GLUCOCORTICOID AND OMEGA-3 FATTY ACID INTERVENTIONS IN ENVIRONMENTAL TRIGGERED INFLAMMATION AND AUTOIMMUNE DISEASE

By

Lauren Kristen Heine

A DISSERTATION

Submitted to
Michigan State University
in partial fulfillment of the requirements
for the degree of

Pharmacology and Toxicology – Environmental Toxicology – Doctor of Philosophy

2023

ABSTRACT

Systemic lupus erythematosus (lupus) is a chronic, debilitating autoimmune disease that predominantly afflicts women of childbearing age and women of color. While genetics plays a critical role in disease onset, environmental exposures to respirable toxicants such as crystalline silica ($cSiO_2$) or Gram-negative bacterial lipopolysaccharide (LPS) have been implicated as triggers for lupus. Pre-clinical studies using lupus-prone mice have shown that pulmonary exposure to $cSiO_2$ leads to unresolved inflammation in the lung, which serves as a nexus for systemic autoimmunity. Similar to what has been observed in human patients, respirable toxicant exposures in lupus-prone mice results in recruitment of auto-reactive B- and T-cells, production of autoantibodies (AAb) and Type-I Interferons (IFNs), and development of glomerulonephritis. Currently, there is no cure for lupus and one of the mainstay treatments is glucocorticoids (GCs). While GCs help quell chronic inflammation, long-term use is associated with many adverse side effects. Interestingly, previous studies from the Pestka lab have shown that dietary supplementation with the omega-3 polyunsaturated fatty acid (PUFA), docosahexaenoic acid (DHA), attenuates $cSiO_2$-triggered autoimmunity and improves survivability in lupus-prone mice. Additionally, DHA treatment in a novel alveolar-like macrophage cell line hinders LPS-primed pro-inflammatory and Type-I IFN transcriptional responses. Given the promising anti-inflammatory nature of DHA, this thesis builds upon previous *in vivo* and *in vitro* models to address the overarching hypothesis that DHA has steroid-sparing properties which can be harnessed to lower requisite doses of GCs needed to attenuate environmental triggered inflammation and autoimmunity.

In this dissertation, four aims were employed to uncover how inflammation and autoimmunity are altered based on therapeutic intervention, age, and environmental stimuli. In the

first aim, thresholds were determined for the GC prednisone's immunomodulatory effects on $cSiO_2$-triggered autoimmunity and secondary toxicity in NZBWF1 lupus-prone mice. A reduction in $cSiO_2$-induced inflammation and autoimmunity was observed at a moderate relevant human equivalent dose (HED) of prednisone. Yet, at this same dose, GC-induced toxicity was observed and there was no improved survivability in $cSiO_2$-exposed mice. In the second aim, age was addressed as contributing factor in $cSiO_2$-induced autoimmunity in NZBWF1 lupus-prone mice. When using adult mice that more appropriately model the age of $cSiO_2$-exposed workers, we observed that $cSiO_2$ exposure resulted in intensified pulmonary inflammation compared to what has been observed in published studies using juvenile mice. In the third aim, environmentally triggered autoimmunity in NZBWF1 lupus-prone mice was assessed using another relevant environmental toxicant, LPS. Here, it was demonstrated that repeated administration of LPS resulted in local unresolved inflammation and systemic autoimmunity in a route of exposure-dependent manner. Lastly, in the fourth aim, the steroid-sparing potential of DHA was assessed in a novel alveolar-like macrophage cell line. In this study, LPS-stimulated proinflammatory and IFN transcriptional responses were reduced upon combination treatment with sub-optimal concentrations of DHA and the GC dexamethasone. Combination treatment was more effective in reducing LPS-induced responses compared to individual treatment with either DHA or the GC alone.

Taken together, each of the present studies has provided novel insights into how therapeutics (e.g., GC and DHA), age, and unique environmental triggers influence inflammation and autoimmunity. Furthermore, these studies demonstrate DHA has the potential to be used as a steroid-sparing adjunct therapy to attenuate environmental-triggered lupus.

This dissertation is dedicated to my loving parents.
Thank you for your unwavering love and support.

ACKNOWLEDGEMENTS

There have been countless people who have guided me through my PhD and made my time in East Lansing memorable. First, I would like to thank my mentors Dr. Jack Harkema and Dr. James Pestka. I consider myself extremely fortunate to have found Dr. Harkema's lab and presented with the opportunity to work on a collaborative project that facilitated a great co-mentorship. I appreciate everything they have taught me about research and professional development. Drs. Harkema and Pestka exemplify what it means to be great mentors, and I cannot thank them enough for their continued support throughout my PhD.

To Dr. Jim Wagner and Ryan Lewandowski, I will always be appreciative of the continued mentorship over the course of my PhD, and for making lab work fun and enjoyable. Seeing you both in lab has always been a source of constant positivity and I will miss seeing you both on a regular basis.

To my guidance committee, Dr. Cheryl Rockwell and Dr. Stepthen Kin Lee, I appreciate your continued support throughout my PhD. I appreciate you each asking the thoughtful and critical questions that helped me grow as a scientist and learn how to design effective and impactful studies.

To the many collaborators I have had the pleasure of working with, thank you for your assistance and expertise on each project. I want to extend a special thank you to Dr. Abby Benninghoff for her time in teaching me valuable molecular and data visualization techniques.

To Drs. Ania Kopec, Kevin Baker, and Kathryn Wierenga, thank you for your guidance since day one of my PhD. Each of you have been amazing mentors in helping me navigate grad school and grow in my professional development. I am very grateful to have met you during my time here. Thank you, also, to Preeti and Dan for the skills you taught me in lab and your continued

friendship.

To each of the undergraduate students I have had the pleasure of working with and mentoring throughout my time at MSU. Liz, Ashleigh, Alexa, Shamya, Tasha, Sarah, Anna, Adrianna, and Riley, thank you all for the time, effort, and positivity each of you brought to every study. These experiments would not have been possible without you.

To my cohort members – Malique, Erin, Olivia, Brad, and Omar – I am grateful for your friendship and to have had such a great support system over the last 5 years.

To all the faculty, my instructors, and support staff in the Pharmacology and Toxicology Department, thank you for your mentorship and guidance.

To John LaPres, thank you for granting me the opportunity to join MSU through the BMS program and for your continued guidance through the EITS program. Additionally, a special thank you to Jake Wier and Amy Swagart for making sure your students consistently have the support they need throughout their PhD.

To all the kind, wonderful, and generous friends I have made here at MSU, thank you for making East Lansing a home. You all became my family over the last 5 years, and I am extremely fortunate to have met each and every one of you.

Lastly, to my Mom and Dad who have been my foundation and my biggest cheerleaders during this long, trying, and rewarding process. I am eternally grateful for having the most supportive parents. Thank you for your unwavering friendship, generosity, and guidance.

TABLE OF CONTENTS

LIST OF ABBREVIATIONS

AA	Arachidonic acid
AAb	Autoantibody
AAg	Autoantigen
AM	Alveolar macrophage
ANOVA	Analysis of variance
ASC	Apoptosis-associated speck-like protein containing a CARD
BALF	Bronchoalveolar lavage fluid
BMDM	Bone marrow-derived macrophage
BSA	Bovine serum albumin
bw	Body weight
CON	Control
CRP	C-reactive protein
$cSiO_2$	Crystalline silica
d	Day
DAMP	Danger-associated molecular pattern
DEG	Differentially expressed gene
DEX	Dexamethasone
DHA	Docosahexaenoic acid
EBV	Epstein-Barr virus
ELS	Ectopic lymphoid structure
ELT	Ectopic lymphoid tissue
EPA	Eicosapentaenoic acid

FBS	Fetal bovine serum
FLAM	Fetal liver-derived alveolar-like macrophage
g	Gram
GC	Glucocorticoid
GLC	Gas-liquid chromatography
GM-CSF	Granulocyte-macrophage colony-stimulating factor
GO	Gene ontology
GR	Glucocorticoid receptor
H&E	Hematoxylin and eosin
hr	Hour
HCQ	Hydroxychloroquine
HED	Human equivalent dose
IFN	Interferon
IN	Intranasal
IP	Intraperitoneal
IRF	Interferon regulatory factor
IRG	Interferon regulated gene
ISG	Interferon stimulated gene
LPS	Lipopolysaccharide
LXR	Liver X Receptor
MARCO	Macrophage receptor with collagenous structure
MAPK	Mitogen-activated protein kinases
mg	Milligram

NF-κB	Nuclear factor kappa B subunit
OA	Oleic acid
OSHA	Occupational Safety and Health Administration
P/S	Penicillin-streptomycin
PAMP	Pathogen associated molecular patterns
PASH	Periodic acid-Schiff hematoxylin
PBS	Phosphate-buffered saline
PI	Post-instillation
PRR	Pattern recognition receptor
PUFA	Polyunsaturated fatty acid
RBC	Red blood cell
RPMI	Roswell Park Memorial Institute
SEM	Standard error of the mean
SPM	Specialized pro-resolving mediators
TF	Transcription factor
TGF-β1	Transforming growth factor beta-1
TLR	Toll-like receptor
VEH	Vehicle
wk	Week

CHAPTER 1: INTRODUCTION AND LITERATURE REVIEW

INTRODUCTION

Systemic lupus erythematosus (lupus) is a chronic autoimmune disease that predominantly afflicts women of childbearing age and women of color. Lupus is characterized by recurring bouts of autoimmunity driven by unresolved inflammation, autoreactive lymphoid cells, and systemic autoantibody (AAb) and Type-I Interferon (IFN) production (1-3). Unattenuated systemic inflammation leads to irreparable damage in the kidney resulting in development of glomerulonephritis and eventually end-stage renal failure (4). While genetic predilection is a major determinant of lupus, environmental toxicants are also linked to onset of autoimmunity (2, 5-7). Occupational exposures to toxicants such as respirable crystalline silica ($cSiO_2$) (8-11) or Gram-negative bacterial lipopolysaccharide (LPS) (12-15) have been implicated as triggers for lupus. Using a preclinical animal model that emulates onset and progression of environmental-triggered lupus, previous studies from our lab have shed light on how pulmonary exposure to $cSiO_2$ leads to autoimmune-mediated glomerulonephritis. In this mouse model, repeated exposure to $cSiO_2$ led to unresolved inflammation in the lung resulting in recruitment of auto-reactive B- and T-cells, perivascular and peribronchiolar ectopic lymphoid tissue (ELT) formation, pathogenic autoantibody (AAb) production, and glomerulonephritis (16-19) (**Figure 1.1**). In line with overactive, aberrant Type-I IFN signaling, which is commonly observed in lupus patients, $cSiO_2$-exposed mice displayed increased Type-I IFN gene expression in pulmonary and renal tissues (20, 21).

As there is no cure for lupus, one of the mainstay treatments utilized to quell chronic inflammation is glucocorticoids (GCs) (22). While GCs are potent anti-inflammatory agents, long-term use is associated with several adverse side effects such as diabetes, muscle wasting, bone loss, and increased susceptibility to infections (22-26). Interestingly, previous studies from our lab

have shown that dietary supplementation with the omega-3 polyunsaturated fatty acid (PUFA) docosahexaenoic acid (DHA), attenuates $cSiO_2$-triggered autoimmunity and improves survivability in lupus-prone mice (16, 18, 21, 27, 28). Additionally, LPS-triggered pro-inflammatory and Type-I IFN transcriptional responses observed in a novel alveolar-like macrophage cell line were impeded when treated with DHA-supplemented medium (29). Based on the findings from these *in vivo* and *in vitro* studies, DHA shows great potential to be used as a cost-effective adjunct therapy in treating environmental-triggered autoimmunity. Together these findings warrant further investigation into whether DHA can be used to lower requisite doses of GCs to quell inflammation while also negating toxicity in models that emulate environmental-triggered lupus.

CHAPTER SUMMARIES

Chapter 1. This introductory chapter contains a brief synopsis of the material found within each section of this dissertation. Additionally, this chapter contains a literature review that provides relevant background information about major topics addressed in this dissertation such as: 1) the underlying mechanisms of lupus, 2) environmental exposures and triggers of autoimmunity, 3) glucocorticoids (GCs) as a cornerstone treatment in lupus, and 4) the anti-inflammatory properties of omega-3 PUFAs.

Chapter 2. While GCs are a cornerstone treatment in lupus, the dosing thresholds necessary for attenuation of inflammation, and conversely where toxicity is observed, have not been elucidated in a preclinical model of lupus. In this chapter, we characterized the dose-dependent immunomodulation and toxicity of the GC prednisone in a preclinical model that emulates onset and progression of $cSiO_2$-triggered lupus. Two cohorts of juvenile female NZBWF1 lupus-prone mice were fed either control AIN-93G diet or one of three AIN-93G diets

containing prednisone at 5, 15, or 50 mg/kg diet which span human equivalent oral doses (HED) currently considered to be low (PL; 5 mg/d HED), moderate (PM; 14 mg/d HED), or high (PH; 46 mg/d HED), respectively. Mice were intranasally instilled with either saline vehicle or 1 mg $cSiO_2$ once weekly for 4 wk. The experimental plan was to 1) terminate one cohort of mice 14 wk after the last $cSiO_2$ instillation for pathology and autoimmunity assessment and 2) to maintain a second cohort to monitor glomerulonephritis development and survival. High dose prednisone treatment resulted in hyperglycemia, muscle wasting, weight loss, and deteriorating health which necessitated early removal of this group from the study. Results from the first cohort revealed that consumption of PM but not PL diet significantly reduced $cSiO_2$-induced pulmonary ectopic lymphoid structure formation, nuclear-specific AAb production, and inflammation/autoimmune gene expression in the lung, splenomegaly, and glomerulonephritis in the kidney. Relative to GC-associated toxicity, PM but not PL diet elicited muscle wasting, but these diets did not affect bone density or cause glucosuria. Finally, neither PM nor PL diet improved latency of $cSiO_2$-accelerated death in the second cohort of mice. Taken together, this preclinical study demonstrates that prolonged dietary administration of prednisone at clinically relevant doses falls short of offering complete protection from $cSiO_2$-induced autoimmunity and can cause significant secondary toxicity at moderate to high doses.

Chapter 3. Published studies from our lab have demonstrated that repeated intranasal exposure to $cSiO_2$ triggers early onset and progression of autoimmunity in the lungs and kidneys of female juvenile NZBWF1 lupus-prone mice. Furthermore, dietary supplementation with the omega-3 fatty acid, DHA, prevented $cSiO_2$-induced lupus in this experimental model. However, it is unknown how $cSiO_2$ exposure and DHA intervention affect adult lupus-prone mice that more appropriately model the age of $cSiO_2$-exposed workers. To address this gap in knowledge, we fed

female adult NZBWF1 mice either purified AIN-93G control diet or AIN-93G diet containing DHA at a HED of 5 g/d. Mice were intranasally instilled with either saline vehicle or 1 mg $cSiO_2$ once per wk for 4 consecutive wks and sacrificed at 1 or 5 wks after the last instillation (PI). Here, $cSiO_2$ exposure led to marked pulmonary pathology and autoimmunity at 5 wk PI. Moderate inflammation and IgG deposition were observed in the kidneys of $cSiO_2$-exposed mice at this same timepoint. Dietary DHA dramatically attenuated $cSiO_2$-triggered responses in both the lung and kidney at 5 wk PI. Overall, we demonstrated that a relevant human dose of the omega-3 fatty acid DHA effectively suppresses $cSiO_2$-triggered pulmonary inflammatory/immune responses in an adult mouse model that more appropriately emulates human occupational exposures.

Chapter 4. Repeated intraperitoneal (IP) exposure to Gram-negative bacterial LPS has been shown to trigger early onset of glomerulonephritis and mortality in lupus-prone mice, yet pulmonary exposure to LPS in preclinical models of lupus has yet to be evaluated. To address this knowledge gap, we assessed the effects of subchronic airway exposure to LPS via intranasal (IN) instillations on the induction of autoimmunity in NZBWF1 lupus-prone mice and related these findings to the effects of equivalent LPS dosing via IP route. Female juvenile NZBWF1 mice were exposed to either sterile saline vehicle or smooth *E. coli* LPS (0.8 μg/g bw) via IN instillation or IP injection twice weekly for 5 consecutive wks. Our findings demonstrated that short-term repeated LPS exposure resulted in local and systemic autoimmunity in a route of exposure-dependent manner. IN exposure to LPS elicited intense lung inflammation and ectopic lymphoid neogenesis, whereas IP exposure drove inflammation that was primarily localized to the spleen and systemic circulation. IP LPS delivery was also more effective in inducing autoimmune-mediated glomerulonephritis compared to the IN route of exposure. Taken together, this is the first study to demonstrate that *E. coli* LPS elicits local and systemic autoimmunity in female NZBWF1

lupus-prone mice through two unique routes of exposure.

Chapter 5. DHA and GCs are both potent anti-inflammatory agents that can be used to quell inflammation and autoimmunity, however DHA's use as a steroid-sparing treatment has yet to be detemined. In this chapter, RNAseq was used to evaluate whether DHA could potentiate the anti-inflammatory effects of the GC dexamethasone (DEX) in LPS-stimulated fetal liver-derived alveolar-like macrophages (FLAMs) isolated from NZBWF1 lupus-prone mice. More specifically, FLAMs were treated were treated with suboptimal concentrations of either DHA alone, DEX alone, or DHA+DEX in combination prior to LPS stimulation for 4 or 8 hr. DHA+DEX co-treatment reduced LPS-triggered proinflammatory and Type-I IFN gene expression in a combinatorial manner, leading to greater suppression of innate immune responses compared to individual treatments. Overall, this study provides compelling evidence that DHA potentiates the anti-inflammatory effects of DEX, and thus DHA can potentially be used to lower requisite amounts of GCs required to reduce inflammation.

Chapter 6. This final chapter discusses conclusions drawn from the present body of work in addition to potential future studies that can be used to build upon the data from this dissertation.

LITERATURE REVIEW

Lupus, demographics, and economic burden

Systemic lupus erythematosus (lupus) is a heterogeneous, debilitating, chronic autoimmune disease that disproportionately afflicts women of child-bearing age and women of color (30, 31). Disease onset and progression are strongly influenced by gene-environment interactions (3). Lupus affects multiple organ systems such as the kidneys, lungs, skin, and central and peripheral nervous systems (1). The kidney is a primary endpoint of concern in lupus because chronic inflammation in the kidney (glomerulonephritis) leads to irreparable organ damage and eventual renal failure.

However, other organ systems affected by chronic inflammation and autoimmunity leave patients susceptible to developing comorbidities that can diminish quality of life (32), lead to increased health care costs (33), and lead to higher incidence of mortality (34). Physical comorbidities identified within lupus patient cohorts that are associated with decreased quality of life include thyroid and metabolic disorders, cardiovascular disease, and allergic disorders, and neurocognitive disorders (35). Patients may also exhibit increased incidences of psychological comorbidities such as depression and anxiety (35). As it pertains to mortality, during the years of 2000-2015, lupus was attributed to 28,411 female deaths and was identified as one of the top 20 leading causes of death in females aged from 5-64 years old (36). Among African American and Hispanic women, lupus has been shown to be among the top 10 leading causes of death among those aged 15-44 (36).

In addition to increased morbidity and mortality, the devastating nature of lupus also extends to the economic burden placed upon patients. In 2016, it was estimated that annual patient costs related to treatment expenses ranged between $15,171-$88,445 (37). Differences in total annual costs for management and treatment of lupus is often dependent upon disease severity (37, 38). Those experiencing mild symptoms incur average annual costs of $27,937 in hospital admission-related care and $10,396 in outpatient care. In comparison, those with severe manifestations incur average annual costs of $49,474 in hospital admission-related care and $23,468 in outpatient care (38). While disease activity dictates annual treatment costs, socioeconomic factors have a determinant role in disease severity, highlighting the complex interplay between health outcomes and potential financial barriers. Socioeconomic factors such as financial status, education level, and health insurance coverage compound each other to influence disease outcomes in lupus patients (31).

Underlying mechanisms of lupus

Lupus is a prototypical autoimmune disease characterized by inflammation and a loss of self-tolerance. Disease activity is driven by B- and T-cells that are activated by self-antigens (1, 2). Additionally, autoreactive B-cells can differentiate plasma cells that secrete large amounts of autoantibodies (AAbs) which target and bind to autoantigens (AAgs) originating from nuclear material and glomerular, phospholipid, or thyroid-related proteins (1, 2, 39, 40). AAb-AAg complexes are distributed via the systemic circulation and deposit in organs such as the spleen or kidney (4). In lupus, this sequence of events continuously reoccurs throughout a patient's lifetime, manifesting in increased measurable disease activity, known as flares (3). These cyclical bouts of autoimmunity lead to increased renal deposition of immunoglobulin complexes, development of glomerulonephritis, and irreparable organ damage that precipitates into end-stage renal failure (41).

Consistent with the diagnostic techniques used to diagnose lupus, disease activity or flaring is monitored through evaluation of organ-specific or non-organ-specific biomarkers (1, 42). Organ-specific biomarkers include urinalysis, which is used to test for elevated levels of protein/creatine or proinflammatory chemokines, which can be indicative of decreased renal function and glomerulonephritis progression (42). Non-organ-specific biomarkers include testing for elevated levels anti-nuclear antibodies, anti-complement antibodies, and Type-I Interferon (IFN) inducible genes and chemokines in the serum (1, 42). It is common for lupus patients to develop aberrant Type-I IFN signaling, sometimes referred to as interferonopathies, where normal IFN-mediated viral responses can longer distinguish between self versus non-self (43). Elevated Type-I IFN signatures are present in approximately 60-80% of lupus patients and lead to increased disease activity (44, 45). Approximately 40 distinct genotypes have been identified and linked to

dysregulated Type-I IFN signaling, suggesting that genetics play a putative role in interferonopathies observed in lupus (43, 46).

Genetic susceptibility plays an essential role in the development of lupus, however, disease onset can also be influenced by external factors such as environmental exposures, hormones, and lifestyle. Currently, over 80 genes considered to be susceptibility loci in humans, have been identified due to their association with incidences of lupus (47). Many of these genes found to be dysregulated in lupus are associated with antigen presentation, maintenance of autoreactive lymphocytes, clearance of intracellular debris, and innate immune response (47, 48). Disease onset is predominantly associated with polygenic traits, meaning either (i) multiple genes considered to be risk alleles are defective in function and together drive a phenotype that results in autoimmunity, or (ii) one or more genes that have defective function are exacerbated by environmental stimuli resulting in autoimmunity (48). While it is rare that an individual gene mutation will result in pathogenic autoimmunity, cases of monogenic lupus do exist (49, 50). These incidences of lupus are predominantly identified in juvenile patients or due to familial history with lupus, however, the mechanisms underlying monogenic cases is still poorly understood (50).

Environmental triggers of lupus

Although genetics highly influence an individual's propensity to develop lupus, environmental factors also play an important role in disease onset. Environmental factors such as medications, UV radiation, infections, occupational exposures, and lifestyle/nutrition can work cooperatively with genetic susceptibility to trigger autoimmunity (51). Some occupational exposures and infections can lead to unresolved inflammation in organs such as the lung or spleen, leading to germinal center formation and increased numbers of autoreactive B-cells, thus prompting a systemic autoimmune response.

Opportunistic pathogens and viruses are recognized by innate immune cells such as monocytes and macrophages as pathogen-associated molecular patterns (PAMPs) which bind to pattern recognition receptors (PPRs) such as toll-like receptors (TLRs) (52, 53). For example, viruses such as Epstein-Barr virus (EBV) activates intracellular TLR3 receptors to initiate a Type-I IFN response (51). Alternatively, pathogens such as bacterial lipopolysaccharide (LPS) can activate TLR4 to elicit proinflammatory cytokine/chemokine and Type-I IFN gene and protein expression in monocytes/macrophages (54, 55). In the case of LPS, autoimmunity can be initiated through multiple routes of exposure. Increased intestinal permeability resulting in a leaky gut syndrome leads to the escape of opportunistic or benign Gram-negative bacterial species into the systemic circulation (13). Alternatively, LPS exposure can occur through respirable sources found in occupations such as agriculture or waste management (13, 14, 52, 56, 57). *In vivo* studies in lupus-prone mice have demonstrated that intraperitoneal exposure to *Salmonella* derived strains of LPS leads to germinal center formation in secondary lymphoid tissues like the spleen and is complemented by increased infiltration of autoreactive B-cells and IgG deposition (58, 59). Furthermore, rheumatoid arthritis (RA)-prone mice exposed to respirable organic LPS-containing dust mixtures develop marked lung pathology, increased Type-I IFN gene expression in pulmonary tissue, and elevated autoreactive IgG AAbs in the serum (54, 60, 61). Taken together, these clinical and preclinical studies provide considerable evidence implicating LPS as a relevant environmental toxicant in autoimmune disease.

Another relevant environmental toxicant that has been linked to autoimmunity in humans is respirable crystalline silica ($cSiO_2$). Occupational $cSiO_2$ exposure has been associated with onset of lupus, RA, scleroderma, ANCA-associated vasculitis (8, 51). According to the Occupational Safety and Health Administration (OSHA), approximately 2.3 million Americans are exposed to

respirable $cSiO_2$ through occupations such as stone cutting, construction, ceramics, and ceramics (62, 63). Due to the small size of $cSiO_2$ (<5 μm), these particles travel down to the distal airways and deposit in the alveoli. In the alveolar airspaces, alveolar macrophages (AMs) serve as the first line of defense against $cSiO_2$ particles and recognize this foreign material through binding of the macrophage receptor with collagenous structure (MARCO) (8). Phagocytosis of $cSiO_2$ particles by AMs results in inflammasome activation, proinflammatory gene expression, and cell death (64-66). Published studies from our lab have demonstrated that repeated intranasal exposure to $cSiO_2$ leads to unresolved pulmonary inflammation in female NZBWF1 lupus-prone mice (17, 18, 67, 68). Moreover, unattenuated inflammation in the lung resulted in perivascular and peribronchiolar infiltration of autoreactive B- and T-cells and formation of ectopic lymphoid tissues (ELTs). As a result, systemic autoimmunity was observed in endpoints such as increased AAb levels detected in the bronchoalveolar lavage fluid (BALF) and plasma, in addition to autoimmune-mediated glomerulonephritis.

In summary, human epidemiological studies and preclinical experimental mouse models have demonstrated that the environmental toxicants LPS and $cSiO_2$ are triggers of autoimmunity and can lead to increased morbidity and mortality in lupus patients (8, 18, 52). Therefore, studies aimed at better elucidating the mechanisms underlying environmentally-triggered lupus will aid in understanding how to better treat and attenuate autoimmunity.

Glucocorticoids and other current treatments for lupus

While there are currently no cures for lupus, several treatment options are available that vary based upon mechanisms of action, off-target side effects, and cost. Each treatment, or combination of treatments, is prescribed with the overall goal of managing lupus flares, slowing disease progression, and reducing the risk of comorbidities that lead to decreased quality of life

and increased mortality. One of the most common treatments perscribed for lupus are glucocorticoids (GCs) such as prednisone (23). While GCs help quell disease activity and are more cost-effective compared to other treatments, prolonged use at moderate to high doses results in deleterious side-effects such as bone loss, muscle wasting, diabetes, cardiovascular disease, and increased risk of opportunistic infections (22-24). Unfortunately, due to the chronic nature of lupus, patients are often reliant on GC treatment for decades leaving them at greater risk of developing unwanted secondary toxicity (69). GCs are heavily utilized due to their fast-acting anti-inflammatory properties, which is of particular importance when a patient is experiencing a flare. Patients who experience moderate to severe flares will often be treated with 125-1000 mg/d of methylprednisolone or prednisolone for ~3 days to achieve rapid immune suppression, followed by a tapered dosing regimen of oral prednisone (23). Doses of oral prednisone prescribed after a flare typically range between 10 to 30 mg/d, while those taken to maintain quiescent disease are <7.5 mg/d (70, 71). The unofficial threshold for GC-mediated toxicity stemming from long-term oral prednisone use is 7.5 mg/d (72-75). While it is recommended that maintenance doses do not exceed 7.5 mg/d in order to avoid adverse outcomes, uncertainty remains in regards to the correct way to taper patients off prednisone while keeping autoimmunity at bay (23).

One method clinicians use to help cut requisite doses of prednisone is to treat patients with a combination of GCs and other drugs such as hydroxychloroquine (HCQ) (76). Hydroxychloroquine is an antimalarial that inhibits B-cell receptor signaling and Type-I IFN production, which are central to lupus pathogenesis. However, HCQ takes up to 6-12 weeks to reduce clinical signs of lupus, which is extremely problematic in managing flares (77). Additionally, HCQ treatment can result in gastrointestinal problems, nausea, and in rare cases cardiomegaly or retinopathy (77). Other therapeutics utilized to manage lupus include

immunosuppressants (e.g., cyclophosphamide) and biologics (e.g., monoclonal antibodies) (76, 78). Similar to HCQ, immunosuppressants and biologics work by suppressing facets of B-cell signaling, TLR signaling, and IFN production. However, these treatments are not always ideal candidates due to their delayed efficacy in reducing inflammation, adverse side effects associated with prolonged use, and increased cost (78, 79). For example, belimumab, a monoclonal antibody that inhibits autoreactive B-cell survival, costs up to $35,000 per year (79). Therefore, there lies a critical need for treatments that are efficacious in attenuating autoimmunity that are both cost-effective and do not generate toxicity.

Omega-3 Polyunsaturated Fatty Acids

Clinical and pre-clinical studies continue to provide mounting evidence that omega-3 polyunsaturated fatty acids (PUFAs) possess potent anti-inflammatory and pro-resolving properties. Clinical trials in humans have shown that increasing intake of dietary omega-3 PUFAs improves pain and fatigue in lupus patients (80-82), in addition to reducing levels of proinflammatory cytokines such as TNF-α in the blood of RA patients (83). Furthermore, increased omega-3 PUFA intake has been shown to reduce omega-6 content in human erythrocytes (84-86). While metabolism of omega-3 PUFAs such as docosahexaenoic acid (DHA) and eicosapentaenoic acid (EPA) result in specialized pro-resolving mediators (SPMs) such as resolvins, protectins, and maresins, metabolites from omega-6 PUFAs like arachidonic acid (AA) include leukotrienes, thromboxanes, and cyclooxygenases and are considered to be proinflammatory (87). Therefore, in clinical studies in humans, by skewing the fatty acid content to favor anti-inflammatory PUFAs, and thereby lowering the omega-6:omega-3 ratio, patients had decreased proinflammatory C-reactive protein (CRP) and IL-6 detected in the blood (84-86).

In line with data from clinical trials, pre-clinical mouse models of lupus have illustrated the potent anti-inflammatory effects of the omega-3 PUFA DHA. Published studies from our lab have shown that dietary DHA administered at a human equivalent dose (HED) of 5 g/d was effective in attenuating inflammation and autoimmunity resulting from repeated intranasal exposure to $cSiO_2$ in female juvenile NZBWF1 lupus-prone mice. More specifically, DHA reduced local pulmonary inflammation (ELT formation, lymphoid cell infiltration, BALF cellularity, AAbs in BALF, proinflammatory gene expression) and systemic autoimmunity (plasma AAbs, glomerulonephritis) (16, 18, 20, 21, 27, 28, 68, 88). Additionally, in female juvenile NZBWF1 lupus-prone mice repeatedly exposed intraperitoneally to Gram-negative *Salmonella*-derived lipopolysaccharide (LPS), oral administration of DHA at 5 g/d HED resulted in reduced LPS-triggered glomerulonephritis (58).

GC and DHA mechanisms of action in monocytes/macrophage

Alveolar macrophages (AMs) are crucial to the detection, sequestration, and clearance of foreign particles in the alveoli. Respirable toxicants, some of which act as pathogen- or danger-associated molecular patterns (PAMPs and DAMPs, respectively), activate AMs by binding to PRRs like TLRs. LPS is a well-characterized PAMP and ligand for TLR4, which activates the mitogen activated protein kinase (MAPK) and nuclear factor-κB (NF-κB) pathways in macrophages (89, 90). Activation of these pathways leads to the translocation of transcription factors (TFs), such as NF-κB or interferon regulatory factors (IRFs), which induce the transcription of proinflammatory genes and type-I IFNs (91). The GC-bound glucocorticoid receptor (GR) can exert anti-inflammatory effects via transrepression and transactivation (25). Transrepression refers to inhibition of a TF via protein-protein interactions to reduce proinflammatory gene expression (92, 93). For example, ligand-bound GR can inhibit TFs such as NF-κB through tethering

mechanisms (92, 93). Transactivation, in comparison, refers to gene expression initiated by protein-protein interactions (40). An example of transactivation is the upregulation of anti-inflammatory mediators, such as dual-specificity phosphatase 1 (DUSP1) and glucocorticoid-induced leucine zipper (GILZ), upon GR activation (94).

Increased expression of DUSP1 preferentially inhibits JUN N-terminal kinase (JNK) and p38 signaling in vitro (25, 95-97). Moreover, depletion of DUSP1 *in vivo* results in increased serum cytokine levels and decreased mortality upon LPS challenge (95, 98). Alternatively, GILZ promotes an anti-inflammatory phenotype by inhibiting NF-κB from binding to DNA, as well as inhibiting ERK1/2 signaling through repression of Raf by direct binding (95-101). GILZ expression in human leukocytes also negatively correlates with lupus disease activity (99). Furthermore, GCs such as Dexamethasone (DEX) used *in vitro*, have been shown to reduce proinflammatory and IFN-regulated gene and protein expression in RAW 264.7 macrophage-like cells and bone marrow-derived macrophages (BMDMs) (102-104). However, attenuation of LPS-triggered proinflammatory responses in an AM cell model have yet to be characterized.

As a tissue-resident macrophage, the AM phenotype is distinct from monocyte-derived macrophages and most transformed *in vitro* macrophage models (105, 106). To circumvent this, the Pestka and Olive labs have optimized a novel, self-renewing AM-like cell model derived from fetal mouse liver. These cells, known as fetal liver-derived alveolar-like macrophages (FLAMs), maintain an AM-like phenotype across multiple passages, greatly reducing the exorbitant number of mice typically required to investigate AM-specific responses (107). Extensive characterization of these cells has confirmed that FLAMs adequately mimic AMs. Notably, FLAMs express both AM-identifying surface markers (*Siglecf* and *CD11c*) and genes (*Marco, Fabp4, Car4, Pparg,* and *Il1a*) (107). Consistent with published literature (108-110), AMs and FLAMs, but not BMDMs,

release IL-1α in response to $cSiO_2$. Conversely, BMDMs, but not AMs and FLAMs, release IL-10 in response to LPS (107). This example of distinct inflammatory responses between *in vitro* macrophage models highlights the importance of using a proper surrogate that accurately reflects the properties of AMs.

By using a combination of RAW-ASC 264.7 and alveolar-like macrophage cell lines, published studies from the Pestka lab have illustrated the anti-inflammatory effects of DHA treatment *in vitro*. DHA treatment of RAW-ASC 264.7 cells and alveolar-like macrophages impeded $cSiO_2$-triggered inflammasome activation, IL-1α expression, and cell death, while also improving efferocytosis (111, 112). Moreover, DHA treatment hindered proinflammatory cytokine and Type-I IFN transcriptional responses in LPS-primed FLAMs (29). Correspondingly, predicted activity of NF-κB and Irf7 TF activity was shown to decrease with DHA treatment. Other *in vitro* studies have revealed that DHA can remedy inflammation through other mechanisms including: (i) alteration of lipid rafts and pro-inflammatory transmembrane receptors (113), (ii) activation of receptors (e.g., GPR120) (114) and transcription factors (e.g., PPARγ) (115) that are inhibitors of NF-κB activity (116), and (iii) production of specialized pro-resolving mediators (SPMs; e.g., resolvins, maresins, and protectins) (117). Based on the literature, it is evident that DHA and GCs work via overlapping, as well as independent, mechanisms of action to reduce proinflammatory gene and protein expression in monocytes/macrophages (**Figure 1.2**). Yet, studies evaluating the concomitant effects of DHA and GC used together *in vitro* to attenuate a proinflammatory alveolar-like macrophage phenotype have yet to be performed.

FIGURES

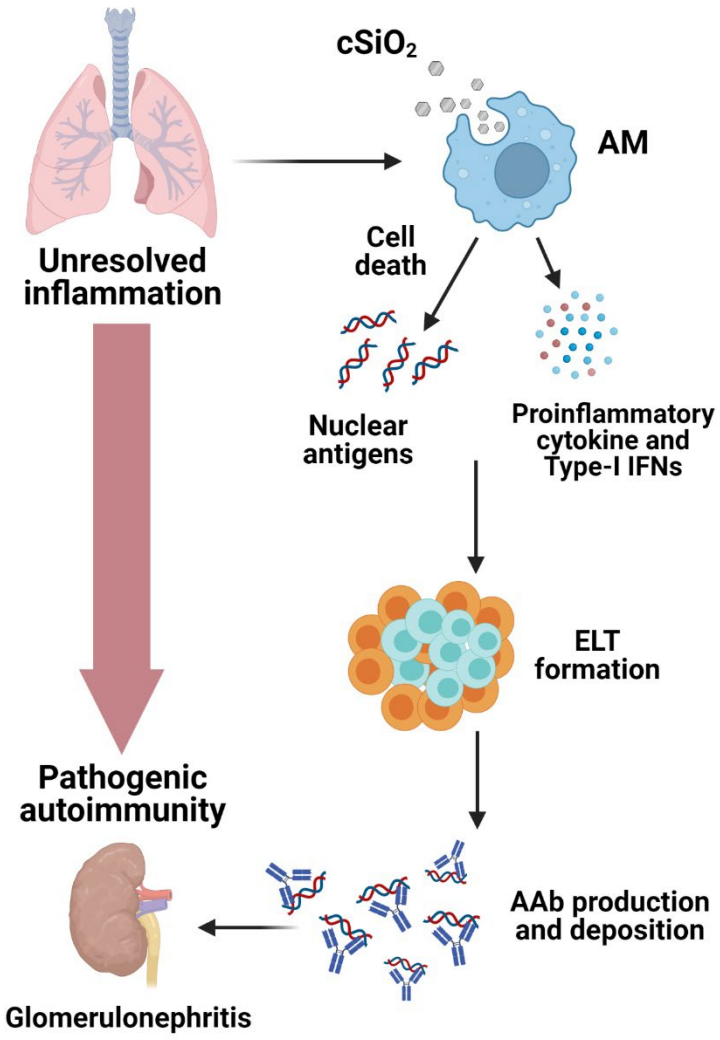

Figure 1.1: Respirable $cSiO_2$-induced inflammation and autoimmune-mediated glomerulonephritis. Upon respiration, $cSiO_2$ particles travel down to the distal airways and deposit in the alveoli due to their small size (<1.5-2 μm). In the alveoli, phagocytosis of $cSiO_2$ by tissue resident alveolar macrophages (AMs) leads to both aberrant proinflammatory cytokine and Type-I IFN signaling in addition to cell death and expulsion of nuclear antigens. Presentation of nuclear antigens to B- and T-cells recruited to the lung prompts the formation of perivascular and peribronchiolar ectopic lymphoid tissue (ELT). ELT contains large numbers of auto-reactive lymphoid cells, including immunoglobulin-secreting plasma cells, creating a nexus of pathogenic autoantibody (AAb) production in the lung. Once bound to cognate self-antigens, AAb-antigen complexes are distributed via systemic circulation and deposit in other organs such as the kidney. Chronic deposition of immune complexes and inflammation results in glomerulonephritis and eventual renal failure.

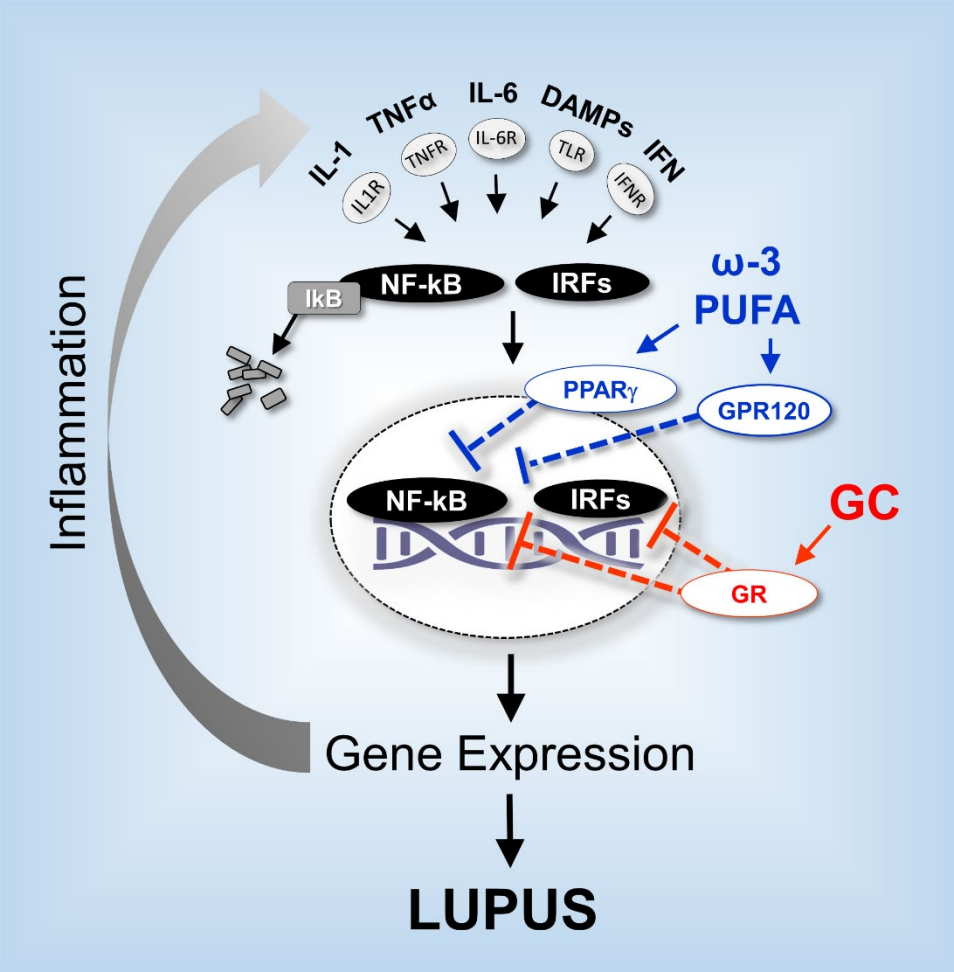

Figure 1.2: DHA and GC reduce inflammation through overlapping mechanisms of action. Immune cells, such as monocytes/macrophages, are activated by binding of DAMPs and proinflammatory cytokines to their respective receptors. Downstream signaling leads to the sequestration and degradation of IkB, which frees NF-kB to translocate into the nucleus and drive proinflammatory gene expression (118, 119). Similarly, interferon regulatory factors (IRFs) are activated and recruited to the nucleus leading to increased IFN gene and protein expression (120). Without breaks in this feed forward loop, continuous unresolved inflammation encourages lupus pathogenesis. Omega (ω)-3 PUFAs inhibit NFkB through activation of GPR120 and PPARγ. GCs also inhibit NFkB, in addition to IRFs, through activation of the GC receptor (GR).

CHAPTER 2: COMPARATIVE EFFECTS OF HUMAN-EQUIVALENT LOW, MODERATE, AND HIGH DOSE ORAL PREDNISONE INTAKE ON AUTOIMMUNITY AND GLUCOCORTICOID-RELATED TOXICITY IN A MURINE MODEL OF ENVIRONMENTAL-TRIGGERED LUPUS

Lauren Heine[1,2], Abby D. Benninghoff[3], Elizabeth A. Ross[4], Lichchavi D. Rajasinghe[4], James G. Wagner[2,5], Ryan P. Lewandowski[5], Alexa L. Richardson[4], Quan-Zhen Li[6], John P. Buchweitz[2,5,7], Justin Zyskowski[7], Ashleigh N. Tindle[5], Anna E. Skedel[5], Nicholas Chargo[8], Laura R. McCabe[2,8], Jack R. Harkema[1,2,5], and James J. Pestka[2,4,9]

[1]Department of Pharmacology and Toxicology, Michigan State University, East Lansing, MI

[2]Institute for Integrative Toxicology, Michigan State University, East Lansing, MI

[3]Department of Animal, Dairy and Veterinary Sciences, School of Veterinary Medicine, Utah State University, Logan, UT

[4]Department of Food Science and Human Nutrition, East Lansing, MI

[5]Department of Pathobiology and Diagnostic Investigation, Michigan State University, East Lansing, MI

[6]Department of Immunology and Internal Medicine, IIMT Microarray Core Facility, University of Texas Southwestern Medical Center, Dallas, TX

[7]Toxicology Section, Michigan State University Veterinary Diagnostic Laboratory, Lansing, MI

[8]Department of Physiology, Michigan State University, East Lansing, MI

[9]Department of Microbiology and Molecular Genetics, Michigan State University, East Lansing, MI

PUBLICATION NOTICE

The following chapter was published in *Frontiers in Immunology*, Volume 13, No. 972108 in Fall 2022, and can be accessed using the doi: https://10.3389/fimmu.2022.972108.

ABSTRACT

Autoimmune diseases can be triggered by environmental toxicants such as crystalline silica dust ($cSiO_2$). Here, we characterized the dose-dependent immunomodulation and toxicity of the glucocorticoid (GC) prednisone in a preclinical model that emulates onset and progression of $cSiO_2$-triggered lupus. Two cohorts of 6-wk-old female NZBWF1 mice were fed either control AIN-93G diet or one of three AIN-93G diets containing prednisone at 5, 15, or 50 mg/kg diet which span human equivalent oral doses (HED) currently considered to be low (PL; 5 mg/d HED), moderate (PM; 14 mg/d HED), or high (PH; 46 mg/d HED), respectively. At 8 wk of age, mice were intranasally instilled with either saline vehicle or 1 mg $cSiO_2$ once weekly for 4 wk. The experimental plan was to 1) terminate one cohort of mice (n=8/group) 14 wk after the last $cSiO_2$ instillation for pathology and autoimmunity assessment and 2) to maintain a second cohort (n=9/group) to monitor glomerulonephritis development and survival. Mean blood concentrations of prednisone's principal active metabolite, prednisolone, in mice fed PL, PM, and PH diets were 27, 105, 151 ng/ml, respectively, which are consistent with levels observed in human blood ≤ 12 h after single bolus treatments with equivalent prednisone doses. Results from the first cohort revealed that consumption of PM but not PL diet significantly reduced $cSiO_2$-induced pulmonary ectopic lymphoid structure formation, nuclear-specific AAb production, and inflammation/autoimmune gene expression in the lung, splenomegaly, and glomerulonephritis in the kidney. Relative to GC-associated toxicity, PM but not PL diet elicited muscle wasting, but these diets did not affect bone density or cause glucosuria. Importantly, neither PM nor PL diet improved latency of $cSiO_2$-accelerated death. PH-fed mice in both cohorts displayed robust GC-associated toxicity including body weight loss, reduced muscle mass, and extensive glucosuria 7 wk after the final $cSiO_2$ instillation requiring their early removal from the study. Taken together,

our results demonstrate that while moderate doses of prednisone can reduce important pathological endpoints of $cSiO_2$-induced autoimmunity in lupus-prone mice such as upstream ectopic lymphoid structure formation, these ameliorative effects come with unwanted GC toxicity and, crucially, none of these three doses extended survival time.

IINTRODUCTION

Systemic lupus erythematosus (lupus) is a devastating chronic human autoimmune disease that primarily affects women of childbearing age. Lupus affects multiple organs and is associated with unresolved inflammation and inadequate clearance of dying cells that precipitates loss of immunological tolerance and production of autoantibodies (AAb). These AAb form immune complexes with autoantigens (AAg) that deposit in tissues provoking recruitment of inflammatory cells, cytokine release, complement activation, and cell death in multiple organ systems (78, 121, 122). Lupus typically involves recurrent, intermittent increases in disease activity known as flares that collectively promote irreversible organ damage often manifesting in glomerulonephritis and end-stage renal disease. While genetic predisposition is a major contributor to an individual's propensity to develop lupus, environmental triggers such as toxicants, UV radiation, infections, or drugs can play critical roles in disease onset, flaring and progression (78, 123-126).

Exposure to respirable crystalline silica ($cSiO_2$) dust particles in occupations such as construction, mining, and stonecutting is etiologically associated with the occurrence of lupus and other autoimmune diseases (125, 127-130). Consistent with epidemiologic investigations, our laboratory has developed a novel preclinical model that emulates gene x environment interaction in $cSiO_2$-triggered lupus. This model employs chronic airway exposure to $cSiO_2$ of lupus-prone female NZBWF1 mice and expresses key lupus hallmarks including unresolved inflammation, loss of immunological tolerance, local/systemic autoantibody production, and glomerulonephritis that

are not evident in similarly treated wild-type mice without lupus predilection (27, 131). Additionally, repeated exposure to $cSiO_2$ in female lupus-prone NZBWF1 mice leads to accelerated AAb production and immune complex-mediated glomerulonephritis approximately 2-3 months earlier (~24 weeks of age) compared to their wild-type counterparts (~32-34 weeks of age) (12). In brief $cSiO_2$ induces in the lung, production of proinflammatory cytokines and chemokines, and Type 1 interferon-regulated gene expression immunogenic macrophage death, and AAg release that together promote early loss of immunological tolerance. This loss is heralded by development of pulmonary ectopic lymphoid structures (ELS) containing follicular dendritic, T, and B-cells that foster development of germinal centers and AAb-producing plasma cells. Resultant AAbs enter the systemic circulation, form immune complexes, and can deposit in the kidney, eliciting glomerulonephritis, and early death (131, 132). We have extensively used this preclinical model to demonstrate that dietary intervention with the omega-3 fatty acid docosahexaenoic acid (DHA) is extremely effective in ameliorating environmental-triggered lupus onset and progression (27, 132-135).

Glucocorticoids (GC) have been a mainstay treatment for autoimmune diseases since the 1950's (136). Prolonged GC treatment can lead to many deleterious side-effects such as muscle and bone loss, diabetes, cardiovascular disease, and increased risk of secondary infection (25, 26, 136-138). Patients with lupus often rely on GCs for the remainder of their lives, putting them at greater risk for GC-induced toxicity (69). The GC prednisone is often used to treat lupus flares and maintain remission due to its potent anti-inflammatory properties, and because it is cost-effective compared to other treatments such as biologics (139). Prednisone doses for treatment of human rheumatological diseases have been classified as low ($\leq$7.5 mg/d), moderate (>7.5 mg $\leq$30 mg/d), and high (>30 mg $\leq$ 100 mg/d) (140). Typical prednisone dosing regimens for patients with lupus

range between 10 to 30 mg/d for treating active flaring and 5 mg/day for maintaining clinically quiescent disease (71). Chronic clinical usage of prednisone doses ranging from 6 to 7.5 mg/day are suggested thresholds for preventing adverse effects and organ damage (72, 141-143).

Much of what is known about prednisone is derived from clinical studies of lupus evaluating i) their effectiveness in alleviating disease flaring and reducing organ damage, and ii) their capacity for eliciting untoward side effects. However, there is a surprising lack of preclinical studies elucidating underlying mechanisms for quelling lupus flaring and progression or identifying toxic thresholds for this potent drug. Moreover, little is known about the formation of pulmonary ELS in the context of lupus and how GCs can regulate ELS when they act as a nexus for autoimmunity. Therefore, the purpose of the present investigation was to test the hypotheses that administration of oral prednisone via the diet would dose-dependently 1) suppresses $cSiO_2$-induced inflammation and autoimmunity and 2) produce secondary GC-induced toxicity in the pre-clinical NZBWF1 lupus-prone mouse model.

MATERIALS AND METHODS

Animals and Diets

Experimental animal procedures were approved by MSU Institutional Animal Care and Use Committee (AUF #PROTO201800113) in accordance with the guidelines of the National Institute of Health. Female 6-week-old NZBWF1 mice were obtained from Jackson Laboratories (Bar Harbor, ME), and upon arrival were randomly divided into two cohorts, Cohort A (n=40, 8 per group) and Cohort B (n=45, 9 per group), and housed 4 per cage or 3 per cage, respectively (**Figure 2.1A**). Mice were kept under a 12-hr light/dark cycle, with free access to both food and water, and at constant temperature and humidity (21°C-24°C and 40-55%, respectively).

Purified, powdered American Institute of Nutrition (AIN)-93G diet containing 70 g/kg oil

was prepared as previously described (135). All diets contained 60 g/kg food-grade high-oleic safflower oil and 10 g/kg food-grade corn oil to supplement essential fatty acids (**Table A2.1**). Unamended AIN-93G was used as control (P0) diet. For treatment diets, prednisone (USP-grade, anhydrous, micronized, Spectrum Chemical) was first dissolved in warm ethanol, then added to 250 g of CON diet. After mechanical mixing and drying overnight in the chemical fume hood, the concentrate was mixed with an additional 750 g CON diet to yield a concentrated prednisone-amended diet stock of 500 mg/kg. This concentrated working stock was then mixed thoroughly with CON AIN-93G using a Kitchen Aid Mixer to achieve low (PL, 5 mg/kg diet), medium (PM, 15 mg/kg diet), and high (PH, 50 mg/kg diet) concentrations. These are estimated to achieve human equivalent doses (HED) of 5, 14, and 46 mg/d, respectively, using an average body weight of 77 kg for women ≥ 20 years of age in the U.S. (143). Prednisone content was verified in representative experimental diets by LC-MS/MS (**Table 2.1**). Diets were prepared bi-weekly and stored at -20°C and provided ad libitum in feed jars designed to minimize spillage during the study. Diet intake for Cohort A mice was measured each week to determine dietary intake/mouse/24 h to determine if prednisone caused hyperphagia or hypophagia (**Figure A2.1**) (144). These measurements indicated each mouse consistently consumed approximately 3-4 grams of diet per 24 h.

Experimental Design

Figure 2.1A depicts experimental design employed for this study. Briefly, 6 wk old NZBWF1 mice were acclimated to P0 diet for 3 days, then groups from Cohorts A and B were administered P0, PL, PM, or PH diet for the duration of the study. Two weeks after initiating experimental diets, mice were anesthetized with 4% isoflurane and intranasally instilled with either with 1.0 mg $cSiO_2$ (Min-U-Sil-5, 1.5-2.0 µm average particle size, Pennsylvania Sand Glass Corporation, Pittsburgh, PA) in 25 µl sterile phosphate buffered saline (PBS) or with 25 µL PBS vehicle (VEH) once per

wk for 4 wk as described previously (131). Starting at 8 wk post final instillation (PI), urine was collected bi-weekly and evaluated for proteinuria (defined as ≥ 300 mg/dL) and glucose using reagent dipsticks (Cortez Diagnostics, Calabasas, CA). Blood was collected via saphenous vein on all Cohort B mice at 7, 9, and 11 wk PI between 8:30 and 11:30 AM for prednisone and prednisolone analysis. All Cohort A mice were sacrificed at 14 wk PI, while Cohort B mice were maintained until they displayed moribund criteria (**Table A2.2**).

Animal Necropsy and Tissue Selection

Mice were euthanized via intraperitoneal injection with sodium pentobarbital at 56 mg/kg body weight. Using heparinized syringes, blood was collected from the abdominal aorta and centrifuged at 3500 x g for 10 min at 4°C to separate the erythrocytes from plasma, and then stored at -80°C. Plasma was later used to analyze blood urea nitrogen (BUN) levels using a colorimetric detection kit (Thermo Fisher Scientific, Wilmington, DE). Bronchoalveolar lavage fluid (BALF) was collected from the lung as described previously (145). The left lung lobe was fixed in 10% neutral buffered formalin (NBF) (Fisher Scientific, Pittsburgh, PA) at a constant pressure of 30 cm H_2O for a minimum of 1 h, then immersed in a large volume of the fixative until further routine processing for light microscopic examination and morphometric analyses described below. Spleens were weighed, then half was stored in NBF along with one kidney until processed for histology. The caudal lung lobe and half a kidney were stored individually in RNAlater (Thermo Fisher Scientific, Wilmington, DE) at 4°C. The remainder of the right lung, half kidney, and half spleen were snap-frozen in liquid nitrogen and stored at -80°C.

Prednisone and Prednisolone Analyses

Experimental diets were analyzed to verify prednisone concentrations and whole blood was evaluated for prednisone and its active metabolite prednisolone by LC-MS/MS at the MSU

Veterinary Diagnostic Laboratory as described in Supplementary Methods.

EchoMRI for Muscle and Fat Composition

An EchoMRI™ (Echo Medical Systems LLC, Houston, TX) was used to measure live body lean muscle and fat composition at 21, 23, and 25 wk of age as described previously (146). Mice were weighed just prior to live body measurement. Random errors in measurements were minimized by using a 4 min scan duration and thereby increasing the number of primary accumulations per body scan.

Inflammatory Cells in BALF

Total leukocytes in the collected BALF were determined using a hemacytometer. Cytological slides were prepared by centrifuging BALF at 400 x g for 10 min using the Shandon Cytospin 3 (Shandon Scientific, PA) and stained with Diff-Quick (Fisher Scientific). Differential cell counts for macrophages/monocytes, neutrophils, lymphocytes, and eosinophils in BALF were assessed using morphological criteria from a total of 200 total cells. Remaining BALF was centrifuged at 2400 x g for 15 min, and supernatant was stored at -80 °C for subsequent autoantibody (AAb) assays.

Tissue Selection for Lung Histology

Randomly selected, transverse tissue blocks were selected from inflation-fixed left lung lobes. Tissues were paraffin embedded, sectioned at a thickness of 5 microns, and were stained with hematoxylin and eosin (H&E) for light microscopic examination. Tissue sections were semi-quantitatively scored for histopathology (lesion severity) by a board-certified veterinary pathologist (JRH) using the following criteria (% of total lung tissue section affected): (0) no lesions associated with exposure; (1) minimal (<10%); (2) mild (10 < 25%); (3) moderate (25 < 50%); (4) marked (50 < 75%); (5) severe (>75%). Lungs were evaluated for the following lung

lesions: (a) ectopic lymphoid tissue (ELS); (b) alveolar proteinosis, and (c) inflammation (alveolitis).

Lung Immunohistochemistry and Morphometry

Formalin-fixed, paraffin embedded lung sections were immunohistochemically stained to identify B and T lymphocytes, and plasma cells, using CD45R, CD3, and IgG antibodies (**Table A2.3**), respectively, as previously described in detail (135). Slides were digitally scanned using the VS110 virtual slide system (Olympus, Hicksville, NY). Two hundred scanned images at 20x magnification were randomly sampled using systematic random sampling NewCast software (Visiopharm, Hoersholm, Denmark). Using the STEPanizer 1.8 Stereology Tool (147), pulmonary $CD45R^+$, $CD3^+$, and IgG^+ lymphoid cells were counted by overlaying a point grid on randomly sampled images (147). Total cell densities were calculated by dividing the number of grid points overlayed with positively stained cells by reference tissue area to get a percentage of total lung area showing positive staining.

Kidney Histopathology

Kidney tissue sections (5 μm) were histochemically stained with periodic acid Schiff and hematoxylin for microscopic examination for renal histopathology. Sections were semi-quantitatively scored (JRH) based on a modified International Society of Nephrology/Renal Pathology Lupus Nephritis Classification system (148) as follows: (0) no tubular proteinosis, normal glomeruli; (1) mild tubular proteinosis with multifocal segmental proliferative glomerulonephritis and occasional early glomerular sclerosis and crescent formation; (2) moderate tubular proteinosis with diffuse segmental proliferative glomerulonephritis, early glomerular sclerosis and crescent formation; (3) marked tubular proteinosis with diffuse global proliferative and sclerosing glomerulonephritis.

Autoantibody Microarray Profiling

BALF and plasma IgG AAb profiling was performed using a high-throughput autoantigen (AAg) microarray at the Microarray and Immune Phenotyping Core Facility at the University of Texas Southwestern Medical Center as we described previously (134). Briefly, BALF and plasma samples were pre-treated with DNAse I to remove free-DNA, then diluted at a 1:25 or 1:50 dilution, respectively. Samples were added and hybridized to protein array plates containing 122 different antigens and 6 controls. Antibody-antigen binding occurring on the plate was detected using Cy3-conjugated anti-mouse IgG (1:2000, Jackson ImmunoResearch Laboratories, PA). Fluorescent images were captured using a Genepix 4200A scanner (Molecular Devices, CA) and were transformed to signal intensity values using GenePix 7.0 software. Signal intensity values for each AAb were first normalized by subtracting the background and normalizing to IgG internal controls, then reported as an antibody score (Ab-score). This Ab-score was calculated based on the normalized signal intensity (NSI) and signal-to-noise ratio (SNR) using the formula:

$$Ab - score = log_2(NSI * SNR + 1)$$

Normalized and unit variance-scaled Ab-score values were visualized using ClustVis software (149). Data were clustered using unsupervised hierarchical co-clustering (HCC). Rows were clustered using Euclidean distance and Ward linkage. Imputation was applied for missing value estimation. Selected AAb-scores were reported as violin plots, generated using Prism 9 (GraphPad Prism v 9.2, San Diego, CA).

NanoString Autoimmune Gene Profiling

RNA was extracted from lungs and kidneys of Cohort A mouse groups with RNeasy Mini Kits with DNase treatment (Qiagen, Valencia, CA). RNA was dissolved in nuclease-free water, quantified with Qubit (Thermo Fisher Scientific), and integrity verified with a TapeStation

(Agilent Technologies). Samples (RNA integrity >8) were analyzed with NanoString Autoimmune Gene Expression assay (XT-CSO-MAIP1-12, NanoString Technologies, Seattle, WA) at the MSU Genomics Core. Assays were performed and quantified on the nCounter MAX system, sample preparation station, and digital analyzer (NanoString Technologies) according to the manufacturer's instructions.

Raw gene expression data were analyzed using NanoString's software nSolver v3.0.22 with the Advanced Analysis Module v2.0. Background subtraction was performed using the eight negative controls included with the module. Genes with counts below a threshold of 2σ of the mean background signal were excluded from subsequent analysis. Data normalization was performed on background-subtracted samples using internal positive controls and selected housekeeping genes that were identified with the geNorm algorithm (https://genorm.cmgg.be/) (**Figure A2.2**).

Differential gene expression analyses were performed as previously described (150, 151) using the nSolver Advanced Analysis Module, which employs several multivariate linear regression models (mixture negative binomial, simplified negative binomial, or log-linear model) to identify significant genes (**Figure A2.3**). Resulting p values were adjusted using the Benjamini-Hochberg (BH) method to control the false discovery rate (**Supplementary File 2.1**). A statistically significant difference in gene expression was defined as 1.5-fold change in expression (log2 >0.58 or <-0.58) with BH q <0.05. Four pairwise comparisons within each time point for each tissue examined were determined a priori, as follows: $cSiO_2$/P0 vs VEH/P0, $cSiO_2$/PL vs $cSiO_2$/P0, $cSiO_2$/PM vs $cSiO_2$/P0, and $cSiO_2$/PM vs $cSiO_2$/PL. Expression data for lung, kidney, and blood samples are available as normalized linear counts in **Supplementary File 2.2**. Venn diagrams of significant differentially expressed genes were generated using BioVenn (152).

To assess the impact of experimental diets on annotated gene sets, global and directed significance scores were calculated for each pathway at each time point, as previously described (151). The global score estimates the cumulative evidence for the differential expression of genes in a pathway. Directed significance scores near zero indicate that a pathway may have many highly regulated genes, but no apparent tendency for those genes to be over- or under-expressed collectively. As a complementary method for comparing pathways and discriminating between experimental groups, pathway Z scores were calculated as the Z-scaled first principal component of the pathway genes' normalized expression. ClustVis (149) was used to perform unsupervised hierarchical cluster analyses (HCC) and principal components analyses (PCA) using log2 transcript count data for DEGs. Spearman rank correlations were performed to examine overall patterns in the gene expression profiles using the pathway Z score compared to other biomarkers of disease in lung or kidney tissues at 14 weeks PI. A significant correlation was inferred when ρ >0.5 or <-0.5 and $p<0.05$. Network analyses for interactions among significant genes were performed using STRING database version 11.5 (http://string-db.org/), with a minimum interaction score > 0.05 and cluster identification using the Markov Cluster (MCL) algorithm with inflation parameter of 1.5. Networks generated by STRING were visualized with Cytoscape v. 3.9. The NanoString nSolver Advanced Analysis software employs the method described by Danaher (153) to measure the abundance of various immune cell populations using marker genes that are expressed stably and specifically in particular cell types. Cell type scores were calculated as the average log-scale normalized expression of their characteristic genes. Relative cell type measurements were based on the total population of infiltrating lymphocytes, which is useful in a sample of heterogenous mix of cell types. Only cell types that exceeded the quality control analysis for correlation of marker gene expression are reported.

Micro-computed Tomography Bone Analysis

Femurs previously fixed in NBF were scanned using the GE Explore Locus micro-computed tomography system (GE Healthcare, Piscataway, NJ) as previously described (154). Analysis is based on the femoral trabecular region defined as 10 % of the total bone length proximal to the distal growth plate extending towards the diaphysis, excluding cortical bone. A fixed threshold of 700 was used (determined by autothreshold and isosurface visualization tools) and all scans included both experimental groups and controls as well as a calibration phantom to normalized grayscale values. Trabecular bone volume fraction (BV/TV%) was obtained using GE Healthcare MicroView Software and was subsequently corrected for body weight (BV/TV/BW) (**Figure A2.4**).

Statistical Analysis

All data were analyzed, and statistical tests were performed using Prism 9 (GraphPad Prism v 9.2, San Diego, CA) except for the NanoString gene expression data discussed above. Data were assessed for outliers using the Grubb's outlier test (with Q=1%) and for normality using the Shapiro-Wilk test ($p<0.01$). Data of histopathological endpoints were analyzed using an unpaired one-tailed t-test to detect $cSiO_2$-induced inflammation and autoimmunity in lupus-prone mice (VEH/P0 vs $cSiO_2$/P0) and a One-Way ANOVA with Dunnett's post-hoc test to address our hypothesis that dietary prednisone would dose-dependently suppress $cSiO_2$-triggered responses ($cSiO_2$/P0 vs $cSiO_2$/PL or $cSiO_2$/PM). Non-normal and semi-quantitative data were analyzed using the nonparametric Mann-Whitney U test (for VEH/P0 vs $cSiO_2$/P0) and the nonparametric Kruskal-Wallis test with a Dunn's post-hoc test ($cSiO_2$/P0 vs $cSiO_2$/PL or $cSiO_2$/PM). Data are presented as mean ± standard error of the mean (SEM), with a p-value ≤ 0.05 being considered as statistically significant.

RESULTS

Prednisone-amended diets dose-dependently increased blood levels of prednisone and prednisolone

LC-MS/MS revealed that consumption of the three prednisone-amended diets dose-dependently increased blood concentrations of prednisone and its active metabolite prednisolone at 19 wk of age in $cSiO_2$-instilled mice (**Figure 2.1B,C**). Mean prednisone and prednisolone concentrations in PL-fed mice were 1.2 ± 0.03 ng/ml and 22.6 ± 0.8 ng/ml, respectively, in PM-fed mice were 4.0 ± 0.04 ng/ml prednisone and 79.8 ± 2.55 ng/ml prednisolone, respectively, and in PH-fed mice were 9.2 ± 0.2 ng/ml and 151 ± 22 ng/ml prednisolone, respectively. Mice fed CON diet had no detectable prednisone and prednisolone in the blood. Prednisone and prednisolone concentrations in the blood remained consistent at 21 and 23 weeks of age for PL- and PM-treated mice (**Figure A2.5**). However, PH-treated mice were terminated at 19 wk of age because of GC-associated toxicity as described in the next section.

Prednisone dose-dependently induced GC-associated toxicity

Mice consuming PH exhibited reduced body weights compared to mice fed P0 beginning at age 8 wk **(Figure A2.6A)** that presaged additional GC-induced toxic effects. PH-fed mice began to lose body weight beginning at age 16 wk (4 wk PI) and displayed a significant reduction of lean muscle mass at age 17 wk (**Figure A2.6B**). By age 19 wk, these mice had high levels of glucose (760 mg/dl) present in their urine indicating that they were extremely hyperglycemic (**Figure A2.6C**). Due to this evidence of deteriorating health, PH-fed mice in Cohorts A and B were euthanized, approximately 7 wk prior to the scheduled necropsy for Cohort A and were not included in further analyses.

Ingestion of PM, but not PL, also impaired body weight gain prior to $cSiO_2$ instillations

starting at age 8 wk and lasted for the duration of Cohort A and B studies (**Figure A2.6A**)**.** Reduced body weights in PM-fed $cSiO_2$-instilled mice corresponded with significant reductions in lean mass, but not fat mass, at age 21 wk (9 wk PI), 23 wk (11 wk PI), and 25 wk (13 wk PI), as compared to $cSiO_2$/CON mice (**Figure 2.2A,B**). $cSiO_2$ did not impact the amount of lean muscle or fat mass measured in CON- or prednisone-fed mice compared to VEH-treated CON-fed mice. Unlike muscle wasting, neither PL nor PM diet affected bone density in $cSiO_2$-exposed mice (**Figure A2.4**). Finally, glycosuria was not detected in to VEH/P0, $cSiO_2$/P0, $cSiO_2$/PL, or $cSiO_2$/PM groups at 19, 21, or 23 wk of age (**Figure A2.6C**).

Prednisone intake did not improve survival time in $cSiO_2$-treated mice

In accordance with a previous study (132), median survival time of Cohort B $cSiO_2$/P0 mice (32 wk of age) was reduced compared to VEH-treated CON-fed mice (>32 wk of age) (**Figure 2.2C**). PL and PM intake reduced median survival times of $cSiO_2$-exposed mice to 26 wk and 29 wk of age, respectively, suggesting that oral prednisone intake was not effective in enhancing the lifespan of $cSiO_2$-exposed lupus-prone mice.

Moderate prednisone intake suppressed $cSiO_2$-induced pulmonary ELS formation

Consistent with prior studies (27, 131, 132), intranasal instillation with $cSiO_2$ induced conspicuous perivascular and peribronchiolar lymphoplasmacytic infiltration (ELS) compared to VEH/P0 mice (**Figure 2.3A.i-ii**). Semi-quantitative severity scoring of pulmonary tissues demonstrated marked ELS formation in $cSiO_2$-instilled mice fed control diet ($cSiO_2$/P0) compared to VEH/P0 mice (**Figure 2.3A.v**). Reflective of the histopathology (**Figure 2.3A.iv**), PM treatment significantly reduced lung severity scores. $cSiO_2$ instillation elicited significant increases in inflammatory cells (neutrophils, lymphocytes, monocyte/macrophages) in BALF of $cSiO_2$/P0 as compared to VEH-instilled mice fed CON diet (**Figure A2.7**). PL and PM consumption did not attenuate $cSiO_2$-

induced increases of inflammatory cell numbers in the BALF. Interestingly, lymphocytic cell numbers significantly increased in BALF of the $cSiO_2$/PM group as compared to the $cSiO_2$/P0 animals.

IHC and morphometry were used to further characterize ELS lymphoid cell populations affected by $cSiO_2$ and prednisone treatments. PM but not PL consumption significantly reduced $cSiO_2$-induced $CD45R^+$ B-cell accumulation in pulmonary perivascular and peribronchiolar regions (**Figure 2.3B**) but neither treatment affected $cSiO_2$-triggered $CD3^+$ T-cell infiltration (**Figure 2.3C**). PM consumption modestly reduced $cSiO_2$-induced increases in pulmonary IgG^+ plasma cell density (**Figure A2.8A**) but not overall IgG deposition (**Figure A2.8B**) whereas PL diet had no effect on either of these responses (**Figure A2.8A,B**).

Prednisone intake selectively inhibited $cSiO_2$-induced nuclear AAbs in the BALF

Consistent with our prior reports, AAg microarray analysis indicated $cSiO_2$ instillation triggered significant increases in IgG AAbs in both the BALF (**Figure 2.4A**) and plasma (**Figure A2.9A**) of $cSiO_2$/P0 mice compared to VEH/P0 mice, which was further reflected in AAb summation scores (**Figure 2.4B; Figure A2.9B**). Prednisone consumption did not significantly reduce AAb summation scores in both the BALF and plasma; however, PL and PM diets were effective at reducing AAbs specific for nuclear AAgs detected in the BALF (**Figure 2.4A,C**) but not the plasma (**Figure A2.9C**).

Moderate prednisone consumption reduced $cSiO_2$-induced splenic lymphoid hyperplasia and splenomegaly

$cSiO_2$/P0 mice exhibited extensive lymphoid hyperplasia in the splenic white pulp that was not observed in the VEH/P0 group (**Figure 2.5A.i, ii**). Hyperplasia was less prominent in $cSiO_2$/PL mice (**Figure 2.5A.iii**) and conspicuously less so in $cSiO_2$/PM mice (**Figure 2.5A.iv**).

Correspondingly, $cSiO_2$/P0 exhibited higher spleen weights than VEH/P0 mice and, furthermore, PM treatment suppressed $cSiO_2$-induced splenic weight increases (**Figure 2.5A.v**).

Moderate prednisone intake inhibited $cSiO_2$-induced glomerulonephritis

Consistent with previous studies (131, 135), histopathological analysis revealed $cSiO_2$ induced glomerulonephritis and protein accumulation in kidneys of $cSiO_2$/P0 mice compared to VEH/P0 mice (**Figure 2.5B.i, ii**). These responses were significantly reduced by PM intake (**Figure 2.5B.iv**). Likewise, the PM significantly reduced $cSiO_2$-induced increases in kidney severity scores (**Figure 2.5C**). $cSiO_2$ treatment resulted in a significant increase in plasma BUN levels (**Figure 2.5D**) and proteinuria (**Figure 2.5E**). PM treatment was effective in significantly reducing plasma BUN values but not protein levels in the urine.

Moderate prednisone intake influenced $cSiO_2$-induced immune pathway transcriptional changes in lung and kidney tissues

NanoString analysis revealed that, in the lung, $cSiO_2$ exposure resulted in 324 differentially expressed genes, and 103 differentially expressed genes with PM treatment. In the kidney, $cSiO_2$ induced 267 differentially expressed genes in P0-fed mice and 20 in PM-fed mice (**Figure 2.6A**). Principal component analyses (PCA) showed distinct gene profiles between VEH/P0 and $cSiO_2$/P0 mice in both lung and kidney tissues (**Figure 2.6B**). Gene profiles were less distinguishable between $cSiO_2$/P0 and $cSiO_2$/PM groups in both tissues.

Immunological pathways significantly affected by $cSiO_2$ and prednisone treatments were identified based on global and directed significance scores (**Figure 2.6C**). $cSiO_2$ exposure led to broad activation of immune pathways in both the lung and kidney. Alternatively, repression of certain nutrient sensing (autophagy and mTOR) and growth factor signaling pathways occurred in the lung, specifically, in response to $cSiO_2$. Prednisone treatment at both low and moderate doses

modestly reduced $cSiO_2$-induced effects on most immune pathways in both tissues. PM treatment demonstrated greater inhibition of $cSiO_2$-stimulated pathways such as those pertaining to cytotoxicity, MHC Class II antigen presentation, T-cell checkpoint signaling, and T-cell receptor signaling. These findings corresponded with calculated Z scores derived from expression values for specific genes assigned to representative immune pathways in the lung (**Figure A2.10A**) and kidney (**Figure A2.10B**). In the lung, network mapping revealed genes associated with innate and adaptive immunity (interleukins, cytokines, IFN), lymphocyte and macrophage function (antigen presentation and MHC), complement, and nuclear proteins were significantly affected by PM treatment (**Figure A2.10C**). Genes associated with inflammation (interleukins, chemokines, cytokines), cell adhesion, apoptosis, lymphocyte and macrophage function (antigen presentation and MHC), and endothelial cell function were most affected by PM treatment in the kidney (**Figure A2.10D**).

Prednisone modulated $cSiO_2$-induced autoimmune-related gene expression in lung and kidney tissues

Heatmaps and bar graphs of representative genes from $cSiO_2$-impacted autoimmune pathways illustrate those most highly influenced by prednisone treatment (**Figure 2.7-8; Figure A2.11**). In accordance with intranasal $cSiO_2$ exposure, the expression of genes coding for nuclear material (*e.g., Hist1hao, Hist1h3b, Sp100*) and associated with AAb production were upregulated in the lung of $cSiO_2$/P0 mice compared to VEH/P0 mice (**Figure 2.7A**). Consistent with previous studies (133, 150), $cSiO_2$ upregulated genes contained in pathways such as MHC II antigen presentation (**Figure 2.7B**), B-cell signaling (**Figure 2.7C**), Fc receptors and phagocytosis (**Figure 2.7D**), lymphocyte tracking (**Figure A2.11A**), oxidative stress (**Figure A2.11B**), cytotoxicity (**Figure A2.11C**), and T-cell checkpoint and receptor signaling (**Figure 2.8A,B**) in both the lung and

kidney. PM treatment markedly reduced some $cSiO_2$-induced autoimmune-related gene expression in the lung and kidney tissues while others remained upregulated (**Figure 2.7-8; Figure A2.11**).

Immune pathways enriched due to $cSiO_2$ exposure, and conversely suppressed by PM treatment, correlated with pathological endpoints evaluated in the lung and kidney (**Figure 2.9; Figure A2.12**). Immune cell type profiling, which was determined based on gene expression data to identify various cell types, revealed significant increases in B- and T-cell infiltration in the lung following $cSiO_2$ exposure (**Figure A2.13A**). Interestingly, B-cell but not T-cell morphometric analysis (**Figure 2.3B.v, 2.3C.v**) was consistent with PM-induced decreases in immune cell scoring. $cSiO_2$ exposure caused B- and T-cells to comprise a large fraction of total infiltrating leukocytes (TILs), which was reduced with PM administration (**Figure A2.13C**). In contrast, PL and PM treatment led to an increase in the fraction of macrophages that comprise TILs. In the kidney, $cSiO_2$ led to significant increases in cytotoxic cells and macrophages (**Figure A2.13B**). Scoring for cytotoxic cells was significantly decreased with PM administration. Prednisone had negligible influence on $cSiO_2$-induced changes in cell fractions of TILs (**Figure A2.13D**). When considering overall TILs, PM treatment effectively suppressed $cSiO_2$-triggered increases in both the lung and kidney tissues (**Figure A12.3C,D**).

$cSiO_2$ and prednisone had modest effects on blood mRNA signatures

NanoString profiling of mRNA isolated from whole blood samples revealed limited effects on immune pathway enrichment and cell type scoring when comparing VEH/P0 vs $cSiO_2$/P0 and $cSiO_2$/P0 vs $cSiO_2$/PL or PM groups (**Figures A2.14-18**). Limited $cSiO_2$-induced transcriptomic changes were observed in blood taken 11 wk PI, whereas prednisone-modulated genes were observed primarily at 7 wk PI (**Figure A2.15A**). $cSiO_2$ exposure had a significant effect on genes

involved in lymphocyte trafficking and stimulation (e.g., *CD3, IL-17r, Ccr7*) and interferon response (e.g., *Irf7, Ifitm3*) (**Figure A2.16**). Similar to what was observed in lung and kidney tissues, genes related to antigen presentation (e.g., *H2-Ob, H2-Dmb2*) and B- and T-cell signaling (e.g., *Cd19, Cd74, Btla*) were significantly modulated by moderate prednisone compared to $cSiO_2$/P0 mice (**Figure A2.16B, A2.17A-B**). However, it is important to note $cSiO_2$ did not significantly upregulate these genes compared to VEH/P0 mice at this same timepoint. At 11 wk PI $cSiO_2$ significantly upregulated genes that factored into immune cell scores for macrophages and neutrophils while decreasing those for cytotoxic cells and T-cells (**Figure A2.18A**). The scoring of these individual immune cell types corresponded with their respective fraction of TILs (**Figure A2.18B**). Only cytotoxic and T-cell fractions of TILs were modulated by PM treatment at this timepoint. Taken together, these data suggest that moderate prednisone offers incomplete protection systemically but does offer significant inhibition of adaptive immune pathways localized to lung and kidney tissues in $cSiO_2$-exposed mice.

DISCUSSION

Major goals in lupus treatment are to achieve drug-free remission in patients, where there is little to no disease activity for 5 or more years, and to slow the progression of organ damage (45). Often, patients with lupus are given bolus IV doses of prednisolone, the active metabolite of prednisone, ranging from 250-1000 mg/d for 3 days to provide quick relief from flaring through non-genomic pathways before starting a tapering regimen of prednisone to maintain inhibition of the inflammation (2, 18, 46). Unfortunately, there are inconsistencies when it comes to tapering and questions surrounding how much prednisone is needed to help patients achieve remission. Thus, tapering regimens can range from lower doses of ≤7.5 mg/d, to medium doses of >7.5-30 mg/d, and finally higher doses of 30-100 mg/d (19). The investigation described herein is the first to

evaluate the dose-dependent response of prolonged prednisone dietary administration on the induction of GC toxicity and the onset/progression of environmental-triggered autoimmunity in a preclinical lupus mouse model. Several novel observations were made. First, we demonstrated the dietary incorporation was a simple and efficient way to deliver clinically relevant prednisone doses to rodents. Second, we found that PH caused significant weight loss, muscle wasting, glucosuria, and mortality, thus necessitating early removal of this experimental group from the study. PM but not PL intake caused muscle wasting and weight loss, however, neither treatment influenced urinary glucose or bone density. Third, PM but not PL was effective in reducing $cSiO_2$-triggered peribronchiolar and perivascular ELS neogenesis, B- and plasma-cell accumulation, and AAb production against nuclear related autoantigens in the lung. However, neither moderate nor low dose prednisone affected $cSiO_2$-induced macrophage, neutrophil, or lymphocyte increases in the BALF, pulmonary and perivascular T-cell accumulation, or plasma AAb responses. Fourth, PM but not PL attenuated $cSiO_2$-induced glomerulonephritis and plasma BUN. Fifth, consistent with the pathological findings, PM significantly reduced $cSiO_2$-triggered gene expression in several inflammation- and autoimmunity-associated pathways in both lung and kidney tissues. Finally, despite the significant inhibition of autoimmunity and glomerulonephritis, PM did not prolong survival of $cSiO_2$-treated mice. Therefore, while GC-associated toxicity endpoints from this study are important to consider, PM was effective in attenuating $cSiO_2$-triggered ELS formation in the lung which importantly serves as the nexus for downstream autoimmunity and resultant glomerulonephritis.

Despite the wide usage of prednisone to manage lupus, there have been limited investigations regarding its therapeutic and toxic properties in preclinical models. These studies have varied in terms of mouse strain, duration of exposure, and route of administration. Relevant

to the present study, the lupus-prone MRL/lpr mouse strain has been used to evaluate suppression of spontaneous autoimmunity following intragastric administration of a prednisone solution daily for 13 weeks (155) or oral administration of a prednisolone solution daily for 4 weeks (156). Alternatively, others have used non-lupus-prone strains such as Crl:CD-1(ICR) (144), C57BL/6 (157), or Dmd^{mdx} (158) mice to evaluate prednisone or prednisolone toxicity in the context of carcinogenicity, insulin resistance, and muscle wasting, respectively. While these studies have provided valuable insights into the anti-inflammatory and toxic effects of oral prednisone and prednisolone exposure, none have assessed both outcomes simultaneously as done here.

A central question arising from our use of prednisone-amended diets relates to their relevance to human intake of the drug in a clinical setting. Oral prednisone has a half-life of 3 to 4 h in humans (41) and is typically prescribed in an immediate release form as a single daily dose or 3 to 4 divided doses/day, or, alternatively, in a delayed release form taken once per day (42). When mice are housed under a standard 12 h light/ 12 h dark cycle, as employed in this study, nearly all their food consumption occurs during the dark cycle, with short episodic feeding occurring during the light cycle (43). Thus, most prednisone ingestion likely occurs during the dark feeding cycle, mimicking intake of the immediate release form of the drug in divided doses with meals throughout the day. Importantly, we found the mice efficiently converted prednisone consumed via the diet to its biologically active metabolite, prednisolone. Mean prednisolone concentrations in blood of mice fed PL, PM, and PH diets were 27, 105, 151 ng/ml, respectively. These results compare favorably to those of Rose et al (41), who gave 5, 20, or 40 mg oral prednisone to healthy human males and observed plasma concentrations of prednisolone between 10-40 ng/ml, 24-80 ng/ml, and 75-200 ng/ml, respectively between 6 and 12 h post-administration. In another study (159), adolescent and young adult patients with lupus were given between 5 and

40 mg of prednisone (mean ± SEM =19.5 ± 11.5) their average prednisolone concentrations were 200, 150, 90, and 50 ng/ml at 2, 4, 6, and 9 h, respectively. Recently, Mangin et al (160) assessed prednisone pharmacokinetics in 107 patients with inflammatory/autoimmune diseases following oral dosing with 5 to 20 mg prednisone and reported 50th percentile levels of approximately 300, 150, and 50 ng/ml at 2, 5, and 9 h after dosing, respectively. Collectively, these reports support the contention that prednisolone concentrations stably attained in blood through feeding prednisone diets in our model are highly consistent with those that might be expected in humans given therapeutic doses of this prodrug.

Consistent with previous studies from our lab, repeated intranasal exposure to $cSiO_2$ beginning at 8-wks of age was effective in initiating unresolved inflammation in the lung leading to a loss of self-tolerance and the development of glomerulonephritis (27, 131, 132, 135). Repeated $cSiO_2$ exposure also led to the production of AAbs corresponding to certain nuclear antigens such as SM, RNP, histone, and DNA-related nucleoproteins which have been commonly implicated in lupus (121, 161, 162). The extent to which prednisone effectively reduced $cSiO_2$-induced inflammation, as demonstrated by the pathological findings, was consistent with mRNA signatures in the lung and kidney. NanoString analysis showed that $cSiO_2$-responsive genes differed based on whether the tissue had direct contact with the $cSiO_2$ particles (lung) or was responding to the systemic autoimmunity initiated by AAbs and immune complexes (kidney). Proinflammatory gene expression initiated by $cSiO_2$ exposure was effectively brought down with the moderate dose of prednisone. Prednisone demonstrated limited efficacy in suppressing $cSiO_2$-induced AAb production detected in the BALF, as it only significantly reduced pathogenic AAbs specific to nuclear and glomeruli-specific antigens. These data were consistent with our NanoString analysis where many of the prednisone-responsive genes under the autoantigen and MHC class II antigen

presentation pathways in the lung were specific to nuclear material (e.g., *Hist1hoa, Hist1h3b, H2-Ob*). Immune cell type enrichment using nSolver analysis indicated $cSiO_2$-dependent increases in macrophages and B-cells in the lung, similar to what was observed via differential cell counts in the BALF and morphometric analysis, respectively. Interestingly, lymphocyte numbers detected in the BALF were significantly increased with moderate prednisone treatment compared to $cSiO_2$ control mice. This suggests that prednisone may exacerbate the upregulation of certain lymphoid cell populations already set in motion by $cSiO_2$. Additionally, prednisone did not reduce overall pulmonary $CD3^+$ T-cell counts as determined with morphometry but did significantly reduce T-cell counts in immune cell profiling using NanoString. It is possible that prednisone promoted T-cell differentiation and replaced inflammatory T-cell populations with those involved in maintaining peripheral tolerance. It has been reported by others that GCs inhibit the differentiation of proinflammatory T-helper cells and enhance the differentiation of anti-inflammatory T-reg cells (163), which could explain the high number of T-cells still present with prednisone treatment in immunohistochemically stained tissues. However, more research is necessary to explain prednisone's preferential inhibition of pulmonary B- rather than T-cell recruitment in our model.

It is well-documented in the literature that prolonged use of GCs such as prednisone can lead to many deleterious side-effects such as cardiovascular disease, osteoporosis, myopathy, diabetes, and increased risk of secondary infection (18-22). It has been suggested that prednisone doses >30-40 mg/d cease to serve any further anti-inflammatory benefits due to saturation of the GC genomic pathway and is also the threshold for undesirable side-effects resulting from GC transactivation pathways (19). This can be extremely problematic for lupus patients considering it is extremely rare for them to achieve drug-free remission (45). Only 3-7% of lupus patients can achieve drug-free remission (47). Additionally, physicians are reported to be more likely to keep

patients on GCs indefinitely if there is evidence of past organ involvement despite decreases in disease activity (18). Due to the unlikelihood of lupus patients attaining drug-free remission, they will likely rely on GCs for the remainder of their lives, putting them at greater risk for GC-induced toxicity (23). Therefore, lower doses of ≤7.5 mg/d have been increasingly recommended as the standard for tapering (18, 19, 45). Our findings that since the PL diet (≈5 mg/day HED) was not toxic but the PM (≈14 mg/d HED) and PH (≈46 mg/d HED) diets were toxic, this suggests the 7.5 mg/d threshold was equivalently relevant in our preclinical model.

A central finding of this study is that while reducing the prednisone dose from PM to PL mostly removes short-term toxicity in our preclinical model, it also largely eliminates efficacy against inflammation and autoimmunity. Equally important, even though the PM dose selectively diminished inflammation/autoimmunity in the lung, spleen, and kidney, it did not have any impact on plasma AAbs or life expectancy of $cSiO_2$-treated lupus-prone mice. Therefore, our findings further highlight the critical need for identifying and developing potential cost-effective, steroid-sparing therapeutics to improve the quality of life in lupus patients. Related to this goal, we have found in prior studies that diets enriched with clinically relevant doses of the omega-3 fatty acid, docosahexaenoic acid (DHA) were highly efficacious in preventing and/or treating $cSiO_2$-induced autoimmunity in the female NZBWF1 mouse (27, 132-135). Unlike prednisone, DHA was effective in reducing both $cSiO_2$-induced B- and T-cell infiltration in the lung. Additionally, DHA was effective in significantly reducing $cSiO_2$-triggered pathogenic AAb in the plasma along with a broader repertoire of AAbs in the BALF compared to prednisone. While prednisone effectively reduced some AAbs in the BALF that are associated with lupus (Smith antigens), DHA also suppressed most of those linked to other autoimmune diseases such as arthritis (fibrinogen), vasculitis (MPO, prednisone3), and myositis (MDA5, Mi-2) (134, 164). In a study by Yan et al.

(155) using MRL/lpr lupus prone mice, prednisone administered intragastrically at doses of 2.5 and 5 mg/kg/d for 13 wks significantly reduced spontaneous production of anti-nuclear AAbs, but not anti-dsDNA AAbs in the serum. Even though we did not observe the same prednisone-induced reduction of AAbs in the systemic circulation, it is interesting to note that those investigators also saw inhibition of anti-nuclear AAbs specifically, similar to the AAb classes affected in our BALF samples. It is also possible that we did not see similar anti-nuclear AAb suppression in the systemic circulation due to our use of lower doses of prednisone.

We conclude that the toxic effects of prednisone outweigh its ameliorative effects on lupus disease which is why there was no improvement in survival. While it was not within the scope of the present study to do a thorough investigation as to why prednisone-fed mice had decreased survivability, incomplete suppression of systemic autoimmunity is a likely factor. While the prednisone was effective in preventing inflammation in the kidney, it was not effective in significantly reducing proteinuria or level of pathogenic autoantibodies in the systemic circulation. So, it is probable that the incomplete protection of prednisone outside of the lung coupled with weight/muscle loss contributed to decreased survival.

One limitation of this investigation is that since the large dose of $cSiO_2$ used here is poorly cleared from lung after instillation, it causes unresolved inflammation that might overwhelm the ameliorative effects of dietary prednisone. It will therefore be useful in future studies to ascertain the dose response effects of dietary prednisone in the context of slower, spontaneous development of autoimmunity and glomerulonephritis in female NZBWF1 mice and other lupus-prone mouse strains. Another limitation of this study is that it focused on the preventive effects of prednisone rather than more clinically relevant therapeutic intervention after autoimmunity onset. It is possible that short term treatment with high dose prednisone, for example for 1 or 2 wk after $cSiO_2$ dosing,

might be effective at reducing $cSiO_2$-triggered autoimmunity with minimal GC-associated toxicity. Similarly, it would be of interest to ascertain whether treating mice with high bolus doses of prednisolone followed by a tapering regimen of prednisone-amended diet could achieve suppression autoimmunity in this model.

Taken together, this preclinical study demonstrates that prolonged dietary administration of prednisone at clinically relevant doses falls short of offering complete protection from $cSiO_2$-induced autoimmunity and can cause significant secondary toxicity at moderate to high doses. While it was not within the scope of our study to investigate why prednisone-fed mice had decreased survivability, we can conclude that secondary GC toxicity likely outweighed the protection which was mainly localized to the lung. However, prednisone's ability to quell inflammation stemming from ELS formation in the lung provides novel insights important to the utilization of prednisone in human lupus triggered by inhaled toxicants. Our findings from this and prior studies highlight the value of this preclinical model for investigating alternative safe, cost-effective therapies for lupus, such as omega-3 fatty acid supplementation, which can lower requisite prednisone doses needed to suppress autoimmunity thereby improving the quality of life of lupus patients.

ACKNOWLEDGEMENTS

First, the authors thank Amy Porter of the Michigan State University Laboratory for Investigative Histopathology for their assistance with histotechnology. Second, they thank Leslie Pittsley and Michigan State University's Campus Animal Resources for their assistance with blood collections. Lastly, they thank Dr. Kevin Childs and the Research Technology Support Genomics Core Facility for processing samples using NanoString nCounter Analysis System.

DATA AVAILABILITY STATEMENT

Original NanoString normalized linear counts (**Supplemental File 2.1**) and statistical analyses (**Supplemental File 2.2**) from autoimmune profiling panel are available in a publicly accessible repository: https://doi.org/10.5061/dryad.2280gb5vx.

AUTHOR CONTRIBUTIONS

LH: study design, coordination, feeding study, necropsy, data curation, data analysis/interpretation, morphometrical analysis, figure preparation, manuscript preparation and submission; AB: data acquisition/analysis, figure preparation, manuscript writing; ER: feeding study, mouse handling, data acquisition; LR: data acquisition/analysis, figure preparation, manuscript writing; JW: necropsy, lab analysis; RL: instillations, necropsy, lab analysis; QZL: microarray; JB and JZ: LC-MS/MS, data analysis, manuscript writing; AR: mouse handling and feeding, data acquisition; AT: morphometric analysis; NC and LM: Micro-CT and manuscript preparation, JH: study design, oversight, lung/kidney histopathology, morphometry, data analysis, manuscript preparation; JP: study design, oversight, funding acquisition, lung/kidney histopathology, morphometry, data analysis, manuscript preparation and submission.

FIGURES

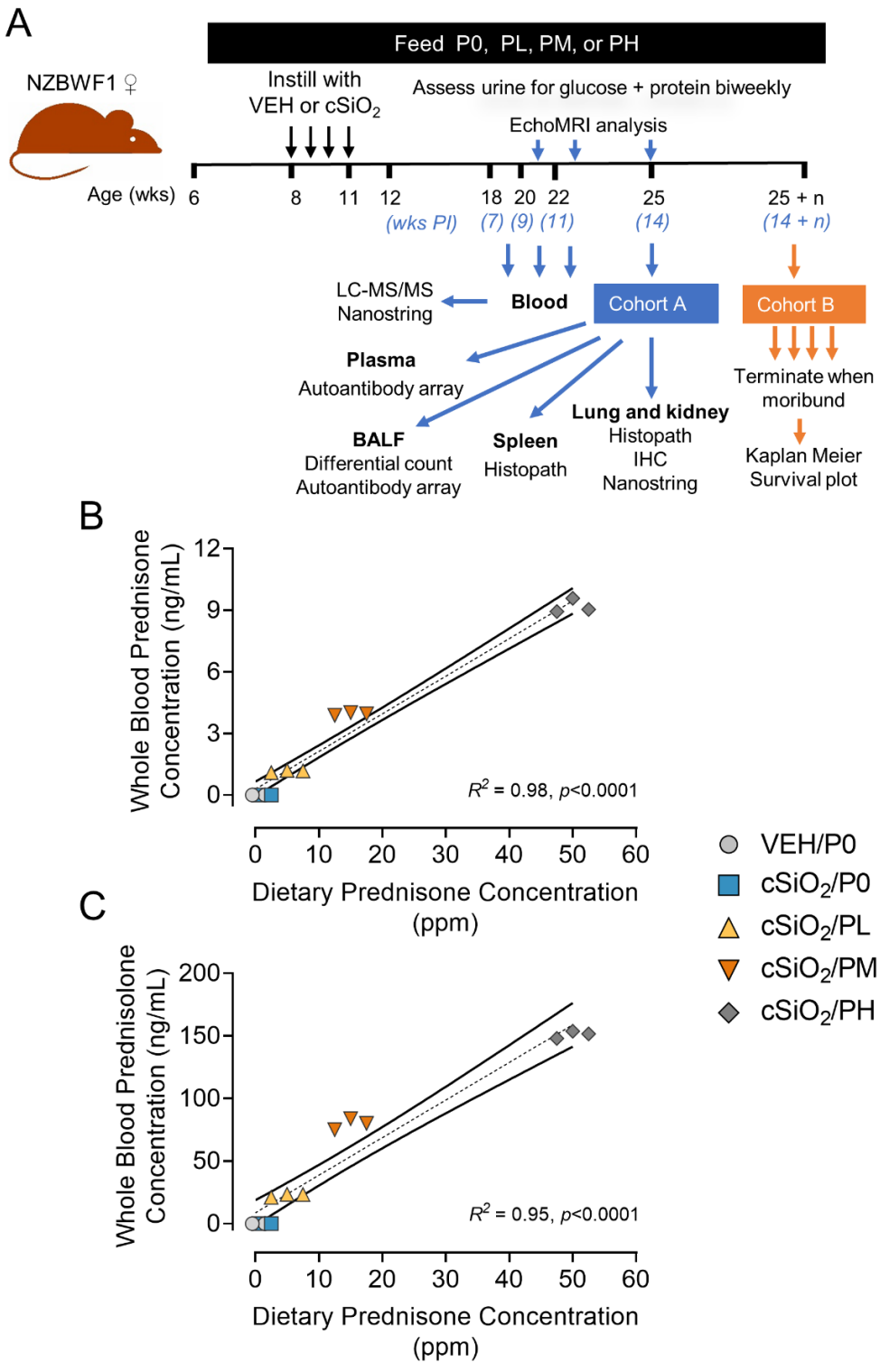

Figure 2.1: Experimental design and confirmation of prednisone and prednisolone levels in whole blood. (A) Female NZBWF1 mice obtained at 6 wk of age were immediately placed on

Figure 2.1 (cont'd):
either control AIN-93G diet containing no prednisone (P0) or prednisone-amended diets. Diets were maintained throughout the duration of the study. Beginning at 8 wk of age, mice were intranasally instilled with either saline vehicle (VEH) or 1 mg of $cSiO_2$ once per week for 4 consecutive weeks. Eight animals per treatment group (Cohort A) were sacrificed at 25 wk of age to evaluate relevant endpoints for onset of pulmonary and renal autoimmunity. The remaining 9 mice per treatment group (Cohort B) were maintained until they met moribund criteria and were humanely sacrificed. Health and proteinuria were monitored following $cSiO_2$ instillations to evaluate disease progression. Food intake, body weights, and fat/lean muscle mass composition were monitored as well to assess prednisone-induced toxicity. **(B)** Levels of and its active metabolite, prednisolone **(C)**, were detected in whole blood samples taken from mice at 19 wk of age determined via LC-MS/MS. Samples were pooled within each cage (n=3/cage), with 3 cages per treatment group resulting in an n=3/group for analysis. Prednisone concentration detected in whole blood is predictable based on dietary prednisone concentrations. For regression analyses, R^2 and p-values are reported. Shaded bands around regression lines represent 95% confidence intervals.

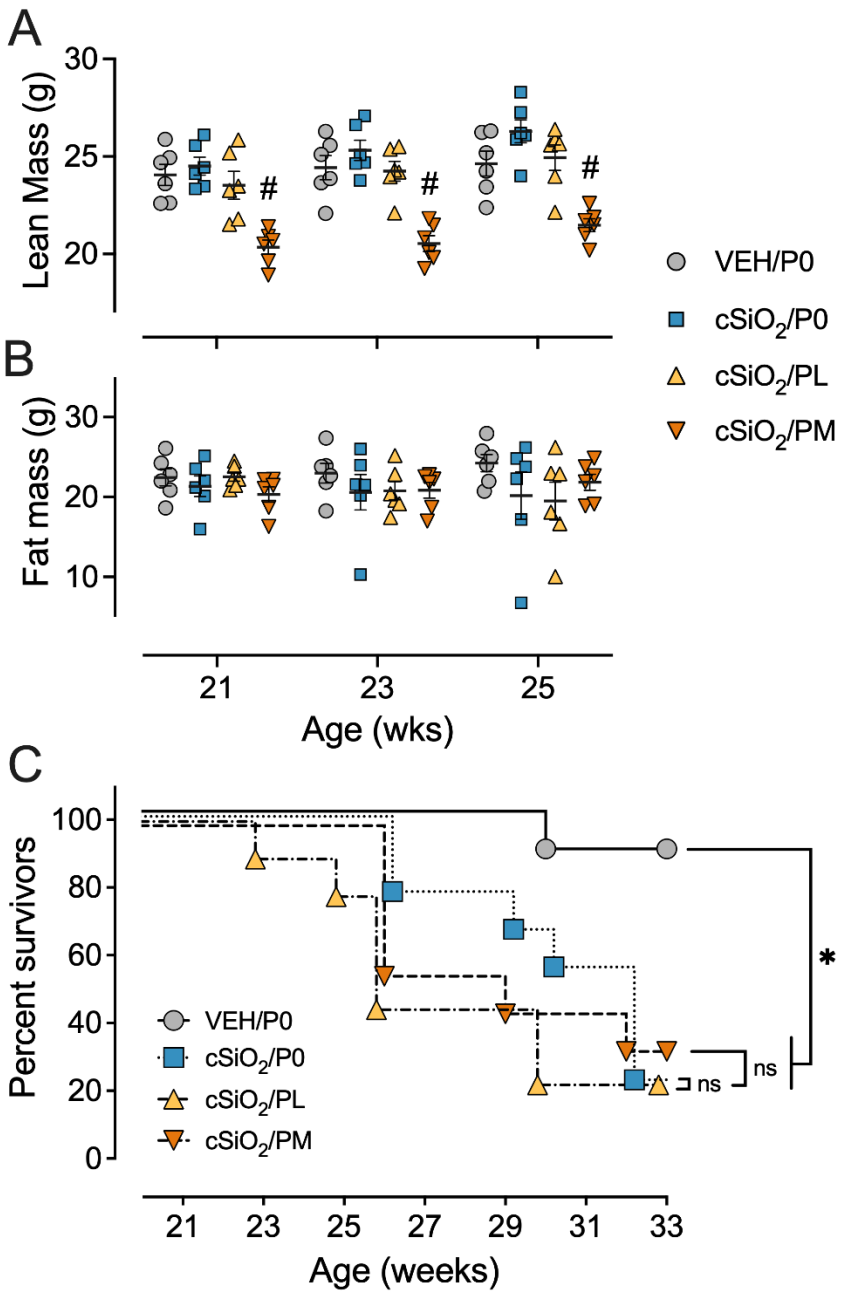

Figure 2.2: Medium dose prednisone treatment significantly reduced lean muscle mass and did not improve survivability. Mice were evaluated for lean muscle **(A)** and fat mass **(B)** using EchoMRI at 21 wk of age (9 wk PI), 23 wk of age (11 wk PI), and 25 wk of age (13 wk PI). PM treatment induced significant lean muscle mass loss compared to $cSiO_2$ control mice. $cSiO_2$ and prednisone had no effects on fat mass. *Indicates $p<0.05$ for VEH/P0 vs $cSiO_2$/P0; $^{\#}$indicates $p<0.05$ for $cSiO_2$/P0 vs $cSiO_2$/PL or $cSiO_2$/PM group as described in Materials and Methods. **(C)** Kaplan-Meier survival plot depicting survival of mice in cohort B which were evaluated weekly using moribund criteria. *Indicates $p<0.05$ for VEH/P0 group survival compared to $cSiO_2$/P0, $cSiO_2$/PL, or $cSiO_2$/PM group survival as determined by the Mantel-Cox log-rank test. No differences in survival between $cSiO_2$/P0 and the $cSiO_2$/PL or $cSiO_2$/PM groups were observed.

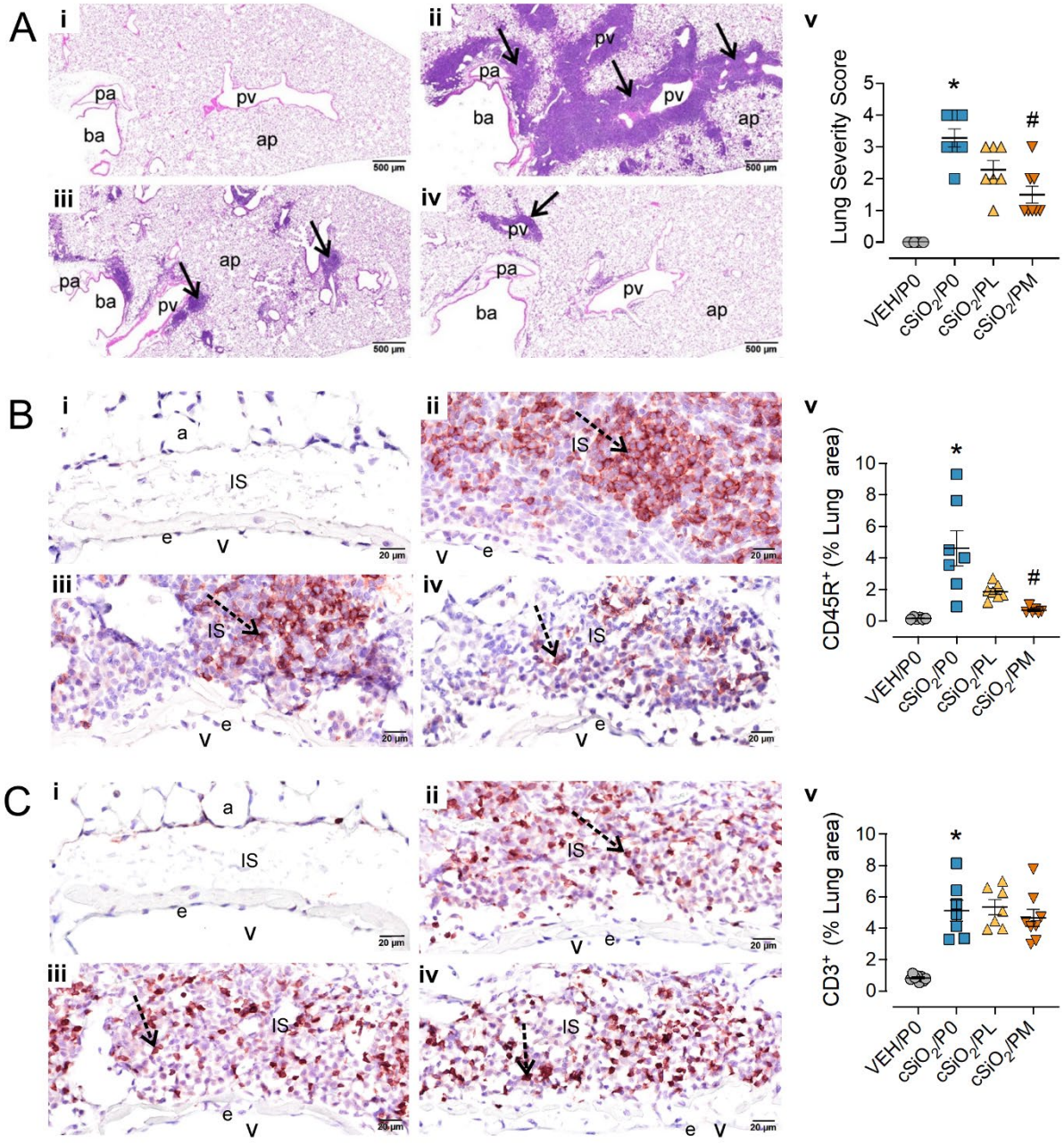

Figure 2.3: Medium dose prednisone (PM) significantly reduced pulmonary peribronchiolar and perivascular formation of Ectopic Lymphoid Structures (ELS) and infiltration of perivascular CD45R+ B cells, but not CD3+ T cells. Light photomicrographs of photomicrographs of hematoxylin and eosin-stained lung tissue sections **(A)** from (i) VEH/P0, (ii) $cSiO_2$/P0, (iii) $cSiO_2$/PL, and (iv) $cSiO_2$/PM mice. $cSiO_2$ treatment resulted in formation of ELS in peribronchiolar and perivascular interstitium (A.ii). Graphic representation of semi-quantitative severity scores following assessment criteria of (1) minimal (<10% of lung tissue affected); (2) slight (10-25%); (3) moderated (26-50%), (4) marked (51-75%), (5) severe (>75%) of total area affected (A.v). PM, but not PL, significantly reduced the amount of ELS (A.iii-v). pa, pulmonary artery; ba, bronchiolar airway; pv, pulmonary vein; alveolar parenchyma; arrows, peri-vascular/bronchiolar ectopic lymphoid structures. Photomicrographs of lung tissue

Figure 2.3 (cont'd):
immunohistochemically stained for **(B)** CD45R+ B lymphoid cells and **(C)** CD3+ T cells in lungs from (i) VEH/P0, (ii) $cSiO_2$/P0, (iii) $cSiO_2$/PL, and (iv) $cSiO_2$/PM mice. e, endothelium; v, venous lumen; IS, perivascular interstitial space; a, alveolus. cSiO2 treatment significantly triggered interstitial infiltration of CD45R+ B cells (B.ii) and CD3+ T cells (C.ii). PM treatment significantly reduced CD45R+ B cell infiltration (B.iv) but had no effect on CD3+ T cells (C.iii-iv). Graphical representation of morphometrically determined density of CD45R+ B cells (B.v), and CD3+ T cells (C.v) in lung tissue. *Indicates $p<0.05$ for VEH/P0 vs $cSiO_2$/P0; #indicates $p<0.05$ for $cSiO_2$/P0 vs $cSiO_2$/PL or $cSiO_2$/PM group.

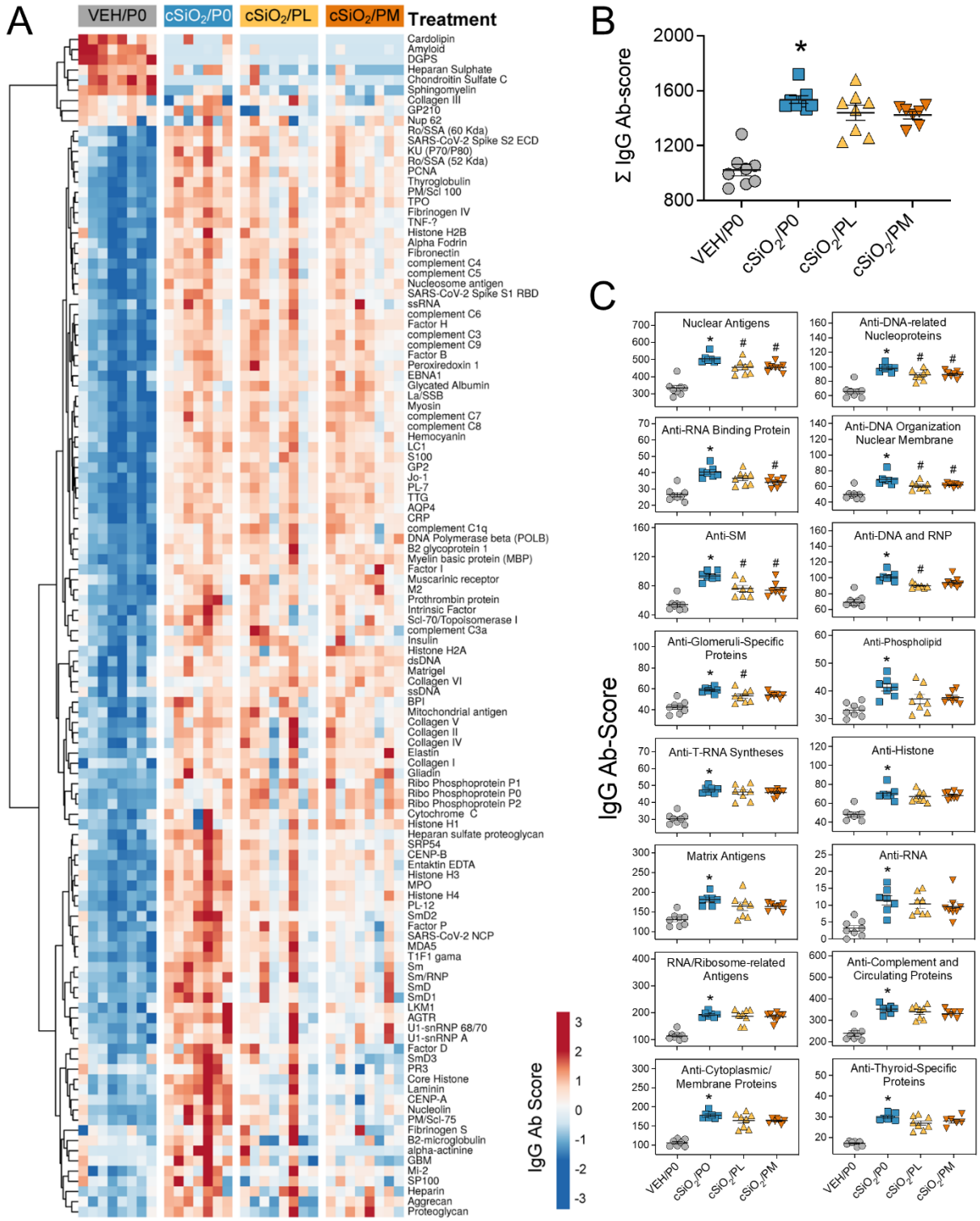

Figure 2.4: Prednisone treatment is effective in reducing a subset of $cSiO_2$-induced AAbs in the BALF. AAbs production was measured in BALF using Cohort A samples collected at time of necropsy (14 wk PI). **(A)** Heat map illustrates unsupervised clustering (Euclidian distance method) of 122 AAbs shown as Ab-score values for IgG expression in BALF. Scale bar values reflect the

Figure 2.4 (cont'd):
range of variance-stabilized Ab scores, which were centered across rows. **(B)** Prednisone does not significantly reduce $cSiO_2$-triggered increased total IgG levels in the BALF. **(C)** prednisone treatment was effective in significantly reducing certain classes of autoantibodies in the BALF compared to $cSiO_2$/P0 positive control. *Indicates $p<0.05$ for VEH/P0 vs $cSiO_2$/P0; $^{\#}$indicates $p<0.05$ for $cSiO_2$/P0 vs $cSiO_2$/PL or $cSiO_2$/PM group.

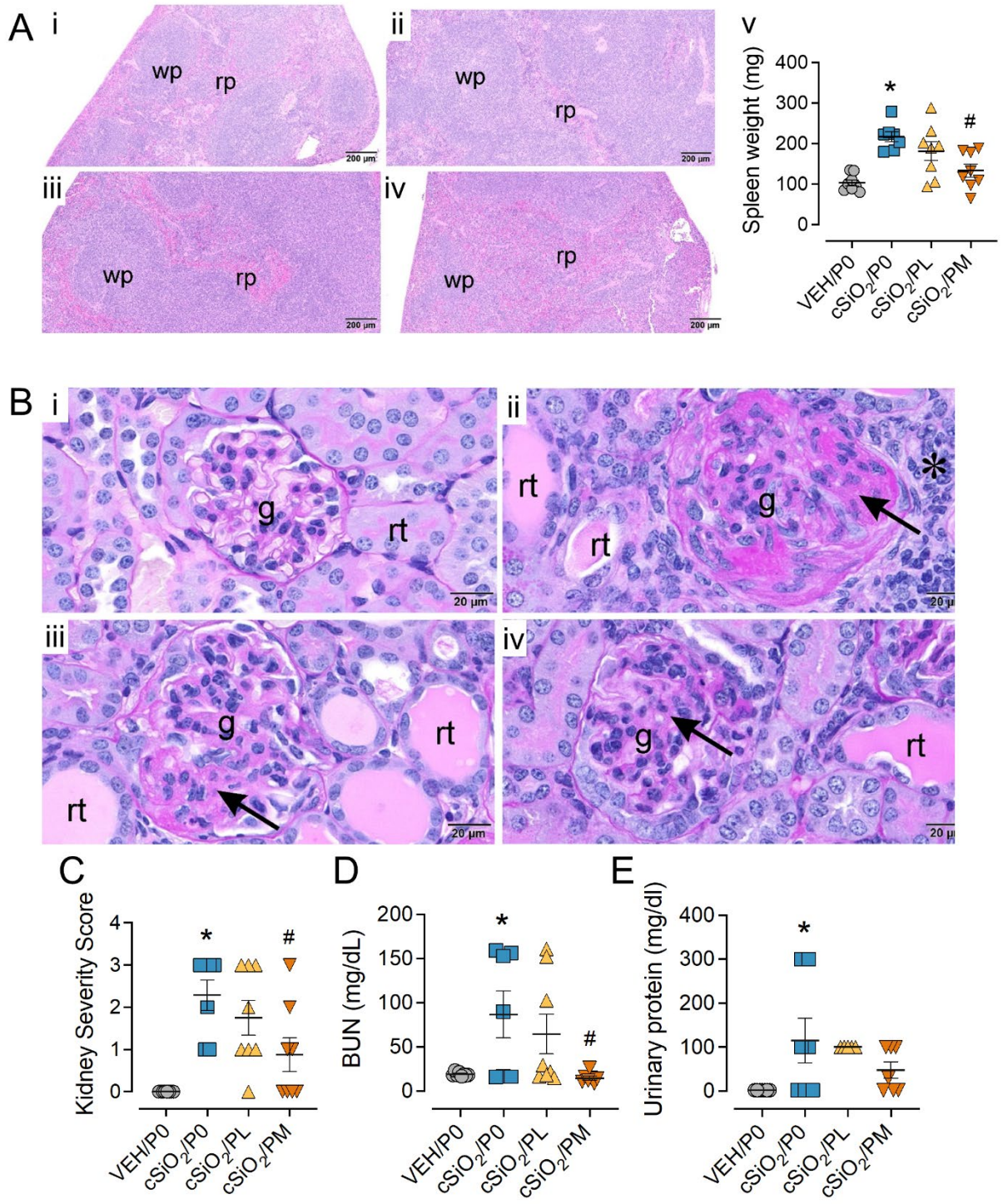

Figure 2.5: Medium dose prednisone (PM) significantly reduced $cSiO_2$-induced splenomegaly and glomerulonephritis. (A) Light photomicrographs of hematoxylin and eosin-stained splenic tissue and **(B)** periodic acid Schiff (PAS) and hematoxylin-stained renal tissue from (i) VEH/P0, (ii) $cSiO_2$/P0, (iii) $cSiO_2$/PL, and (iv) $cSiO_2$/PM mice. Splenic white pulp (wp) is increased (lymphoid cell hyperplasia) in A.ii and A.iii compared to A.i. WP is similar in VEH/P0 (A.i) and $cSiO_2$/PM (A.iv) mice. Glomeruli (g) in B.ii and B.iii are enlarged and hypercellular with

Figure 2.5 (cont'd):
PAS-stained membranous tissue (arrows). Dilated renal tubules (rt) with luminal proteinaceous material are present in B.ii and B.iii, but not in B.i. PM treatment results in modest glomerular and renal tubular histopathology in B.iv. **(C)** Individual kidney sections were semi-quantitatively scored based on the modified International Society of Nephrology/Renal Pathology Lupus Nephritis Classification system described methods for lupus nephritis score. **(D)** PM treatment significantly reduced $cSiO_2$-induced plasma BUN at time of necropsy **(E)** but was ineffective in significantly reducing urinary protein assessed at 12 wks of age. Statistical analyses were performed as described in Methods. *Indicates $p<0.05$ for VEH/P0 vs $cSiO_2$/P0; #indicates $p<0.05$ for $cSiO_2$/P0 vs $cSiO_2$/PL or $cSiO_2$/PM group.

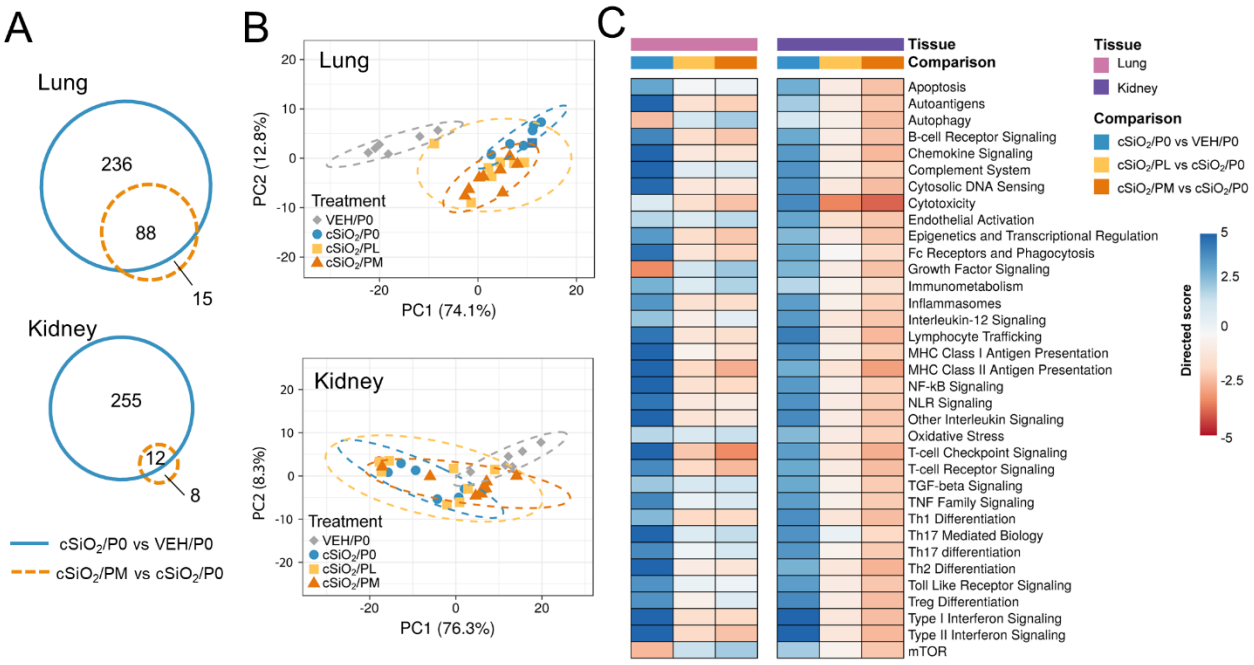

Figure 2.6: Effect of prednisone treatment on $cSiO_2$-induced transcriptional changes in lung and kidney tissues of mice 14 weeks post instillation. (A) Venn diagrams depicting overlap of genes differentially regulated in mice with $cSiO_2$/P0 vs VEH/P0 treatment or $cSiO_2$/PM vs $cSiO_2$/P0 treatment (FDR $q<0.05$, 1.5-fold change). The overlap regions indicate genes affected by silica exposure that were also differentially regulated with medium-dose prednisone. No significant differentially expressed genes were identified when comparing $cSiO_2$/PL to $cSiO_2$/P0 for either lung or kidney. **(B)** Principal components analyses of differentially expressed genes in lung and kidney tissues of mice with low- ($cSiO_2$/PL) or medium-dose prednisone ($cSiO_2$/PM) as compared to VEH/CON and $cSiO_2$-exposed ($cSiO_2$/P0) tissue-matched control diets. PC1 and PC2 are shown with 95% confidence intervals (dashed ellipses). **(C)** Directed significance scores for autoimmune pathways were determined using nSolver (see Materials and Methods) by comparing $cSiO_2$/P0 to tissue-matched VEH/P0 control group or by comparing $cSiO_2$/PL or $cSiO_2$/PM treatments to tissue matched $cSiO_2$/P0 treatment group. Abbreviations: $cSiO_2$, crystalline silica; P0, zero prednisone; PL, low-dose prednisone; PM, medium-dose prednisone; VEH, vehicle control.

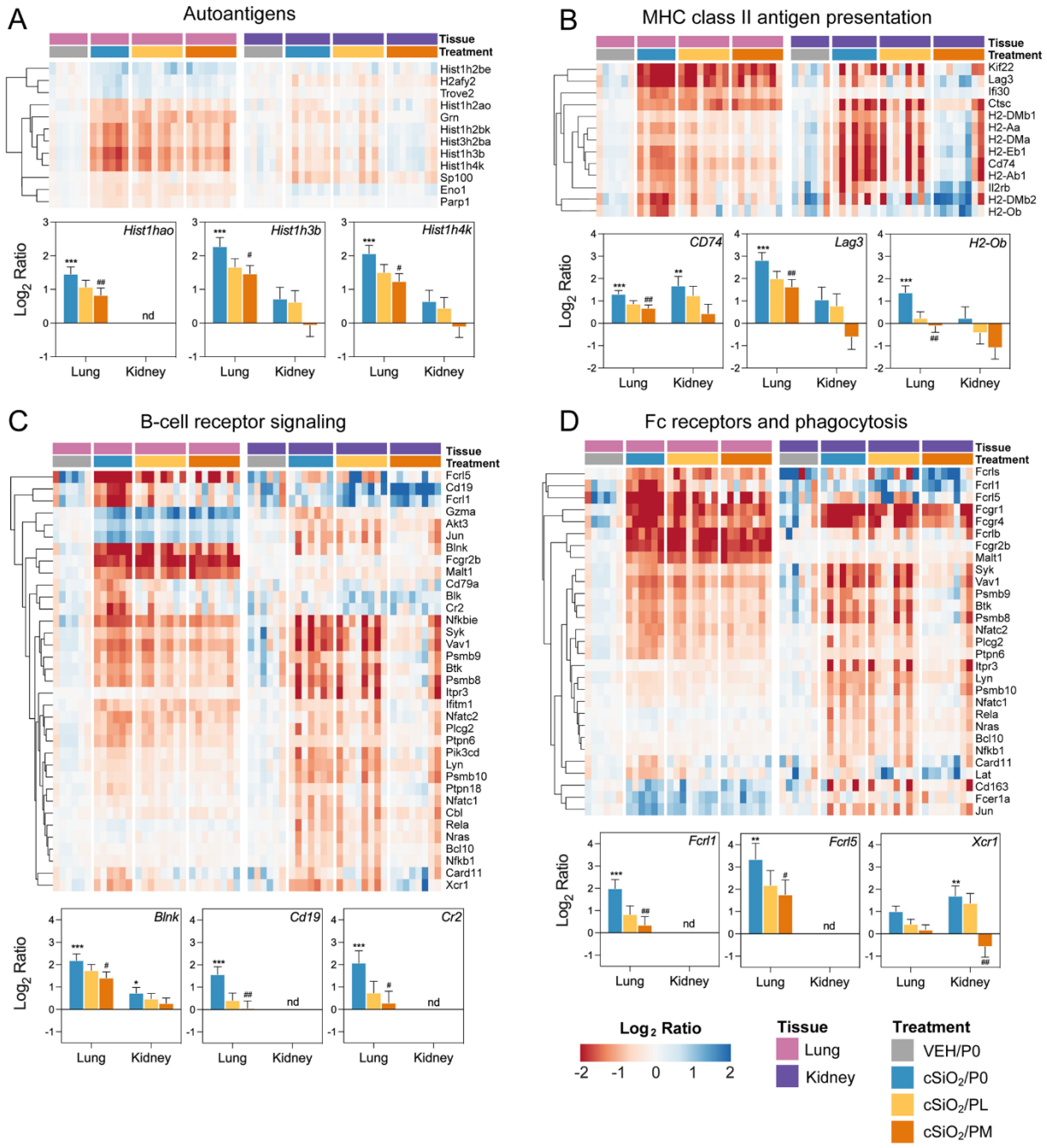

Figure 2.7: Comparison of prednisone-responsive genes associated with (A) autoantigen, (B) MHC class II antigen presentation, (C) B-cell receptor signaling, and (D) Fc receptors and phagocytosis pathways in lung or kidney tissues 14 weeks post instillation with $cSiO_2$. Gene expression data were obtained using the NanoString Autoimmune Profiling gene panel and are shown as log2 ratios for $cSiO_2$/P0, $cSiO_2$/PL, and $cSiO_2$/PM treatment groups with respect to the tissue-matched VEH/P0 control group (log2 ratio = 0). For each pathway, heatmaps with unsupervised hierarchical clustering (Euclidian distance method) by gene show log2 expression values for all genes identified as differentially expressed in response to either $cSiO_2$ exposure or medium-dose prednisone (FDR $q<0.05$, 1.5-fold change) in either of the selected tissues. The mean

Figure 2.7 (cont'd):
log2 ratio values + SEM for selected genes of interest are also shown for each pathway. For for $cSiO_2$/P0 as compared to VEH/P0, *, FDR-corrected $q<0.05$; **, $q<0.01$; and ***, $q<0.001$. For $cSiO_2$/PL or $cSiO_2$/PM vs $cSiO_2$/P0, #, FDR-corrected $q<0.05$; ##, $q<0.01$; and ###, $q<0.001$. See Supplementary File 1 for test specifications and FDR-corrected q-values for all genes in the panel for all comparisons. Abbreviations: $cSiO_2$, crystalline silica; P0, zero prednisone; PL, low-dose prednisone; PM, medium-dose prednisone; VEH, vehicle control.

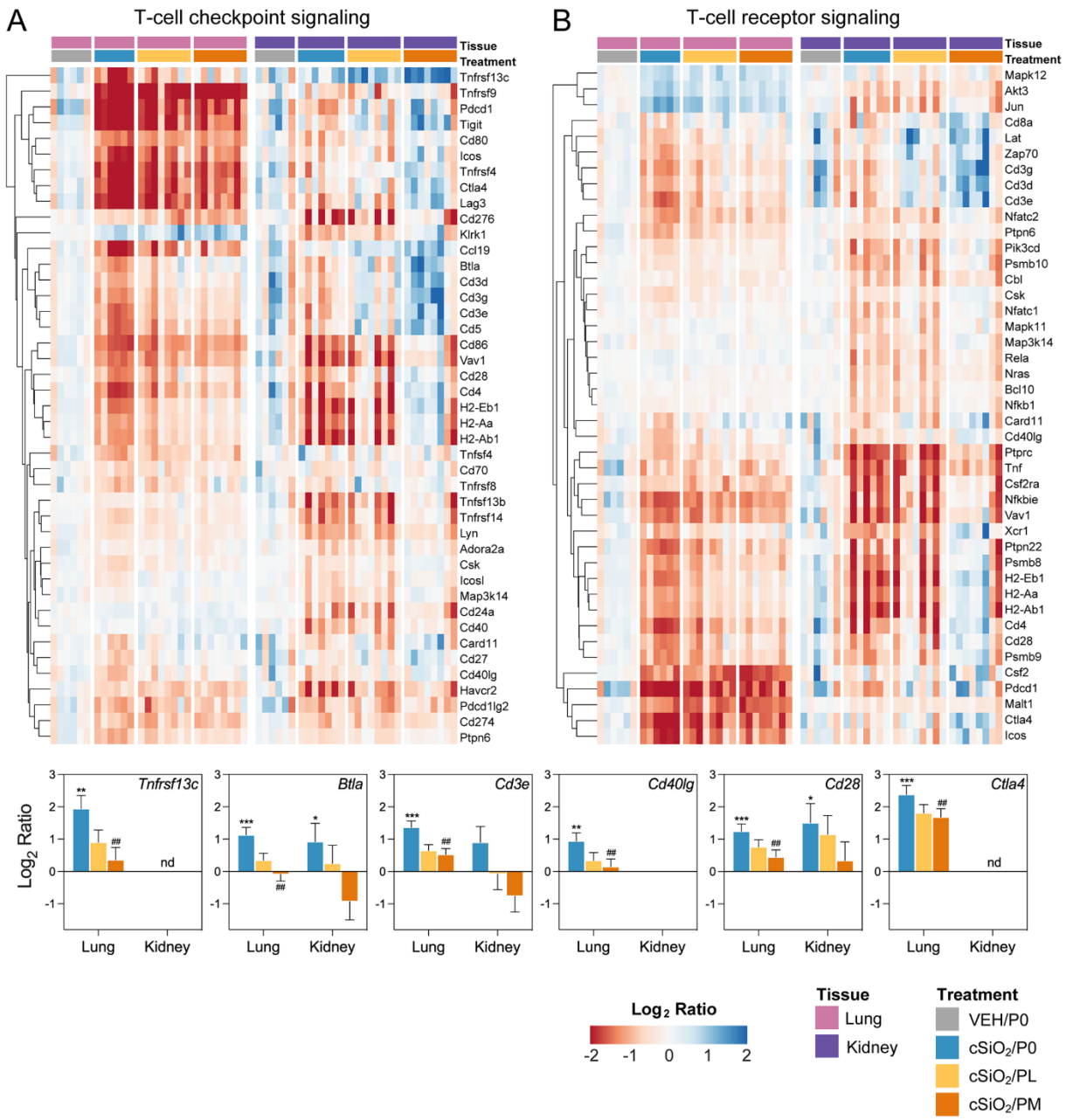

Figure 2.8: Comparison of prednisone-responsive genes associated with (A) T-cell checkpoint signaling and (B) T-cell receptor signaling pathways in lung or kidney tissues 14 weeks post instillation with $cSiO_2$. Gene expression data were obtained using the NanoString Autoimmune Profiling gene panel and are shown as log2 ratios for $cSiO_2$/P0, $cSiO_2$/PL, and $cSiO_2$/PM treatment groups with respect to the tissue-matched VEH/P0 control group (log2 ratio = 0). For each pathway, heatmaps with unsupervised hierarchical clustering (Euclidian distance method) by gene show log2 expression values for all genes identified as differentially expressed in response to either $cSiO_2$ exposure or medium-dose prednisone (FDR $q<0.05$, 1.5-fold change) in either of the selected tissues. The mean log2 ratio values + SEM for selected genes of interest are also shown. For $cSiO_2$/P0 as compared to VEH/P0, *, FDR-corrected $q<0.05$; **, $q<0.01$; and ***, $q<0.001$. For cSiO2/PL or $cSiO_2$/PM vs $cSiO_2$/P0, #, FDR-corrected $q<0.05$; ##, $q<0.01$; and

Figure 2.8 (cont'd):
###, q<0.001. See Supplementary File 1 for test specifications and FDR-corrected q-values for all genes in the panel for all comparisons. Abbreviations: $cSiO_2$, crystalline silica; P0, zero prednisone; PL, low-dose prednisone; PM, medium-dose prednisone; VEH, vehicle control.

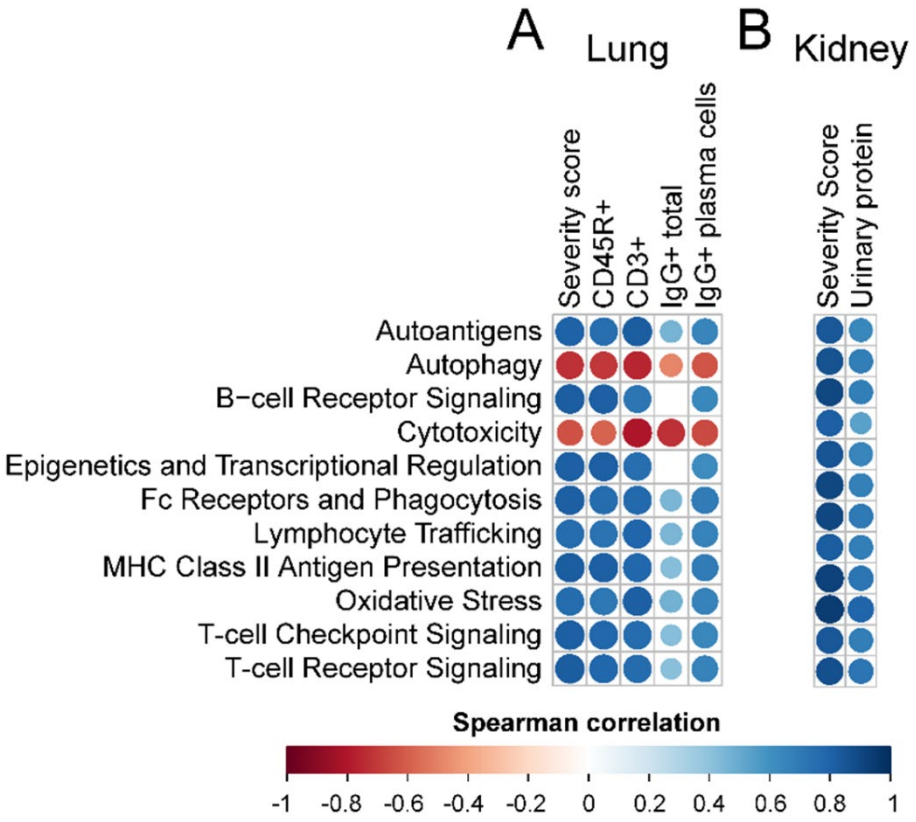

Figure 2.9: Correlation analyses of selected autoimmune pathways. For all treatment groups, spearman ρ values were calculated by correlating pathway Z scores with **(A)** lung severity score or the percent positive staining for $CD45R^+$, $CD3^+$, or IgG^+ in lung tissue or IgG^+ in lung tissue plasma cells; or **(B)** kidney severity score, kidney blood urea nitrogen (BUN), or kidney urinary protein. Significant correlation values ($p<0.05$) are represented as circles colored by the correlation value (blue, positive; red, negative); non-significant correlations are indicated by blank cells.

TABLES

Table 2.1: Relation of prednisone concentrations in experimental diet to mouse and human daily doses.

Experimental Diet[a]	Prednisone			
	Concentration[b] (mg/kg diet)	Mouse dose[c] (mg/kg bw/d)	HED[d] (mg/kg bw/d)	HED[e] (mg/d)
P0 (CON)	0 (0)	0	0	0
PL	5 (5.0)	0.75	0.06	5
PM	15 (15.2)	2.25	0.18	14
PH	50 (49.8)	7.5	0.6	46

[a] Abbreviations: CON refers to control diet; PL, PM and PH correspond to low, moderate and high dose prednisone diets.
[b] Values in parentheses refer to LC-MS analysis of a representative lot of experimental diets.
[c] Mouse dose was calculated by multiplying dietary concentration by the FDA conversion factor of 0.15 (165).
[d] Human equivalent dose was-calculated by multiplying mouse dose by FDA drug interspecies conversion factor of 0.08 (166).
[e] Daily human equivalent dose based on average body weight of 77 kg for women ≥ 20 years of age in the U.S. (143)

CHAPTER 3: CHARACTERIZATION OF SILICA-TRIGGERED AUTOIMMUNITY AND OMEGA-ACID INTERVENTION IN ADULT LUPUS-PRONE MOUSE MODEL

Lauren K. Heine[1,2], Tasha Scarlett[3], James G. Wagner[2,3], Ryan P. Lewandowski[3], Abby D. Benninghoff[4], Ashleigh N. Tindle[3], Anna E. Skedel[3], James J. Pestka[2,5,6], and Jack R. Harkema[2,3]

[1]Department of Pharmacology and Toxicology, Michigan State University, East Lansing, MI

[2]Institute for Integrative Toxicology, Michigan State University, East Lansing, MI

[3]Department of Pathobiology and Diagnostic Investigation, Michigan State University, East Lansing, MI

[4]Department of Animal, Dairy and Veterinary Sciences, School of Veterinary Medicine, Utah State University, Logan, UT

[5]Department of Food Science and Human Nutrition, Michigan State University, East Lansing, MI

[6]Department of Microbiology and Molecular Genetics, Michigan State University, East Lansing, MI

PUBLICATION NOTICE

The following chapter is in preparation to be submitted to *Frontiers in Immunology*.

ABSTRACT

Introduction: Occupational exposure to respirable crystalline silica dust ($cSiO_2$) has been epidemiologically linked to the systemic autoimmune disease lupus. We have previously found intranasal $cSiO_2$ instillation can trigger early onset and progression of autoimmunity in the lungs and kidneys of juvenile, 8-wk-old female NZBWF1 lupus-prone mice. Furthermore, we have demonstrated that dietary supplementation with the omega-3 fatty acid, docosahexaenoic acid (DHA), prevents $cSiO_2$-induced lupus. However, it is unknown how $cSiO_2$ exposure and DHA intervention affect adult lupus-prone mice that more appropriately model the age of $cSiO_2$-exsposed workers.

Methods: In the present study, we fed adult female 14-wk-old NZBWF1 mice either purified AIN-93G control diet (CON) or AIN-93G diet containing DHA at a human equivalent dose (HED) of 5 g/d. Beginning at 16-wk of age, mice were intranasally instilled with either saline vehicle (VEH) or 1 mg $cSiO_2$ once per wk for 4 consecutive wks and sacrificed at 1 or 5 wks after the last instillation (PI). Lung and kidney tissues were processed for light microscopy, immunohistochemistry, and morphometric analysis. Bronchoalveolar lavage fluid (BALF) was collected for total and differential inflammatory cell counts.

Results: VEH/CON mice had no pulmonary or renal pathology at either 1 or 5 wks PI. $cSiO_2$/CON mice had mild pulmonary ectopic lymphoid tissue (ELT) formation at 1-wk PI, with a marked increase at 5 wks PI. Correspondingly, lungs of $cSiO_2$/CON mice had increases in BALF cellularity, $CD3^+$ T-cell, $CD45R^+$ B-cell, and IgG^+ plasma cell densities, and proinflammatory gene and protein expression at both timepoints compared to VEH/CON mice. Kidneys from $cSiO_2$/CON mice had conspicuous glomerular IgG deposition compared to VEH/CON mice. Dietary DHA supplementation dramatically attenuated $cSiO_2$-triggered lung pathology including

ELT formation, increases in $CD3^+$ T-cell, $CD45R^+$ B-cell and IgG^+ plasma cell densities, and inflammatory cell counts in BALF at both 1 and 5 wk PI. Proinflammatory gene and protein expression was reduced in a time-dependent manner at one or both timepoints. $cSiO_2$/DHA mice also had no IgG deposition in renal glomeruli.

Discussion: Our findings demonstrate that repeated intranasal $cSiO_2$ exposure in adult female NZBWF1 lupus-prone mice resulted in pulmonary pathology that was more severe compared to what has previously been observed in juveniles. Nevertheless, translationally relevant DHA supplementation markedly ablated $cSiO_2$-triggered lupus pathology in adult mice, in a manner similar to that observed in juvenile mice.

INTRODUCTION

Systemic lupus erythematosus (lupus) is a chronic, heterogeneous, multi-organ autoimmune disease that primarily afflicts women of child-bearing age. Lupus is associated with unresolved inflammation and loss of tolerance to self-antigens leading to the recruitment of autoreactive B- and T-cells which perpetuates a robust pathogenic autoantibody (AAb) response (1, 2). Resulting AAbs bind their cognate autoantigens (AAgs) forming immune complexes that are distributed via the systemic circulation and deposit in various organs such as the kidney. This process chronically reoccurs, manifesting in cyclical bouts of inflammation and autoimmunity known as lupus flares (3). These flares negatively impact quality of life and increase morbidity and mortality in lupus patients (3). Importantly, repeated flaring promotes development of glomerulonephritis and irreparable damage to the kidney eventually leading to end-stage renal failure (4).

Lupus onset, flaring, and progression is strongly influenced by gene-environment interactions (2). Disease susceptibility can be largely impacted by known genetic predispositions (5), yet environmental exposures to toxicants, infections, UV radiation, and certain medications have also

been linked to lupus onset and progression (6, 7). Exposure to the environmental toxicant, respirable crystalline silica ($cSiO_2$), has been implicated in the development of autoimmune diseases such as lupus, rheumatoid arthritis, scleroderma, and ANCA-associated vasculitis (8-10). According to the Occupational Health and Safety Administration (OSHA), approximately 2.3 million workers practicing occupations such as stonecutting, construction, ceramics, and mining are exposed to respirable $cSiO_2$ dusts (https://www.osha.gov/silica-crystalline). Additionally, lupus risk has been shown to increase in accordance with duration of exposure for women of color in $cSiO_2$-exposing occupations (11).

Consistent with human epidemiological studies focused on the association between $cSiO_2$ exposure and autoimmunity, our lab has demonstrated that $cSiO_2$ triggers autoimmune disease onset and progression in juvenile female NZBWF1 lupus-prone mice. Specifically, short-term repeated $cSiO_2$ instillations (1 mg/wk for 4 consecutive wks) beginning at 8 wks of age accelerated disease onset with glomerulonephritis being observed at 20-22 wk of age (17). In comparison, unexposed female NZBWF1 mice spontaneously develop glomerulonephritis as they age into adults at approximately 32-34 wks of age (167). Prior to evident kidney disease, $cSiO_2$ exposure triggers formation of pulmonary ectopic lymphoid tissue (ELT), robust AAb responses in bronchoalveolar lavage fluid (BALF) and plasma, and proinflammatory gene expression in lung and kidney tissues (17, 20, 88). Altogether, these juvenile mouse studies show that inhalation of $cSiO_2$ leads to extensive pulmonary inflammation, creating a nexus for a local and systemic autoimmune response leading to downstream renal pathology. Although occupational exposures occur in adults (>25 years old), $cSiO_2$ exposure in adult mice that more appropriately model the age of adult workers, and who also have underlying genetic susceptibility to autoimmunity, has yet to be studied.

Like environmental exposures, lifestyle choices such as diet can impact lupus disease progression. It has been shown in clinical and pre-clinical studies that increased consumption of polyunsaturated fatty acids, such as the ω-3 fatty acid (FA) docosahexaenoic acid (DHA), can reduce disease symptoms in lupus and RA patients (81, 82, 117, 168, 169). Our lab has previously shown *in vivo* that juvenile female NZBWF1 mice exposed to $cSiO_2$ and fed DHA enriched diets exhibited blunted autoimmunity (18, 21, 67, 68, 88). More specifically, mice fed a human equivalent dose (HED) of 5 g/d DHA had significantly less pulmonary ELT formation, pathogenic AAb detected in the BALF and plasma, and glomerulonephritis compared to $cSiO_2$-exposed mice non-DHA diets.

A key limitation of the aforementioned preclinical studies focused on $cSiO_2$-triggered lupus and omega-3 intervention was that they were conducted in juvenile mice with a human age equivalence of 12-17 years (**Figure 1A**) (170). In this study, we addressed this limitation by employing adult NZBWF1 mice that more appropriately model the age of $cSiO_2$-exposed workers (20-30 years of age). Specifically, we tested two hypotheses: (i) adult female NZBWF1 mice receiving the same instilled dose of $cSiO_2$ used in previous studies would develop similar or more severe pulmonary and renal pathology compared to that observed in juveniles, and (ii) DHA-amended diet (HED 5 g/d) administered to $cSiO_2$-exposed adult mice would significantly attenuate the systemic autoimmune response, similar to what has been previously observed in juveniles.

MATERIALS AND METHODS

Animals and diets

All mouse experiments were approved by the Institutional Animal Care and Use Committee (IACUC) at Michigan State University (AUF# 201800113). Adult 14-wk-old female NZBWF1 mice, which more appropriately model the age of $cSiO_2$-exposed workers (**Figure 1A**), were

obtained from Jackson Laboratories (Bar Harbor, ME) were housed three per cage and given access to food and water throughout the course of the experiment. The animal facility was maintained at a constant temperature (21-24°C) and humidity (40-55%) with a 12-hour light/dark cycle.

Control (CON) American Institute of Nutrition (AIN)-93G diet (171) or an AIN-93G diet containing DHA were prepared as described previously (67) (**Table 1**). Briefly, CON diet contained 70 g/kg of fat, 10 g/kg from food-grade corn oil and 60 g/kg from high-oleic safflower oil (LouAna, Brea, CA), to provide sufficient basal essential fatty acids. For DHA-supplemented diet, safflower oil was partially replaced with 25 g/kg microalgal oil containing 40% DHA (DHASCO; provided by Dr. Kevin Hadley, DSM Nutritional Products, Columbia, MD). This supplementation yielded a diet containing 10 g/kg DHA which is calorically equivalent to a human equivalent dose (HED) of 5 g/d (16). Diets were prepared weekly to prevent oxidation of fatty acids and were stored at -20°C. Mice were given fresh food every day.

Experimental Design

Upon arrival, 14-wk-old female NZBWF1 mice were randomly sorted into experimental groups and fed either CON or DHA-supplemented diets. Beginning at 16 wks of age, mice were intranasally instilled once weekly for 4 consecutive wks with either 25 μL PBS vehicle (VEH) or 1.0 mg of $cSiO_2$ (Min-U-Sil-5, 1.5-2.0 μm average particle size, Pennsylvania Sand Glass Corporation, Pittsburgh, PA) suspended in PBS (**Figure 1B**). Therefore, there were a total of 3 experimental groups as follows: (i) VEH treated mice fed CON diet (VEH/CON, n = 12), (ii) $cSiO_2$-instilled mice administered CON diet ($cSiO_2$/CON, n = 12), and (iii) $cSiO_2$-instilled mice administered DHA-supplemented diet ($cSiO_2$/DHA, n = 12). For instillations, mice were anesthetized with 4% isoflurane. Following the final $cSiO_2$ instillation (19 wks of age), urine was

collected weekly until the time of necropsy and evaluated for proteinuria (≥300 mg/dL protein) using reagent dipsticks (Cortez Diagnostics, Calabasas, CA). One cohort of mice (n = 6) from each experimental group was sacrificed 1 wk post-instillation last $cSiO_2$ instillation (PI) while the remaining mice were sacrificed at 5 wk PI.

Animal Necropsy, Tissue Selection and Lung Lavage

Prior to death by exsanguination via the abdominal aorta, mice were anesthetized with an intraperitoneal injection of sodium pentobarbital (56 mg/kg). Abdominal cavity was exposed, and blood was collected from the abdominal vena cava for analysis of plasma and RBCs as described below. Immediately after death, the trachea was exposed and cannulated, and the heart and lungs were excised en bloc from the carcass. A volume of 0.8 mL saline was intratracheally instilled in the lung and withdrawn to recover bronchoalveolar lavage fluid (BALF). A second saline lavage was performed and the collected BALF was combined with the first sample for analysis. The left lung lobe was inflation fixed via the trachea with 10% neutral buffered formalin (NBF) (Fischer Scientific, Pittsburgh, PA) at a constant pressure of 30 cm H_2O for a minimum of 1 hr. The lung lobe was immersed in fixative for at least 48 hr prior to tissue processing for light microscopy. Collected venous blood was spun down by centrifuge at 3500 x g for 10 min at 4°C to separate the plasma and RBCs. Both plasma and RBCs were stored at -80°C for AAb microarray and fatty acid analysis, respectively.

BALF Cytology

A hemocytometer was used to determine total BALF leukocyte cell counts. Centrifugal forces (40 x g for 10 min) were used to immobilize BALF cells onto glass slides (Shandon Cytospin 3) that were then air dried and stained with Diff-Quick (Fisher Scientific). Unused BALF was centrifuged at 465 x g for 15 min and resultant supernatant was stored at -80°C. BALF differential

inflammatory cell counts were performed based on morphological criteria to identify monocytes, neutrophils, lymphocytes, and eosinophils out of a total of 200 cells per cytological slide.

Fatty Acid Analysis

Fatty acid content of red blood cells (RBCs) was determined using gas liquid chromatography by OmegaQuant Analytics, LLC (Sioux Falls, SD). The RBC Omega-3 Index, a biomarker for tissue omega-3 content (172), was calculated by taking the sum of EPA and DHA (%EPA+DHA) as a percent of total fatty acids.

Lung and Kidney Histopathology

Formalin fixed left lung lobes were cut into 4 transverse tissue blocks (~2 mm each) and embedded in paraffin. Tissue sections (5 μm thickness) were deparaffinized and stained with hematoxylin and eosin (H&E) to be microscopically assessed for histopathology. A board-certified veterinary pathologist, without knowledge of individual animal exposure/diet ("blind analysis"), scored the severity of lung lesions that included (a) perivascular and peribronchiolar ectopic lymphoid tissue (ELT), (b) alveolar proteinosis, (c) alveolitis, (d) alveolar type II epithelial cell hyperplasia, and (e) mucous cell metaplasia in bronchiolar epithelium. Similarly, fixed kidney tissues were cut into 3 transverse sections and processed for histopathology. Tissues sections were stained with Periodic acid-Schiff and hematoxylin (PASH) stain or immunohistochemically stained with IgG. Kidneys were also evaluated by a board-certified veterinary pathologist to assess tubular proteinosis and global proliferative and sclerosing glomerulonephritis using a modified International Society of Nephrology/Renal Pathology Lupus Nephritis Classification system (173) and for glomerular IgG deposition.

Immunohistochemistry and Morphometric Analysis of Lung and Kidney

Immunohistochemistry (IHC) was performed on formalin-fixed, paraffin embedded lung and

kidney tissue sections. In the lung, B-cells were identified using 1:600 rat anti-CD45R monoclonal antibody and T-cells were identified using 1:250 rabbit anti-CD3 polyclonal antibody (**Table A3.1**). IgG^+ plasma cells in the lung and IgG deposition in the kidney were identified using goat anti-IgG polyclonal antibody (**Table A3.1**). Slides were scanned using the VS200 virtual slide system (Olympus, Hicksville, NY). Using NewCast software (Visiopharm, Hoersholm, Denmark), each whole glass slide was randomly subsampled to obtain at least 100 digital microscopic images from lung tissue sections captured at 20X magnification. Using the STEPanizer 1.8 Stereology Tool (147), pulmonary $CD45R^+$, $CD3^+$, and IgG^+ lymphoid cells were counted by overlaying a point grid on randomly sampled images. Total cell densities were calculated by dividing the number of grid points overlayed with positively stained cells by reference tissue area to get a percentage of total lung area showing positive staining.

Multiplex Analysis of Cytokines

Right cranial lung lobes were weighed out and placed in appropriate amounts of 1X RIPA buffer (Thermo Fisher Scientific) and protease inhibitor (1:100 dilution; Thermo Fisher Scientific) to make 20% homogenates. Lung tissue was homogenized using the Qiagen TissueLyser bead mill, and a BCA assay was used to determine the protein concentration of each sample (Thermo Fisher Scientific). Protein concentrations were then normalized to 1000 ug/mL/sample and all samples were submitted to Eve Technologies Corp. (Calgary, Alberta) for multiplexed quantification of multiple mouse cytokines and chemokines using the Mouse Cytokine Multiplex Discovery Assay® (MilliporeSigma, Burlington, Massachusetts, USA). The multiplex contained MCP-5, IP-10, MIP-1α, MIP-1β, MIP-3β, MIG, MCP-1, and KC. Assay sensitivities of these markers ranged from 0.3 – 30.6 pg/mL.

NanoString autoimmune gene profiling

RNA was extracted from lung tissue (1 and 5 wk PI) with RNeasy Mini Kits with DNase treatment (Qiagen, Valencia, CA). RNA was dissolved in nuclease-free water, quantified with Qubit (Thermo Fisher Scientific), and integrity verified with a TapeStation (Agilent Technologies). Samples (RNA integrity >8) were analyzed with NanoString Autoimmune Gene Expression assay (XT-CSO-MAIP1-12, NanoString Technologies, Seattle, WA) at the MSU Genomics Core. Assays were performed and quantified on the nCounter MAX system, sample preparation station, and digital analyzer (NanoString Technologies) according to the manufacturer's instructions.

Gene expression data was analyzed as performed as previously described (19-21, 174). Briefly, raw gene expression data were analyzed using NanoString's software nSolver v3.0.22 with the Advanced Analysis Module v2.0. For differential gene expression, a statistically significant difference in gene expression was defined as 1.5-fold change in expression (log2 >0.58 or <-0.58) with BH q <0.05. Two pairwise comparisons within each timepoint (1 and 5 wk PI) were determined a priori, as follows: $cSiO_2$/CON vs VEH/CON and $cSiO_2$/CON vs $cSiO_2$/DHA.

To assess the impact of $cSiO_2$ exposure and experimental diets on annotated gene sets, global and directed significance scores were calculated for each pathway at each time point, as previously described (174). The global score estimates the cumulative evidence for the differential expression of genes in a pathway. As a complementary method for comparing pathways and discriminating between experimental groups, pathway Z scores were calculated as the Z-scaled first principal component of the pathway genes' normalized expression. ClustVis (175) was used to perform unsupervised hierarchical cluster analyses (HCC) using log2 transcript count data for DEGs. Spearman rank correlations were performed to examine overall patterns in the gene expression profiles using the pathway Z score compared to other biomarkers of disease in lung

tissues at 1 and 5 wk PI. A significant correlation was inferred when ρ >0.5 or <-0.5 and p<0.05.

Autoantibody microarray

BALF and plasma samples were assessed for presence of AAbs by GeneCopoeia (Rockville, Maryland). Briefly, dilutions of plasma and BALF samples were incubated on microscope slides, each containing 16 identical OmicsArray™ panels of 120 known autoantigens adhered to nitrocellulose filters. One panel was reserved for a PBS negative sample control. Following incubation, the slides were washed, then incubated with Cy3-labeled anti-mouse IgG and Cy5-labeled anti-mouse IgM secondary antibodies. Next the slides were washed, and fluorescent signals (532nm for Cy3/IgG, 635nm for Cy5/IgM) were detected using a GenePix™ 4000B two-channel laser microarray scanner (Molecular Devices, San Jose, California). Fluorescent signal intensities were determined using GenePixPro™ 7.0 software (Molecular Devices, San Jose, California). Antibody scores were calculated using normalized signal intensities (NSI) and signal-to-noise ratios (SNR), and by using the following equation:

$$Ab\ score = \log_2(NSI * SNR + 1)$$

Normalized and unit variance-scaled Ab-score values were visualized using ClustVis software (175). Data were clustered using unsupervised hierarchical co-clustering (HCC). Rows were clustered using Euclidean distance and Ward linkage. Imputation was applied for missing value estimation. Selected AAb-scores were reported as violin plots, generated using Prism 9 (GraphPad Prism v 9.2, San Diego, CA).

Statistical Analysis

All data were analyzed, and statistical tests were performed using Prism 9 (GraphPad Prism v 9.2, San Diego, CA), excluding the NanoString gene expression data as discussed above. Data were assessed for outliers using the Grubb's outlier test (with Q=1%) and for normality using the

Shapiro-Wilk test ($p<0.01$). Data of histopathological endpoints were analyzed using a One-Way ANOVA to address our hypothesis that dietary DHA would suppress $cSiO_2$-triggered responses. Non-normal and semi-quantitative data were analyzed using the nonparametric Kruskal-Wallis test. Data are presented as mean ± standard error of the mean (SEM), with a p-value ≤ 0.05 being considered as statistically significant.

RESULTS

Body Weights and RBC Fatty Acid Composition

The effects of intranasal $cSiO_2$ instillation were compared in CON- and DHA-fed adult female NZBWF1 mice using the Experimental Design depicted in **Figure 3.1B**. Mean mouse body weights increased approximately 7 g from ages 14 to 23 wks of age across all experimental groups (**Figure A3.1**). $cSiO_2$ exposure and experimental diets did not influence body weight increases. Consistent with previous studies (67, 68), replacement of high-oleic sunflower oil with DHA-enriched algal oil in DHA-enriched diets corresponded with increased omega-3 PUFA content in RBCs from mice necropsied at both 1 and 5 wk PI (**Table 3.2; Figure 3.2**). Concomitantly, $cSiO_2$/DHA mice had a significant reduction in the percentage of total omega-6 PUFAs in their RBCs compared to $cSiO_2$/CON-fed mice (**Table 3.2; Figure 3.2**). DHA PUFA content in RBCs was significantly increased in DHA-fed mice compared to those on CON diet at the expense of arachidonic acid. Moreover, the omega-3 index, which describes the sum of the omega-3 PUFAs DHA and eicosapentaenoic acid (EPA) as a percentage of total fatty acids, was three times higher in $cSiO_2$/DHA mice (17-19%) compared to either VEH/CON and $cSiO_2$/CON mice (5-6%).

DHA attenuated $cSiO_2$-triggered pulmonary ELT formation

The most conspicuous lung lesions in mice instilled with $cSiO_2$ and fed CON diet were lymphoplasmacytic infiltrations in perivascular and peribronchiolar interstitial tissue (ectopic

lymphoid tissue, ELT) (**Figure 3.3A**). These $cSiO_2$-instilled mice also had mild to moderate mixed inflammatory cell infiltrates in the alveolar parenchyma (alveolitis; composed of neutrophils, lymphocytes, and monocytes) that were associated with accumulations of extracellular proteinaceous material (proteinosis) and $cSiO_2$ particles (extracellular and intracellular) throughout the alveolar airspaces. $cSiO_2$ particle-laden alveolar macrophages with morphologic features of degeneration (vacuolation) and necrosis (cellular enlargement, cytoplasmic vacuolation and nuclear pyknosis or karyorrhexis) was another frequent finding in these $cSiO_2$-instilled lungs at both 1- and 5-wks PI. The lungs of mice at 5 wks, but not 1 wk PI, also had widely scattered small granulomas, composed of macrophages, lymphocytes and $cSiO_2$ particles, in alveolar septa.

ELT onset was most severe in the lungs of mice 5 wks after the last $cSiO_2$ instillation (**Figure 3.3A**), with significantly lesser amounts in mice 1 wk PI. No or minimal perivascular/bronchiolar lymphoid cell infiltrates were present in VEH/CON mice at both timepoints. VEH/CON mice were also devoid of any other lung histopathology (e.g., alveolitis). In contrast to the large amounts of ELT in $cSiO_2$/CON mice, $cSiO_2$-exposed DHA-fed mice had only small amounts of ELT in their lungs at both 1 and 5 wk PI (**Figure 3.3A**). Dietary DHA supplementation, however, had minimal to no apparent attenuation of other $cSiO_2$-triggered pulmonary pathology including alveolar accumulation of amorphous protein, silica, macrophages, and inflammatory cells. Semi-quantitative severity scores of lung lesions supported histopathological observations that $cSiO_2$ exposure led to significantly increased inflammation, ELT formation, and alveolar proteinosis at both timepoints (**Figure 3.3B**). Similarly, dietary supplementation with DHA markedly attenuated ELT formation, but only had modest to no effect on alveolitis and alveolar proteinosis (**Figure 3.3B**).

$cSiO_2$ exposure led to significantly elevated numbers of total leukocytes, monocytes, and

neutrophils at 1 and 5 wk PI in the BALF as compared to VEH/CON mice. In contrast, DHA reduced numbers of total leukocytes and monocytes in the BALF but resulted in increased neutrophil numbers at 5 wk PI as compared to $cSiO_2$/CON mice (**Figure 3.3C**).

Lymphoid cell populations in ELT were identified using IHC (**Figure 3.4A**) and quantified using standard morphometric techniques (**Figure 3.4B**). $cSiO_2$-induced ELT was composed predominantly of $CD3^+$ T-cells and $CD45R^+$ B-cells, with lesser numbers of IgG^+ plasma cells located in the margins of ELT. $cSiO_2$-triggered lymphoid cell infiltration was significant at 1 wk PI and markedly increased at 5 wk PI. Dietary supplementation with DHA significantly reduced $CD45R^+$ B-cell, $CD3^+$ T-cell, and IgG^+ plasma cell infiltration at 5 wk PI.

Consistent with increased lymphoplasmacytic infiltrations in $cSiO_2$-exposed mice, there was increased chemokine protein expression in lung tissue (**Figure 3.5**). More specifically, $cSiO_2$ exposure led to increased expression of monocyte chemoattractant proteins (MCP-5, MCP-1), macrophage inflammatory proteins (MIP-3β, MIP-1β, MIP-1α), IFN-induced proteins (IP-10), and chemokines (MIG, KC) at 1 or 5 wk PI. DHA supplementation attenuated $cSiO_2$-triggered MCP-5, IP-10, MCP-1, and KC protein expression in lung tissue.

NanoString global and directed significance scores revealed immunological pathways were significantly altered in lung tissue by both $cSiO_2$ exposure and diet (**Figure 3.6**). $cSiO_2$ exposure led to the activation of autoimmune-related pathways such as MHC Class I antigen presentation, Nod-like receptor (NLR) signaling, and Type I/II IFN signaling at both 1 and 5 wk PI. DHA-fed $cSiO_2$-exposed mice had significantly reduced enrichment of these pathways at 1 wk PI.

$cSiO_2$ exposure resulted in the upregulation of several genes associated with significantly enriched pathways at both 1 and 5 wk PI compared to VEH/CON mice (**Figure 3.7** and **3.8**). DHA significantly downregulated genes associated with NLR signaling (e.g., *Cyld, Tlr4, Casp4*)

(**Figure 3.7A**), MHC Class I antigen presentation (e.g., *Fcgr1, Herc6*) (**Figure 3.7B, D**), cytosolic DNA sensing (e.g., *Ddx58, Zbp1*) (**Figure 3.7C**), and Type I/II IFN signaling (e.g., *Irf7, Mx1, Isg15*) (**Figure 3.8A-C**) at 1 wk PI.

$cSiO_2$ exposure induced significant IgG AAb response in BALF

Increased levels of total IgG (**Figure 3.9**) and IgM (**Figure A3.2**) AAbs detected in the BALF of $cSiO_2$/CON mice compared to VEH/CON mice. DHA diet modestly reduced levels of total IgG AAbs in the BALF compared to $cSiO_2$/CON mice (**Figure 3.9**), but levels of IgM AAbs remained unchanged (**Figure A3.2**). Significant differences were not detected among VEH/CON, $cSiO_2$/CON, and $cSiO_2$/DHA groups in regard to IgG AAbs in the plasma (**Figure A3.3**).

$cSiO_2$-induced kidney pathology and IgG deposition is suppressed by DHA

Mild histopathological changes were observed in renal tissue from $cSiO_2$/CON mice at 5 wk PI (**Figure 3.10**). These mice had modest glomerular hypertrophy (**Figure 3.10B**) and mild renal IgG deposition (**Figure 3.10E**) compared to VEH/CON mice (**Figure 3.10A,D**). Renal pathology and IgG immunohistochemical staining was absent in $cSiO_2$/DHA mice (**Figure 3.10C,F**). Consistent with histopathological analysis, semiquantitative-severity scoring revealed increased glomerular hypertrophy and renal IgG deposition at 5 wk PI (**Figure 3.10G-H**). $cSiO_2$-induced glomerular changes were attenuated in DHA-fed mice. Urinalysis revealed no evidence of proteinuria in mice exposed to $cSiO_2$ (**Supplemental Figure** 3.**4**).

DISCUSSION

While our lab has previously used juvenile 8-wk old female NZBWF1 mice as a means of determining if $cSiO_2$ exposure is capable of accelerating lupus onset, here we wanted to determine if increased age would prompt a heightened autoimmune response compared to juveniles when instilled with the same dose of $cSiO_2$. Additionally, we wanted to evaluate whether age would

influence DHA's efficacy in ameliorating $cSiO_2$-triggered autoimmunity at the same HED. By utilizing adult female NZBWF1 mice that more appropriately model the age of $cSiO_2$-exposed workers, we were able to draw comparisons between juvenile and adult mice regarding exposure and diet outcomes. First, repeated $cSiO_2$ instillation in adult female NZBWF1 mice triggered increased pulmonary ELT formation, pulmonary lymphocyte infiltration of $CD45R^+$ B- and $CD3^+$ T-cells, BALF leukocyte cellularity, levels of IgG and IgM AAbs in BALF, and pro-inflammatory gene and protein expression in lung tissue. Second, dietary DHA orally administered at 5 g/d HED was effective in attenuating $cSiO_2$-triggered pulmonary ELT formation, pulmonary $CD45R^+$ B- and $CD3^+$ T-cell infiltration, monocyte cellularity in the BALF, and pro-inflammatory gene and protein expression in the lungs of adult mice. Third, adult mice exposed to $cSiO_2$ exhibited significantly more B- and T-cell infiltration around the perivascular and peribronchiolar airways compared to that previously observed in juveniles. By using data available from our lab's previous studies which utilized the same mouse strain and exposure/treatment model (17, 67), we were able to draw indirect comparisons between juveniles and adults. Here, adult lupus-prone mice from the present study exposed to $cSiO_2$ had significantly greater pulmonary $CD45R^+$ B-cell and $CD3^+$ T-cell infiltration compared to juveniles from previous studies (**Figure 3.11**) (17, 27). Baseline levels of T-cells in VEH/CON adult mice were also significantly greater compared to juveniles. A significant difference was not detected between juvenile and adult $cSiO_2$/DHA mice regarding $CD45R^+$ B-cells, whereas adult $cSiO_2$/DHA mice had significantly more $CD3^+$ T-cells compared to their juvenile counterparts.

In present study, repeated $cSiO_2$ exposure resulted in an age-dependent response in the lungs of female NZBWF1 mice (**Figure 3.12**). Compared to juvenile mice of the same strain who were also exposed to the same repeated $cSiO_2$ dosing regimen (16), at 5 wk PI we observed more

advanced pulmonary pathology and IgG AAb responses in the BALF of $cSiO_2$/CON mice. Interestingly, adult $cSiO_2$/CON mice sacrificed at 5 wk PI exhibited pulmonary inflammation comparable to juvenile $cSiO_2$/CON mice sacrificed at much later timepoints such as 9 and 13 wk PI (16, 88). It is important to note that VEH-instilled adult mice sacrificed at 5 wk PI also had elevated pulmonary $CD3^+$ T-cell densities and Σ IgG AAbs levels detected in the BALF compared to VEH-instilled juvenile mice sacrificed at 5 wk PI. Due to the advanced age of the adult mice at the time of first $cSiO_2$-instillation it is likely that adult mice developed a baseline autoimmune response that primes them to develop more severe lung pathology in a shorter time frame following the last $cSiO_2$ instillation.

Contrary to the effects of $cSiO_2$ exposure in this adult mouse model, the effectiveness of DHA-amended diets in ameliorating $cSiO_2$-triggered lupus was not age-dependent. Based on the histopathological findings, morphometric analysis of lymphoid cell densities contained in ELT, and BALF monocyte counts, DHA demonstrated significant attenuation of $cSiO_2$-induced responses in the lung at both 1 and 5 wks PI, similar to what has been observed in juveniles (16). Similarly, in line with previous juvenile mouse studies (21), DHA significantly reduced $cSiO_2$-triggered Type I/II IFN, innate, and adaptive immune response gene signatures in the lung. Interestingly, the 5 g/d DHA-enriched diet only modestly decreased IgG AAbs detected in the BALF at 5 wk PI, whereas IgG-related AAbs were significantly decreased in juveniles sacrificed at the same timepoint (88). Thus, apart from the pathogenic IgG AAb in the BALF, DHA effectively reduced a majority of $cSiO_2$-triggered pulmonary pathology independent of age.

While the pre-clinical adult mouse model described here was informative with regards to $cSiO_2$-triggered endpoints in the lung, we only observed mild pathology in the kidney at 5 wk PI. Based on previous studies centred around $cSiO_2$-triggered glomerulonephritis in juvenile

NZBWF1 mice, proteinuria develops at approximately 10-wks after $cSiO_2$-exposure with concomitant renal pathology observed at 12 wk PI (17). While we hypothesized that these adult $cSiO_2$-instilled mice would exhibit advanced systemic autoimmunity, pathology in the kidney did not follow an age-dependent response like the lung. Considering the lung serves as the nexus for respirable $cSiO_2$-mediated autoimmune responses in this model, it is likely a threshold of recurring inflammation originating from the lung that is necessary for resultant downstream damage to the kidney was not met in this experimental model. Moderate changes in renal pathology were consistent with unaltered IgG AAb responses present in the plasma of $cSiO_2$/CON mice. We speculate if $cSiO_2$-exposed adult mice were terminated at a later timepoint (e.g., 9 wk PI) we would see more advanced glomerulonephritis. Therefore, this model illustrated that while $cSiO_2$-induced lung pathology was age-dependent, downstream renal inflammation was relatively less pronounced.

Despite these minor limitations in experimental design, we have found that a relevant human dose of the omega-3 fatty acid DHA can effectively suppress $cSiO_2$-triggered pulmonary inflammatory/immune responses in adult mice. Furthermore, oral administration of DHA at 5 g/d ameliorated the more pronounced age-dependent immune response in adult lupus-prone mice that more appropriately model the age of $cSiO_2$-exposed workers. Currently, the most common drugs used for treating lupus are glucocorticoids (e.g., prednisone), antimalarials (e.g., hydroxychloroquine), immunosuppressants (e.g., cyclophosphamide), and monoclonal antibodies (76). Although treatment with these drugs have been shown to be effective in managing and slowing disease progression, their chronic use has also been associated with significant adverse effects (24, 176). While newer biologic therapies have not demonstrated similar off-target toxic effects, they are expensive and remain unaffordable for many lupus patients (79). Therefore, there

lies a critical need for non-toxic, cost-effective therapies to protect against environmental-triggered lupus. The findings of our present, and previous studies (16, 21, 67, 68, 88), provide substantial pre-clinical evidence to further investigate the use of DHA as a potential steroid-sparing therapeutic to prevent/treat lupus flares triggered by environmental/occupational exposures to toxic agents like airborne $cSiO_2$ dust.

ACKNOWLEDGEMENT

The authors thank Amy Porter of the Michigan State University Laboratory for Investigative Histopathology for their assistance with histotechnology. The authors also thank Dr. Kevin Childs and the Research Technology Support Genomics Core Facility for processing samples using NanoString nCounter Analysis System.

AUTHOR CONTRIBUTIONS

LH: study design, coordination, feeding study, necropsy, data curation, data analysis/interpretation, figure preparation, manuscript preparation and submission; TS: morphometric analysis, data acquisition and interpretation; JW: study design, necropsy, lab analysis; RL: instillations, necropsy, lab analysis; AB: data procurement and statistical analysis; AS: morphometric analysis; AT: animal handling, urinalysis; JH: study design, oversight, lung/kidney histopathology, morphometry, data analysis, manuscript preparation; JP: study design, oversight, funding acquisition, data analysis, manuscript preparation.

FIGURES

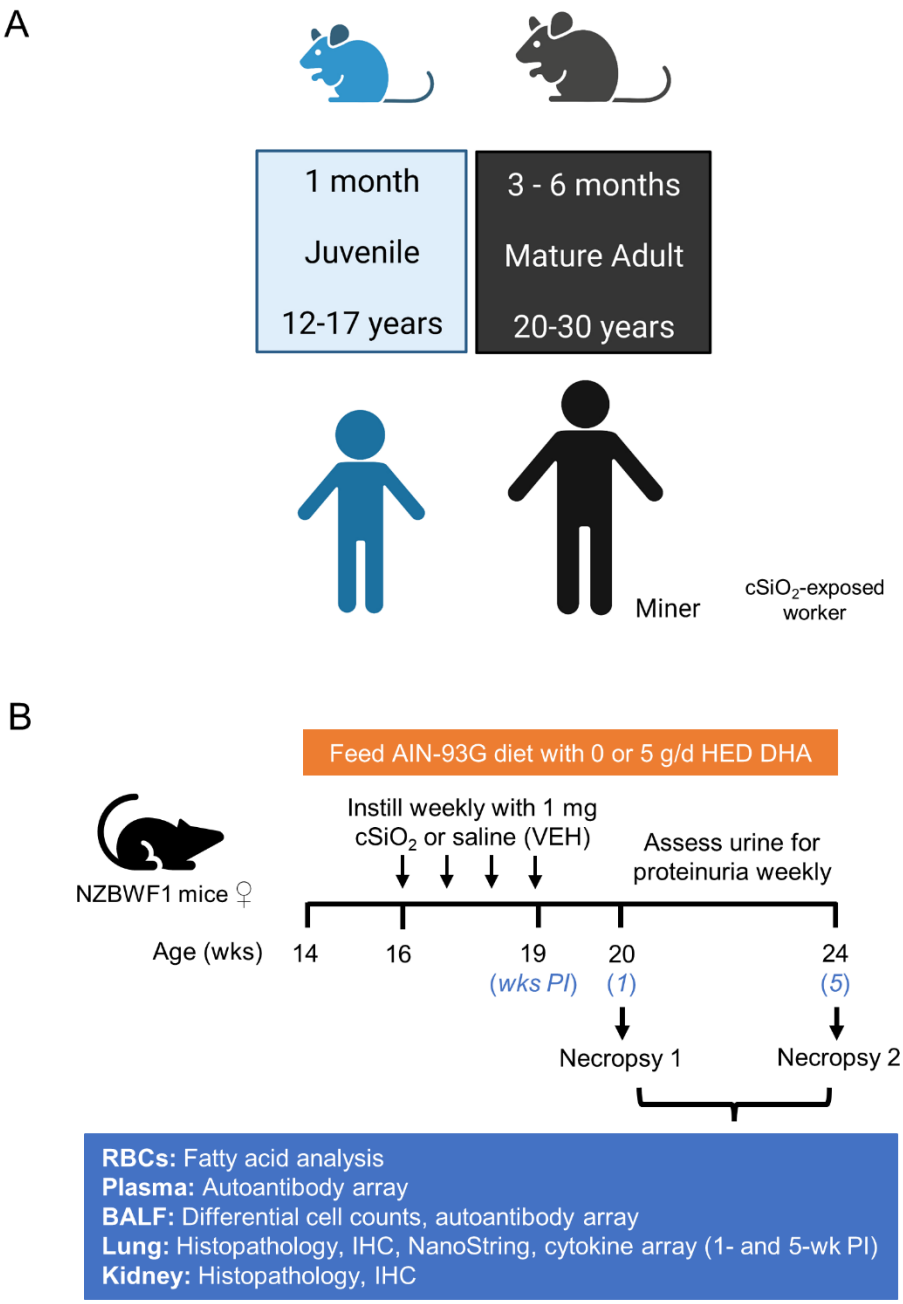

Figure 3.1: Rationale for mouse age selection and experimental design. (A) Graphical depiction of approximate age comparisons between mice and humans. Mice between 3-6 months of age more appropriately model the age of adult humans, and by extension, $cSiO_2$-exposed workers (170). **(B)** Female NZBWF1 mice were obtained at 14 wks of age and were initiated on either AIN-93G (CON) diet or diet enriched with 1% DHA (5 g/d HED). Beginning at 16 wks of age, mice were intranasally instilled with either saline (VEH) or 1 mg $cSiO_2$ once a wk for 4

Figure 3.1 (cont'd):
consecutive wks. Proteinuria was assessed weekly starting at 20 wks of age to monitor disease progression. Six animals per exposure/treatment group were sacrificed at 20 wks of age (1 wk PI), and the remaining 6 mice per group/treatment were euthanized at 24 wks of age (5 wk PI). At both timepoints, BALF was collected for differential cell counts and AAb microarray; plasma was collected for AAb microarray and fatty acid analysis; lung and kidney tissues were collected for histopathology, IHC, morphometric analysis, NanoString, and cytokine multiplex array.

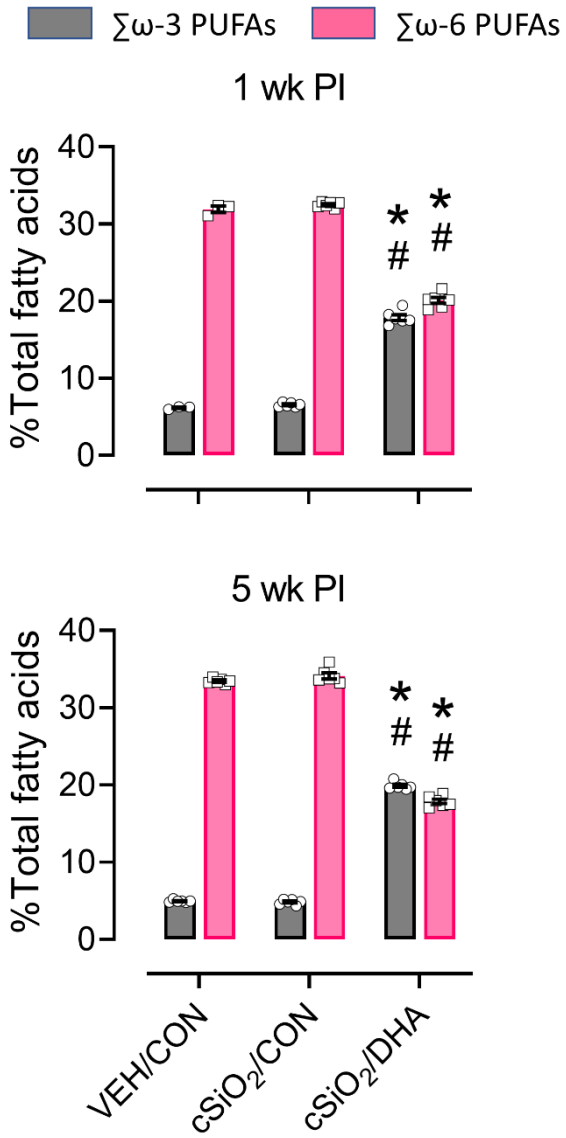

Figure 3.2: DHA supplementation skews long chain PUFA profile. In VEH/CON and $cSiO_2$/CON mice total omega-6 fatty acids were more abundant than omega-3 fatty acids in RBC cell membranes at both 1- and 5-wk PI. In $cSiO_2$/DHA mice, total omega-6 fatty acids were significantly reduced whereas total omega-3 fatty acids were significantly increased at both timepoints. p <0.05; * Significantly different from VEH/CON, # Significantly different from $cSiO_2$/CON.

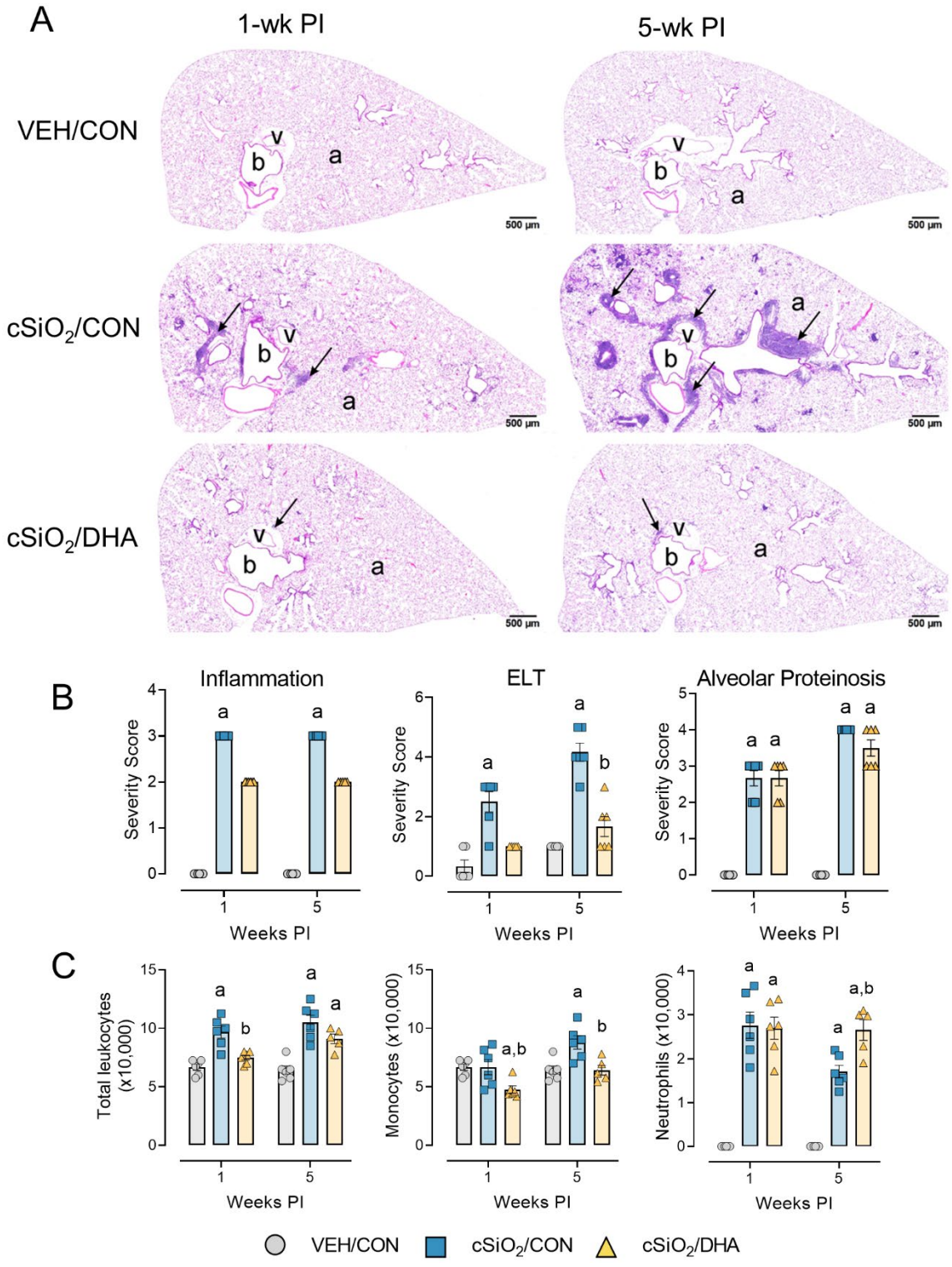

Figure 3.3: DHA suppresses $cSiO_2$-induced pulmonary perivascular and peribronchiolar lymphoid cell infiltrate. (A) Light photomicrographs of hematoxylin and eosin-stained lung tissue sections from mice instilled with saline vehicle fed CON diet (VEH/CON), mice instilled with $cSiO_2$ fed CON diet ($cSiO_2$/CON), and mice instilled with $cSiO_2$ fed DHA-enriched diet

Figure 3.3 (cont'd):
($cSiO_2$/DHA). $cSiO_2$ exposure resulted in perivascular and peribronchiolar infiltration of mononuclear lymphoid cells at 1 wk PI, with even greater infiltration (ectopic lymphoid tissue, ELT, arrows) at 5 wks PI. DHA attenuated ELT formation at both timepoints. b, bronchioles; v, blood vessel; a, alveolar parenchyma. **(B)** Graphic representation of semi-quantitative severity scores following assessment criteria of (1) minimal (<10%); (2) slight (10-25%); (3) moderate (26-50%); (4) marked (51-75%); and (5) severe (>75%) amount of tissue affected. **(C)** $cSiO_2$ instillation caused significant increase in total leukocytes, monocytes, and neutrophils in the BALF. DHA significantly reduced total leukocyte and monocyte cellularity in the BALF but did not influence neutrophils. $p<0.05$; a, Significantly different from VEH/CON; b, Significantly different from $cSiO_2$/CON.

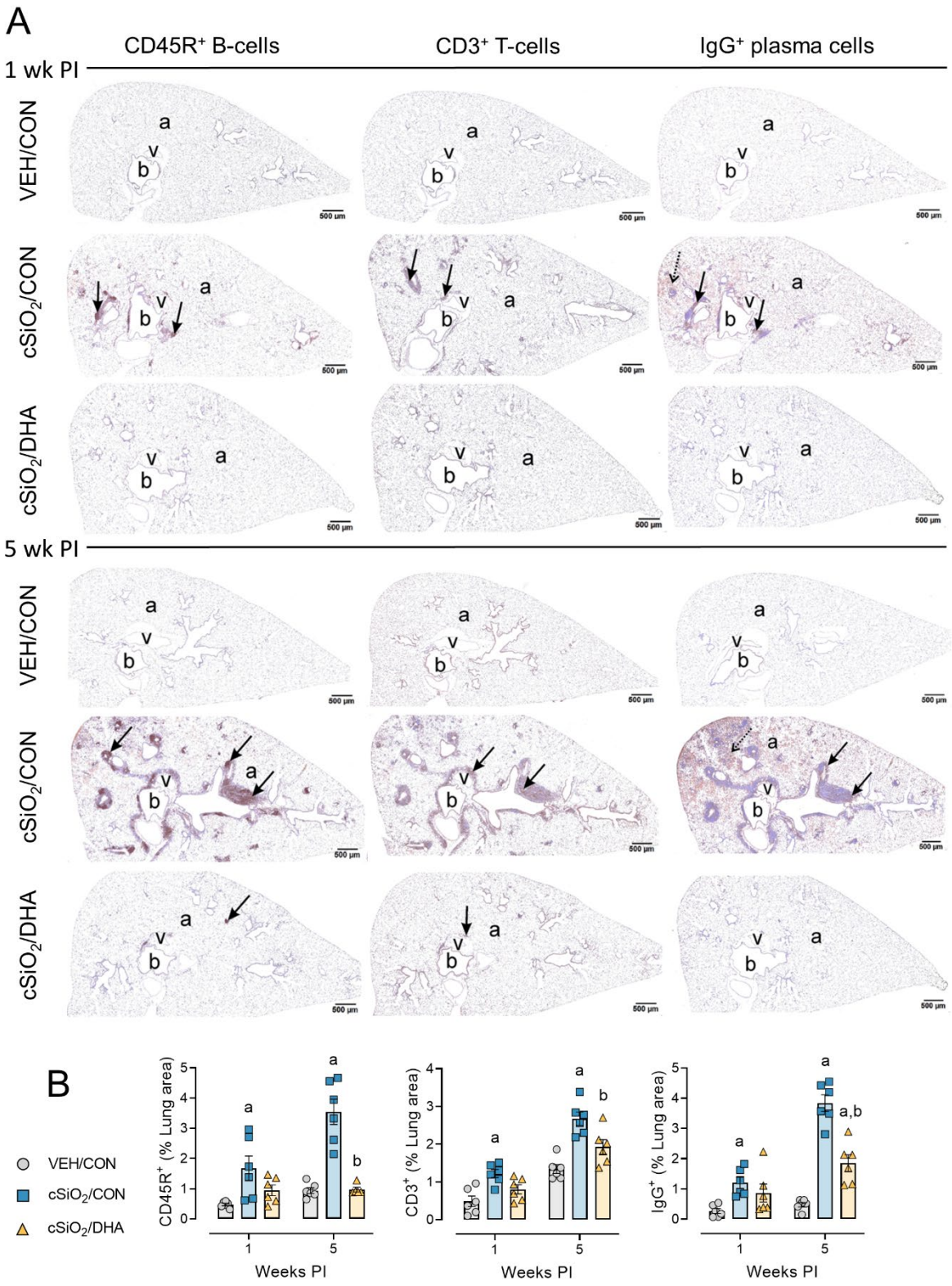

Figure 3.4: DHA inhibits lung infiltration of perivascular CD45R$^+$ B-cells, CD3$^+$ T-cells, and IgG$^+$ plasma cells. Light photomicrographs of perivenous ectopic lymphoid tissue (ELT)

Figure 3.4 (cont'd):
immunohistochemically stained for $CD45R^+$ B lymphoid cells, $CD3^+$ T-cells, and IgG^+ plasma cells in lungs of VEH/CON, $cSiO_2$/CON, and $cSiO_2$/DHA mice **(A)**. $cSiO_2$ treatment triggered interstitial infiltration of $CD45R^+$ B-cells, $CD3^+$ T-cells, and IgG^+ plasma cells at 1 wk PI, with even greater lymphoid infiltrates at 5 wk PI. Arrows, lymphoid cell infiltrates; b, bronchioles; v, blood vessels; a, alveolar parenchyma. DHA treatment significantly attenuated lymphoid cell infiltration present at 1 and 5 wk PI. **(B)** Graphical representation of morphometrically determined density of $CD45R^+$ B-cells, $CD3^+$ T-cells, and IgG^+ plasma cells in lung tissue. p <0.05; a, Significantly different from VEH/CON; b, Significantly different from $cSiO_2$/CON.

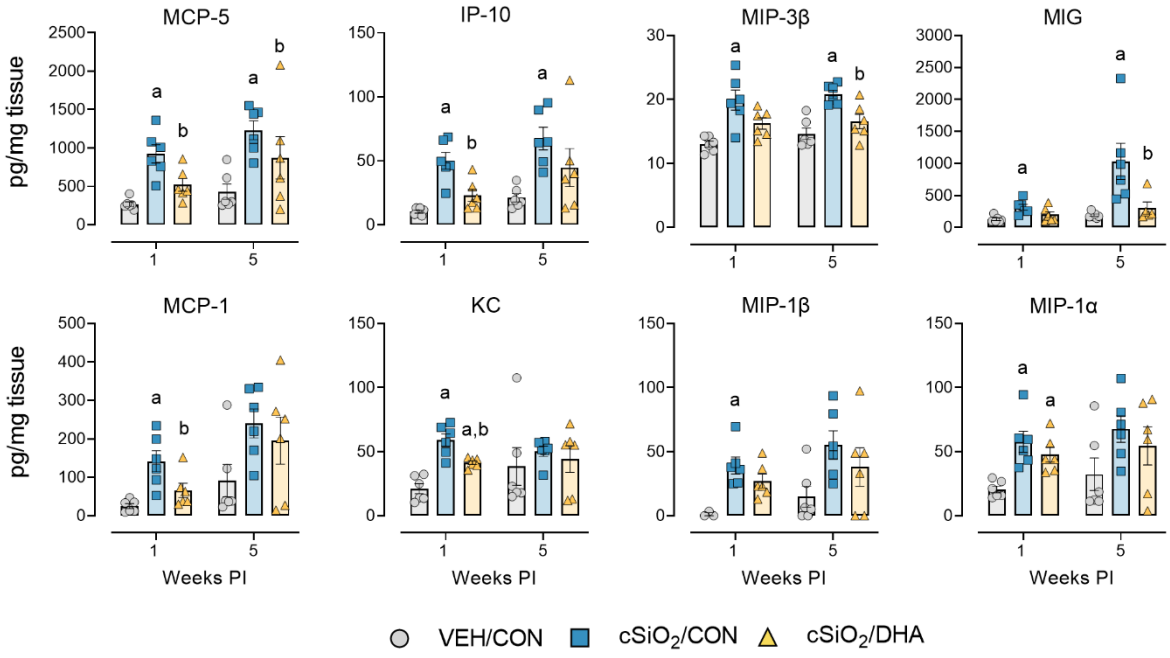

Figure 3.5: DHA consumption suppressed $cSiO_2$-induced chemokine protein expression in lung tissue. Proinflammatory cytokine production was measured in lung tissue homogenate using a multiplex cytokine discovery assay. Cytokine production significantly increased with $cSiO_2$ exposure and was attenuated with the DHA-enriched diets at either 1 or 5 wk PI. p<0.05; a, Significantly different from VEH/CON; b, Significantly different from $cSiO_2$/CON.

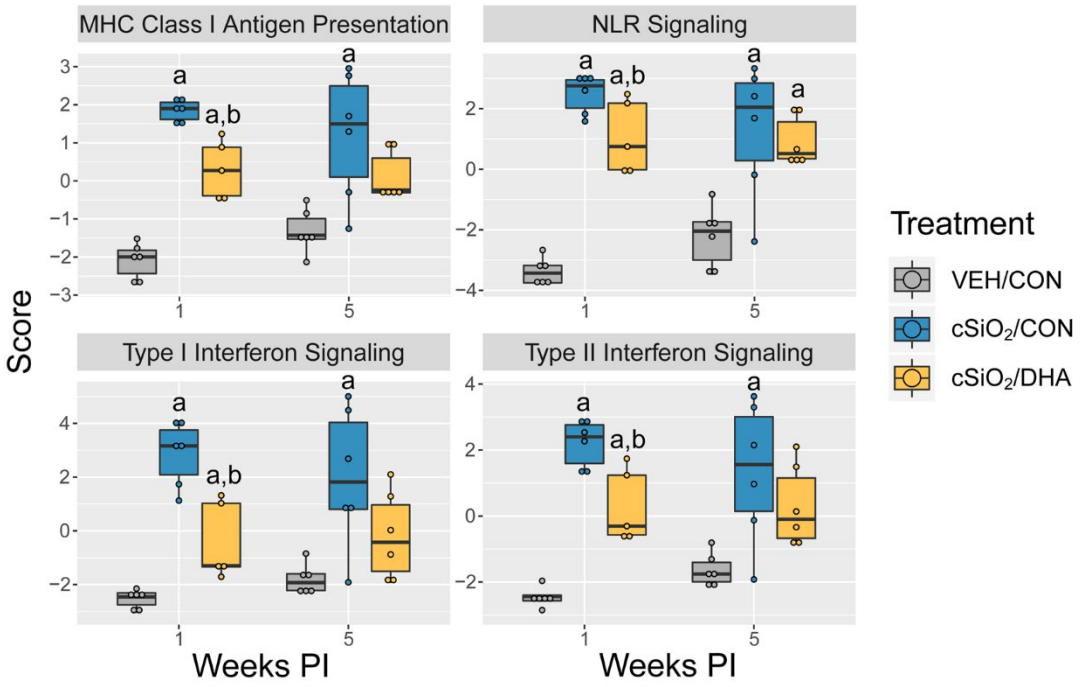

Figure 3.6: Effect of DHA-enriched diet on select autoimmune pathways in lung tissue 1- and 5-wks post-$cSiO_2$ instillation. Pathway Z scores are presented as Tukey box-plots for select pathways of interest for lung tissue. Within a tissue type, different letters indicate that the treatment groups are significantly different ($p<0.05$) as described in Materials and Methods. $cSiO_2$ exposure led to significant enrichment of MHC Antigen Presentation, NLR signaling, and Type I/II Interferon Signaling Pathways. DHA significantly reduced pathway Z scores for MHC Antigen Presentation and Type I/II Interferon Signaling at 1-wk PI and for NLR signaling at both 1 and 5 wk PI. p <0.05; a, Significantly different from VEH/CON; b, Significantly different from $cSiO_2$/CON.

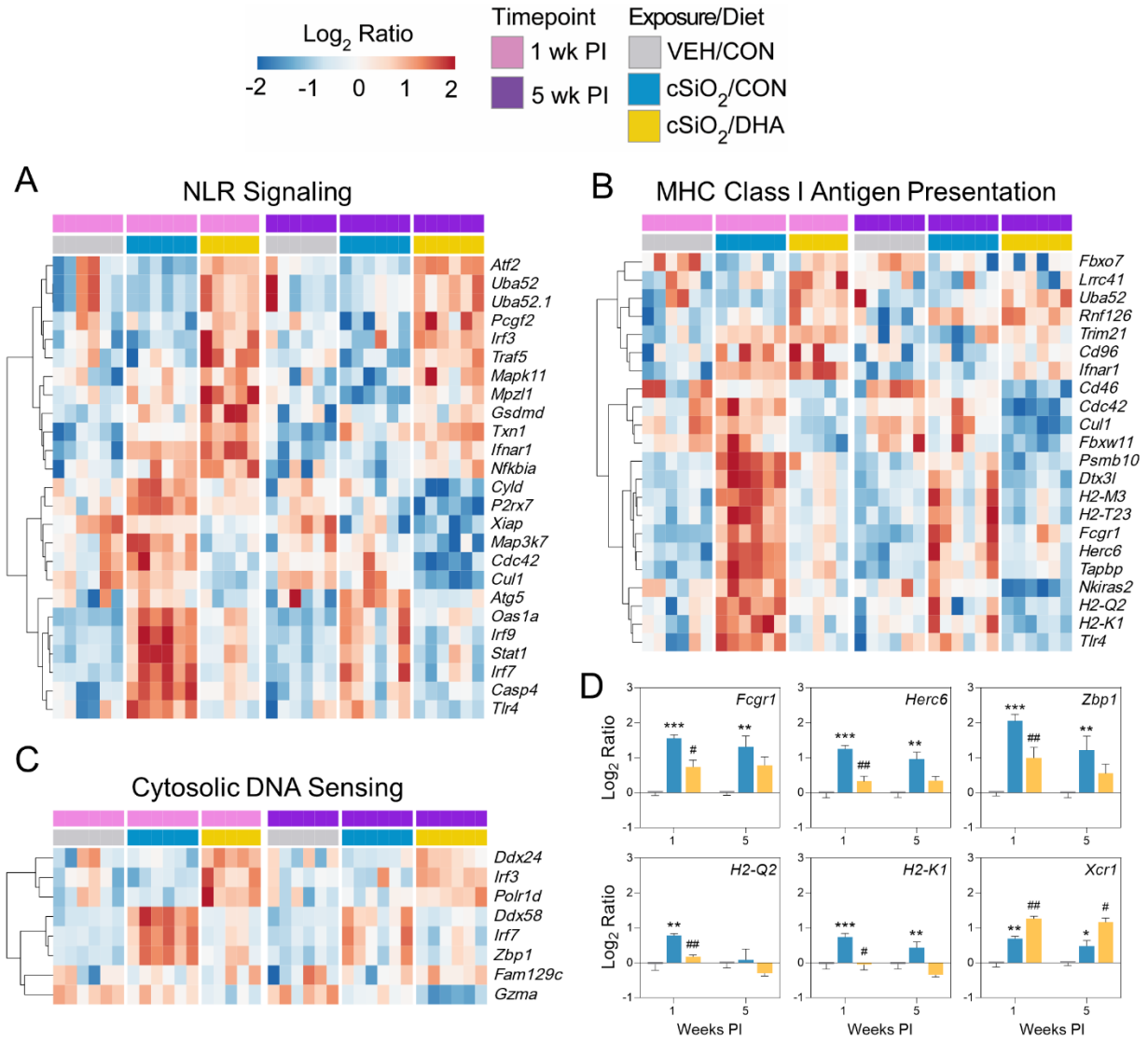

Figure 3.7: Representative DHA-responsive genes associated with (A) NLR Signaling, (B) Cytosolic DNA Sensing, and (C) MHC Class I Antigen Presentation pathways in lung tissue 1 and 5 wk PI with $cSiO_2$. Gene expression data were obtained using the NanoString Autoimmune Profiling gene panel and are shown as $\log_2$ ratios for $cSiO_2$/CON and $cSiO_2$/DHA treatment groups with respect to the VEH/CON group ($\log_2$ ratio = 0). For each pathway, heatmaps with unsupervised hierarchical clustering (Euclidian distance method) by gene show $\log_2$ expression values for all genes identified as differentially expressed in response to either $cSiO_2$ exposure or DHA-enriched diet (FDR q<0.05, 1.5-fold change). **(D)** The mean $\log_2$ ratio values + SEM for selected genes of interest are also shown for each pathway. For $cSiO_2$/CON as compared to VEH/CON, *, FDR-corrected q<0.05; **, q<0.01; and ***, q<0.001. For $cSiO_2$/DHA vs $cSiO_2$/CON, $^{\#}$, FDR-corrected q<0.05; $^{\#\#}$, q<0.01; and $^{\#\#\#}$, q<0.001.

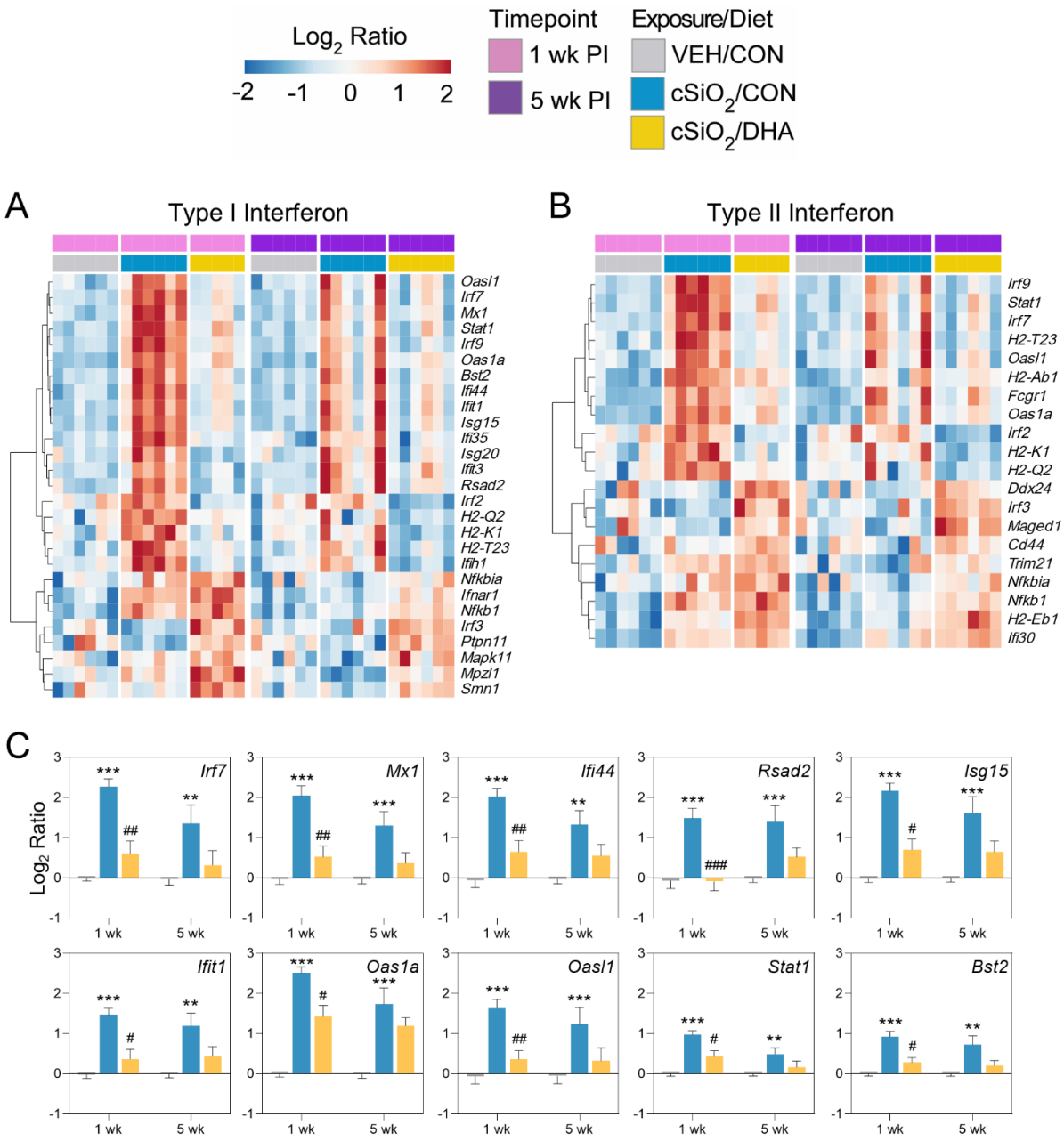

Figure 3.8: Representative DHA-responsive genes associated with (A) Type I Interferon and (B) Type II Interferon pathways in lung tissue 1 and 5 wks post instillation with $cSiO_2$. Gene expression data were obtained using the NanoString Autoimmune Profiling gene panel and are shown as log_2 ratios for $cSiO_2$/CON and $cSiO_2$/DHA treatment groups with respect to the VEH/CON group (log_2 ratio = 0). For each pathway, heatmaps with unsupervised hierarchical clustering (Euclidian distance method) by gene show log_2 expression values for all genes identified as differentially expressed in response to either $cSiO_2$ exposure or the DHA-enriched diet (FDR q<0.05, 1.5-fold change). **(C)** The mean log_2 ratio values + SEM for selected genes of interest is also shown for each pathway. For $cSiO_2$/CON as compared to VEH/CON, *, FDR-corrected q<0.05; **, q<0.01; and ***, q<0.001. For $cSiO_2$/DHA vs $cSiO_2$/CON, $^{\#}$, FDR-corrected q<0.05; $^{\#\#}$, q<0.01; and $^{\#\#\#}$, q<0.001.

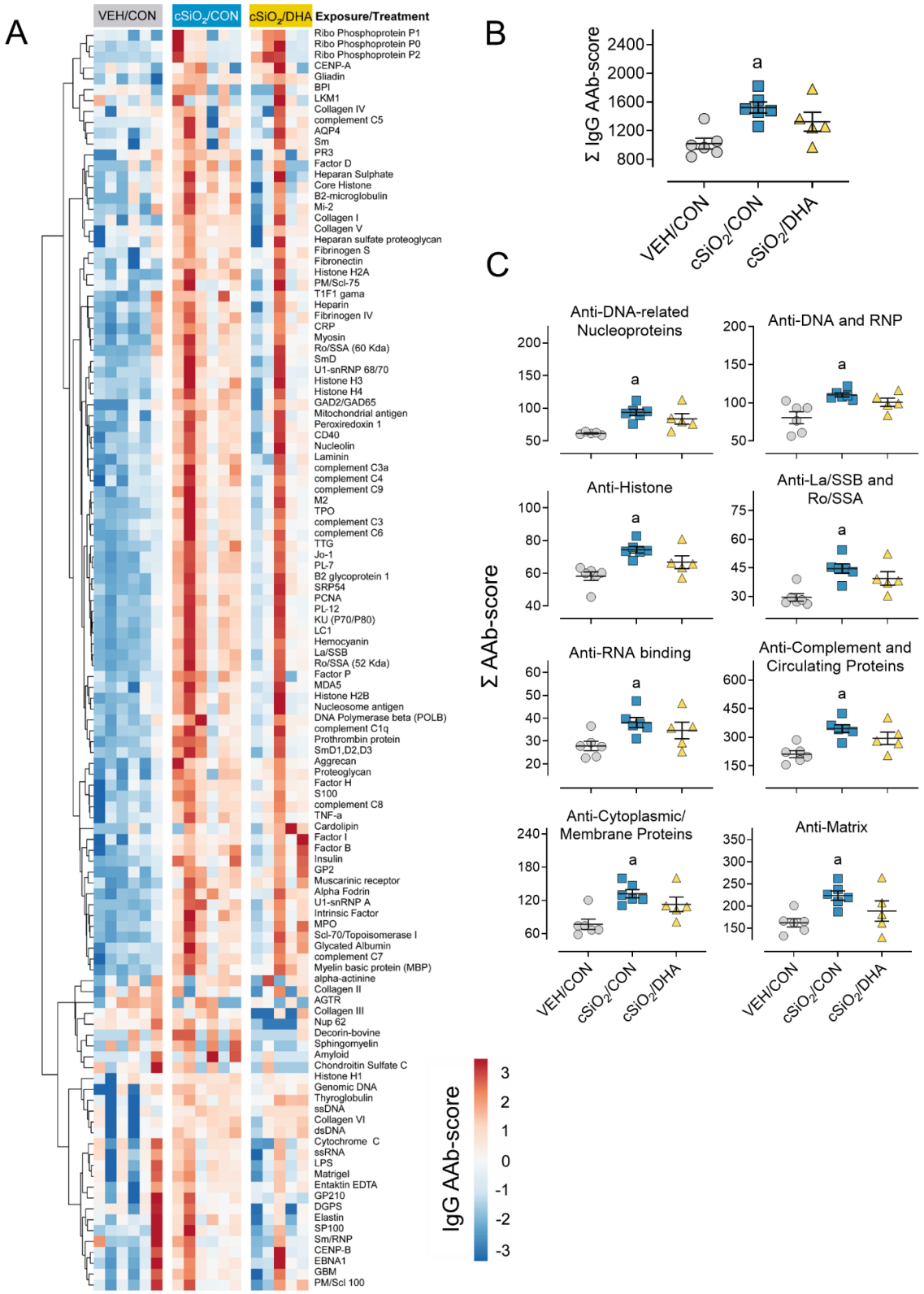

Figure 3.9: DHA feeding modestly affects $cSiO_2$ induced IgG AAb responses in the BALF of adult mice at 5 wks PI. (A) AAb-score values for the expression of 120 IgG AAbs are illustrated

Figure 3.9 (cont'd):
in a heatmap using unsupervised clustering (Euclidian distance method). Scale bar values reflect the range of variance stabilized AAb scores, which are centered across rows. **(B)** DHA did not significantly reduce $cSiO_2$-triggered total IgG detected in the BALF. **(C)** $cSiO_2$ exposure significantly increased various classes of autoimmunity-related AAbs detected in the BALF. A downward trend was observed in the same classes of $cSiO_2$-triggered AAbs when mice were fed DHA. $p < 0.05$; a, Significantly different from VEH/CON.

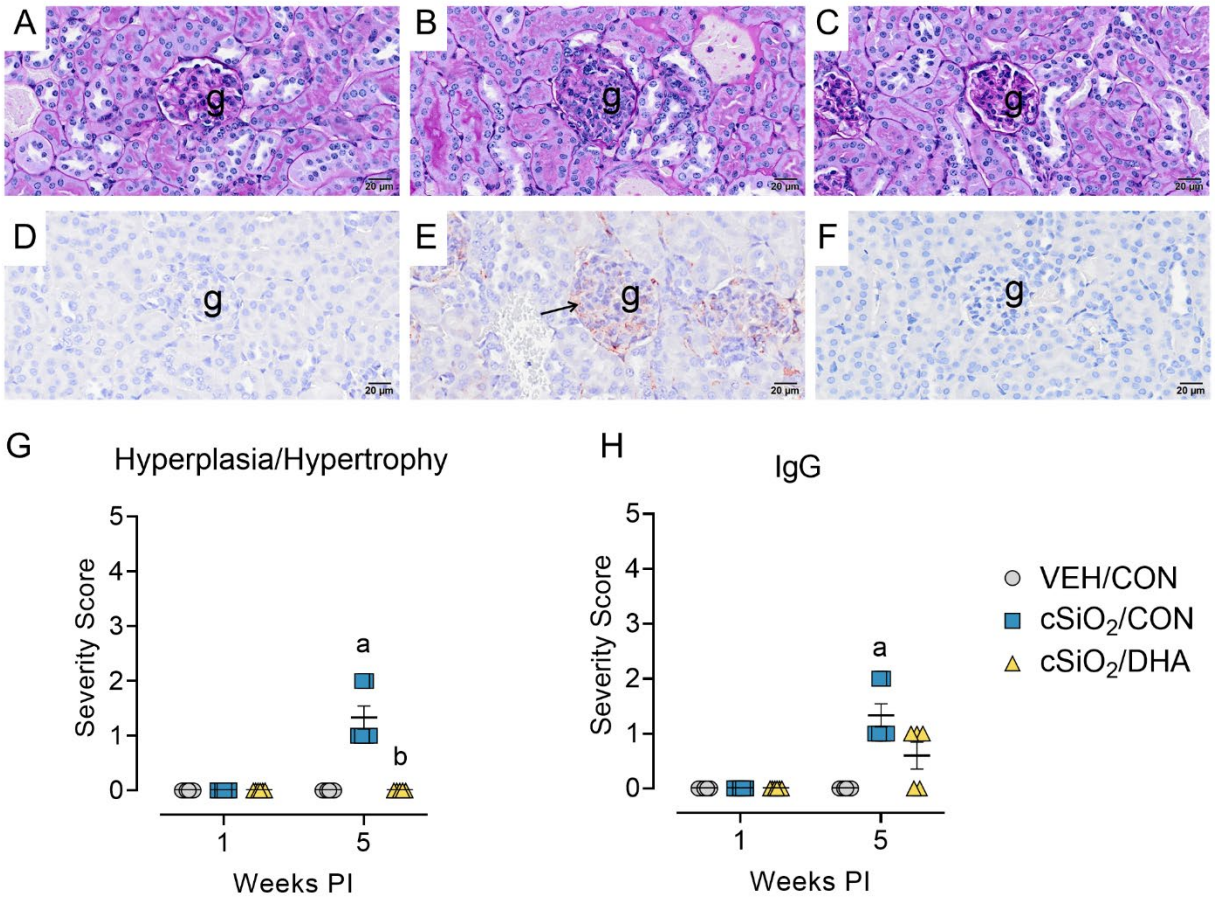

Figure 3.10: $cSiO_2$-triggered membranoproliferative glomerulonephritis and glomerular IgG deposition at 5 wk PI and DHA-induced attenuation. Light photomicrographs of kidney tissue stained with periodic acid Schiff (PAS) and hematoxylin **(A, B, C)** and immunohistochemically stained for IgG with hematoxylin counterstain **(D, E, F).** VEH/CON **(A, D)**, $cSiO_2$/CON **(B, E)**, and $cSiO_2$/DHA mice **(C, F)**. $cSiO_2$-exposed mice **(B, E)** had modest increases in glomerular size, cellularity, size, and IgG deposition. No histopathology was observed in VEH/CON mice **(A, D)** and DHA-fed mice **(C, F).** Individual kidney sections were semi-quantitatively scored based on the modified International Society of Nephrology/Renal Pathology Lupus Nephritis Classification system described methods for lupus nephritis score for hyperplasia/hypertrophy **(G)** and IgG deposition **(H)**. $cSiO_2$/CON mice had significantly increased severity scores for hyperplasia/hypertrophy and IgG deposition at 5-wk PI. DHA enriched diets attenuated renal hyperplasia and hypertrophy. g, glomeruli; arrow, IgG proteinaceous material. $p < 0.05$; a, Significantly different from VEH/CON; b, Significantly different from $cSiO_2$/CON.

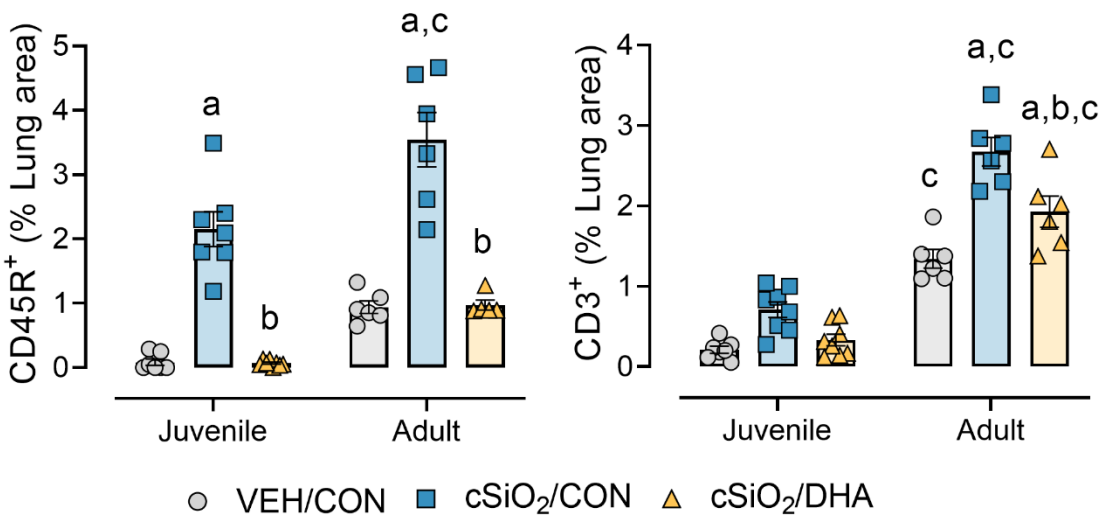

Figure 3.11: $cSiO_2$-triggered infiltration of lymphoid cells is greater in adult NZBWF1 mice compared to juveniles from previous studies. $cSiO_2$ exposure induced significant infiltration of **(A)** $CD45R^+$ B-cells at 5 wks PI in both juvenile and adult mice. $cSiO_2$ exposure induced significant infiltration of **(B)** $CD3^+$ T-cells at 5 wks PI only in adult mice and not in juveniles (16). $CD45R^+$ B-cell and $CD3^+$ T-cell density was significantly greater in adult mice compared to juveniles. DHA significantly reduced $CD45R^+$ B-cell infiltration in both juvenile and adult mice, and $CD3^+$ T-cell infiltration in adult $cSiO_2$-exposed mice. Morphometric data from the present study and a previous study (16) was compared using a Two-Way ANOVA. p <0.05; a, Significantly different from VEH/CON; b, Significantly different from $cSiO_2$/CON.; c, Significantly different from juvenile mice within same exposure/treatment group.

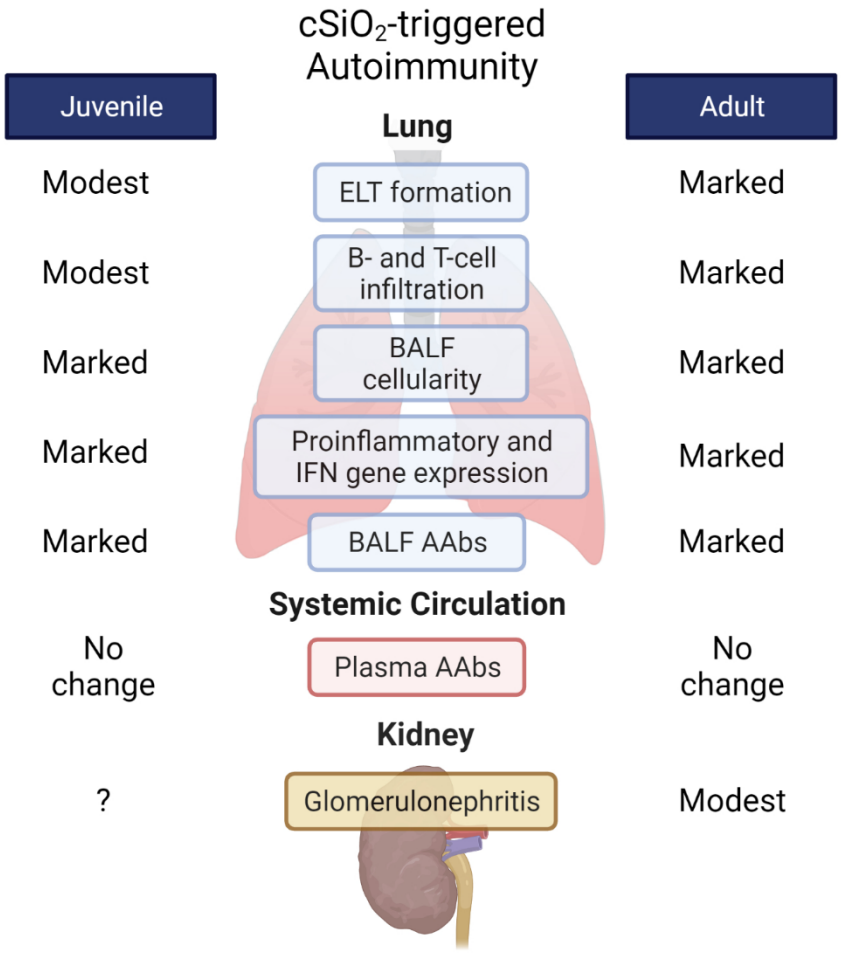

Figure 3.12: Age-dependent responses in $cSiO_2$-triggered endpoints observed at 5 wk PI. Diagrammatical summary of severity of $cSiO_2$-triggered endpoints in juvenile and adult female NZBWF1 mice necropsied at 5-wk PI. In a previous study from our lab, it has been demonstrated that $cSiO_2$ exposure in juveniles leads to a mixture of modest to marked changes in the lung, and no observable changes regarding plasma AAbs and glomerulonephritis at 5 wk PI (16). In the present study, $cSiO_2$ exposure in adult mice sacrificed at 5 wk PI resulted in more marked pulmonary pathology and modest renal pathology demonstrating the age-dependent response to $cSiO_2$ in this experimental model.

TABLES

Table 3.1: Formulation of experimental diets.

	Experimental Diet	
	CON	**DHA**
Macronutrient	**(g/kg total diet)**	
Carbohydrates		
Corn Starch	398	398
Maltodextrin (Dyetrose)	132	132
Sucrose	100	100
Cellulose	50	50
kcal (%total)	63.2	63.2
Proteins		
Casein	200	200
L-Cysteine	3	3
kcal (% of total)	19.7	19.7
Fats		
Corn Oil	10	10
High-Oleic Sunflower Oil	60	35
DHA-enriched Algal Oil	0	25
kcal (% of total)	17.1	17.1
Other		
AIN93G Mineral Mix	35	35
AIN93G Vitamin Mix	10	10
Choline Bitartrate	3	3
TBHQ Antioxidant	0.01	0.01

Values are shown as mass g/kg diet. Composition of diet based on manufacturer descriptions. Corn oil contained 612 g/kg linoleic acid and 26 g/kg oleic acid. High-oleic safflower oil contained 750 g/kg oleic acid and 140 g/kg linoleic acid. Algal oil contained 395 DHA g/kg and 215 g oleic acid g/kg. 10 g/kg diet is calorically equivalent to a human equivalent dose of 5 g/d.

Table 3.2 Fatty acid content of RBCs at 1 and 5 wk post-instillation.

		Experimental group					
		1 wk PI			5 wk PI		
		VEH/CON	$cSiO_2$/CON	$cSiO_2$/DHA	VEH/CON	$cSiO_2$/CON	$cSiO_2$/DHA
Common Name	Chemical Formula	*(% of total fatty acid)*					
Lauric Acid	C14:0	0.16 ± 0.01	0.16 ± 0.00	0.26 ± 0.01*†	0.14 ± 0.00	0.16 ± 0.00	0.25 ± 0.01*†
Palmitic Acid	C16:0	28.38 ± 0.06	28.02 ± 0.09	31.85 ± 0.26*†	27.1 ± 0.07	26.37 ± 0.39	30.88 ± 0.35†
Palmitelaidic Acid	C16:1n7t	0.13 ± 0.03	0.09 ± 0.01	0.10 ± 0.01	0.10 ± 0.01	0.12 ± 0.02	0.08 ± 0.01
Palimitoleic Acid	C16:1n7	0.51 ± 0.01	0.58 ± 0.02	0.53 ± 0.01	0.50 ± 0.01	0.58 ± 0.04	0.55 ± 0.30
Stearic Acid	C18:0	13.76 ± 0.21	13.45 ± 0.11	12.90 ± 0.16*	14.21 ± 0.02	14.12 ± 0.2	13.21 ± 0.14*†
Elaidic Acid	C18:1t	0.37 ± 0.12	0.20 ± 0.02	0.23 ± 0.04	0.29 ± 0.06	0.24 ± 0.05	0.21 ± 0.02
Oleic Acid	C18:1 ω-9	17.68 ± 0.44	17.56 ± 0.12	15.47 ± 0.15*†	18.33 ± 0.11	18.57 ± 0.07	16.30 ± 0.10*†
Linoelaidic Acid	C18:2 ω-6t	0.13 ± 0.02	0.07 ± 0.01*	0.08 ± 0.01	0.12 ± 0.02	0.08 ± 0.01	0.08 ± 0.00
Linoleic Acid	C18:2 ω-6	8.31 ± 0.08	9.16 ± 0.23*	10.94 ± 0.15*†	7.59 ± 0.07	8.77 ± 0.62	10.40 ± 0.24*
Arachidic Acid	C20:0	0.13 ± 0.02	0.10 ± 0.00	0.10 ± 0.01*	0.11 ± 0.00	0.11 ± 0.00	0.10 ± 0.00*†
Gamma-Linolenic Acid	C18:3 ω-6	0.05 ± 0.01	0.05 ± 0.00	0.02 ± 0.00*†	0.06 ± 0.00	0.06 ± 0.01	0.03 ± 0.00*†
Eicosenoic Acid	C20:1n9	0.32 ± 0.02	0.29 ± 0.00	0.19 ± 0.01*†	0.32 ± 0.01	0.33 ± 0.01	0.19 ± 0.01*†
Alpha-Linolenic Acid	C18:3 ω-3	0.02 ± 0.00	0.03 ± 0.00	0.03 ± 0.00	0.02 ± 0.00	0.02 ± 0.00	0.02 ± 0.00
Eicosadienoic Acid	C20:2 ω-6	0.26 ± 0.01	0.26 ± 0.01	0.20 ± 0.01*†	0.22 ± 0.01	0.22 ± 0.01	0.19 ± 0.01*†
Behenic Acid	C22:0	0.10 ± 0.01	0.09 ± 0.01	0.07 ± 0.00*†	0.12 ± 0.04	0.07 ± 0.00	0.08 ± 0.01
Dihomo-gamma-linolenic Acid	C20:3 ω-6	1.23 ± 0.02	1.27 ± 0.03	0.99 ± 0.05*†	1.27 ± 0.01	1.22 ± 0.03	1.11 ± 0.06*
Arachidonic Acid	C20:4 ω-6	19.35 ± 0.40	19.34 ± 0.20	7.32 ± 0.24*†	21.03 ± 0.13	20.84 ± 0.24	5.82 ± 0.20*†
Lignoceric Acid	C24:0	0.18 ± 0.02	0.19 ± 0.01	0.18 ± 0.02	0.17 ± 0.01	0.17 ± 0.01	0.17 ± 0.01
Eicosapentaenoic Acid (EPA)	C20:5 ω-3	0.25 ± 0.01	0.30 ± 0.02	3.65 ± 0.18*†	0.09 ± 0.01	0.10 ± 0.01	4.45 ± 0.16*†
Nervonic Acid	C24:1 ω-9	0.17 ± 0.03	0.17 ± 0.01	0.15 ± 0.02	0.18 ± 0.01	0.18 ± 0.01	0.19 ± 0.01
Docosatetraenoic Acid	C22:4n6	2.01 ± 0.02	1.82 ± 0.04*	0.42 ± 0.01*†	2.23 ± 0.03	2.02 ± 0.13	0.20 ± 0.01*†
Adrenic Acid	C22:4 ω-6	2.01 ± 0.02	1.82 ± 0.04	0.42 ± 0.01	2.23 ± 0.03	2.02 ± 0.13	0.2 ± 0.01
Omega-6 Docosapentaenoic Acid	C22:5 ω-6	0.58 ± 0.02	0.55 ± 0.03	0.12 ± 0.00*†	0.95 ± 0.02	0.92 ± 0.04	0.05 ± 0.00*†
Omega-3 Docosapentaenoic Acid	C22:5 ω-3	0.66 ± 0.01	0.65 ± 0.01	0.92 ± 0.02*†	0.32 ± 0.01	0.29 ± 0.02	0.9 ± 0.01*†
Docosahexaenoic Acid (DHA)	C22:6 ω-3	5.25 ± 0.08	5.60 ± 0.09	13.28 ± 0.22*†	4.53 ± 0.06	4.44 ± 0.11	14.52 ± 0.13*†
Omega-3 Index: EPA + DHA	C20:5 ω-3 + C22:6 ω-3	5.50 ± 0.09	5.90 ± 0.11	16.93 ± 0.36*†	4.62 ± 0.07	4.54 ± 0.12	18.97 ± 0.20*†
	Σ SFA	42.71 ± 0.12	42.02 ± 0.13*	45.35 ± 0.18*†	41.85 ± 0.09	41.0 ± 0.35	44.69 ± 0.25*†
	Σ MUFA	19.18 ± 0.65	18.90 ± 0.12	16.67 ± 0.18*†	19.72 ± 0.14	20.03 ± 0.13	17.53 ± 0.13*†
	Σ PUFA (ω-3)	6.19 ± 0.10	6.57 ± 0.12	17.88 ± 0.36*†	4.96 ± 0.07	4.84 ± 0.14	19.90 ± 0.20*†
	Σ PUFA (ω-6)	31.93 ± 0.43	32.52 ± 0.14	20.10 ± 0.39*†	33.46 ± 0.14	34.13 ± 0.40	17.89 ± 0.29*†

Analysis of fatty acid profiles of RBCs from experimental groups 1 and 5 wk post-instillation as determined by OmegaQuant Analytics, LLC. $p < 0.05$; * Significant compared to VEH/CON, † Significant compared to $cSiO_2$/CON.

CHAPTER 4: COMPARATIVE EFFECTS OF INTRANASAL AND INTRAPERITONEAL E. COLI LIPOPOLYSACCHARIDE EXPOSURE ON INDUCTION OF INFLAMMATION AND AUTOIMMUNITY IN LUPUS-PRONE NZBWF1 MICE

Lauren K. Heine[1,2], Lichchavi D. Rajasinghe[3], James G. Wagner[2,4], Ryan P. Lewandowski[4], Quan-Zhen Li[5], Alexa L. Richardson[3], Ashleigh N. Tindle[4], Jenan J. Shareef[4], Jack R. Harkema[2,4], and James J. Pestka[2,3,6]

[1]Department of Pharmacology and Toxicology, Michigan State University, East Lansing, MI

[2]Institute for Integrative Toxicology, Michigan State University, East Lansing, MI

[3]Department of Food Science and Human Nutrition, Michigan State University, East Lansing, MI

[4]Department of Pathobiology and Diagnostic Investigation, Michigan State University, East Lansing, MI

[5]Department of Immunology and Internal Medicine, IIMT Microarray Core Facility, University of Texas Southwestern Medical Center, Dallas, TX

[6]Department of Microbiology and Molecular Genetics, Michigan State University, East Lansing, MI

PUBLICATION NOTICE

The following chapter is in preparation to be submitted to *Frontiers in Immunology*.

ABSTRACT

Introduction: Systemic lupus erythematosus (lupus) is a chronic, prototypical autoimmune disease driven by a combination of heredity and exposures to environmental agents such as microbes and toxicants. While repeated intraperitoneal (IP) exposure to gram negative bacterial lipopolysaccharide (LPS) triggers early onset in autoimmune glomerulonephritis and mortality in lupus-prone mice, the effects of pulmonary exposure to LPS in this preclinical model of lupus has yet to be evaluated. To address this knowledge gap, we assessed the effects of subchronic airway exposure to LPS via intranasal (IN) instillations on the induction of autoimmunity in NZBWF1 lupus-prone mice and related these findings to the effects of equivalent LPS dosing via IP route.

Methods: Female 8-wk old NZBWF1 mice were exposed to either sterile saline vehicle (VEH) or smooth *Escherichia coli* (*E. coli*) LPS (0.8 μg/g bw) via IN instillation or IP injection twice per wk for 5 consecutive wks. Mice were necropsied 1 wk following the last LPS exposure and selected tissues were assessed for markers of inflammation/autoimmunity using conventional histopathology, immunohistochemistry, RT-PCR, and autoantigen protein microarray.

Results: LPS/IN mice exhibited inflammatory cell influx in bronchioalveolar lavage fluid (BALF), pulmonary ectopic lymphoid tissue (ELT) formation, and inflammatory gene expression in lung tissue compared to VEH/IN mice. In addition to pulmonary pathology, IN exposure to LPS elicited robust increases in IgM and IgG autoantibodies (AAb) for diverse autoantigens (AAgs) in BALF and, to a much lesser extent, in the plasma. In comparison, LPS/IP mice did not exhibit pulmonary pathology or AAb responses in the BALF but did demonstrate robust IgM AAb and modest IgG AAb responses in the plasma. Both LPS/IN and LPS/IP groups had enlarged spleens with conspicuous IgG deposition compared to their respective VEH controls. In the kidney, there were signs of early glomerulonephritis (hypertrophy, hypercellularity, and IgG deposition) that was most prominent in LPS/IP mice.

Discussion: Our findings demonstrate that i) short-term repeated IN exposure to LPS elicits intense lung inflammation and ectopic lymphoid neogenesis concurrently with pulmonary and systemic autoimmunity, ii) responses to short-term repeated IP exposure to LPS is primarily localized to the spleen and systemic circulation, and iii) IP LPS delivery was more effective in inducing autoimmune-mediated glomerulonephritis than the IN route.

INTRODUCTION

Systemic lupus erythematosus (lupus) is a devastating chronic autoimmune disease that affects multiple organ systems and predominantly afflicts women of color and child-bearing age (30). Lupus is characterized by unresolved inflammation and a breakdown of self-recognition by autoreactive lymphoid cells (e.g., B- and T-cells) leading to robust production of autoantibodies (AAbs) (177). Resultant AAbs bind to cognate autoantigens (AAgs) which deposit in other organs such as the kidney, leading to glomerulonephritis and eventually renal failure (178).

While genetic predilection plays an essential role in development of lupus, exposures to microbes and pathogen-associated molecular patterns (PAMPs) have been associated with lupus onset and increased morbidity and mortality (13, 52, 56, 57). Of high relevance, Gram-negative bacterial lipopolysaccharide (LPS) has been implicated in chronic inflammatory and autoimmune diseases (13-15, 177). Exposure to LPS can occur systemically as a result of Gram-negative bacterial infections such as salmonellosis or from the escape of opportunistic and benign Gram-negative bacterial species from the large intestine via a leaky gut (13). LPS exposure leads to classical activation of innate immune cell populations through toll-like receptor 4 (TLR4) which stimulates proinflammatory cytokine/chemokine and Type-I IFN expression via the activation of NF-κB and IFN regulatory factors (IRFs), respectively (177). LPS can also further exacerbate autoimmunity through triggering immunogenic cell death with consequent stimulation of

autoreactive B- and T-cells and breaking of immunological tolerance (56).

Consistent with the hypothesis that LPS is a trigger of autoimmunity, subchronic LPS exposure via the intraperitoneal route has been reported to induce autoimmunity in previous studies utilizing non-autoimmune C57BL/6 and BALB/c mice (179-182). Moreover, IP LPS treatment also accelerates autoimmune disease development in lupus prone NZBWF1, MRL/lpr (MRL) and BXSB mice (183-186). Autoimmune disease triggered by LPS has been linked to polyclonal B-cell activation, decreased immune complex uptake by macrophages, impaired clearance of circulating immune complexes, and elevated renal immune complex deposition (179-188).

In addition to systemic exposure, humans are also commonly exposed to LPS via inhalation, which can lead Gram-negative bacterial pulmonary infections (189, 190). Individuals can also inhale LPS when engaging in occupations centered around agriculture, textiles, and waste management (14, 191-193). Airborne LPS-containing organic dust mixtures, have been shown to incite inflammation with long-term exposure leading to diminished lung function (14). *In vivo* studies have likewise reported that inhalation exposure to LPS-containing organic dust mixtures leads to increased pulmonary pathology, proinflammatory and Type-I Interferon (IFN) gene responses in lung tissue, and induction of circulating AAbs present in the serum of rheumatoid arthritis (RA)-prone mice (54, 60).

Several preclinical studies have demonstrated that LPS can accelerate autoimmunity in female NZBWF1 lupus-prone mice (58, 194-196). A consistent constraint of these investigations is that they focused only on the effects of systemic exposure via intraperitoneal (IP) injections, in addition to only assessing endpoints in the serum and kidney (58, 194, 196, 197). Moreover, these same studies utilized LPS from pathogenic *Salmonella* species as a trigger for glomerulonephritis rather than LPS derived from other clinically and environmentally relevant strains such as *E. coli*.

To address these limitations, we ascertained how subchronic airway exposure to *E. coli* LPS via intranasal (IN) instillation influences inflammation and autoimmunity in NZBWF1 mice, and further compared these findings to those elicited from systemic IP LPS exposure using an equivalent dosing regimen.

MATERIALS AND METHODS

Animals and experimental design

Escherichia coli O55:B5 (Sigma Aldrich, Catalog #L2880) was dissolved into a solution for IP injections and IN instillations and were prepared fresh prior to each exposure. For both routes of exposure, stock LPS solutions were suspended in sterile phosphate buffered saline (PBS) and dissolved by sonication for 10 min and vortexed for 30 seconds.

Animal experiments were approved by the Michigan State University (MSU) Institutional Animal Care and Use Committee (IACUC) (AUF# 201800113). Six-wk-old female NZBWF1 mice (Jackson Laboratories, Bar Harbor, ME) were randomized into experimental groups following their arrival. Mice were housed three per cage and maintained at a constant temperature (21-24°C) and humidity (40-55%) with a 12-hr light/dark cycle throughout the study. For the entirety of the study, mice were fed modified American Institute of Nutrition (AIN)-93G diet (171) containing 70 g/kg of fat, 10 g/kg from food-grade corn oil and 60 g/kg from high-oleic safflower oil (LouAna, Brea, CA) which provided basal essential fatty acids. Diet was prepared biweekly, and mice were provided fresh food daily. Food reserves were stored at -20°C when not in use. Mice had access to food and water throughout the study.

The experimental design for this study is depicted in **Figure 4.1A**. Beginning at 8 wks of age, mice were treated one of four ways as designated by their assigned experimental group: (i) injected IP with sterile phosphate buffered saline (PBS) vehicle (VEH) (VEH/IP, n = 6), (ii)

injected IP with LPS (0.8 μg/g) (LPS/IP, n = 6), (iii) instilled IN with 25 μL sterile PBS VEH (VEH/IN, n = 6), or (iv) instilled IN with 25 μL LPS (0.8 μg/g) (LPS/IN, n = 6). Injections and instillations took place twice a wk for 5 consecutive wks. Prior to both injections and instillations, mice were anesthetized using 4% isoflurane. Each wk of LPS treatment, urine was collected from all experimental groups to monitor proteinuria (≥300 mg/dL protein) using reagent dipsticks (Cortez Diagnostics, Calabasas, CA) to assess nephritis progression. All mice were sacrificed following the last wk of exposures at 13 wks of age.

Necropsy

All experimental groups were terminated 1 wk after the final exposure at 13 wks of age. Mice were first anesthetized with sodium pentobarbital (56 mg/kg) administered via IP injection, followed by euthanasia through exsanguination of the abdominal aorta. Heparinized syringes were used to collect the blood from the abdominal aorta. Plasma was isolated from blood samples spun down at 3500 x g for 10 min at 4°C. Plasma was stored at -80°C for AAb microarray analysis. Bronchoalveolar lavage fluid (BALF) was collected from the whole lung as described previously (198). After completing inflammatory cell quantification in the BALF, samples were spun down at 465 x g for 15 min at 4°C and the cell fraction was used to perform differential cell counts. Remaining supernatant was stored at -80°C for AAb microarray analysis. Left lung lobes were fixed in 10% neutral buffered formalin (NBF) (Fischer Scientific, Pittsburgh, PA) for 1 hr at a constant pressure of 30 cm H_2O. Spleens were weighed prior to sectioning. The head of the spleen was fixed in 10% NBF, along with one whole kidney. The caudal lung lobe was stored in RNAlater at (Thermo Fisher Scientific, Wilmington, DE) at 4°C for 16 hr, then moved to -80°C. All tissues fixed in NBF remained in fixative for 48 hrs prior to being processed for histology. Remaining right lung lobes and half a kidney were snap frozen and stored at -80°C.

BALF cell quantitation and identification

Total leukocyte cell counts in BALF were performed using a hemocytometer. In preparation of differential cell counts, BALF cells were immobilized on glass slides using centrifugal forces (Shandon Cytospin 3) and spun down at 40 x g for 10 min. Cytological slides were air dried and then stained using Diff-Quick (Fisher Scientific). The remaining BALF was centrifuged at 465 x g for 15 min and supernatant was collected and stored at -80°C for subsequent AAb analysis. Differential cell counts were performed by counting 200 cells total per cytological slide and morphological criteria was used to identify the number of macrophages/monocytes, neutrophils, and lymphocytes.

Lung histopathology

Left lung lobes were intratracheally fixed in formalin for 48 hrs at a constant gravimetric fluid pressure of 30 cm. Using random start, the lobe was sectioned into four transverse lung blocks (~2 mm each). Tissue blocks were embedded in paraffin and tissues were cut at 5 μm thickness, deparaffinized, and stained with hematoxylin & eosin (H&E). Light microscopic examination was performed by a board-certified veterinary pathologist (JRH) without knowledge of individual animal exposure.

Lung immunohistochemistry and morphometric analysis

Formalin-fixed, paraffin embedded lung tissues were immunohistochemically stained for $CD45R^+$ B-cells, $CD3^+$ T-cells, and IgG^+ plasma cells (**Table A4.1**). Slides were scanned using the VS200 virtual slide system (Olympus, Hicksville, NY). Using NewCast software (Visiopharm, Hoersholm, Denmark), each whole glass slide was randomly subsampled to obtain at least 100 digital microscopic images from lung tissue sections captured at 20X magnification. Morphometric analysis used to quantify $CD45R^+$ B-cells, $CD3^+$ T-cells, and IgG^+ plasma cells in

the lung was performed using the STEPanizer 1.8 stereology tool (147). Briefly, lymphoid cell densities were quantified by overlaying a point grid on randomly subsampled images. The number of grid points overlayed with positively stained cells was divided by reference tissue area to obtain a percentage of the total lung area showing positive IHC staining.

Quantitative PCR for lung tissue

Total RNA was extracted from the caudal lung lobes using TissueLyser II and a RNeasy Mini Kit (Qiagen, cat. #74104) per manufacturer's instructions. RNA was eluted using RNase-free water provided by the RNeasy kit and quantified using the Nanodrop ND-1000 spectrophotometer (Thermo Fisher Scientific, Waltham, MA). High-Capacity cDNA Reverse Transcriptase Kit (Thermo Fisher Scientific, cat. #4368814) RNA was used to prepare cDNA. Taqman assays were run in technical triplicate using the TakaraBio smartchip real-time PCR system at the MSU Genomics Core to assess gene expression. Exposure-dependent gene expression was assessed for cytokines (*Tnfa, Il1b, Il6, Ifng*), chemokines (*Ccl3, Ccl4, Ccl8, Cxcl1, Cxcl3, Cxcl9, Cxcl10, Cxcl13*), IFN-regulated genes (*Zbp1, Oas1a, Oasl1, Irg1*), lymphocyte activation and differentiation (*Ly6i, Bcl6, Il12b*), cell death (*Bax, Bcl2, Nlrp3, Casp1, Casp4*), oxidative stress (*Nos2, Lcn2, Keap1, Nrf2*), and housekeeping genes (*Actb, Gapd*). ΔCt values were calculated by subtracting the average raw Ct value of the housekeeping genes from the raw Ct value for each gene of interest. ΔΔCt values were calculated by subtracting the average ΔCt value of the respective VEH group from the average ΔCt value of the corresponding route of exposure LPS group. ΔΔCt values are shown in units of fold increase relative to VEH control mice for each gene of interest.

Autoantibody Microarray

IgG and IgM AAb profiling was performed using a high-throughput autoantigen (AAg) microarray

at the Microarray and Immune Phenotyping Core Facility at the University of Texas Southwestern Medical Center as described previously (88) for BALF and plasma samples. Briefly, BALF and plasma samples were pre-treated with DNAse I to remove free-DNA and then diluted 1:25 or 1:50, respectively. Samples were added and incubated on protein array plates containing 122 different antigens and 6 controls. Antibody-antigen binding occurring on the plate was detected using Cy3-conjugated anti-mouse IgG (1:2000, Jackson ImmunoResearch Laboratories, PA). Fluorescent images were captured using a Genepix 4200A scanner (Molecular Devices, CA) and were transformed to signal intensity values using GenePix 7.0 software. Signal intensity values for each AAb were first normalized by subtracting the background and normalizing to IgG internal controls, then reported as an antibody score (Ab-score). This Ab-score was calculated based on the normalized signal intensity (NSI) and signal-to-noise ratio (SNR) using the formula:

Ab-score = $log_2\ (NSI * SNR + 1)$

Normalized and unit variance-scaled Ab-score values were visualized using ClustVis software (36). For heat maps, data were clustered using unsupervised hierarchical co-clustering (HCC) and rows were clustered using Euclidean distance and Ward linkage. Imputation was applied for missing value estimation. ClustVis was also used for Principal Component Analysis (PCA) to calculate and illustrate similarities between exposure groups. Prism 9 (GraphPad Prism v 9.2, San Diego, CA) was used to graph select classes of IgG and IgM AAbs (88).

Kidney and spleen histopathology and immunohistochemistry

Spleen heads fixed in formalin were placed into individual tissue blocks, embedded with paraffin, and cut at a 5 μm thickness. Deparaffinized splenic tissue was immunohistochemically stained for IgG (**Table A4.1**) and counterstained with hematoxylin. Light microscopic examination of germinal center formation and extracellular proteinaceous IgG deposition was assessed (JRH).

Kidney tissue sections (5 μm) were histochemically stained with H&E and light microscopic examination was performed by a board-certified veterinary pathologist (JRH) without knowledge of individual animal exposure. Glomerulonephritis severity scores were based on a modified Society of Nephrology/Renal Pathology Lupus Nephritis Classification system (173): (0) no tubular proteinosis, normal glomeruli; (1) mild tubular proteinosis with multifocal segmental proliferative glomerulonephritis and occasional early glomerular sclerosis and crescent formation; (2) moderate tubular proteinosis with diffuse segmental proliferative glomerulonephritis, early glomerular sclerosis, and crescent formation; (3) marked tubular proteinosis with diffuse global proliferative and sclerosing glomerulonephritis. Kidney tissue sections were also immunohistochemically stained for IgG and counterstained with H&E, and semi-quantitative scoring of renal IgG deposition was performed.

Statistical analysis

Data and statistical analyses were performed using (GraphPad Prism v 9.2, San Diego, CA). The Grubb's test (Q=1%) and Shapiro-Wilk test ($p<0.01$) were used to test for outliers and normality, respectively. A One-Way ANOVA was used on all data to detect significant differences with LPS treatment relative to VEH (VEH/IP vs LPS/IP, VEH/IN vs LPS/IN) and between routes of exposure (VEH/IP vs VEH/IN, LPS/IP vs LPS/IN). Non-normal and semi-quantitative data were analyzed using the Kruskal-Wallis non-parametric test. Data are presented as the mean ± standard error of the mean (SEM), with a p-value ≤ 0.05 being considered statistically significant.

RESULTS

Mice in the four experimental groups did not exhibit evident signs of deteriorating health such as lethargy, rough coat, dyspnea, or decreased ambulation. However, weight gain was suppressed in the LPS/IN group compared to VEH/IN group, but not in the LPS/IP group (**Figure 4.1B**).

Intranasal LPS exposure led to a significant increase in total leukocytes, macrophages/monocytes, and neutrophils in the BALF compared to VEH controls (**Figure 4.2A**). Consistent with induction of BALF cellularity, histopathologic analysis revealed that mice in the LPS/IN group predominantly had a mononuclear cell bronchopneumonia, consisting mainly of lymphocytes, plasma cells, and macrophages/monocytes, with lesser numbers of neutrophils (**Figure 4.2B**). Lung lesions were most severe in the hilar region of the lung lobe. LPS-induced bronchiolitis/alveolitis consisted of conspicuous accumulations of T- and B-lymphoid cells in the interstitial tissue surrounding bronchioles and blood vessels (ELT) and alveolar accumulations of enlarged and often vacuolated macrophages. Hyperplasia of type 2 alveolar epithelial cells was occasionally present in the inflamed alveolar parenchyma as well as bronchiolar epithelial hypertrophy/hyperplasia in small diameter pre-terminal and terminal bronchioles.

IP injections with LPS did not affect BALF cellularity (**Figure 4.2A**). Lung lesions were not present in VEH/IN mice, except for occasional small inflammatory foci randomly scattered in the alveolar parenchyma and composed of a mixed inflammatory cell infiltrate (neutrophils, monocytes, and macrophages) (**Figure 4.2B**). These small foci were often associated with a minute foreign body, e.g., inhaled bedding or food material. No exposure-related histopathology was microscopically evident in the lungs of mice exposed IP to LPS or VEH.

IHC and morphometric analysis were used to quantify lymphoid cell populations in ELT in mice exposed via the IN route. LPS/IN mice exhibited significant infiltration of $CD45R^+$ B cells (**Figure 4.3A**) and $CD3^+$ T cells (**Figure 4.3B**) around the perivascular and peribronchiolar regions of the lung compared to VEH/IN mice. Correspondingly, mice subjected to LPS/IN exhibited increased numbers of IgG^+ plasma cells located in ELT (**Figure 4.4A-B**). While mice exposed to LPS via IP injection did not have increased presence of IgG^+ plasma cells, there was still noticeable

extracellular IgG^+ proteinaceous material deposition in the lung compared to VEH/IP mice (**Figure 4.4A-C**).

IN LPS exposure upregulated expression of genes in lung tissue pertaining to cytokines (*Tnfa, Il1b, Il6, Ifng*) (**Figure 4.5A**), chemokines (*Ccl3, Ccl4, Ccl8, Cxcl1, Cxcl3, Cxcl9, Cxcl10, Cxcl13*) (**Figure 4.5B**), and IFN response (*Zbp1, Oas1a, Oasl1, Irg1*) (**Figure 4.5C**). IN exposure to LPS also induced genes associated with lymphocyte activation and differentiation (*Ly6i, Bcl6, Il12b*), cell death (*Bax, Nlrp3, Casp1, Casp4*), and oxidative stress (*Nos2, Lcn2*) (**Figure 4.6**). Genes downregulated with IN exposure to LPS compared to VEH/IN mice were *Bcl6* (germinal center T cells), *Bcl2* (apoptosis), and *Nrf2* and *Keap1* (oxidative stress) (**Figure 4.6**). Of these, only *Cxcl13, Oas1a, Casp1,* and *Casp4* were modestly induced by IP exposure to LPS (**Figure 4.5,6**).

LPS/IN mice exhibited robust increases of both IgM AAbs (**Figure 4.7A,B**) and IgG AAbs (**Figure 4.8A,B**) in BALF compared to their respective controls. In comparison, IgM and IgG AAbs were modestly elevated. PCA analysis revealed distinct clustering of VEH/IN samples from LPS/IN, VEH/IP, and LPS/IP groups for IgM AAb (**Figure 4.7C**) and IgG AAb (**Figure 4.8C**) responses in the BALF. Specificities for IgM and IgG AAbs in LPS/IN mice, and IgG AAbs in LPS/IP mice, were highly diverse and extended over a wide range of AAgs including DNA-related nucleoproteins, anti-DNA organization and nuclear membrane, phospholipid antigens, and complement and circulating proteins. (**Figures 4.7D and 4.8D**). Comparatively, only select classes of IgM AAbs demonstrated a significant LPS-response in the IP group compared to VEH/IP control mice (**Figures 4.7 and 4.8**).

In the plasma, LPS/IP mice exhibited marked increases in IgM AAbs, while these responses were much more muted in the LPS/IN mice (**Figure 4.9A-C**). IgM AAbs in LPS/IP

mice reacted with most AAgs on the microarray, whereas IgM AAbs in LPS/IN mice reacted with a smaller subset of AAgs (**Figure 4.9D**). Both the LPS/IP and LPS/IN groups exhibited modest increases in IgG AAbs (**Figure 4.10A-C**). IP or IN LPS IgG AAbs reacted with approximately three quarters of microarray AAgs (**Figure 4.10D**).

Both LPS/IP and LPS/IN groups had significant increases in spleen weights compared to their respective VEH controls, with spleen weights being greater in LPS/IP mice compared to LPS/IN mice (**Figure 4.11A**). LPS/IP mice had extensive formation of germinal centers, which were absent or less evident in VEH/IP, LPS/IN, and VEH IN mice (**Figure 4.11B**). LPS-exposed mice from both IP and IN groups had marked increases in IgG deposition in the spleen compared to their respective controls.

LPS exposure resulted in glomerulonephritis for both routes of exposure compared to their respective VEH controls (**Figure 4.12A**). Mice exposed to LPS via IP injection, however, had marked glomerular hypertrophy/hypercellularity and mild IgG deposition compared to their VEH controls. In contrast, mice exposed to LPS intranasally exhibited only minimal to mild glomerular hypertrophy and scarce IgG deposition compared to VEH/IN mice (**Figure 4.12B**). Proteinuria was not detected in the urine of any experimental groups throughout the study.

DISCUSSION

While subchronic IP exposure to *Salmonella* LPS triggers accelerated glomerulonephritis in various lupus-prone mouse strains (179-181, 183-186, 188), it is unclear how pulmonary exposure impacts autoimmunity in these same preclinical models of lupus. Growing evidence from humans studies (177) and pre-clinical mouse models of RA (54, 60) suggest that pulmonary exposure to LPS is likely a trigger for autoimmunity. Here, we compared for the first time the effects of subchronic airway and systemic LPS-triggered inflammation and autoimmunity in female

NZBWF1 lupus-prone mice. As depicted in **Figure 4.13**, we found responses were highly dependent on the route of exposure. Specifically, IN exposure to LPS induced robust BALF leukocyte cellularity, pulmonary ELT formation, infiltration of $CD45R^+$ B- and $CD3^+$ T-lymphocytes, IgG^+ plasma cells, and pro-inflammatory gene expression in lung tissue which was not evident in LPS/IP and VEH-instilled mice. These responses in the lung were unique to LPS/IN mice and were not detected in LPS/IP mice. While both routes of LPS exposure triggered splenomegaly and splenic IgG deposition, splenic germinal center formation was evident only in LPS/IP mice. Furthermore, IgM and IgG AAb induction were more prominent in the BALF after IN LPS exposure, while more vigorous AAb responses in the plasma were evident after IP LPS exposure. Lastly, glomerulonephritis with IgG deposition was more prominent in LPS/IP mice than LPS/IN animals.

Similar to what has been observed following subchronic IN exposure to crystalline silica in NZBWF1 mice (17, 18), IN LPS exposure drove unresolved inflammation and autoimmunity in the lung. Pulmonary ELTs likely served as a source for robust IgM and IgG responses in the BALF of mice intranasally exposed to LPS (**Figure 4.13**). IP LPS exposure, in comparison, did not lead to significant pulmonary pathology. Yet, IgG was immunohistochemically detected in lung vasculature, including alveolar capillaries, and in some alveolar airspaces. Likewise, small amounts of IgM and IgG AAbs were detected in the BALF of LPS/IP mice.

In contrast to LPS IN delivery to the lung, IP exposure to LPS effectively triggered plasma AAb responses reflecting systemic autoimmunity that was likely driven by polyclonal B-cell activation and development of splenic germinal centers. Similar to ELT in the lung, germinal centers in the spleen contain large numbers of proliferating B-cells that could have been activated by either LPS or self-antigens (199, 200). Zhang et al. and coworkers (59) found that spontaneous

splenic germinal center formation in MLR/lpr lupus-prone mice led to significantly elevated serum IgG and IgM anti-dsDNA and splenic IgG deposition. These findings support the notion that IP delivery of LPS elicited splenic pathology which likely led to the robust IgM and IgG AAb responses in the plasma (**Figure 4.13**).

Our preclinical mouse model exemplifies the importance of AAbs in driving lupus pathogenesis regardless of route of exposure to environmental toxicants such as LPS. Elevated levels of IgM and IgG AAbs detected in the BALF and plasma in IN and IP LPS-exposed mice, respectively, demonstrated that isotype switching continued to take place until termination of the study. Considering naïve B-cells produce IgM prior to maturation and isotype switching, this suggests that there were a significant number of immature B-cells at sites of inflammation still present in the lung and spleen in addition to mature IgG producing B-cells. Unresolved inflammation, in part attributed to B-cell activation, resulted in not only a broad repertoire of antibodies targeting self-antigens, but also increased IgG deposition in both the lung and spleen. Deposition of IgG pathogenic immune complexes are associated with increased tissue damage in lupus patients (178). Our results suggest that IP LPS exposure in female NZBWF1 mice resulted in IgG AAb-mediated responses that are consistent with those observed in humans.

In addition to LPS-mediated inflammation in the lung, spleen, and plasma, IN and IP treatment with LPS resulted in moderate renal pathology compared to VEH control mice. In other studies where female NZBWF1 mice were exposed to *Salmonella*-derived LPS via IP injection using the same dose as in the present model, more severe glomerulonephritis and renal immune complex deposition was present compared to the LPS/IN mice in this study (58, 194, 196, 197). We have recently demonstrated that severity of glomerulonephritis is particularly dependent on the chemotype of Gram-negative bacteria used in the exposure model (58). Repeated IP injections

with rough *Salmonella* LPS induced advanced glomerulonephritis in NZBWF1 mice, whereas repeated IP injections with smooth *Salmonella* LPS elicited minimal renal pathology. Interestingly, although the *E. coli* LPS strain used in the present study is a smooth serotype, there was more robust renal pathology observed in mice treated IP with *E. coli* compared to mice injected with smooth *Salmonella* LPS in the aforementioned study. Thus, severity of LPS-accelerated autoimmune nephritis in NZBWF1 mice may not only be chemotype-dependent, but also influenced by the type of Gram-negative bacterium from which the LPS was derived.

While severe glomerulonephritis did not develop in mice exposed to LPS either via the IN or IP route, we did observe some glomerular pathology with both routes of exposure. These findings support the idea that chronic LPS exposure, regardless of route of administration, was indeed capable of creating pathology in the kidneys of NZBWF1 mice due to unresolved inflammation and systemic autoimmunity. However, additional studies are needed to determine if LPS-induced glomerulonephritis progresses with additional exposures or time post-exposure in these NZBWF1 lupus-prone mice. Overall, this is the first study to demonstrate that exposure to the clinically relevant environmental toxicant *E. coli* LPS leads to local and systemic autoimmunity in female NZBWF1 lupus-prone mice through multiple routes of exposure.

ACKNOWLEDGEMENTS

The authors thank Amy Porter of the Michigan State University Laboratory for Investigative Histopathology for their assistance with histotechnology.

AUTHOR CONTRIBUTIONS

LH: study design, coordination, animal handling, necropsy, data curation, data analysis/interpretation, figure preparation, manuscript preparation and submission; LR: data curation and visualization; JW: study design, necropsy, lab analysis; RL: instillations/injections, necropsy, lab analysis; QZL: AAb microarray; AR: animal handling, urinalysis; AT and JS:

morphometric analysis; JH: study design, oversight, lung/kidney histopathology, morphometry, data analysis, manuscript preparation; JP: study design, oversight, funding acquisition, data analysis, manuscript preparation.

FIGURES

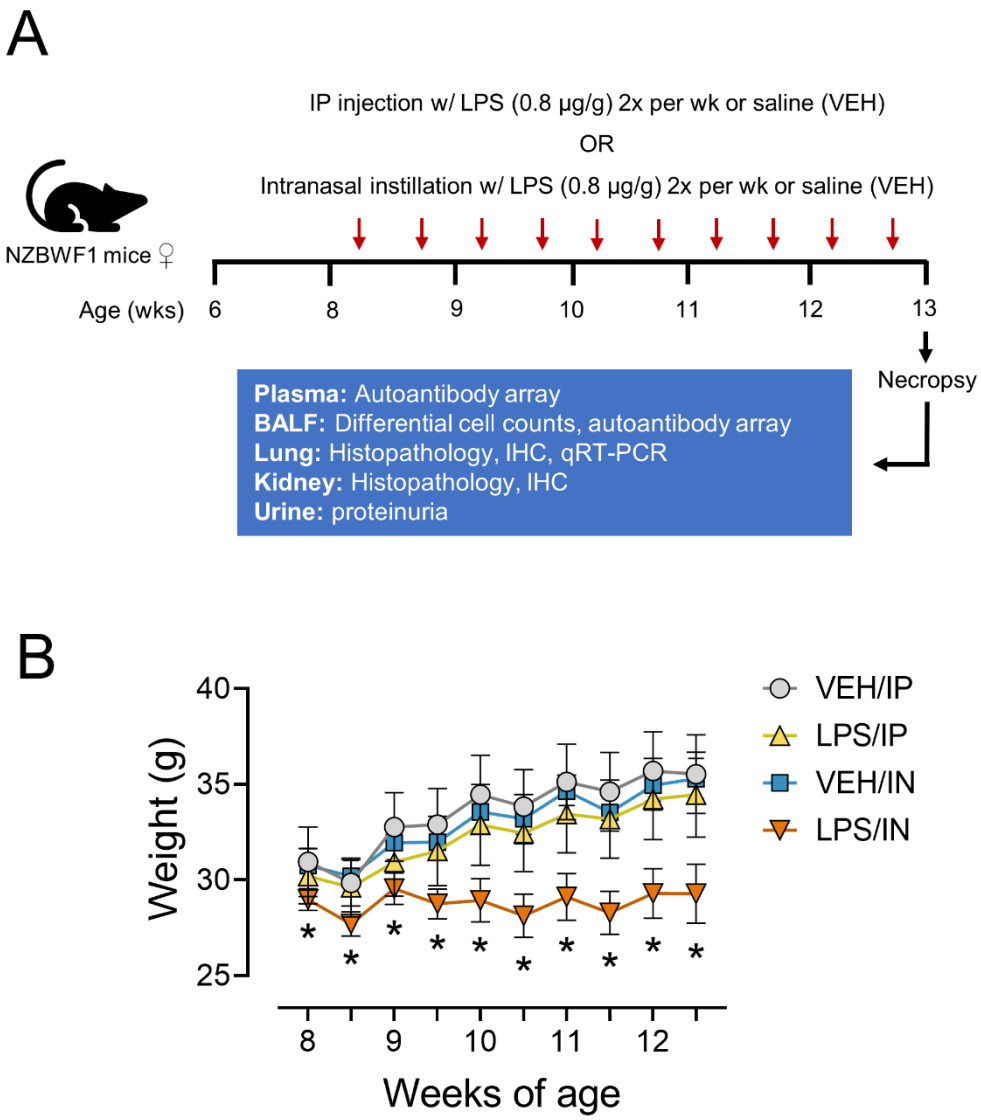

Figure 4.1: (A) Experimental design. Female NZBWF1 mice were obtained at 6 wks of age and were allowed to acclimate for 2 wks. Beginning at 8 wks of age, mice were treated with either 1) IP injection with saline vehicle, 2) IP injection with LPS, 3) intranasal instillation with saline vehicle, or 4) intranasal instillation with LPS. Mice were injected IP or intranasally instilled with the appropriate treatment twice per wk for 5 consecutive wks. Proteinuria was assessed weekly starting at 8 wks of age to monitor disease progression. All animals were sacrificed at 13 wks of age. At the time of necropsy, BALF was collected for differential cell counts and AAb microarray; plasma was collected for AAb microarray; lung and kidney tissues were collected for histopathology, IHC, morphometric analysis, and qRT-PCR. **(B)** Body weight changes were observed with intranasal LPS exposure treatment in female NZBWF1 mice. Animals were weighed twice per wk beginning at 8 wks of age. LPS/IN mice had significantly lower body weights throughout the duration of the study compared to VEH/IN mice and mice treated via IP injection. LPS/IP mice had no significant changes in body weight compared to VEH/IP mice.

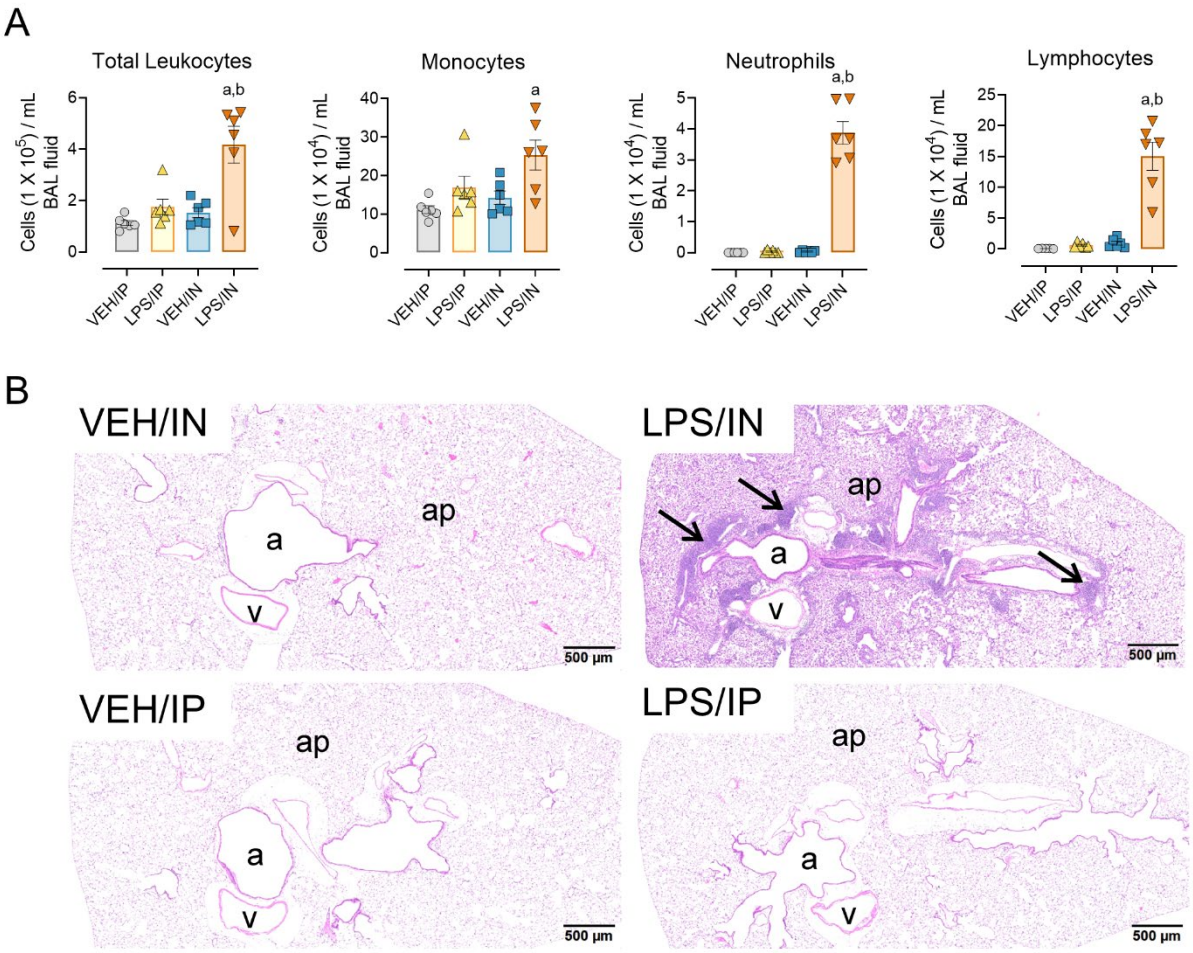

Figure 4.2: Intranasal LPS exposure results in significant BALF cellularity and pulmonary ELT formation. (A) LPS intranasal instillation led to increased total leukocytes, monocytes, neutrophils, and lymphocytes in the BALF (B). $p<0.05$; a, Significantly different from VEH control within same route of exposure; b, Significantly different from LPS/IP group. **(B)** Light photomicrographs of hematoxylin and eosin-stained lung tissue sections from mice intranasally instilled with saline vehicle (VEH/IN), mice intranasally instilled with LPS (LPS/IN), mice injected IP with saline vehicle (VEH/IP), and mice injected IP with LPS (LPS/IN). Intranasal LPS exposure resulted in perivascular and peribronchiolar ELT formation at 13 wks of age compared to VEH/IN mice. Abbreviations: a, pulmonary airways; v, pulmonary vessels; ap, alveolar parenchyma; arrows, peri-vascular/bronchiolar ectopic lymphoid structures.

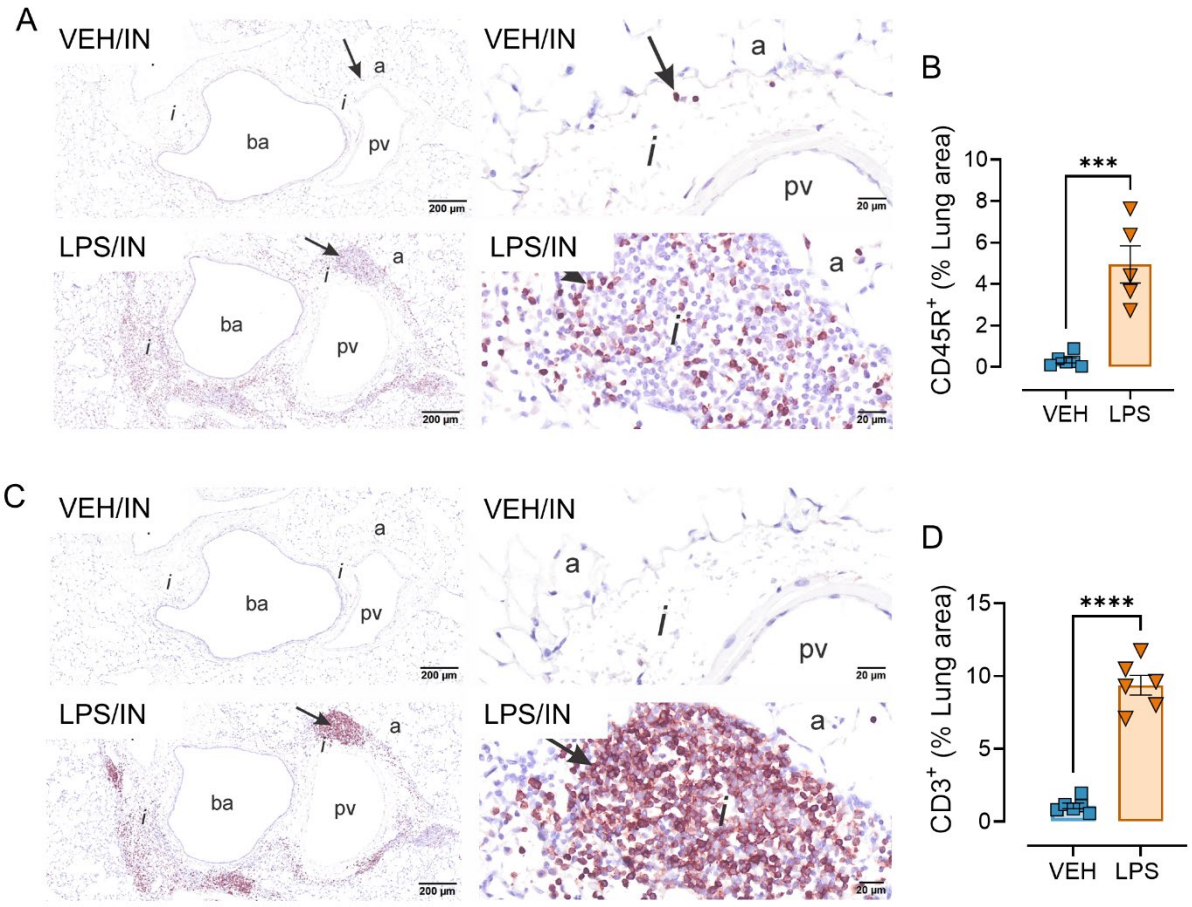

Figure 4.3: Intranasal LPS exposure increased lung infiltration of perivascular CD45R$^+$ B-cells and CD3$^+$ T-cells. Light photomicrographs of perivenous ectopic lymphoid tissue (ELT) immunohistochemically stained for **(A,B)** CD45R$^+$ B lymphoid cells and **(C,D)** CD3$^+$ T cells in lungs from VEH/IN and LPS/IN mice. Abbreviations: pv, pulmonary vein; ba, bronchiolar airway; i, peribronchiolar and perivascular interstitium; a, alveolar parenchyma; arrows, perivascular/bronchiolar ectopic lymphoid tissue; arrow, arrow, positively stained lymphoid cells. Intranasal LPS exposure triggered significant interstitial infiltration of CD45R$^+$ B-cells **(A)** and CD3$^+$ T-cells **(C)** compared to VEH/IN mice. Graphical representation of morphometrically determined density of CD45R$^+$ B-cells **(B)** and CD3$^+$ T-cells **(D)** in lung tissue. *** $p<0.001$, **** $p<0.0001$ for VEH/IN vs LPS/IN.

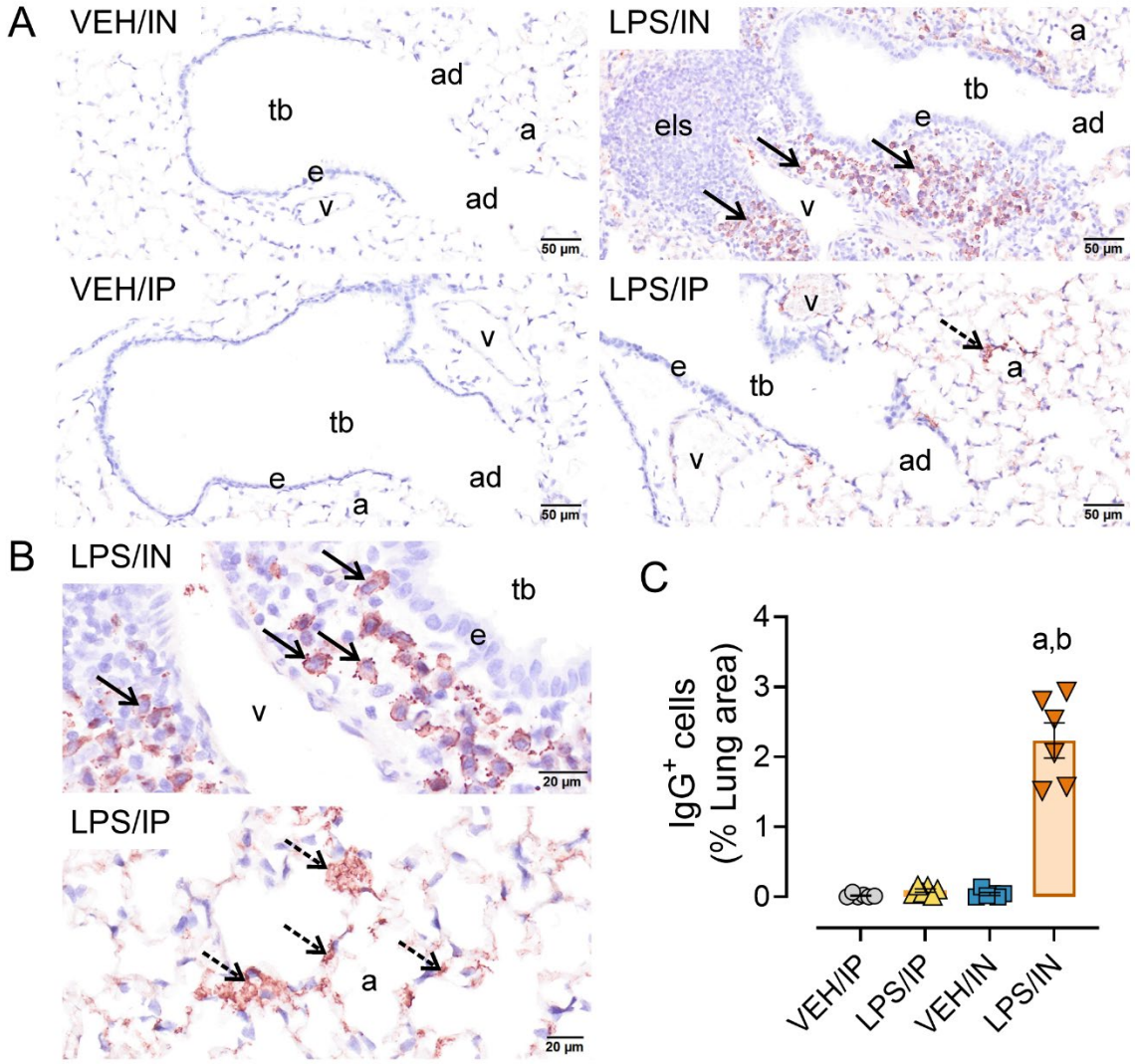

Figure 4.4: Intranasal LPS exposure triggered a significant increase in pulmonary IgG$^+$ plasma cells in the lung. Light photomicrographs of perivenous ectopic lymphoid tissue (ELT) immunohistochemically stained for IgG$^+$ plasma cells (arrows), and alveolar parenchyma immunohistochemically stained for extracellular IgG$^+$ proteinaceous material (stippled arrows) in alveolar airspace **(A)**. Zoomed in photomicrographs IgG$^+$ stained tissue around pulmonary vessel in LPS exposed mice **(B)**. Abbreviations: tb, terminal bronchiole; e, epithelium; v, pulmonary vein; a; alveolar parenchyma; els, ectopic lymphoid structure/tissue. Graphical representation of morphometrically determined lung density of IgG$^+$ plasma cells **(C)**. LPS/IP mice did not lead to increased IgG$^+$ plasma cell infiltration, but extracellular IgG deposition in lung tissue was still present. Tissues counterstained with hematoxylin. $p<0.05$; a, Significantly different from VEH control within same route of exposure; b, Significantly different from LPS/IP group.

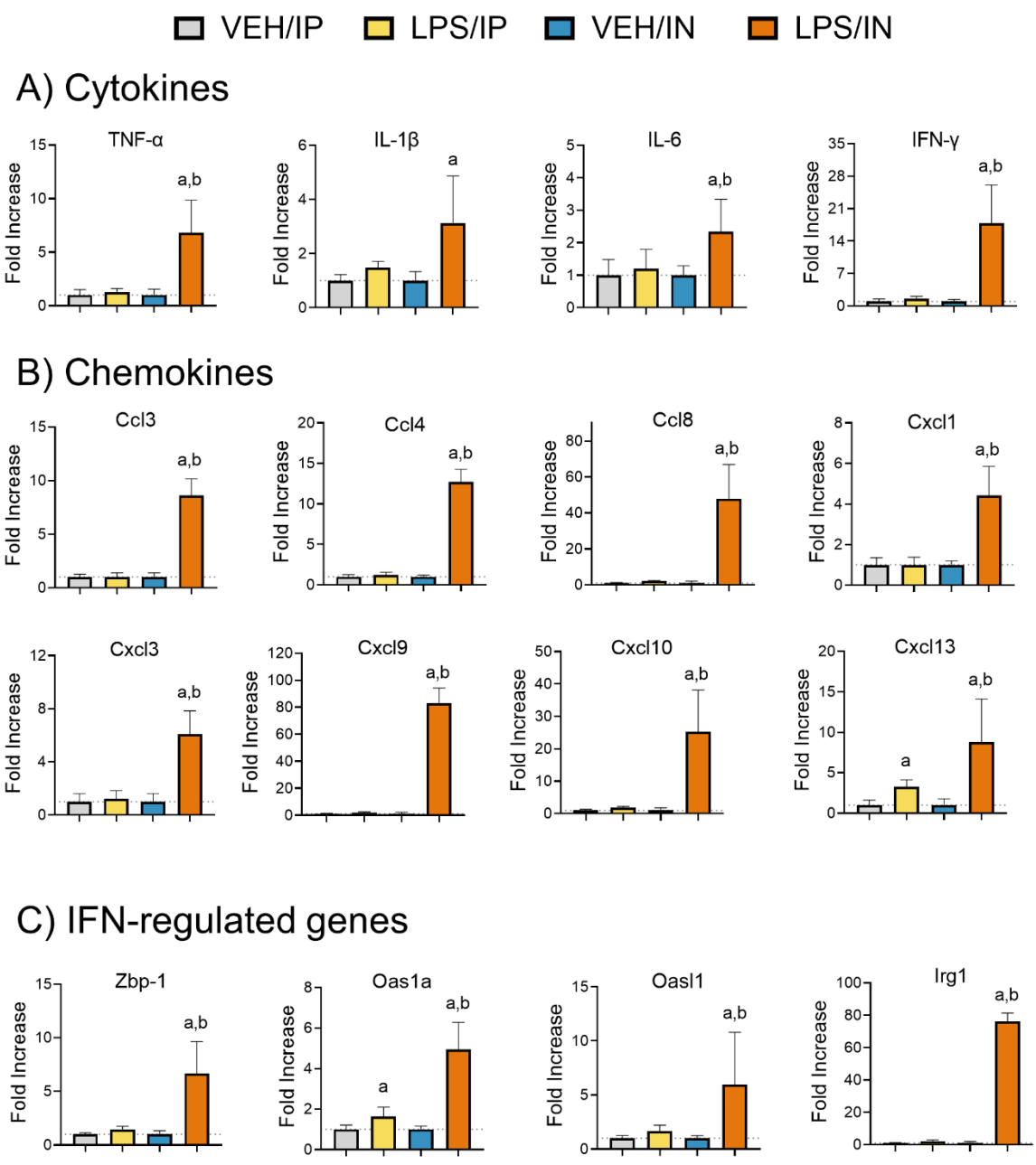

Figure 4.5: IN but not IP LPS exposure induced expression of cytokine (A), chemokine (B), IFN-regulated genes (C) the lung qRT-PCR was used to assess exposure-dependent changes in gene expression within the lung tissue. Letters: a, differs from VEH control within same route of exposure ($p<0.05$); b, differs from LPS/IP group ($p<0.05$).

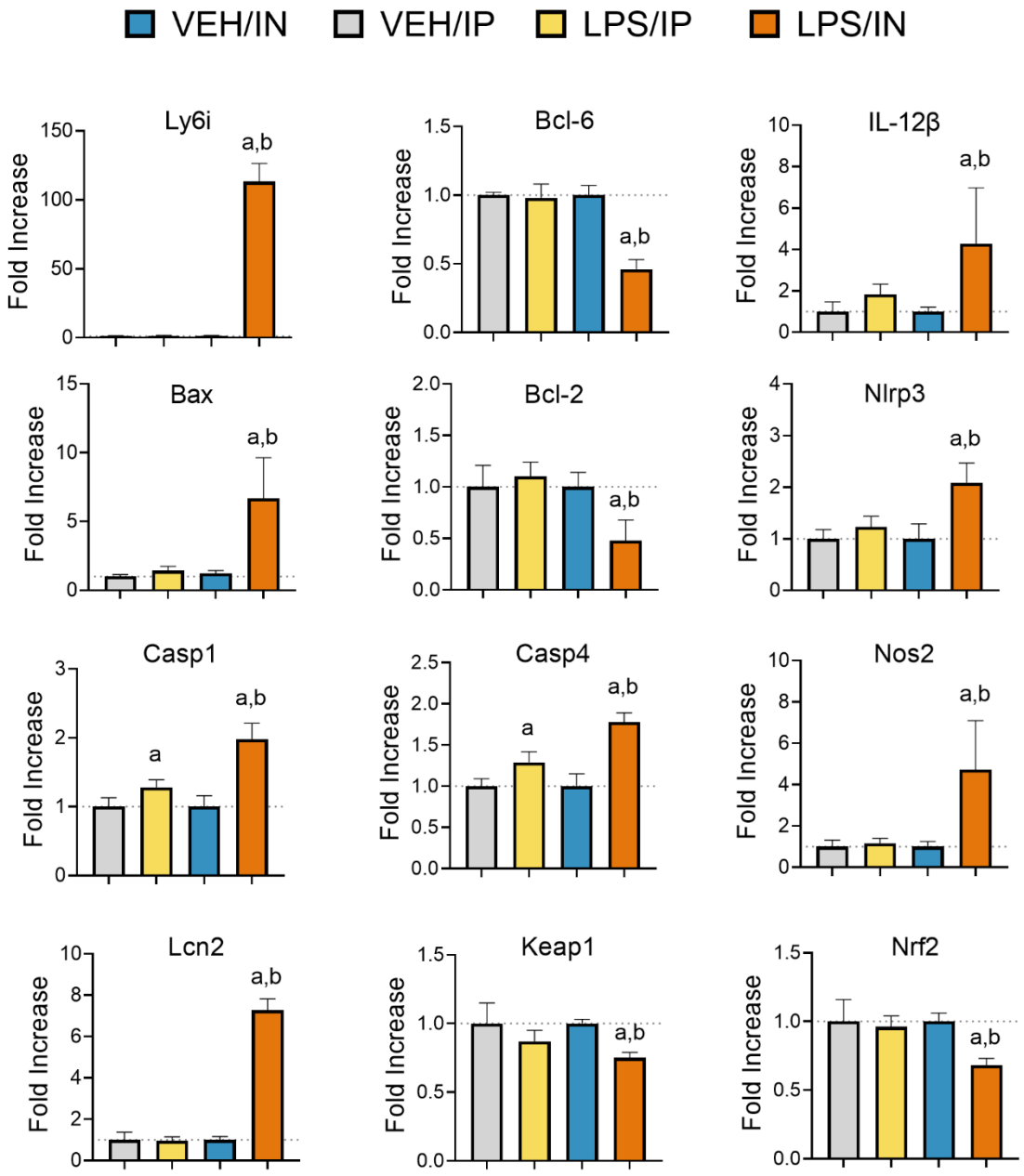

Figure 4.6: IN but not IP LPS exposure influences gene expression associated with lymphocyte activation/differentiation (*Ly6i, Bcl-6, Il12b*) cell death (*Bax, Bcl-2. Nlrp3, Casp1, Casp4*), and oxidative stress (*Nos2, Lcn2, Keap1, Nrf2*). Letters: a, differs from VEH control within same route of exposure ($p<0.05$); b, differs from LPS/IP group ($p<0.05$).

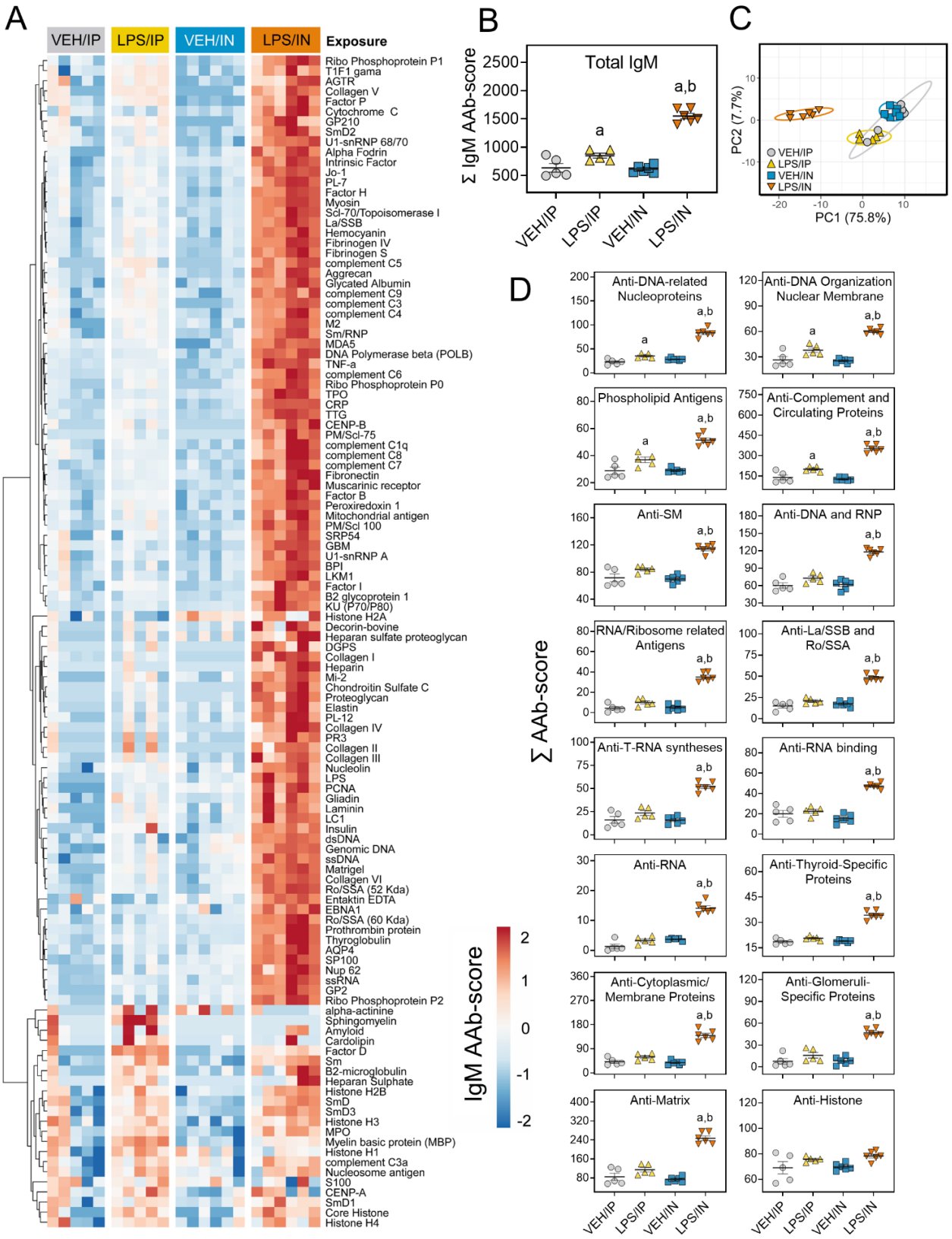

Figure 4.7: LPS exposure resulted in significantly elevated IgM AAbs in the BALF. AAb

Figure 4.7 (cont'd):
production was measured in BALF samples collected at the time of necropsy. **(A**) Heat map illustrates unsupervised clustering (Euclidian distance method) of 122 AAbs shown as AAb-score values for IgM expression in BALF. Scale bar values reflect the range of variance-stabilized AAb scores, which were centered across rows. **(B)** IP and intranasal LPS exposure increased total IgM levels in the BALF. **(C)** PCA of differentially expressed IgM AAbs in the BALF of VEH and LPS-exposed mice for both routes of exposure. Ellipses illustrate 95% confidence intervals. **(D)** Both IP and intranasal LPS exposure led to increases in various classes of AAbs in the BALF compared to their respective VEH control mice. $p<0.05$; a, Significantly different from VEH control within same route of exposure; b, Significantly different from LPS/IP group.

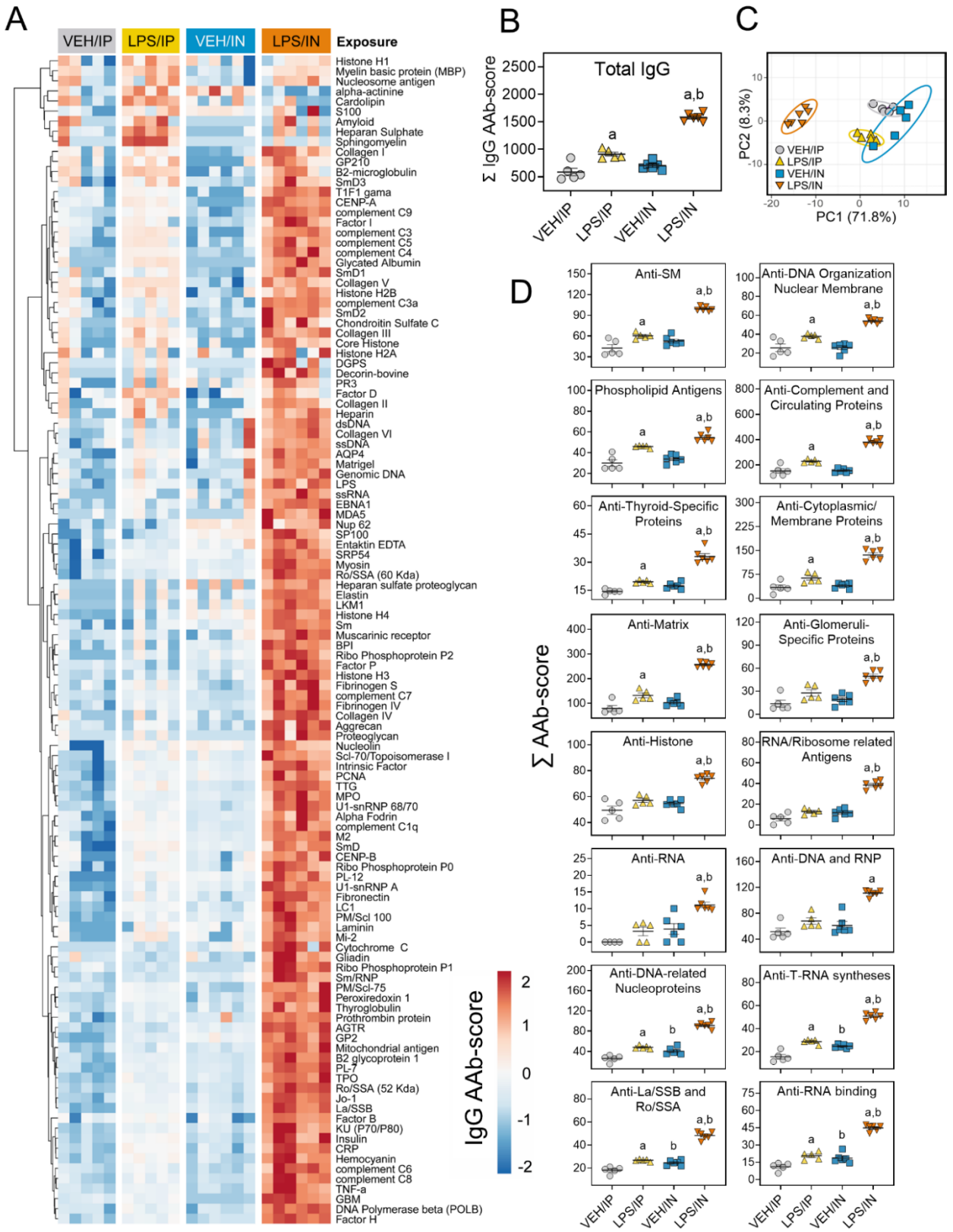

Figure 4.8: LPS exposure resulted in significantly elevated IgG AAbs in the BALF. AAb

Figure 4.8 (cont'd):
production was measured in BALF samples collected at the time of necropsy. **(A)** Heat map illustrates unsupervised clustering (Euclidian distance method) of 122 AAbs shown as AAb-score values for IgG expression in BALF. Scale bar values reflect the range of variance-stabilized AAb scores, which were centered across rows. **(B)** IP and intranasal LPS exposure increased total IgG levels in the BALF. **(C)** PCA of differentially expressed IgG AAbs in the BALF of VEH and LPS-exposed mice for both routes of exposure. Ellipses illustrate 95% confidence intervals. **(D)** Both IP and intranasal LPS exposure led to increases in various classes of AAbs in the BALF compared to their respective VEH control mice. $p<0.05$; a, Significantly different from VEH control within same route of exposure; b, Significantly different from LPS/IP group.

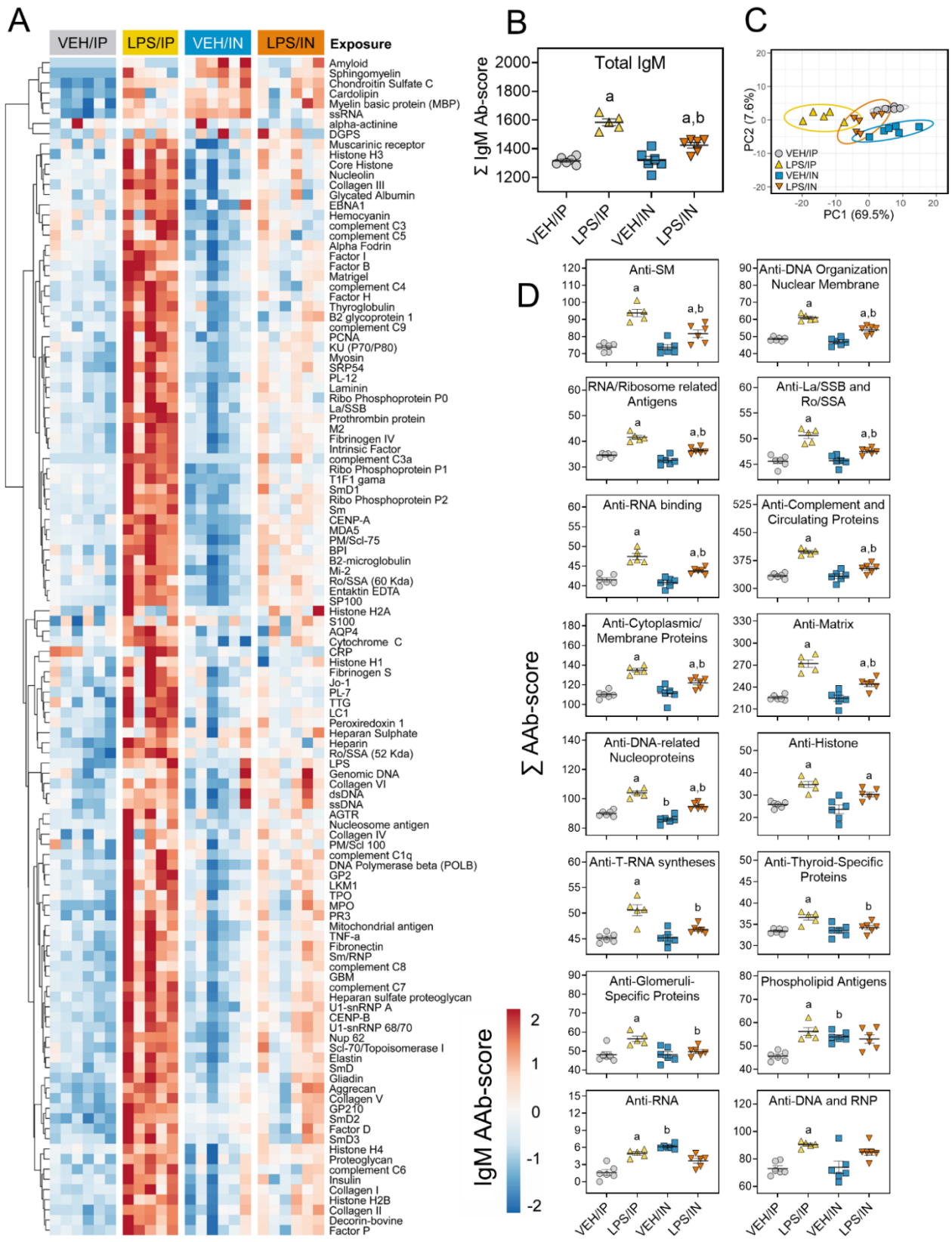

Figure 4.9: LPS exposure resulted in significantly elevated IgM AAbs in the plasma. AAb

Figure 4.9 (cont'd):
production was measured in plasma samples collected at the time of necropsy. **(A)** Heat map illustrates unsupervised clustering (Euclidian distance method) of 122 AAbs shown as AAb-score values for IgM expression in plasma. Scale bar values reflect the range of variance-stabilized AAb scores, which were centered across rows. **(B)** IP and intranasal LPS exposure increaseed total IgM levels in the plasma. **(C)** PCA of differentially expressed IgM AAbs in the plasma of VEH and LPS-exposed mice for both routes of exposure. Ellipses illustrate 95% confidence intervals. **(D)** Both IP and intranasal LPS exposure led to increases in various classes of AAbs in the plasma compared to their respective VEH control mice. $p<0.05$; a, Significantly different from VEH control within same route of exposure; b, Significantly different from LPS/IP group.

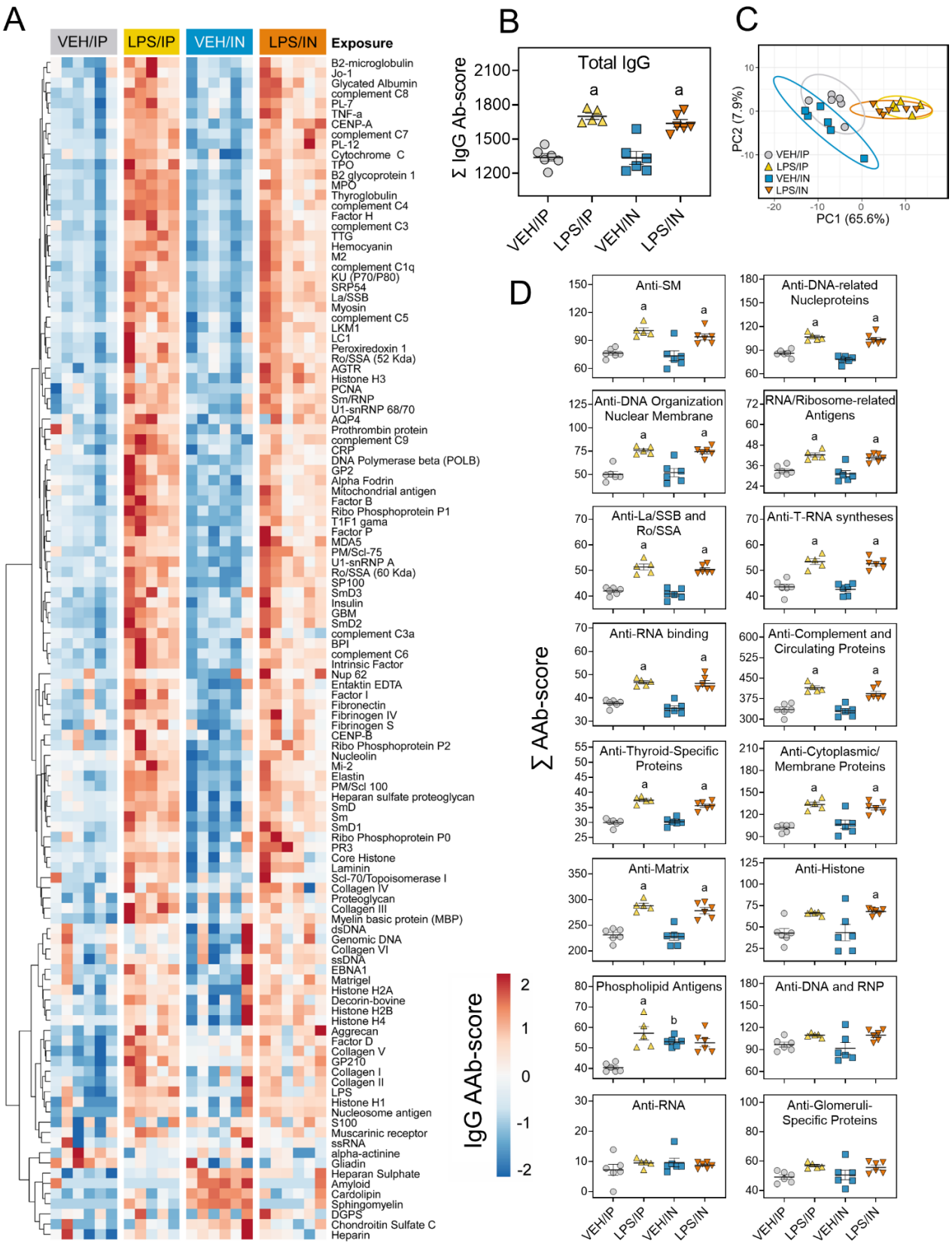

Figure 4.10: LPS exposure resulted in significantly elevated IgG AAbs in the plasma. AAb

Figure 4.10 (cont'd):
production was measured in plasma samples collected at the time of necropsy. **(A)** Heat map illustrates unsupervised clustering (Euclidian distance method) of 122 AAbs shown as AAb-score values for IgG expression in plasma. Scale bar values reflect the range of variance-stabilized AAb scores, which were centered across rows. **(B)** IP and intranasal LPS exposure increased total IgG levels in the plasma. **(C)** PCA of differentially expressed IgG AAbs in the plasma of VEH and LPS-exposed mice for both routes of exposure. Ellipses illustrate 95% confidence intervals. **(D)** Both IP and intranasal LPS exposure led to increases in various classes of AAbs in the plasma compared to their respective VEH control mice. $p<0.05$; a, Significantly different from VEH control within same route of exposure; b, Significantly different from LPS/IP group.

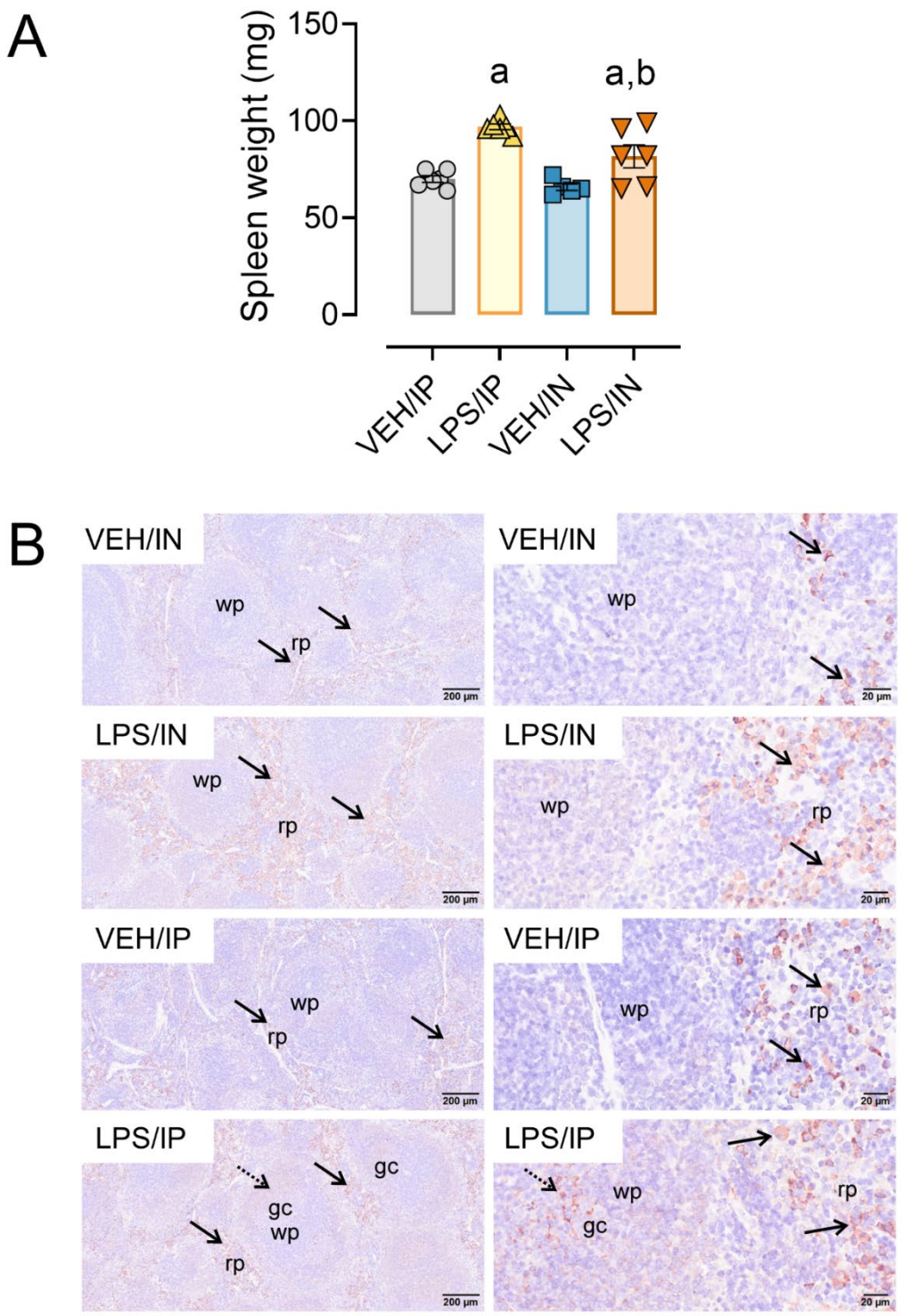

Figure 4.11: LPS exposure resulted in splenomegaly and IgG deposition. Spleen weights from LPS/IP and LPS/IN mice were significantly greater compared to VEH/IP and VEH/IN mice, respectively **(A)**. Light photomicrographs of splenic tissue immunohistochemically stained for extracellular IgG^{+} proteinaceous material and counterstained with hematoxylin **(B)**. Splenic white pulp (wp) increased (lymphoid cell hyperplasia) in mice exposed to LPS IP and intranasally.

Figure 4.11 (cont'd):
Germinal center formation was present in LPS/IP mice. Increased IgG deposition was present in mice exposed to LPS both IP and intranasally compared to the respective VEH controls. Abbreviations: wp, white pulp; rp, red pulp; gc, germinal center; arrows, IgG^+ stained tissue. $p<0.05$; a, a, Significantly different from VEH control within same route of exposure; b, Significantly different from LPS/IP group.

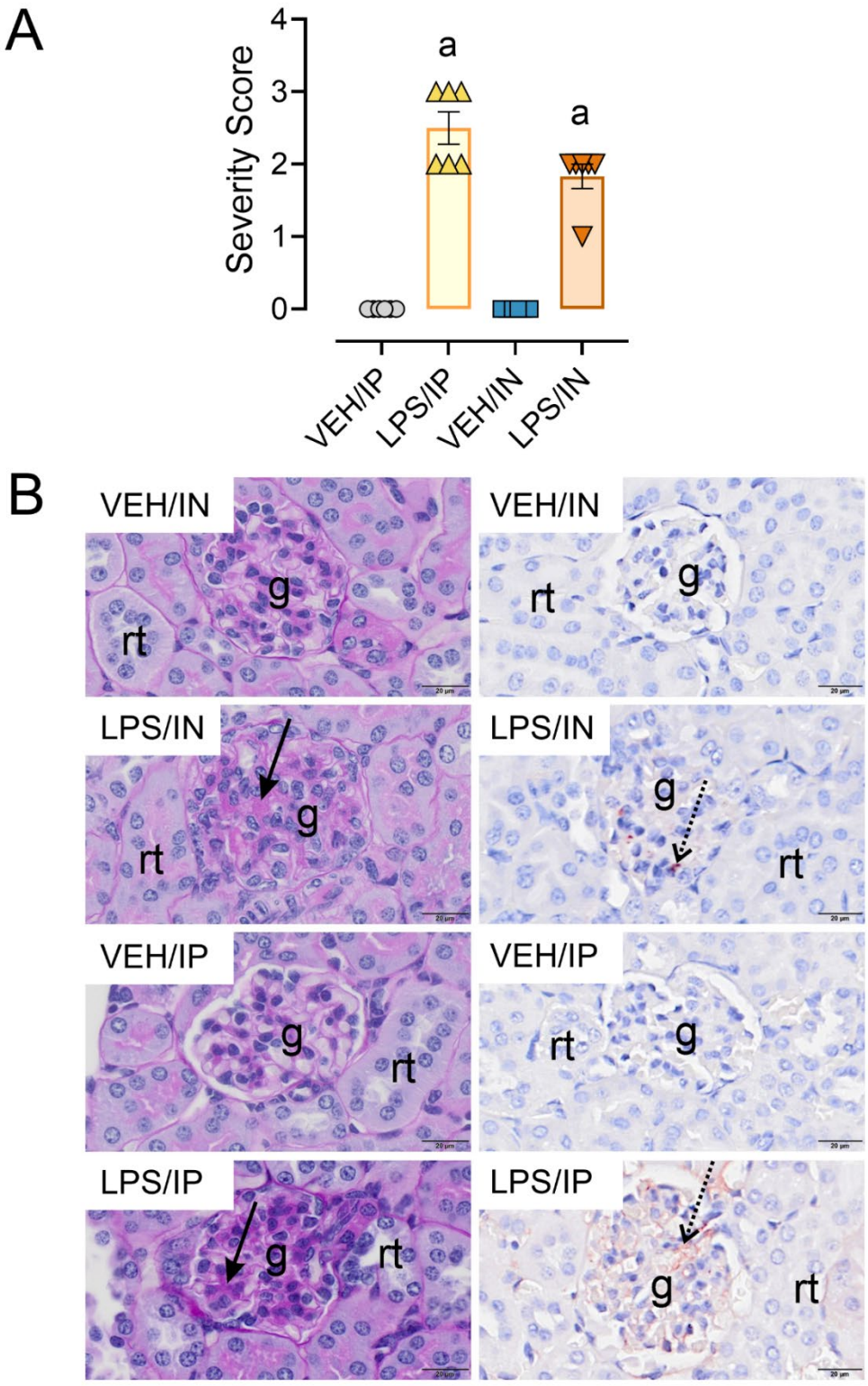

Figure 4.12: LPS resulted in moderate renal pathology and elevated glomerulonephritis severity scores. Individual kidney sections were semi-quantitatively scored based on the modified International Society of Nephrology/Renal Pathology Lupus Nephritis Classification system

Figure 4.12 (cont'd):
described methods for lupus nephritis score **(A)**. Both IN and IP LPS exposure resulted in elevated glomerulonephritis scores compared to respective VEH controls. **(B)** Light photomicrographs of kidney sections histochemically stained with Periodic Acid Schiff stain (left panel) or immunohistochemically stained with IgG (right panel) and counterstained with hematoxylin. LPS/IN mice exhibited mild glomerular hypertrophy and little IgG deposition compared to VEH/IN mice, and LPS/IP mice had marked glomerular hypertrophy and mild IgG deposition compared to VEH/IP mice. $p<0.05$; a, Significantly different from VEH control within same route of exposure; b, Significantly different from LPS/IP group.

CHAPTER 5: OMEGA-3 FATTY ACID AND GLUCOCORTICOID COMBINATORIAL SUPPRESSION OF PROINFLAMMATORY AND INTERFERON GENE EXPRESSION IN LPS-PRIMED ALVEOLAR-LIKE MACROPHAGE CELL MODEL

Lauren K. Heine[1,2†], Rance Nault[2,3†], Andrew Thompson[4,5,6], Ingo Braasch[5,6], Olivia K. Favor[1,2], Jack R. Harkema[2,8], James J. Pestka[2,9,10]

[1]Department of Pharmacology and Toxicology, Michigan State University, East Lansing, MI

[2]Institute for Integrative Toxicology, Michigan State University, East Lansing, MI

[3]Department of Biochemistry & Molecular Biology, Michigan State University, East Lansing, MI

[4]Department of Biological Sciences, Western Michigan University, Kalamazoo, MI

[5]Department of Integrative Biology, Michigan State University, East Lansing, MI

[6]Ecology, Evolution, and Behavior Program, Michigan State University, East Lansing, MI

[7]Department of Integrative Biology, Michigan State University, East Lansing, MI

[8]Department of Pathobiology and Diagnostic Investigation, Michigan State University, East Lansing, MI

[9]Department of Food Science and Human Nutrition, Michigan State University, East Lansing, MI

[10]Department of Microbiology and Molecular Genetics, Michigan State University, East Lansing, MI

[†]These authors contributed equally to this work and share first authorship

PUBLICATION NOTICE

The following chapter is in preparation to be submitted to *Frontiers in Immunology*.

ABSTRACT

Introduction: Glucocorticoids (GC) are one of the most common anti-inflammatory treatments for autoimmune diseases such as systemic lupus erythematosus (lupus). Chronic use of GCs leads to several deleterious side-effects and diminished quality of life, inciting a need for steroid-sparing therapeutics. Polyunsaturated fatty acids (PUFA), such as docosahexaenoic acid (DHA), have been shown to inhibit pro-inflammatory and Type I Interferon (IFN) gene signatures in macrophages, which are central to initiation of autoimmunity triggered by inhaled environmental toxicants such as bacterial lipopolysaccharide (LPS). The goal of the present study was to determine whether combination treatment with suboptimal concentrations of DHA and GC in LPS-primed alveolar-like macrophages could potentiate the anti-inflammatory effects of DHA and GC individual treatment.

Methods: RNAseq was used to evaluate whether DHA could potentiate the anti-inflammatory effects of the GC dexamethasone (DEX) in LPS-stimulated fetal liver-derived alveolar-like macrophages (FLAMs) isolated from NZBWF1 lupus-prone mice. FLAMs were treated with suboptimal concentrations of either DHA alone, DEX alone, or DHA+DEX in combination prior to LPS stimulation (20 ng/mL) for 4 or 8 hr.

Results: LPS stimulation resulted in significant enrichment of innate immunity and Type I/II IFN pathways with corresponding upregulation of gene sets falling within these pathways at both timepoints. LPS-primed FLAMs treated in combination with suboptimal concentrations of DHA and DEX exhibited superior combinatorial affects compared those observed with DHA and DEX treatment alone. DHA+DEX cotreatment resulted in downregulation of innate immunity and Type I/II IFN pathways initially altered by LPS treatment. Lastly, DHA+DEX cotreatment exhibited superior downregulation of individual Type I/II IFN genes compared to individual treatments.

Discussion: Our findings demonstrate that while DHA and DEX can significantly alter LPS-stimulated gene expression in alveolar-like macrophages when used in high enough concentrations alone, DHA can be used to potentiate the anti-inflammatory effects of DEX when both are used at lower concentrations. This study provides promising evidence that DHA can potentially be used to lower requisite amounts GCs required to reduce inflammation.

INTRODUCTION

The lung is host to a variety of immune cell types which aid in preservation of homeostatic functions as well as defense against harmful pathogens (201, 202). Many inhaled toxicants travel to the distal airways and alveoli where they interact with alveolar macrophages (AMs), which serve as the first line of defense against environmental insults (203). AMs, which arise from fetal liver monocytes, recognize various pathogen-associated molecular patterns (PAMPs) and damage-associated molecular patterns (DAMPs) via pattern-recognition receptors (PRRs). Activation of AMs by various PAMPs and DAMPs elicits effector functions such as proinflammatory cytokine/chemokine production, secretion of Type I/II Interferons (IFNs), phagocytosis, and cell death (204-206). Proinflammatory AMs, classically referred to as the "M1" phenotype, have been implicated in the pathology of various autoimmune diseases (e.g., lupus, arthritis) (207-209) and pathogenic infections (e.g., *Mycobacterium tuberculosis*, influenza) (204).

Systemic lupus erythematosus (lupus) is a debilitating, prototypical autoimmune disease that is characterized by chronic inflammation and a loss of self-tolerance (10). Lupus onset is dependent on a combination of genetic susceptibility and environmental exposures (2, 210). Epidemiologic studies have implicated environmental toxicants such as respirable crystalline silica ($cSiO_2$) (8, 9) and bacterial lipopolysaccharide (LPS)-containing dusts (14, 191-193) in the development of lupus. LPS, a component of the outer membrane of gram-negative bacteria, is a

well-known, potent activator the innate immune system (55). Upon interaction with AMs following inhalation exposure, LPS acts by binding the TLR4 receptor which stimulates MAP kinases, NF-κB, and interferon regulatory factors (IRFs) (203). These events lead to the upregulation of various proinflammatory cytokines/chemokines and Type I/II IFNs. Type I IFNs have been identified as an important part of lupus pathogenesis, and interferon-stimulated gene (ISG) expression is present in approximately 60-80% of lupus patients (1, 44). Robust IFN responses detected in lupus patients is associated with more active disease states and is believed to contribute to perpetuation of autoimmunity through the recruitment and activation of lymphocytes (44). Thus, pro-inflammatory and IFN responses resulting from interactions between AMs and environmental toxicants are crucial elements of chronic inflammatory diseases.

As it stands, one of the most common courses of treatment for lupus is glucocorticoids (GCs) such as prednisone. GCs are cost-effective anti-inflammatory agents that can quell chronic, cyclical bouts of increased disease activity (flares) (78). Yet, chronic use at moderate to high doses (≥7.5 mg/d) has been associated with several adverse side-effects such as osteoporosis, hyperglycemia, muscular atrophy, and cardiovascular disease (24-26). Additionally, a preclinical study conducted by our lab determined that $cSiO_2$-exposed NZBWF1 lupus-prone mice treated orally with moderate to high human equivalent doses of prednisone exhibited significant muscle wasting, hyperglycemia, and increased morbidity (19). Importantly, prednisone treatment also did not improve the survivability of $cSiO_2$-exposed mice. Based on mounting evidence from clinical and preclinical studies, it is evident that there is a critical need for cost-effective, steroid-sparing treatments for lupus patients.

Interestingly, omega-3 polyunsaturated fatty acids such as docosahexaenoic acid (DHA) have shown increasing promise as an anti-inflammatory therapeutic for autoimmune disorders

such as lupus and rheumatoid arthritis (83, 168, 172). Preclinical *in vivo* studies have demonstrated that dietary DHA supplementation effectively reduces environmental-triggered pulmonary inflammation and proinflammatory and ISG gene expression in NZBWF1 lupus-prone mice (16, 21, 67). Furthermore, *in vitro* studies have revealed that DHA can mediate inflammation via several mechanisms including: (i) alteration of lipid rafts and proinflammatory transmembrane receptors (113), (ii) activation of receptors (e.g., GPR120) (114) and transcription factors (e.g., PPARγ) (115) that are inhibitors of NF-κB activity (116), and (iii) production of specialized pro-resolving mediators (SPMs; e.g., resolvins, maresins, and protectins) (117). A recent study from our lab by Wierenga et al., demonstrated that DHA treatment was effective in attenuating LPS-stimulated Type I IFN responses in a novel macrophage cell model (211). Taken together, results from these previous studies suggest that the anti-inflammatory properties of DHA could potentially be harnessed to lower requisite doses of GCs required by lupus patients.

While previous *in vitro* studies have elucidated the anti-inflammatory mechanisms of action of DHA and GCs (e.g., dexamethasone, DEX) individually in macrophage-like cell lines, DHA and GC concomitant treatment has yet to be evaluated. Therefore, we designed a study to determine if DHA could potentiate the anti-inflammatory effects of the GC DEX in fetal liver-derived alveolar-like macrophages (FLAMs) isolated from the NZBWF1 lupus-prone mouse strain. Here, we tested the hypothesis that cotreatment of LPS-primed FLAMs with sub-optimal concentrations of both DHA and DEX would additively suppress proinflammatory and Type I/II IFN gene responses compared to individual treatment.

METHODS

Animals and FLAM cultures

NZBWF1 mice (Jackson Laboratories, Bar Harbor, ME) were housed at Michigan State

University's animal facility which was maintained at a constant temperature (21-24°C), humidity (40-55%), and 12-hour light/dark cycle. Animal experimental protocols for the following study were approved by the Institutional Animal Care and Use Committee (IACUC) at Michigan State University (MSU; AUF# 201800113). After mice were bred, dams were euthanized between 14-18 gestational days. Mice were euthanized via CO_2 inhalation for 10 minutes to ensure death to neonates, and cervical dislocation was used as a secondary form of euthanasia for the dam. Fetuses were promptly removed from the dam, and the loss of access to the maternal blood supply served as the secondary form of euthanasia for the neonates.

Fetal livers were excised from neonates and further processed to generate FLAM cell cultures as previously described (107, 108, 211). Briefly, fetal livers were dissociated in sterile phosphate buffered saline (PBS) to create a cell suspension. Suspensions were filtered through a 70-micron filter and centrifuged at 220 x g for 5 min. Two wash steps were performed using sterile PBS before resuspending cells in modified RPMI media (mRPMI, Thermo Fisher) containing 10% fetal bovine serum (FBS, Thermo Fisher), 1% penicillin-streptomycin (P/S, Thermo Fisher), 30 ng/mL murine granulocyte-monocyte colony stimulating factor (GM-CSF, PeproTech), and 20 ng/mL recombinant human TGF-β1 (PeproTech). Cells were plated in 10 cm culture plates (1 liver/plate). mRPMI media was replaced every ~2 days until cells created an adherent monolayer and exhibited a round AM-like morphology (~1 wk). Cells were then frozen down until needed for this study. FLAMs were thawed and cultured in mRPMI media for the duration of this experiment, and cells between passages 10 and 11 were used for all subsequent analyses.

Experimental Design

The experimental design for all experiments is described in **Figure 5.1A**. Briefly, FLAMs were seeded in 6-well plates at -48 hr in mRPMI media. At -24 hr, cells were gently washed, and media

was replaced with mRPMI containing 0 or 10 μM DHA (NuCheck Prep, Elysian, MN). Beginning at the DHA treatment step, mRPMI media containing 0.25% FBS was used to optimize DHA incorporation into the cell membrane by limiting competing fatty acids present in the media. At -1 hr, FLAMs were treated with mRPMI media containing 0 or 100 nM DEX (Sigma-Aldrich). At 0 hr, FLAMs were treated with mRPMI medium (CON Veh) or media containing 20 ng/mL LPS (LPS Veh; Salmonella enterica serotype typhimurium containing <1% impurities, Millipore Sigma). Cells were collected at either 4 or 8 hours depending on the designated endpoint. All treatment groups were as follows: (i) CON Veh (collected at 4 hr), (ii) LPS Veh (collected at 4 and 8 hr); (iii) DHA (collected at 4 and 8 hr); (iv) DEX (collected at 4 and 8 hr); (v) DHA+DEX (collected at 4 and 8 hr).

RNAseq

Cells reserved for RNAseq analysis were lysed using RLT lysis buffer (Qiagen) and RNA was isolated from cells using RNeasy Mini Kits (Qiagen). RNA was quantified with Qubit (Thermo Fisher Scientific) and integrity was verified with TapeStation (Agilent Technologies). Samples (RNA integrity >8) were library prepped at the MSU Genomics Core using the Illumina Stranded mRNA Library Preparation, Ligation Kit with IDT for Illumina Unique Dual Index adapters following the manufacturer's recommendations except that half volume reactions were used. Libraries were pooled in equimolar proportions and quantified using the Invitrogen Collibri Quantification qPCR kit. Samples were sequenced on the NovaSeq 6000 S4 flow cell in a 2x150bp paired end format using a NovaSeq v1.5, 300 cycle reagent kit. Base calling was done by Illumina Real Time Analysis (RTA) v3.4.4 and output of RTA was demultiplexed and converted to FastQ format with Illumina Bcl2fastq v2.20.0. RNAseq reads were trimmed using Trimmomatic v0.39 (212) and evaluated for quality control using FastQC 0.11.7

(https://www.bioinformatics.babraham.ac.uk/projects/fastqc/). Reads were aligned to the mouse reference genome (GRCm39 release 109) using STAR v2.7.9a (213) in the GeneCounts quantMode. Genes with fewer than 10 reads in at least one sample were filtered out prior to differential expression using DESeq2 (214). Genes were considered differentially expressed when |fold-change| ≥ 2 and adjusted p-value ≤ 0.5.

Enrichment Analyses

Gene set enrichment analysis (GSEA) using the fgsea R package (v1.20.0) was performed on fold-change ranked genes for the Gene Ontology (GO) and Kyoto Encyclopedia of Genes and Genomes (KEGG) gene sets obtained from the Gene Set Knowledgebase (GSKB; http://ge-lab.org/gskb/). Pathway-level information extractor (PLIER) v0.99.0 was used to identify modules of gene co-expression and collapse the patterns into latent variables (LVs) (Mao et al.). GO and KEGG gene sets obtained from GSKB were used as prior knowledge mapped to the identified LVs to identify putative changes in pathway activities. LVs were considered high confidence when area under the curve (AUC) ≥ 0.7 and false detection rate (FDR) ≤ 0.05. LV estimates were used to evaluate differences between treatment groups using a 3-way ANOVA (factors; DHA treatment, DEX treatment, Time) and Tukey HSD pairwise post-hoc test. Top contributing genes were extracted using the plotTopZ function. Inference of transcription factor (TF) activity was performed using the decoupleR R package (215). High confidence (level "A") mouse TFs and their target genes were obtained from DoRothEA (216).

Quantitative PCR

Cells were treated in 12-well plates following the same experimental design depicted in **Figure 5.1A**. Approximately $5x10^5$ cells/well were collected for RNA extraction. Total RNA was extracted RNeasy Mini Kits (Qiagen) per manufacturer's instructions. RNA was eluted using

RNase-free water provided by the RNeasy kit and quantified using the Nanodrop ND-1000 spectrophotometer (Thermo Fisher Scientific, Waltham, MA). Using a High-Capacity cDNA Reverse Transcriptase Kit (Thermo Fisher Scientific) RNA was used to prepare cDNA. Taqman assays were run in technical triplicate using the TakaraBio smartchip real-time PCR system with the assistance of the MSU Genomics Core to assess gene expression. Expression of IFN-stimulated genes (*Mx1, Irf7, Ifit1, Isg15, Oasl1, Rsad2*) and housekeeping genes (*Actb, Hprt*) were assessed. ΔCt values were calculated by subtracting the average raw Ct value of housekeeping genes from the raw Ct value for each gene of interest. To evaluate LPS proinflammatory gene induction, ΔΔCt values were calculated by subtracting average ΔCt value of the respective CON Veh group from the average ΔCt value of the LPS Veh treatment. ΔΔCt values are shown in units of fold increase relative to LPS Veh for each gene of interest. Similarly, to assess DHA/DEX treatment on LPS-stimulated FLAMs, ΔΔCt values were calculated by subtracting average ΔCt value of the respective LPS Veh group from the average ΔCt value of the corresponding DHA/DEX treatment. ΔΔCt values are shown in units of fold increase relative to LPS Veh for each gene of interest.

Fatty Acid Analysis

Cell pellets from (i) CON Veh, (ii) LPS Veh, (iii) DHA, (iv) DEX, and (v) DHA+DEX groups (**Figure 5.1A**) were stored in 100% methanol at -80°C prior to fatty acid composition analysis preformed at OmegaQuant using gas chromatography (GC) with flame ionization detection. Cell pellets in solution were transferred into a screw-cap glass vials and dried in a speed vac. After drying methanol containing 14% boron trifluoride (Sigma-Aldrich, St. Louis, MO) was added. The vial was briefly vortexed and heated in a hot bath at 100˚C for 10 minutes. After cooling, hexane (EMD Chemicals, USA) and HPLC grade water were added sequentially. The vials were recapped, vortexed and centrifuged help to separate layers. An aliquot of the hexane layer was

transferred to a GC vial. GC was carried out using a GC2010 Gas Chromatograph (Shimadzu Corporation, Columbia, MD) equipped with a SP2560, 100-m fused silica capillary column (0.25 mm internal diameter, 0.2 um film thickness; Supelco, Bellefonte, PA).

Fatty acids were identified by comparison with a standard mixture of fatty acids characteristic of RBC (GLC OQ-A, NuCheck Prep, Elysian, MN) which was also used to determine individual fatty acid calibration curves. The following 24 fatty acids (by class) were identified: saturated (14:0, 16:0, 18:0, 20:0, 22:0 24:0); cis monounsaturated (16:1, 18:1, 20:1, 24:1); trans [16:1, 18:1*, 18:2* - see below for more details); cis n-6 polyunsaturated (18:2, 18:3, 20:2, 20:3, 20:4, 22:4, 22:5); cis n-3 polyunsaturated (18:3, 20:5, 22:5, 22:6). Fatty acid composition was expressed as a percent of total identified fatty acids. The omega-3 index is defined as the sum of 20:5n-3 (EPA) and 22:6n-3 (DHA). The chromatographic conditions used in this study were sufficient to isolate the C16:1trans isomers and the C18:2 Δ 9t-12c, 9t-12t, and 9c-12t isomers, which is reported as C18:2n6t. However, each individual C18:1 trans molecular species (i.e., C18:1 Δ6 thru Δ13) could not be segregated but appeared as two blended peaks that eluted just before oleic acid. The areas of these two peaks were summed and referred to a C18:1 trans.

Data visualization and statistics

Visualization of RNAseq differential expression and functional enrichment analyses was performed using R v4.1.2. Visualization of individual gene graphs was performed using Prism 9 (GraphPad Prism v 9.2, San Diego, CA).

RESULTS

Increased DHA incorporation in DHA-treated FLAMs

DHA treatment of LPS-stimulated FLAMs resulted in approximately a 3-fold increase of DHA incorporated into the phospholipid membrane (**Figure 5.1B** and **Table 5.1**). Concurrent reductions

in oleic acid (OA) and arachidonic acid (AA) were observed in DHA-treated cells. Significant differences in DHA, OA, and AA content were not detected in LPS-primed FLAMs treated with DEX alone. Interestingly, DEX did not alter DHA incorporation, or conversely the displacement in OA and AA, in the phospholipid membrane of cells that were cotreated with DHA+DEX.

Concentration-dependent suppression of IFN gene expression with DHA and DEX treatment

LPS-treatment increased the expression of Type I IFN regulated genes in FLAMs compared to those treated with CON Veh (**Figure 5.2A-C**). DHA treatment alone resulted in decreased IFN gene expression at the 25 μM concentration (**Figure 5.2A**), but not at the 10 μM (**Figure 5.2B**) and 5 μM (**Figure 5.2C**) for all genes. LPS-primed FLAMs treated with varying concentrations of DEX alone demonstrated decreased IFN gene expression at the 1 μM concentration for all genes. Some, but not all, genes were affected by DEX treatment at 100 and 10 nM. LPS-primed FLAMs treated with both DHA and DEX at the same concentrations that were otherwise ineffective in reducing IFN gene expression when used alone, significantly altered gene expression when combined.

LPS-stimulated enrichment of innate immunity pathways

LPS treatment in FLAMs resulted in 3632 and 3572 differentially expressed genes (DEGs) at 4 and 8 hr, respectively (**Figure 5.3A**) compared to CON Veh-treated FLAMs. Of these total DEGs, 1772 were upregulated at 4 hr and 1574 were upregulated at 8 hr. Additionally, there were 1860 and 1998 DEGs downregulated with LPS treatment at 4 and 8 hr, respectively. Gene set enrichment analysis (GSEA) performed to identify biological processes associated with gene expression revealed that LPS treatment at both 4 and 8 hr showed increased expression of genes involved in various innate immunity pathways such as response to lipopolysaccharide, cellular response to IFNγ, and cytokine and chemokine activity (**Figure 5.3B**). Using DecoupleR, the top 10 inferred

active transcription factors (TFs) in response to LPS treatment were identified for both 4 and 8 hr timepoints (**Figure 5.3C**). Several proinflammatory TFs, such as IRF1, STAT1/2, NFKB1, had increased predicted activity with LPS treatment. Although certain TFs were more positively enriched at either 4 or 8 hr, 9 out of 10 TFs were preserved as the most positively enriched TFs with LPS treatment.

Suppression of LPS-induced proinflammatory response with DHA+DEX cotreatment

DHA individual treatment in LPS-primed FLAMs resulted in 16 DEGs at 4 hr and 83 DEGs at 8 hr (**Figure 5.4A**). DEX treatment alone resulted in 48 DEGs at 4 hr and 160 DEGs at 8 hr. Few to no DEGs were shared between DHA and DEX individual treatments at each timepoint. Interestingly, DHA+DEX co-treatment led to a greater number of DEGs being expressed at 4 and 8 hr compared to DHA and DEX treatment alone. DHA+DEX co-treatment resulted in 247 DEGs in LPS-primed FLAMs at 4 hr and 347 DEGs at 8 hr. DHA+DEX treatment also resulted in greater overlap of DEGs shared between co-treatment and individual treatments.

PLIER analysis identified 9 high confidence LVs representing groups of co-expressed genes associated with multiple pathways shown in the U matrix (**Figure 5.4B**). DHA+DEX cotreatment resulted in significantly altered LV estimates for LV2, which was broadly represented by genes associated with pathways involving cellular response to IFNγ, cellular response to IFNβ, and antigen processing and presentation (**Figure 5.4B,C**). This was further evidenced based on evaluation of the top 40 genes that contributed to LV2 (**Figure 5.5**). Genes identified within this list pertained to IFN and anti-viral response (e.g., *Mx1, Mx2, Oasl1, Ifit1, Sp140, Gm5431*), MCH I antigen processing and presentation (e.g., *H2-dma, H2-ab1, H2-aa, H2-eb1*), cytokine receptor signaling (e.g., *CD74, Ccr5, Ccl2*), and apoptosis and proliferation (e.g., *Mxd1, Daxx, Zeb1*). DHA+DEX cotreatment led to greater repression of these genes when compared to the DHA and

DEX treatments alone.

Combinatorial downregulation of LPS-triggered proinflammatory gene expression with DHA+DEX treatment

Of the total DEGs resulting from DHA+DEX treatment, 75 genes were downregulated with cotreatment at 4 hr and 291 were downregulated at 8 hr (**Figure 5.6A**). DHA+DEX treatment-related effects on TF enrichment opposed those observed in FLAMs primed with LPS (**Figure 5.6B,C**). DHA+DEX co-treatment resulted in decreased predicted activity of TFs that are drivers of inflammatory gene expression such as IRF1, STAT1/2/3, and NFKB1 at both 4 and 8 hr. Correspondingly, genes downstream of the same proinflammatory TFs altered by DHA+DEX treatment were also downregulated with cotreatment. Moreover, combinatorial affects were observed with DHA+DEX co-treatment compared to individual treatment. Individual DEGs pertaining to Type I/II IFNs (**Figure 5.7A**), cytokine signaling (**Figure 5.7B**), and antigen processing and presentation (**Figure 5.7C**) were downregulated compared to LPS treatment at 8 hr. Downregulation of each gene was potentiated with cotreatment and DHA+DEX co-treated cells were significantly different compared to cells treated with DHA and DEX individually. Combinatorial effects were observed for some but not all genes at the 4 hr timepoint.

Limited upregulation of genes with DHA+DEX cotreatment

Combination treatment with DHA+DEX led to the upregulation 112 DEGs at 4 hr and 48 DEGs upregulated at 8 hr (**Figure 5.8A**). Of these genes, 39 DEGs at 4 hr and 22 DEGs at 8 hr are not currently annotated and their functions are unknown. Furthermore, only 12 genes at 4 hr and 1 gene at 8 hr were shown to have co-treatment effects resulting in significant differences between DHA+DEX and DHA or DEX individual treatments. DHA+DEX co-treatment resulted in predicted increased activity of TFs that reduce inflammation (e.g., PPARG, YBX1, TWIST1),

proliferation (e.g., BCL6, E2F4), differentiation and development (e.g., MYC, GLI2, NFI, RUNX3), glucocorticoid signaling (NR3C1), circadian rhythm (CLOCK), and metabolism (e.g., ARNTL, SREBP2) (**Figure 5.8B,C**).

DISCUSSION

Alveolar macrophages are central to the detection, sequestration, and initiation of targeted immune responses towards respirable environmental toxicants. However, there are currently few cell models that (i) appropriately model and retain an alveolar macrophage phenotype or (ii) provide sufficient cell numbers to perform series of experiments. The FLAM cell model provided an opportunity carry out a series of novel experiments designed to elucidate the steroid-sparing potential of DHA in cells that closely resemble alveolar macrophages (107). Here, we made several novel observations by utilizing bulk transcriptomics in NZBWF1-derived FLAMs. First, RNAseq data revealed that LPS treatment led to the upregulation of several pathways involved in innate immunity such as cytokine/chemokine and IFN signaling. Correspondingly, inferred TF activity analysis revealed predicted upregulated activity of TFs involved in inflammatory signaling such as NFKB, STAT1, and IRF1. Second, DHA+DEX co-treatment in LPS primed FLAMs led to a greater total of DEGs compared to DHA and DEX treatment alone. Third, DHA+DEX co-treatment downregulated several pathways also involved in innate immunity, such as cytokine, Type-I IFN (IFNβ), and Type-II IFN (IFNγ) signaling. TF activity, likewise, showed decreased predicted activity of the TFs NFKB, STAT1/2, and IRF1. Fourth, greater downregulation of individual IFN, cytokine, and antigen presentation and processing genes resulted from DHA+DEX cotreatment compared to individual DHA and DEX treatment. Lastly, while DEGs and TFs that were upregulated by DHA+DEX cotreatment were not as prominent in these analyses, cotreatment did demonstrate a modest impact TFs associated with proliferation, differentiation, and anti-

inflammatory mediators such as PPARG.

In line with what has been demonstrated in previous studies using alveolar like-macrophages (211), LPS served as a potent activator of IFN-related gene signaling in FLAMs at multiple timepoints. Type-I IFNs are key mediators of lupus pathogenesis in human patients and are often associated with more severe disease activity (44, 217). In the context of environmental triggered lupus, preclinical studies have demonstrated that respirable toxicants such as crystalline silica and LPS-containing organic dust mixtures, elicit upregulated Type-I IFN gene signatures in lupus- and rheumatoid arthritis (RA)-prone mice, respectively (20, 21, 54). Interestingly, several of the IFN-related genes upregulated as a result of pulmonary silica or LPS exposure in the aforementioned *in vivo* studies were consistent with LPS-responsive IFN genes identified within the present dataset. Furthermore, RA-prone mice exposed to LPS demonstrated increased IFN gene expression within monocyte-macrophage populations isolated from the lung (54). Considering the overall importance of IFNs in lupus, in addition to their relevance concerning monocyte-macrophage populations in the lung, this experimental model provides important information about Type-I IFN gene responses specific to specialized pulmonary monocyte-macrophage cell types such as the alveolar macrophage.

While DHA or DEX treatments have been used individually elucidate potential mechanisms by which each reduces proinflammatory gene expression in various macrophage cell lines (102-104, 111, 211), cotreatment had yet to be evaluated prior to this study. Based on the amount of DEGs that were downregulated versus upregulated with DHA+DEX cotreatment, it was evident that repression of proinflammatory gene expression was the primary method by which DHA+DEX helped FLAMs return to an M2 anti-inflammatory phenotype. Here, not only was DHA+DEX co-treatment in LPS-primed FLAMs effective in reducing proinflammatory and IFN

gene signatures, but significant differences were detected between cotreatment and individual treatments. Though upregulated gene responses resulting from cotreatment were less prominent, several of the TFs predicted to have increased activity are associated with anti-inflammatory and differentiation pathways. Furthermore, many of these identified TFs work together to reduce either inflammation or differentiation. For example, Pparγ has been shown to inhibit inflammatory gene expression through interactions with with the LXR (218), but it has also been shown work in combination with Myc to create an M2 phenotype in monocytes (219). Similar to Pparγ and Myc, other combinations of TFs such as Ybx1 and Pgrn, Twist and Srebp, or Clock and Bmal2 can work cooperatively to reduce TNF-α binding (220), TNF-α production (221), and complement (222), respectively. Taken together, the DEGs specific to cotreatment work together to attenuate the proinflammatory phenotype of LPS-primed FLAMs.

The evidence provided by the present study supports the idea that DHA has steroid-sparing properties whereby it can potentiate the anti-inflammatory effects of GCs, like DEX, to attenuate inflammation in the alveolar macrophage. Given that chronic use of GCs moderate to high doses can lead to significant toxicity and diminished quality of life in lupus patients, there is a critical need for interventions that can be used in conjunction with GCs to lessen toxicity while also reducing inflammation and autoimmunity. Overall, these findings support the need for further investigations *in vtiro* and *in vivo* to determine the full extent of DHA's steroid-sparing effects in treating environmentally triggered inflammation and autoimmunity.

ACKNOWLEDGMENTS

The authors thank the Michigan State University Genomics Core Facility for their expertise and assistance with sequencing and procession RNAseq samples.

AUTHOR CONTRIBUTIONS

LH: study design, data analysis/interpretation, figure preparation, manuscript preparation; RN: data curation, figure preparation, manuscript preparation; AT and IB: study design; OF: FLAM isolation; JH: study design, project funding, manuscript preparation; JP: study design, project funding, manuscript preparation.

FIGURES

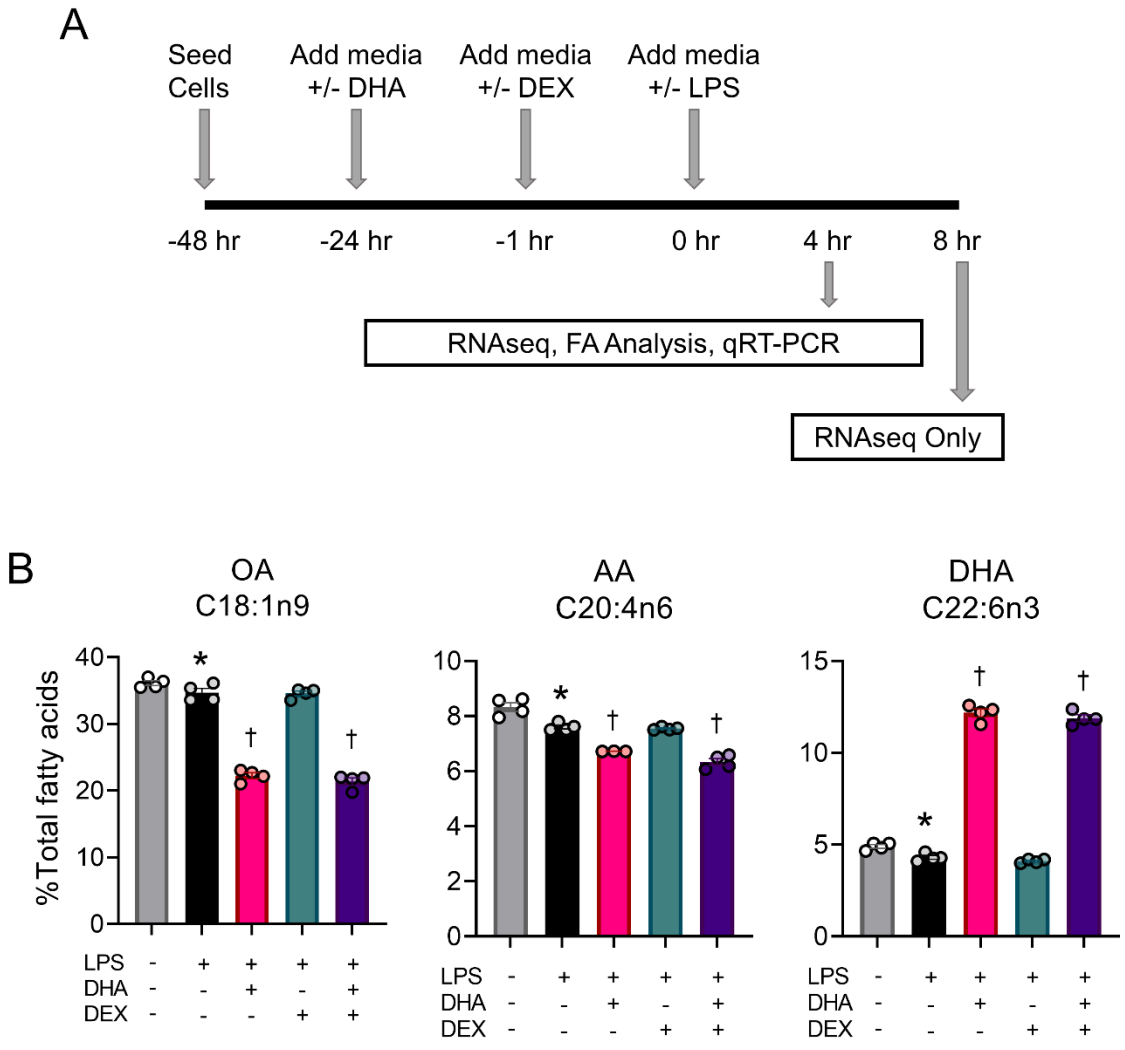

Figure 5.1: Experimental design. (A) FLAMS were seeded in 6-well plates 48 hours prior to LPS stimulation in mRPMI media with 10% FBS and 1% P/S. 24 hours pre-stimulation, media was replaced with mRPMI containing either DHA or EtOH Veh containing 0.25% FBS and 1% P/S. 1 hour pre-stimulation media was replaced with mRPMI containing either DEX or EtOH Veh. At time 0, media was discarded, and cells were treated with mRPMI media containing either 20 ng/mL LPS or PBS Veh. Cells were collected at either 4 or 8 hours post-LPS stimulation for RNAseq. **(B)** DHA supplementation resulted in increased phospholipid DHA with accompanied decreases in arachidonic acid and oleic acid. $p<0.05$; *Significant differences between VEH and LPS VEH were determined using a Student's t-test; †Significant differences between LPS VEH and DHA/DEX treatments were determined using a One-Way ANOVA.

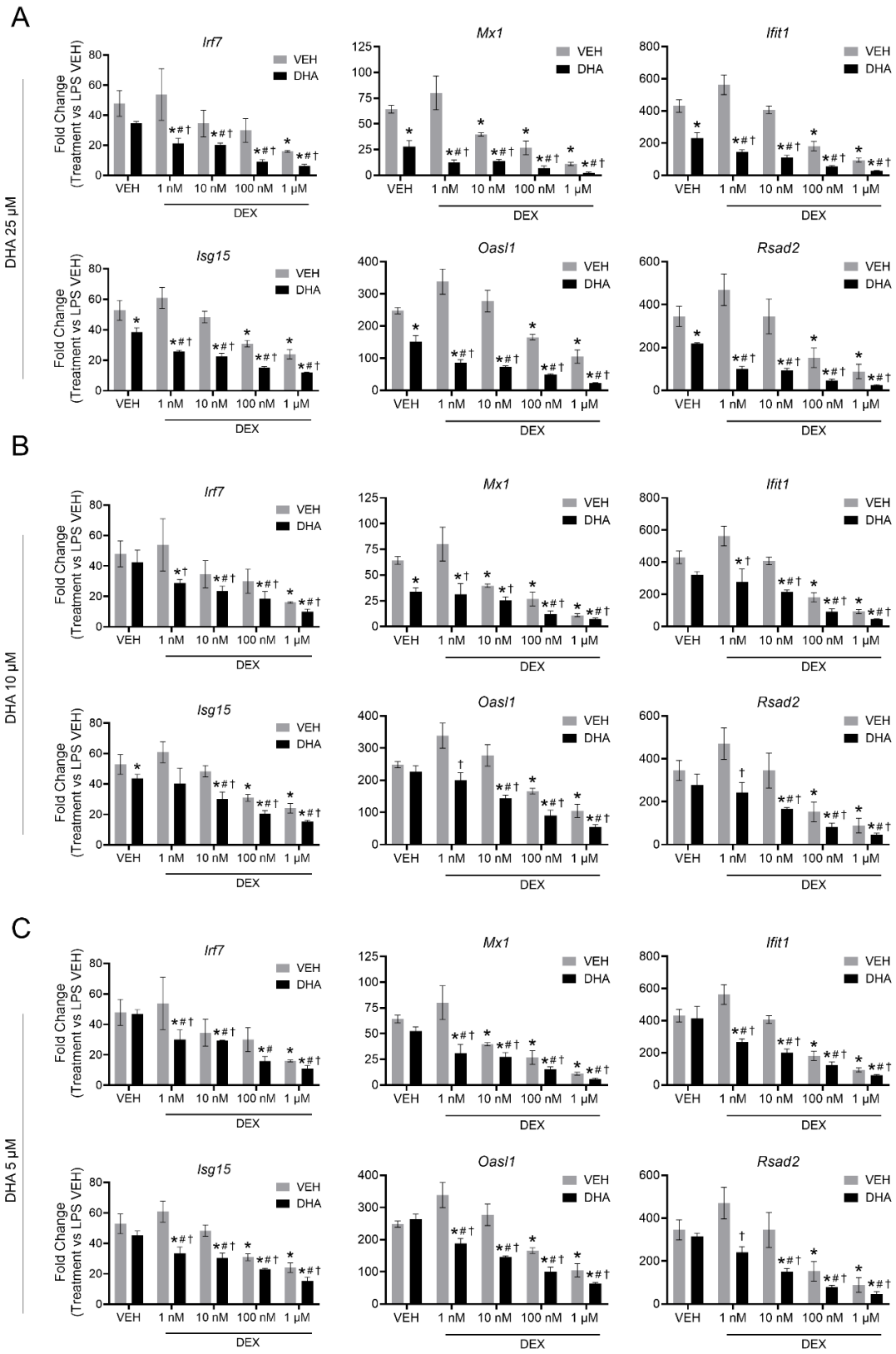

Figure 5.2: DHA+DEX combination treatment suppresses IFN-regulated gene expression.

Figure 5.2 (cont'd):
qRT-PCR was performed on FLAMs stimulated with LPS (20 ng/mL) for 4 hr. Cells were pre-treated with either VEH containing no DHA or RPMI media containing 25 μM **(A)**, 10 μM **(B)**, or 5 μM **(C)** DHA at -24 hr. Cells were then treated with VEH containing no DEX or varying concentrations of DEX (1 nM-1 μM) -1 hr prior to LPS treatment. Fold change is shown as DHA and/or DEX treatment relative to LPS VEH ± SEM. n=3 biological replicates. $p<0.05$; *Significant compared to LPS VEH; #Significant compared to DHA alone; †Significant compared to DEX alone.

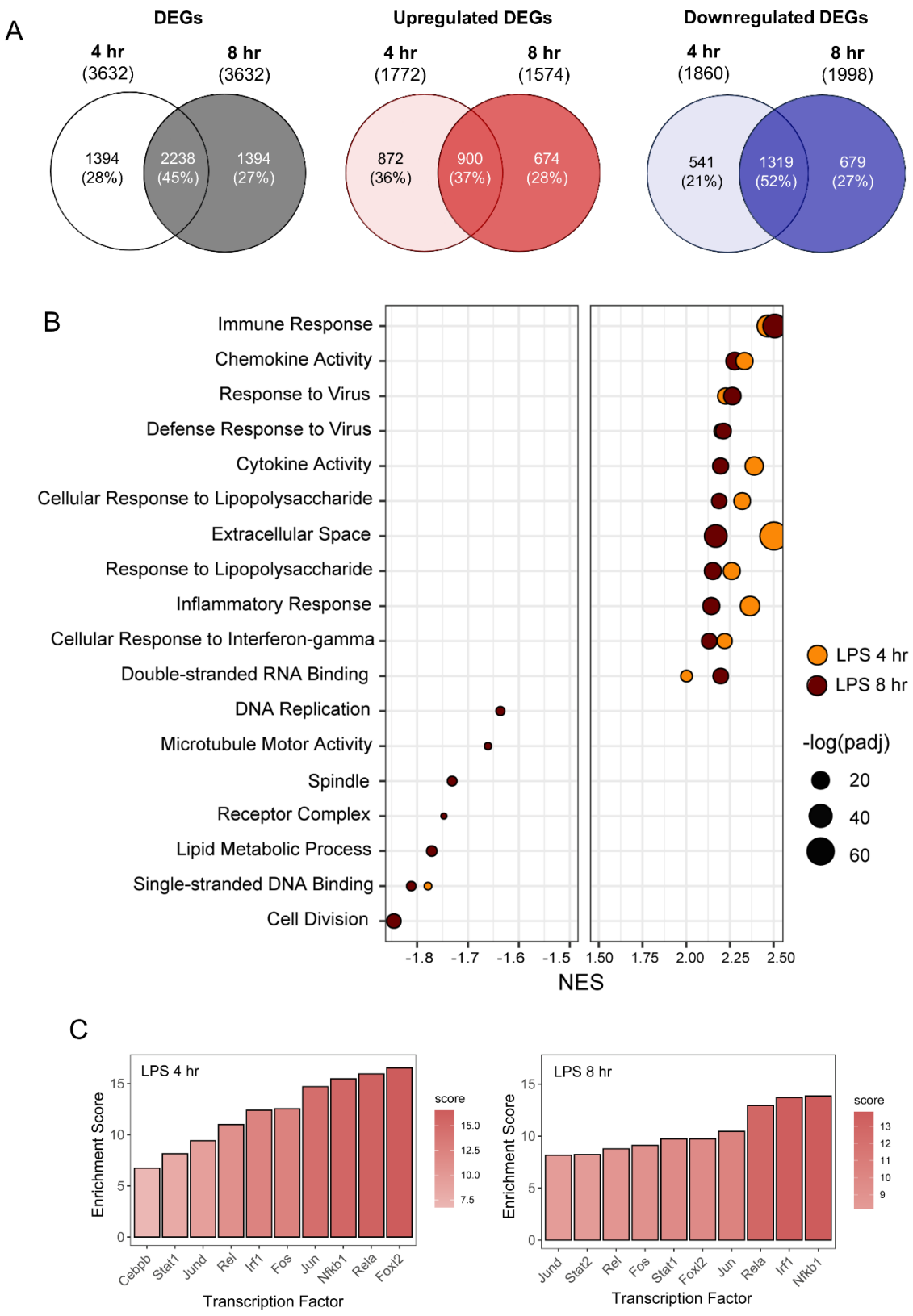

Figure 5.3: LPS-induced transcriptional responses in FLAMs. (A) Differentially expressed

Figure 5.3 (cont'd):
genes (DEGs) were determined using DESeq2 (214) filtering for genes exhibiting a |log2 fold change| >= 2 and adjusted p-value <= 0.05 between the LPS treatment group and vehicle control (CON) group. Venn diagrams for total DEGs, upregulated DEGs, and downregulated DEGs are shown for the 4 hr timepoint (left circle), 8 hr timepoint (right circle), and both timepoints (intersection). **(B)** Functional enrichment analysis using the GSEA method was used to identify the top 10 biological processes associated with up- and downregulated genes at each timepoint which was subsequently manually curated to focus on immune-related pathways. **(C)** Top 10 inferred active transcription factors following LPS treatment were identified for both timepoints using DecoupleR (215).

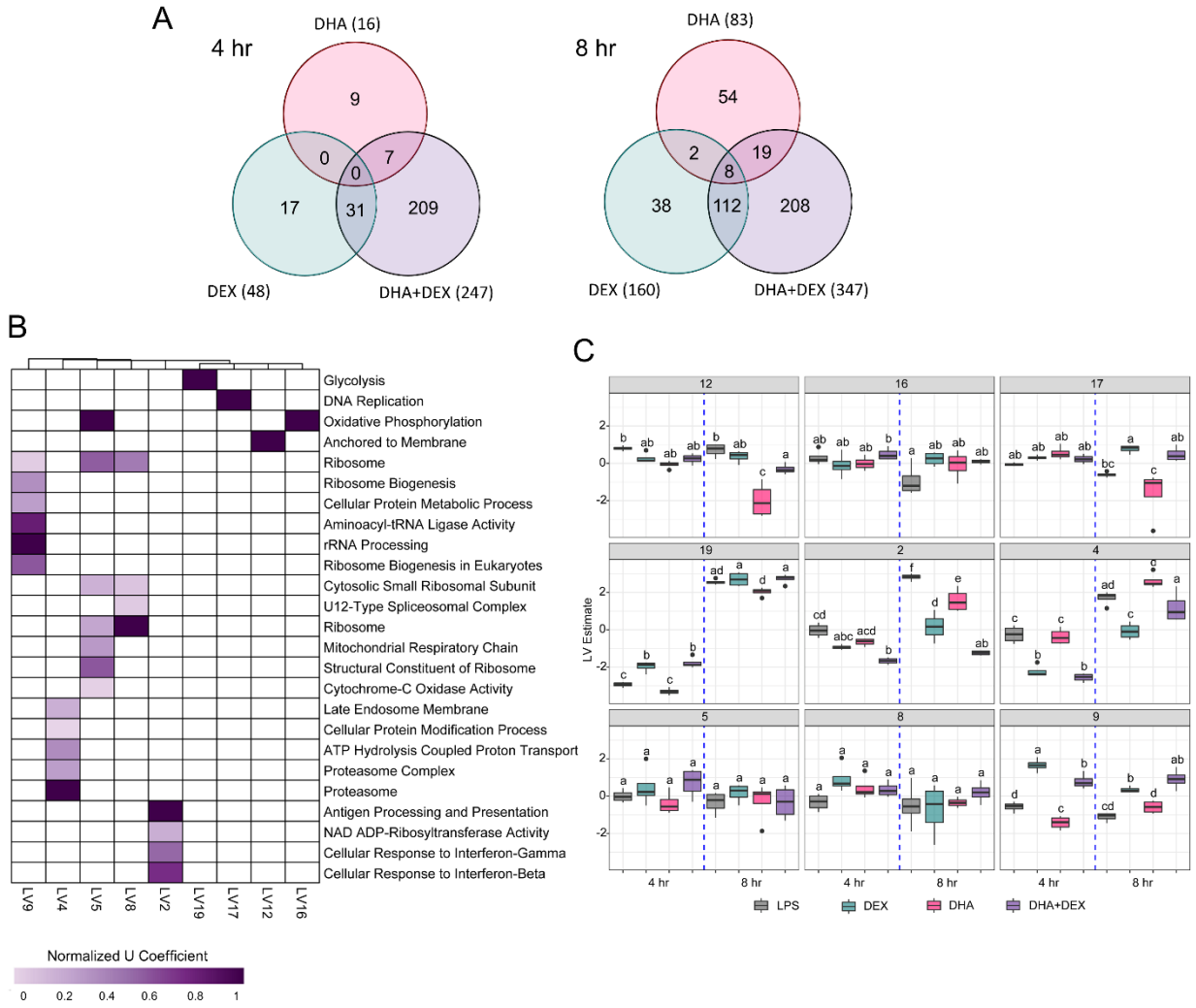

Figure 5.4: DHA and DEX individual and co-treatment transcriptional responses in LPS-stimulated FLAMs. (A) Differentially expressed genes (DEGs) were determined using DESeq2 (214) filtering for genes exhibiting a |log2 fold change| >= 2 and adjusted p-value <= 0.05 between DHA, DEX, or DHA+DEX treatment relative to LPS control. Venn diagrams for the number of treatment-dependent unique gene symbols for 4 and 8 hr timepoints. **(B)** Functional enrichment analysis using the PLIER method was used to identify significantly enriched biological processes associated with DHA+DEX co-treatment. Pathway-level information extractor (PLIER) was used to identify high confidence latent variables (LVs; AUC >= 0.7 and FDR <= 0.05) mapped to Gene Ontology and KEGG gene sets. **(C)** LV estimates for high confidence LVs are shown for each treatment group. Treatment groups were assessed by 3-way ANOVA and different letters indicate significant differences (p <= 0.05).

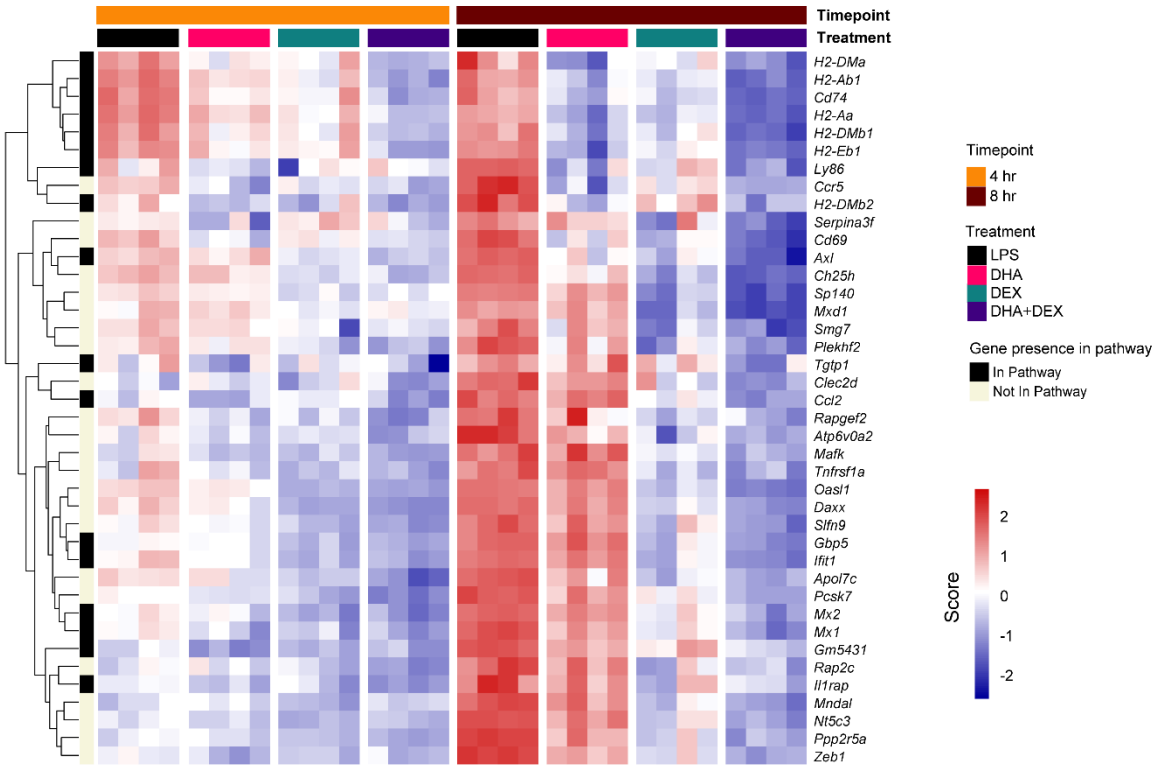

Figure 5.5: Altered genes within antigen processing and presentation pathway with DHA+DEX cotreatment. Top 40 genes enriched by co-treatment were determined using pathway-level information extractor (PLIER). Color scale corresponds to scaled expression value with red being highly expressed genes and blue corresponding to downregulated genes.

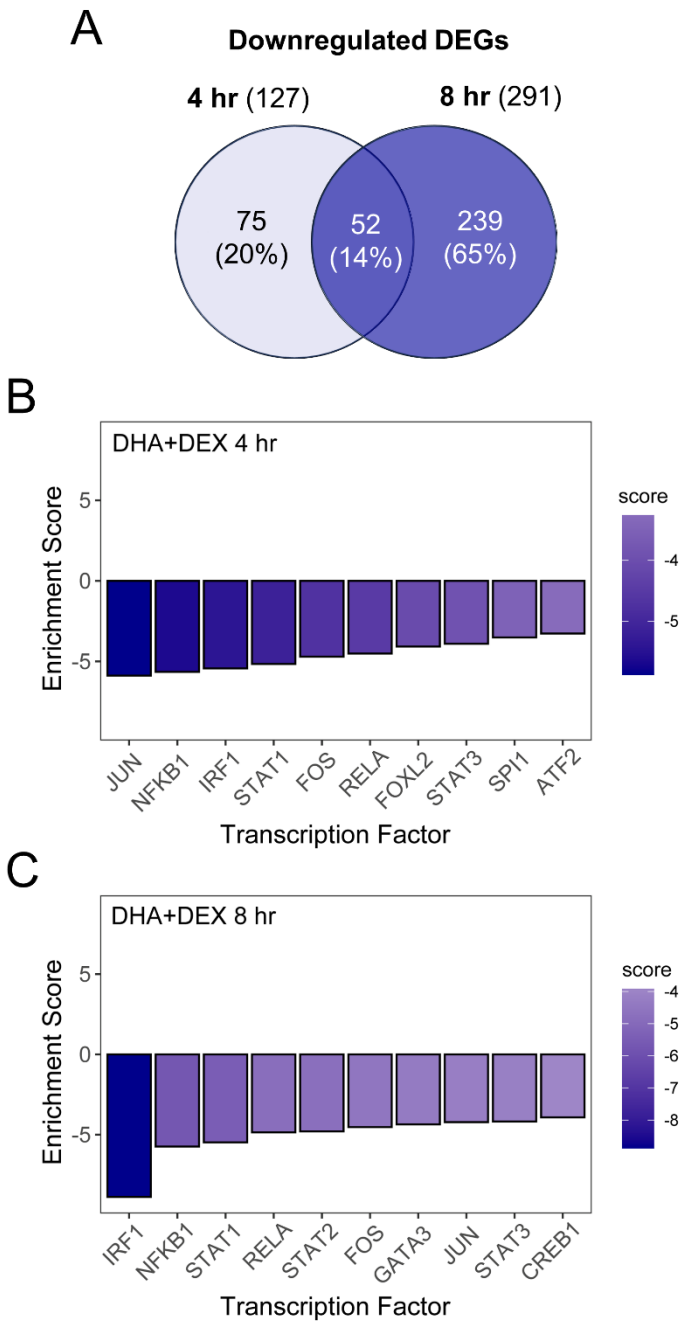

Figure 5.6: Downregulated DEGs and decreased transcription factor activity with DHA+DEX cotreatment. (A) Downregulated differentially expressed genes (DEGs) were determined using DESeq2 (214) filtering for genes exhibiting a |log2 fold change| >= 2 and adjusted p-value <= 0.05 between the LPS treatment group and vehicle control (CON) group. Venn diagrams for downregulated DEGs are shown for the 4 hr timepoint (left circle), 8 hr timepoint (right circle), and both timepoints (intersection). Top 10 inferred transcription factors that experience a reduction in activity following DHA+DEX co-treatment relative to LPS Veh were identified for 4 hr **(B)** and 8 hr **(C)** timepoints using DecoupleR (215).

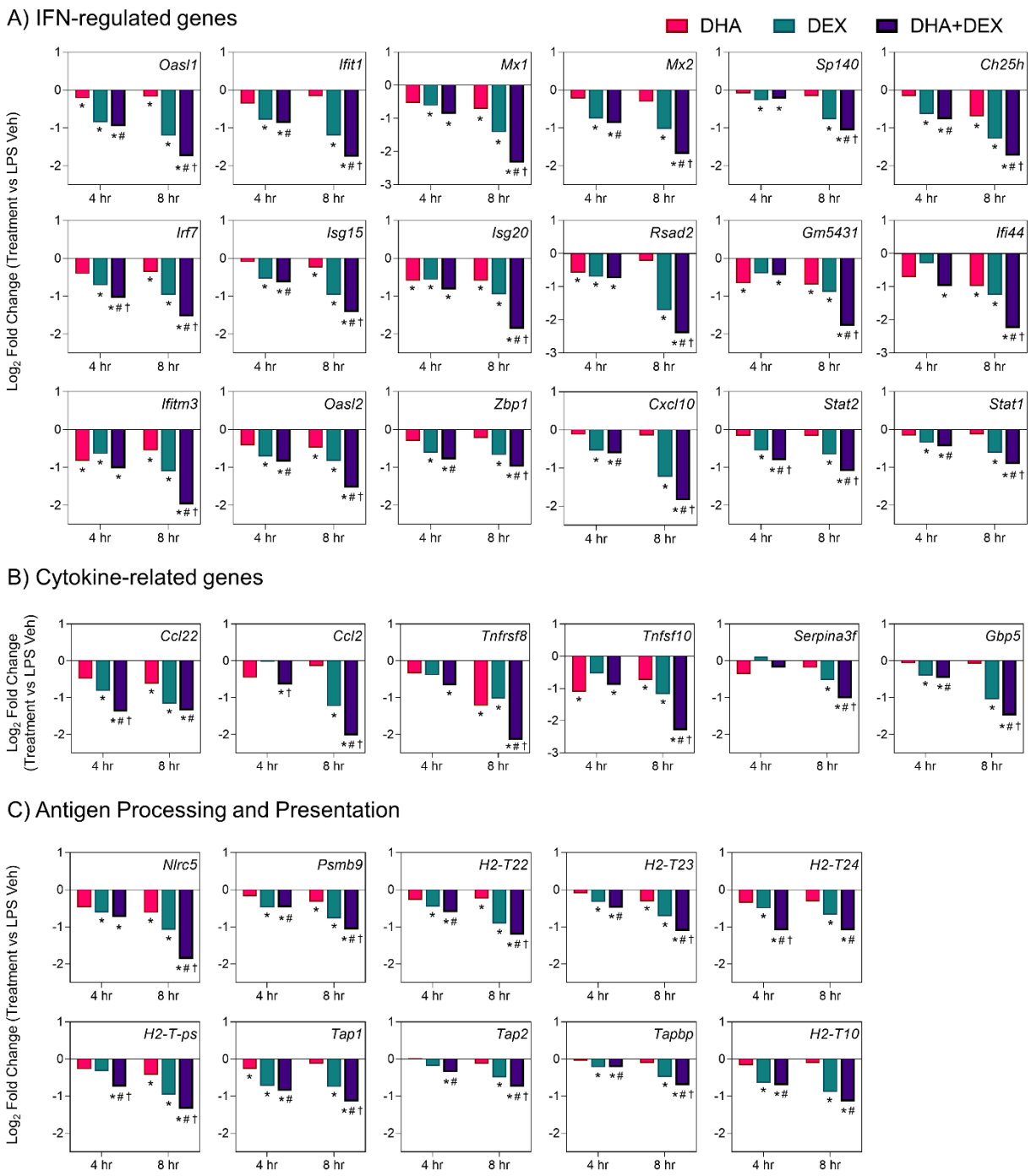

Figure 5.7: DHA+DEX combinatorial effects on suppression of innate immunity-related genes. Representative individual differentially expressed genes related to **(A)** Type I IFNs, **(B)** cytokine signaling, and **(C)** antigen processing and presentation that exhibited combinatorial affects compared to individual DHA or DEX treatment were isolated from RNAseq dataset. Log2 fold change was determined relative to LPS Veh. $p<0.05$; *Significant compared to LPS VEH; #Significant compared to DHA alone within respective timepoint; †Significant compared to DEX alone within respective timepoint.

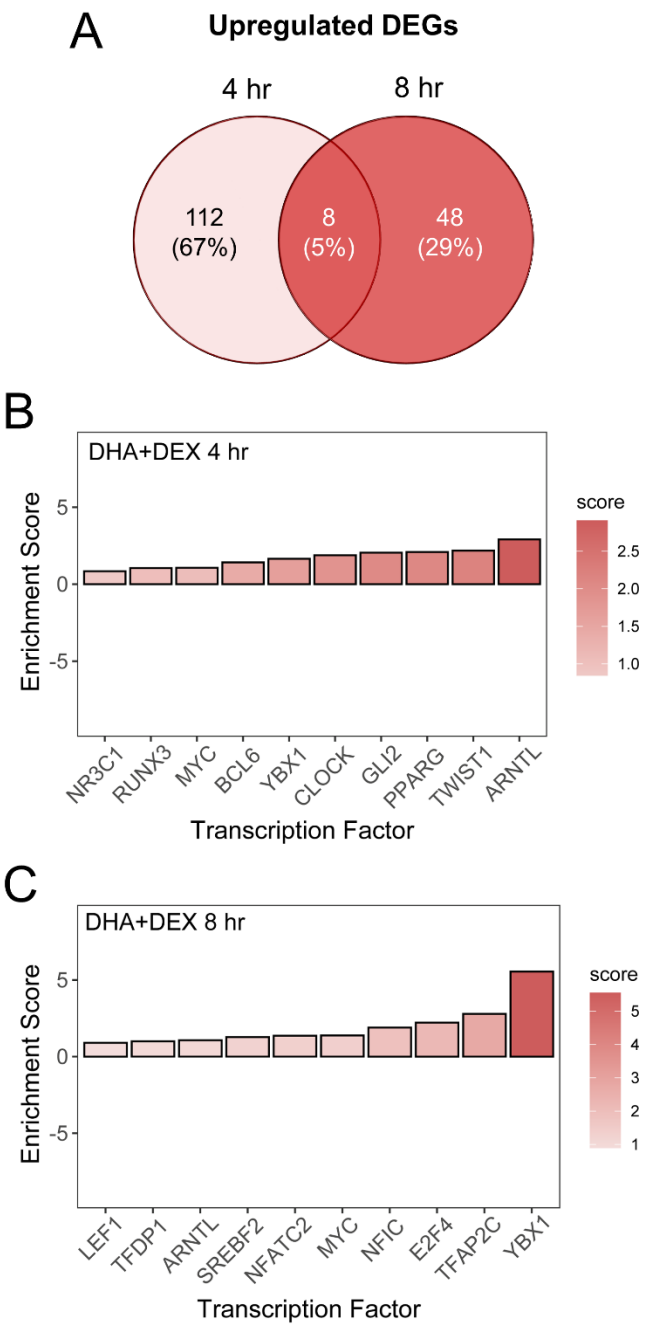

Figure 5.8: Upregulated DEGs and increased transcription factor activity with DHA+DEX cotreatment. (A) Downregulated differentially expressed genes (DEGs) were determined using DESeq2 (214) filtering for genes exhibiting a |log2 fold change| >= 2 and adjusted p-value <= 0.05 between the LPS treatment group and vehicle control (CON) group. Venn diagrams for downregulated DEGs are shown for the 4 hr timepoint (left circle), 8 hr timepoint (right circle), and both timepoints (intersection). **(B)** Top 10 inferred transcription factors that experience a increase in activity following DHA+DEX co-treatment relative to LPS Veh were identified for both timepoints using DecoupleR (215).

TABLES

Table 5.1: Fatty acid composition of FLAMs.

Fatty Acid	Chemical Formula	% of total fatty acids, mean ± SEM				
		VEH CON	LPS VEH	DHA	DEX	DHA+DEX
Myristic acid	C14:0	2.66 ± 0.02	2.40 ± 0.20	2.15 ± 0.28	1.85 ± 0.19	1.75 ± 0.33
Palmitic acid	C16:0	18.92 ± 0.42	23.61 ± 1.02*	28.46 ± 1.04†	24.96 ± 0.70	30.11 ± 0.88†
Palmitelaidic acid	C16:1n7t	0.24 ± 0.02	0.18 ± 0.01*	0.10 ± 0.01†	0.21 ± 0.01	0.12 ± 0.01†
Palmitoleic acid	C16:1n7	3.10 ± 0.03	3.04 ± 0.06	2.61 ± 0.03†	2.99 ± 0.06	2.46 ± 0.07†
Stearic acid	C18:0	13.83 ± 0.34	13.01 ± 0.14*	14.14 ± 0.14†	12.90 ± 0.04	13.95 ± 0.15†
Elaidic acid	C18:1t	0.41 ± 0.03	0.40 ± 0.02	0.25 ± 0.02†	0.43 ± 0.02	0.23 ± 0.02†
Oleic acid	C18:1n9	36.11 ± 0.36	34.67 ± 0.63*	22.24 ± 0.45†	34.57 ± 0.36	21.36 ± 0.54†
Linoelaidic acid	C18:2n6t	0.52 ± 0.02	0.47 ± 0.03	0.26 ± 0.01†	0.48 ± 0.03	0.26 ± 0.02†
Linoleic acid	C18:2n6	1.07 ± 0.02	0.97 ± 0.02*	0.84 ± 0.02†	0.97 ± 0.01	0.84 ± 0.00†
Arachidic acid	C20:0	0.87 ± 0.02	0.86 ± 0.04	0.85 ± 0.00	0.75 ± 0.02	1.02 ± 0.05†
gamma-Linolenic acid	C18:3n6	0.02 ± 0.00	0.01 ± 0.00*	0.01 ± 0.00	0.02 ± 0.01	0.01 ± 0.00
Eicosenoic acid	C20:1n9	0.50 ± 0.03	0.53 ± 0.03	0.23 ± 0.01†	0.49 ± 0.01	0.21 ± 0.01†
alpha-Linolenic acid	C18:3n3	0.02 ± 0.00	0.01 ± 0.00*	0.01 ± 0.00	0.01 ± 0.00	0.01 ± 0.00
Eicosadienoic acid	C20:2n6	0.07 ± 0.01	0.06 ± 0.00	0.03 ± 0.01†	0.04 ± 0.00†	0.02 ± 0.01†
Behenic acid	C22:0	0.51 ± 0.04	0.47 ± 0.06	0.62 ± 0.04	0.46 ± 0.03	0.82 ± 0.06†
Dihomo-g-linolenic acid	C20:3n6	0.91 ± 0.03	0.79 ± 0.00*	0.90 ± 0.00†	0.84 ± 0.01†	0.98 ± 0.02†
Arachidonic acid	C20:4n6	8.33 ± 0.16	7.61 ± 0.07*	6.61 ± 0.12†	7.55 ± 0.03	6.34 ± 0.12†
Lignoceric acid	C24:0	0.53 ± 0.03	0.52 ± 0.03	0.54 ± 0.03	0.47 ± 0.02	0.67 ± 0.02†
Eicosapentaenoic acid	C20:5n3	0.55 ± 0.02	0.48 ± 0.02*	1.81 ± 0.08†	0.49 ± 0.01	1.87 ± 0.10†
Nervonic acid	C24:1n9	0.08 ± 0.00	0.09 ± 0.02	0.08 ± 0.02	0.07 ± 0.00	0.07 ± 0.00
Docosatetraenoic acid	C22:4n6	1.56 ± 0.03	1.50 ± 0.02	0.96 ± 0.02†	1.49 ± 0.01	0.89 ± 0.04†
Docosapentaenoic - n6	C22:5n6	0.24 ± 0.00	0.21 ± 0.01*	0.13 ± 0.01†	0.22 ± 0.02	0.13 ± 0.01†
Docosapentaenoic - n3	C22:5n3	4.03 ± 0.07	3.82 ± 0.13	4.00 ± 0.12	3.65 ± 0.02	3.99 ± 0.06
Docosahexaenoic	C22:6n3	4.91 ± 0.10	4.31 ± 0.11*	12.17 ± 0.22†	4.10 ± 0.05	11.90 ± 0.18†
Total SFA		37.32 ± 0.73	40.86 ± 0.97*	46.76 ± 0.90†	41.38 ± 0.51	48.30 ± 0.68†
Total MUFA		40.45 ± 0.40	38.92 ± 0.72	25.52 ± 0.49†	38.75 ± 0.42	24.46 ± 0.60†
Total n6		12.72 ± 0.22	11.61 ± 0.11*	9.74 ± 0.16†	11.62 ± 0.07	9.47 ± 0.09†
Total n3		9.50 ± 0.18	8.61 ± 0.24*	17.99 ± 0.38†	8.25 ± 0.06	17.77 ± 0.30†
Omega-3 Index		5.45 ± 0.12	4.78 ± 0.11*	13.98 ± 0.27†	4.59 ± 0.06	13.76 ± 0.24†

Fatty acid composition of FLAMs treated following experimental design detailed in **Figure 1A**.

Table 5.1 (cont'd):
$p<0.05$; *Significant change in LPS VEH vs VEH CON group; †Significant change in DHA/DEX treatment groups vs LPS VEH.

CHAPTER 6: CONCLUSIONS AND FUTURE DIRECTIONS

CONCLUSION

The primary goal of this dissertation was to gain better insight into how different therapeutics, age, and environmental stimuli mediate inflammation and autoimmunity. This goal was achieved by employing multiple preclinical murine models that emulate environmental-triggered lupus. Furthermore, mechanistic studies looking at the intersection between LPS-primed inflammation and GC/DHA treatment were performed in a novel alveolar-like macrophage cell model. Overall, these studies provide a framework for future *in vivo* and *in vitro* studies aimed at further elucidating the steroid-sparing effects of DHA.

PRIMARY FINDINGS AND FUTURE DIRECTIONS

Utilization of adult female NZBWF1 lupus-prone mice

As was seen in **Chapter 3**, we not only developed a more appropriate model that accounted for the age of $cSiO_2$-exposed workers, but we also witnessed intensified $cSiO_2$-induced pulmonary inflammation at 5 wk PI compared that observed in juveniles from previous studies (16). Consequently, adult female NZBWF1 lupus-prone mice serve as an appropriate model to evaluate $cSiO_2$-triggered inflammation and autoimmunity in the lung. However, a limitation of this study was that we did not see increased AAb production in the plasma or severe glomerulonephritis at 5 wk PI. These findings suggest that sacrificing mice at a timepoint between 9-13 wk PI would be more appropriate to evaluate systemic and renal endpoints. For future studies focused on $cSiO_2$ exposure *in vivo*, I would propose using the same experimental design detailed in Chapter 3, with the exception that mice would be necropsied at 9-wk PI.

Evaluating the steroid-sparing effects of DHA in a murine model of $cSiO_2$-triggered lupus

Like previous studies from our lab which have detailed the dose-dependent attenuation of $cSiO_2$-

triggered autoimmunity by DHA (16, 18, 21, 27, 88), we have now elucidated the same thresholds for prednisone. As shown in **Chapter 2**, the moderate HED of prednisone (14 mg/d), but not the low HED (5 mg/d), was effective in reducing $cSiO_2$-triggered inflammation in the lung and kidney. However, adverse side effects were observed at the moderate and high HEDs of prednisone. Therefore, these results support the need for a non-toxic, steroid-sparing therapy that can be used to sustain remission of autoimmunity while also offsetting toxicity.

Consistent with previous studies (16, 18, 27), **Chapter 3** of this dissertation demonstrated that DHA strongly attenuates $cSiO_2$-triggered autoimmunity. Thus, an area of interest for future studies would be to address the hypothesis that DHA could be used in conjunction with prednisone to attenuate $cSiO_2$-induced inflammation while reducing unwanted toxicity. One approach to address this hypothesis would be to use a combination of the high dose prednisone-amended diet and DHA-amended diets. In this study, I would intranasally instill 16-wk-old adult female NZBWF1 lupus-prone mice with either saline vehicle or 1 mg $cSiO_2$ once weekly for 4 consecutive weeks. To more appropriately model treatment regimens found in clinic, I would wait to administer both prednisone and DHA-amended diets until after autoimmunity onset was triggered by $cSiO_2$. Following the last $cSiO_2$ instillation, I would start the mice on either a control AIN93-G diet or high dose prednisone diet (46 mg/d HED) for approximately 2 weeks. At the end of these 2 weeks, mice would be maintained on either a control AIN93-G or DHA-amended diet (5 g/d or 2 g/d HED) for the remainder of the study until mice were necropsied at 9 wk following the last $cSiO_2$ instillation. In previous studies from our lab, the high (5 g/d) but not the low (2 g/d) dose of DHA was effective in attenuating $cSiO_2$-triggered inflammation (16, 18, 27). Therefore, it will need to be ascertained if these findings change with prior prednisone treatment. For this study, I would hypothesize that DHA-amended diets would be able to maintain suppression of $cSiO_2$-triggered

autoimmunity initiated by short-term high dose prednisone treatment, while also avoiding toxicity due to the abbreviated duration of GC use.

While this proposed experiment would provide answers to address the initial hypothesis, the parameters of this preclinical model could be adjusted to address additional questions in follow up studies. For example, mice could be maintained on DHA diets past the fixed necropsy timepoint to assess survivability. Alternatively, a second fixed timepoint could be added (e.g., 13 wk PI) to assess whether suppression of autoimmunity is maintained across a broader length of time. Lastly, if DHA is not able to maintain attenuation of disease in $cSiO_2$-exposed mice, combination diets can be employed. More specifically, a combination diet that incorporates each respective suboptimal dose of prednisone (5 mg/d HED) and DHA (2 g/d), could be administered following short-term high dose prednisone treatment with the maintained goal of ameliorating autoimmunity while still avoiding secondary toxicity.

Evaluating age and therapeutic interventions in a murine model of LPS-induced lupus

As shown in **Chapter 4**, *E. coli* LPS triggers autoimmunity in female juvenile NZBWF1 lupus-prone mice through both intranasal and intraperitoneal routes of exposure. While it would be of great interest to determine if GC and DHA combination treatment is effective in attenuating LPS-induced autoimmunity, limitations of the study described in **Chapter 4** would have to be addressed. These limitations include: (i) determining if, and when, severe glomerulonephritis develops in this model and (ii) if increased age leads to exaggerated inflammation and autoimmunity in LPS-exposed mice. The first limitation can be addressed by terminating mice at a later timepoint or by increasing the number of exposures (instillations/injections) to LPS. Similar to the experiment detailed in **Chapter 3**, female adult NZBWF1 lupus-prone mice can be used to determine if increased age intensifies local and systemic autoimmunity resulting from LPS

exposure. Additionally, using adult mice is likely a more relevant model when considering the age of LPS-exposed workers. Once these questions are answered, prednisone/DHA combination treatment, as described in the preceding $cSiO_2$ experiment, can be used to ascertain if prednisone and DHA treatment quells LPS-triggered inflammation and autoimmunity.

Further evaluation of GC+DHA combination treatment *in vitro*

In **Chapter 5**, it was shown that combination treatment with suboptimal concentrations of DHA and the GC DEX was able to promote an anti-inflammatory phenotype in LPS-stimulated FLAMs. These results were mediated primarily though the concomitant repression of proinflammatory gene expression. However, additional follow-up studies can be performed to create an even more compelling story. While not included in **Chapter 5**, ATAC-seq was also performed to evaluate treatment-dependent changes in chromatin remodeling at 4 hr. However, major global changes in chromatin remodeling were not observed at this timepoint. Therefore, additional timepoints (e.g., 30-60 minutes) will need to be assessed to determine when treatment-dependent chromatin remodeling occurs. In addition to looking at upstream regulation of gene expression, future studies can also evaluate the impact of individual and combination treatments on protein expression in LPS-stimulated FLAMs. Such analyses include measurement of proinflammatory protein expression by ELISA and Western blots, in addition to performing ChIPseq as validation of TF enrichment analysis. Furthermore, extra investigation into why certain genes, such as *Dusp1* and *Gilz* did not exhibit increased gene expression with DHA/DEX treatment as previously hypothesized can be addressed in future experiments.

SUMMARY

In summation, each of the proposed studies is aimed at better elucidating the steroid-sparing effects of DHA in order to reduce requisite doses of GCs and thereby improve quality of life for lupus

patients.

REFERENCES

1. Yu H, Nagafuchi Y, Fujio K. Clinical and Immunological Biomarkers for Systemic Lupus Erythematosus. *Biomolecules* (2021) 11(7):928. doi: 10.3390/biom11070928

2. Tsokos GC. Systemic Lupus Erythematosus. *New England Journal of Medicine* (2011) 365(22):2110-21. doi: 10.1056/nejmra1100359

3. Adamichou C, Bertsias G. Flares in systemic lupus erythematosus: diagnosis, risk factors and preventive strategies. *Mediterranean Journal of Rheumatology* (2017) 28(1):4-12. doi: 10.31138/mjr.28.1.4

4. Yu F, Haas M, Glassock R, Zhao MH. Redefining lupus nephritis: Clinical implications of pathophysiologic subtypes. Nature Publishing Group; 2017. p. 483-95.

5. Ramos PS, Brown EE, Kimberly RP, Langefeld CD. Genetic Factors Predisposing to Systemic Lupus Erythematosus and Lupus Nephritis. *Seminars in Nephrology* (2010) 30(2):164-76. doi: 10.1016/j.semnephrol.2010.01.007

6. Zucchi D, Elefante E, Schilirò D, Signorini V, Trentin F, Bortoluzzi A, et al. One year in review 2022: systemic lupus erythematosus. *Clinical and Experimental Rheumatology* (2022) 40(1):4-14. doi: 10.55563/clinexprheumatol/nolysy

7. Wu H, Chang C, Lu Q. The Epigenetics of Lupus Erythematosus. Springer Singapore; 2020. p. 185-207.

8. Hoy RF, Chambers DC. Silica-related diseases in the modern world. *Allergy* (2020) 75(11):2805-17. doi: 10.1111/all.14202

9. Parks CG, Conrad K, Cooper GS. Occupational exposure to crystalline silica and autoimmune disease. *Environmental Health Perspectives* (1999) 107(suppl 5):793-802. doi: 10.1289/ehp.99107s5793

10. Parks CG, De Souza Espindola Santos A, Barbhaiya M, Costenbader KH. Understanding the role of environmental factors in the development of systemic lupus erythematosus. *Best Practice & Research Clinical Rheumatology* (2017) 31(3):306-20. doi: 10.1016/j.berh.2017.09.005

11. Finckh A, Cooper GS, Chibnik LB, Costenbader KH, Watts J, Pankey H, et al. Occupational silica and solvent exposures and risk of systemic lupus erythematosus in urban women. *Arthritis & Rheumatism* (2006) 54(11):3648-54. doi: 10.1002/art.22210

12. Tsokos GC, Lo MS, Costa Reis P, Sullivan KE. New insights into the immunopathogenesis of systemic lupus erythematosus. *Nat Rev Rheumatol* (2016) 12(12):716-30. doi: 10.1038/nrrheum.2016.186

13. Mu Q, Zhang H, Luo XM. SLE: Another Autoimmune Disorder Influenced by Microbes and Diet? *Frontiers in Immunology* (2015) 6:608-. doi: 10.3389/FIMMU.2015.00608

14. Farokhi A, Heederik D, Smit LAM. Respiratory health effects of exposure to low levels of airborne endotoxin - A systematic review. *Environmental Health* (2018) 17(1). doi: 10.1186/s12940-018-0360-7

15. He S, Liang Y, Shao F, Wang X. Toll-like receptors activate programmed necrosis in macrophages through a receptor-interacting kinase-3-mediated pathway. *Proceedings of the National Academy of Sciences of the United States of America* (2011) 108(50):20054-9. doi: 10.1073/pnas.1116302108

16. Bates MA, Akabari P, Gilley KN, Wagner JG, Li N, Kopec AK, et al. Dietary Docosahexaenoic Acid Prevents Silica-Induced Development of Pulmonary Ectopic Germinal Centers and Glomerulonephritis in the Lupus-Prone NZBWF1 Mouse. *Front Immunol* (2018) 9:2002. doi: 10.3389/fimmu.2018.02002

17. Bates MA, Brandenberger C, Langohr I, Kumagai K, Harkema JR, Holian A, et al. Silica triggers inflammation and ectopic lymphoid neogenesis in the lungs in parallel with accelerated onset of systemic autoimmunity and glomerulonephritis in the lupus-prone NZBWF1 mouse. *PLoS ONE* (2015) 10(5):1-25. doi: 10.1371/journal.pone.0125481

18. Pestka JJ, Akbari P, Wierenga KA, Bates MA, Gilley KN, Wagner JG, et al. Omega-3 Polyunsaturated Fatty Acid Intervention Against Established Autoimmunity in a Murine Model of Toxicant-Triggered Lupus. *Frontiers in Immunology* (2021) 12. doi: 10.3389/fimmu.2021.653464

19. Heine LK, Benninghoff AD, Ross EA, Rajasinghe LD, Wagner JG, Lewandowski RP, et al. Comparative effects of human-equivalent low, moderate, and high dose oral prednisone intake on autoimmunity and glucocorticoid-related toxicity in a murine model of environmental-triggered lupus. *Front Immunol* (2022) 13:972108. doi: 10.3389/fimmu.2022.972108

20. Bates MA, Benninghoff AD, Gilley KN, Holian A, Harkema JR, Pestka JJ. Mapping of Dynamic Transcriptome Changes Associated With Silica-Triggered Autoimmune Pathogenesis in the Lupus-Prone NZBWF1 Mouse. *Frontiers in Immunology* (2019) 10(MAR):632-. doi: 10.3389/fimmu.2019.00632

21. Benninghoff AD, Bates MA, Chauhan PS, Wierenga KA, Gilley KN, Holian A, et al. Docosahexaenoic Acid Consumption Impedes Early Interferon- and Chemokine-Related Gene

Expression While Suppressing Silica-Triggered Flaring of Murine Lupus. *Frontiers in Immunology* (2019) 10:2851-. doi: 10.3389/fimmu.2019.02851

22. Tani C, Elefante E, Signorini V, Zucchi D, Lorenzoni V, Carli L, et al. Glucocorticoid withdrawal in systemic lupus erythematosus: Are remission and low disease activity reliable starting points for stopping treatment? A real-life experience. *RMD Open* (2019) 5(2):e000916-e. doi: 10.1136/rmdopen-2019-000916

23. Porta S, Danza A, Arias Saavedra M, Carlomagno A, Cecilia Goizueta M, Vivero F, et al. Glucocorticoids inSystemic Lupus Erythematosus. Ten Questions and Some Issues. *Journal of Clinical Medicine* (2020) 9(9). doi: 10.3390/jcm9092709

24. Flammer JR, Rogatsky I. Minireview: Glucocorticoids in autoimmunity: unexpected targets and mechanisms. *Molecular endocrinology (Baltimore, Md)* (2011) 25(7):1075-86. doi: 10.1210/me.2011-0068

25. Cain DW, Cidlowski JA. Immune regulation by glucocorticoids. Nature Publishing Group; 2017. p. 233-47.

26. Ugarte A, Danza A, Ruiz-Irastorza G. Glucocorticoids and antimalarials in systemic lupus erythematosus: an update and future directions. NLM (Medline); 2018. p. 482-9.

27. Bates MA, Brandenberger C, Langohr, II, Kumagai K, Lock AL, Harkema JR, et al. Silica-Triggered Autoimmunity in Lupus-Prone Mice Blocked by Docosahexaenoic Acid Consumption. *PLoS One* (2016) 11(8):e0160622. doi: 10.1371/journal.pone.0160622

28. Rajasinghe LD, Bates MA, Benninghoff AD, Wierenga KA, Harkema JR, Pestka JJ. Silica Induction of Diverse Inflammatory Proteome in Lungs of Lupus-Prone Mice Quelled by Dietary Docosahexaenoic Acid Supplementation. *Front Immunol* (2021) 12:781446. doi: 10.3389/fimmu.2021.781446

29. Wierenga KA, Riemers FM, Westendorp B, Harkema JR, Pestka JJ. Single cell analysis of docosahexaenoic acid suppression of sequential LPS-induced proinflammatory and interferon-regulated gene expression in the macrophage. *Front Immunol* (2022) 13:993614. doi: 10.3389/fimmu.2022.993614

30. Catalina MD, Owen KA, Labonte AC, Grammer AC, Lipsky PE. The pathogenesis of systemic lupus erythematosus: Harnessing big data to

understand the molecular basis of lupus. *Journal of Autoimmunity* (2020) 110. doi: 10.1016/j.jaut.2019.102359

31. Carter EE, Barr SG, Clarke AE. The global burden of SLE: prevalence, health disparities and socioeconomic impact. *Nature Reviews Rheumatology* (2016) 12(10):605-20. doi: 10.1038/nrrheum.2016.137

32. Rizk A, Gheita TA, Nassef S, Abdallah A. The impact of obesity in systemic lupus erythematosus on disease parameters, quality of life, functional capacity and the risk of atherosclerosis. *Int J Rheum Dis* (2012) 15(3):261-7. doi: 10.1111/j.1756-185X.2011.01698.x

33. Han G-M, Han X-F. Comorbid Conditions are Associated With Emergency Department Visits, Hospitalizations, and Medical Charges of Patients With Systemic Lupus Erythematosus. *JCR: Journal of Clinical Rheumatology* (2017) 23(1):19-25. doi: 10.1097/rhu.0000000000000437

34. Yang Y, Thumboo J, Earnest A, Yong SL, Fong KY. The effect of comorbidity on hospital mortality in patients with SLE from an Asian tertiary hospital. *Lupus* (2014) 23(7):714-20. doi: 10.1177/0961203314522340

35. Gergianaki I, Garantziotis P, Adamichou C, Saridakis I, Spyrou G, Sidiropoulos P, et al. High Comorbidity Burden in Patients with SLE: Data from the Community-Based Lupus Registry of Crete. *Journal of Clinical Medicine* (2021) 10(5):998. doi: 10.3390/jcm10050998

36. Yen EY, Singh RR. Brief Report: Lupus-An Unrecognized Leading Cause of Death in Young Females: A Population-Based Study Using Nationwide Death Certificates, 2000-2015. *Arthritis & Rheumatology* (2018) 70(8):1251-5. doi: 10.1002/art.40512

37. Jiang M, Near AM, Desta B, Wang X, Hammond ER. Disease and economic burden increase with systemic lupus erythematosus severity 1 year before and after diagnosis: a real-world cohort study, United States, 2004–2015. *Lupus Science & Medicine* (2021) 8(1):e000503. doi: 10.1136/lupus-2021-000503

38. Murimi-Worstell IB, Lin DH, Kan H, Tierce J, Wang X, Nab H, et al. Healthcare Utilization and Costs of Systemic Lupus Erythematosus by Disease Severity in the United States. *The Journal of Rheumatology* (2021) 48(3):385-93. doi: 10.3899/jrheum.191187

39. Pisetsky DS, Lipsky PE. New insights into the role of antinuclear antibodies in systemic lupus erythematosus. *Nature Reviews Rheumatology* (2020) 16(10):565-79. doi: 10.1038/s41584-020-0480-7

40. Dema B, Charles N. Autoantibodies in SLE: Specificities, Isotypes and Receptors. *Antibodies* (2016) 5(1):2. doi: 10.3390/antib5010002

41. Yung S, Chan TM. Mechanisms of kidney injury in lupus nephritis - the role of anti-dsDNA antibodies. Frontiers Media S.A.; 2015.

42. Liu C-C, Kao AH, Manzi S, Ahearn JM. Biomarkers in systemic lupus erythematosus: challenges and prospects for the future. *Therapeutic Advances in Musculoskeletal Disease* (2013) 5(4):210-33. doi: 10.1177/1759720x13485503

43. Crow YJ, Stetson DB. The type I interferonopathies: 10 years on. *Nature Reviews Immunology* (2022) 22(8):471-83. doi: 10.1038/s41577-021-00633-9

44. Northcott M, Jones S, Koelmeyer R, Bonin J, Vincent F, Kandane-Rathnayake R, et al. Type 1 interferon status in systemic lupus erythematosus: a longitudinal analysis. *Lupus Science & Medicine* (2022) 9(1):e000625. doi: 10.1136/lupus-2021-000625

45. Psarras A, Emery P, Vital EM. Type I interferon-mediated autoimmune diseases: pathogenesis, diagnosis and targeted therapy. *Rheumatology (Oxford)* (2017) 56(10):1662-75. doi: 10.1093/rheumatology/kew431

46. Rodero MP, Crow YJ. Type I interferon–mediated monogenic autoinflammation: The type I interferonopathies, a conceptual overview. *Journal of Experimental Medicine* (2016) 213(12):2527-38. doi: 10.1084/jem.20161596

47. Vaughn SE, Kottyan LC, Munroe ME, Harley JB. Genetic susceptibility to lupus: the biological basis of genetic risk found in B cell signaling pathways. *J Leukoc Biol* (2012) 92(3):577-91. doi: 10.1189/jlb.0212095

48. Harley ITW, Sawalha AH. Systemic lupus erythematosus as a genetic disease. *Clin Immunol* (2022) 236:108953. doi: 10.1016/j.clim.2022.108953

49. Alperin JM, Ortiz-Fernández L, Sawalha AH. Monogenic Lupus: A Developing Paradigm of Disease. *Front Immunol* (2018) 9:2496. doi: 10.3389/fimmu.2018.02496

50. Belot A, Cimaz R. Monogenic forms of systemic lupus erythematosus: new insights into SLE pathogenesis. *Pediatric Rheumatology* (2012) 10(1):21. doi: 10.1186/1546-0096-10-21

51. Barbhaiya M, Costenbader KH. Environmental exposures and the development of systemic lupus erythematosus. *Current Opinion in Rheumatology* (2016) 28(5):497-505. doi: 10.1097/bor.0000000000000318

52. Battaglia M, Garrett-Sinha LA. Bacterial infections in lupus: Roles in promoting immune activation and in pathogenesis of the disease. *J Transl Autoimmun* (2020) 4(100078). doi: 10.1016/j.jtauto.2020.100078

53. Zindel J, Kubes P. DAMPs, PAMPs, and LAMPs in Immunity and Sterile Inflammation. *Annual Review of Pathology: Mechanisms of Disease* (2020) 15(1):493-518. doi: 10.1146/annurev-pathmechdis-012419-032847

54. Gaurav R, Mikuls TR, Thiele GM, Nelson AJ, Niu M, Guda C, et al. High-throughput analysis of lung immune cells in a combined murine model of agriculture dust-triggered airway inflammation with rheumatoid arthritis. *PLOS ONE* (2021) 16(2):e0240707. doi: 10.1371/journal.pone.0240707

55. Kovach MA, Standiford TJ. Toll like receptors in diseases of the lung. *International Immunopharmacology* (2011) 11(10):1399-406. doi: 10.1016/j.intimp.2011.05.013

56. Qiu CC, Caricchio R, Gallucci S. Triggers of Autoimmunity: The Role of Bacterial Infections in the Extracellular Exposure of Lupus Nuclear Autoantigens. *Front Immunol* (2019) 10. doi: 10.3389/fimmu.2019.02608

57. Huffnagle GB, Dickson RP, Lukacs NW. The respiratory tract microbiome and lung inflammation: a two-way street. *Mucosal Immunology* (2017) 10(2):299-306. doi: 10.1038/mi.2016.108

58. Favor OK, Chauhan PS, Pourmand E, Edwards AM, Wagner JG, Lewandowski RP, et al. Lipidome modulation by dietary omega-3 polyunsaturated fatty acid supplementation or selective soluble epoxide hydrolase inhibition suppresses rough LPS-accelerated glomerulonephritis in lupus-prone mice. *Front Immunol* (2023) 14:1124910. doi: 10.3389/fimmu.2023.1124910

59. Zhang Q, Xiang L, Zaman MH, Dong W, He G, Deng GM. Predominant Role of Immunoglobulin G in the Pathogenesis of Splenomegaly in Murine Lupus. *Front Immunol* (2019) 10:3020. doi: 10.3389/fimmu.2019.03020

60. Poole JA, Thiele GM, Janike K, Nelson AJ, Duryee MJ, Rentfro K, et al. Combined Collagen-Induced Arthritis and Organic Dust-Induced Airway Inflammation to Model Inflammatory Lung Disease in Rheumatoid Arthritis. *Journal of Bone and Mineral Research* (2019) 34(9):1733-43. doi: 10.1002/jbmr.3745

61. Johnson AN, Harkema JR, Nelson AJ, Dickinson JD, Kalil J, Duryee MJ, et al. MyD88 regulates a prolonged adaptation response to environmental dust exposure-induced lung disease. *Respiratory Research* (2020) 21(1). doi: 10.1186/s12931-020-01362-8

62. Olsson AR. Occupations and exposures in the work environment as determinants for rheumatoid arthritis. *Occupational and Environmental Medicine* (2004) 61(3):233-8. doi: 10.1136/oem.2003.007971

63. B. C. Doney WEM, J. M. Hale, and G. Syamlal. Estimation of the number of workers exposed to respirable crystalline silica by industry: Analysis of OSHA compliance data (1979-2015). *Am J Ind Med* (2020) 63(6):465-77. doi: 10.1002/ajim.23109

64. Dostert C, Pétrilli V, Van Bruggen R, Steele C, Mossman BT, Tschopp J. Innate immune activation through Nalp3 inflammasome sensing of asbestos and silica. *Science* (2008) 320(5876):674-7. doi: 10.1126/science.1156995

65. Joshi GN, Knecht DA. Silica phagocytosis causes apoptosis and necrosis by different temporal and molecular pathways in alveolar macrophages. *Apoptosis* (2013) 18(3):271-85. doi: 10.1007/s10495-012-0798-y

66. Gilberti RM, Joshi GN, Knecht DA. The Phagocytosis of Crystalline Silica Particles by Macrophages. *American Journal of Respiratory Cell and Molecular Biology* (2008) 39(5):619-27. doi: 10.1165/rcmb.2008-0046oc

67. Bates MA, Brandenberger C, Langohr II, Kumagai K, Lock AL, Harkema JR, et al. Silica-triggered autoimmunity in lupus-prone mice blocked by docosahexaenoic acid consumption. *PLoS ONE* (2016) 11(8):1-31. doi: 10.1371/journal.pone.0160622

68. Gilley KN, Wierenga KA, Chauhuan PS, Wagner JG, Lewandowski RP, Ross EA, et al. Influence of total western diet on docosahexaenoic acid suppression of silica-triggered lupus flaring in NZBWF1 mice. *PLoS ONE* (2020) 15(5). doi: 10.1371/journal.pone.0233183

69. Felten R, Arnaud L. Is it possible to stop glucocorticoids in systemic lupus? : Elsevier Masson SAS; 2020.

70. Buttgereit F, Da Silva JAP, Boers M, Burmester G-R, Cutolo M, Jacobs J, et al. Standardised nomenclature for glucocorticoid dosages and glucocorticoid treatment regimens: current questions and tentative answers in rheumatology. *Annals of the Rheumatic Diseases* (2002) 61(8):718-22. doi: 10.1136/ard.61.8.718

71. Mathian A, Pha M, Haroche J, Cohen-Aubart F, Hié M, Pineton de Chambrun M, et al. Withdrawal of low-dose prednisone in SLE patients with a clinically quiescent disease for more than 1 year: a randomised clinical trial. *Ann Rheum Dis* (2020) 79(3):339-46. doi: 10.1136/annrheumdis-2019-216303

72. Ruiz-Arruza I, Barbosa C, Ugarte A, Ruiz-Irastorza G. Comparison of high versus low-medium prednisone doses for the treatment of systemic lupus erythematosus patients with high activity at diagnosis. Elsevier; 2015. p. 875-9.

73. Al Sawah S, Zhang X, Zhu B, Magder LS, Foster SA, Iikuni N, et al. Effect of corticosteroid use by dose on the risk of developing organ damage over time in systemic lupus erythematosus - the Hopkins Lupus Cohort. *Lupus Science & Medicine* (2015) 2(1). doi: 10.1136/lupus-2014-000066

74. Thamer M, Hernan MA, Zhang Y, Cotter D, Petri M. Prednisone, Lupus Activity, and Permanent Organ Damage. *Journal of Rheumatology* (2009) 36(3):560-4. doi: 10.3899/jrheum.080828

75. Fryar C, Carroll M, Gu Q, Afful J, Ogden C. Anthropometric reference data for children and adults: United States, 2015–2018. *National Center for Health Statistics Vital Health Stat* (2021) 3(46). doi:

76. Basta F, Fasola F, Triantafyllias K, Schwarting A. Systemic Lupus Erythematosus (SLE) Therapy: The Old and the New. *Rheumatology and Therapy* (2020) 7(3):433-46. doi: 10.1007/s40744-020-00212-9

77. Dima A, Jurcut C, Chasset F, Felten R, Arnaud L. Hydroxychloroquine in systemic lupus erythematosus: overview of current knowledge. *Therapeutic Advances in Musculoskeletal Disease* (2022) 14:1759720X2110730. doi: 10.1177/1759720x211073001

78. Fava A, Petri M. Systemic lupus erythematosus: Diagnosis and clinical management. Academic Press; 2019. p. 1-13.

79. Lamore R, Parmar S, Patel K, Hilas O. Belimumab (Benlysta): A breakthrough therapy for systemic lupus erythematosus. *P and T* (2012) 37(4):212-26. doi:

80. Charoenwoodhipong P, Harlow SD, Marder W, Hassett AL, McCune WJ, Gordon C, et al. Dietary Omega Polyunsaturated Fatty Acid Intake and Patient-Reported Outcomes in Systemic Lupus Erythematosus: The Michigan Lupus Epidemiology and Surveillance Program. *Arthritis Care Res (Hoboken)* (2020) 72(7):874-81. doi: 10.1002/acr.23925

81. Arriens C, Hynan LS, Lerman RH, Karp DR, Mohan C. Placebo-controlled randomized clinical trial of fish oil's impact on fatigue, quality of life, and disease activity in Systemic Lupus Erythematosus. *Nutrition Journal* (2015) 14(1). doi: 10.1186/s12937-015-0068-2

82. Li X, Bi X, Wang S, Zhang Z, Li F, Zhao AZ. Therapeutic Potential of ω-3 Polyunsaturated Fatty Acids in Human Autoimmune Diseases. *Front Immunol* (2019) 10:2241. doi: 10.3389/fimmu.2019.02241

83. Adam O, Beringer C, Kless T, Lemmen C, Adam A, Wiseman M, et al. Anti-inflammatory effects of a low arachidonic acid diet and fish oil in patients with rheumatoid arthritis. *Rheumatology International* (2003) 23(1):27-36. doi: 10.1007/s00296-002-0234-7

84. Farzaneh-Far R, Harris WS, Garg S, Na B, Whooley MA. Inverse association of erythrocyte n-3 fatty acid levels with inflammatory biomarkers in patients with stable coronary artery disease: The Heart and Soul Study. *Atherosclerosis* (2009) 205(2):538-43. doi: 10.1016/j.atherosclerosis.2008.12.013

85. Fontes JD, Rahman F, Lacey S, Larson MG, Vasan RS, Benjamin EJ, et al. Red blood cell fatty acids and biomarkers of inflammation: A cross-sectional study in a community-based cohort. *Atherosclerosis* (2015) 240(2):431-6. doi: 10.1016/j.atherosclerosis.2015.03.043

86. Grenon SM, Conte MS, Nosova E, Alley H, Chong K, Harris WS, et al. Association between n-3 polyunsaturated fatty acid content of red blood cells and inflammatory biomarkers in patients with peripheral artery disease. *Journal of Vascular Surgery* (2013) 58(5):1283-90. doi: 10.1016/j.jvs.2013.05.024

87. Innes JK, Calder PC. Omega-6 fatty acids and inflammation. *Prostaglandins, Leukotrienes and Essential Fatty Acids* (2018) 132:41-8. doi: 10.1016/j.plefa.2018.03.004

88. Rajasinghe LD, Li Q-Z, Zhu C, Yan M, Chauhan PS, Wierenga KA, et al. Omega-3 fatty acid intake suppresses induction of diverse autoantibody repertoire by crystalline silica in lupus-prone mice. *Autoimmunity* (2020) 53(7):415-33. doi: 10.1080/08916934.2020.1801651

89. Bagaev AV, Garaeva AY, Lebedeva ES, Pichugin AV, Ataullakhanov RI, Ataullakhanov FI. Elevated pre-activation basal level of nuclear NF-κB in native macrophages accelerates LPS-induced translocation of cytosolic NF-κB into the cell nucleus. *Scientific Reports* (2019) 9(1):1-16. doi: 10.1038/s41598-018-36052-5

90. Bode JG, Ehlting C, Häussinger D. The macrophage response towards LPS and its control through the p38 MAPK-STAT3 axis. 2012. p. 1185-94.

91. Heil M, Land WG. Danger signals – Damaged-self recognition across the tree of life. Frontiers Media S.A.; 2014. p. 578-.

92. Scheschowitsch K, Leite JA, Assreuy J. New insights in glucocorticoid receptor signaling-more than just a ligand-binding receptor. Frontiers Research Foundation; 2017. p. 16-.

93. Vandevyver S, Dejager L, Tuckermann J, Libert C. New insights into the anti-inflammatory mechanisms of glucocorticoids: An emerging role for glucocorticoid-receptor-mediated transactivation. Oxford Academic; 2013. p. 993-1007.

94. Xavier AM, Anunciato AKO, Rosenstock TR, Glezer I. Gene expression control by glucocorticoid receptors during innate immune responses. Frontiers Media S.A.; 2016. p. 31-.

95. Hoppstädter J, Ammit AJ. Role of dual-specificity phosphatase 1 in glucocorticoid-driven antiinflammatory responses. Frontiers Media S.A.; 2019. p. 1446-.

96. Shah S, King EM, Chandrasekhar A, Newton R. Roles for the Mitogen-activated Protein Kinase (MAPK) Phosphatase, DUSP1, in Feedback Control of Inflammatory Gene Expression and Repression by Dexamethasone * □ S. (2014). doi: 10.1074/jbc.M113.540799

97. Shipp LE, Lee JV, Yu C-Y, Pufall M, Zhang P, Scott DK, et al. Transcriptional Regulation of Human Dual Specificity Protein Phosphatase 1 (DUSP1) Gene by Glucocorticoids. doi: 10.1371/journal.pone.0013754

98. Chi H, Barry SP, Roth RJ, Wu JJ, Jones EA, Bennett AM, et al. Dynamic regulation of pro-and anti-inflammatory cytokines by MAPK phosphatase 1 (MKP-1) in innate immune responses. 2006.

99. Ayroldi E, Godot V, Flynn JK, Morand EF, Dankers W. Could GILZ Be the Answer to Glucocorticoid Toxicity in Lupus? *Frontiers in Immunology | wwwfrontiersinorg* (2019) 1:1684-. doi: 10.3389/fimmu.2019.01684

100. Hoppstädter J, Kessler SM, Bruscoli S, Huwer H, Riccardi C, Kiemer AK. Glucocorticoid-Induced Leucine Zipper: A Critical Factor in Macrophage Endotoxin Tolerance. *The Journal of Immunology* (2015) 194(12):6057-67. doi: 10.4049/jimmunol.1403207

101. Ayroldi E, Macchiarulo A, Riccardi C. Targeting glucocorticoid side effects: selective glucocorticoid receptor modulator or glucocorticoid-induced leucine zipper? A perspective. doi: 10.1096/fj.14-254755

102. Flammer JR, Dobrovolna J, Kennedy MA, Chinenov Y, Glass CK, Ivashkiv LB, et al. The type I interferon signaling pathway is a target for glucocorticoid inhibition. *Molecular and cellular biology* (2010) 30(19):4564-74. doi: 10.1128/MCB.00146-10

103. Chinenov Y, Gupte R, Dobrovolna J, Flammer JR, Liu B, Michelassi FE, et al. Role of transcriptional coregulator GRIP1 in the anti-inflammatory actions of glucocorticoids. *Proceedings of the National Academy of Sciences* (2012) 109(29):11776-81. doi: 10.1073/pnas.1206059109

104. Bhattacharyya S, Zhao Y, Kay TWH, Muglia LJ. Glucocorticoids target suppressor of cytokine signaling 1 (SOCS1) and type 1 interferons to regulate Toll-like receptor-induced STAT1 activation. *Proceedings of the National Academy of Sciences of the United States of America* (2011) 108(23):9554-9. doi: 10.1073/pnas.1017296108

105. Lavin Y, Winter D, Blecher-Gonen R, David E, Keren-Shaul H, Merad M, et al. Tissue-Resident Macrophage Enhancer Landscapes Are Shaped by the Local Microenvironment. *Cell* (2014) 159(6):1312-26. doi: 10.1016/j.cell.2014.11.018

106. Fejer G, Sharma S, Gyory I. Self-renewing macrophages – A new line of enquiries in mononuclear phagocytes. *Immunobiology* (2015) 220(2):169-74. doi: 10.1016/j.imbio.2014.11.005

107. Thomas ST, Wierenga KA, Pestka JJ, Olive AJ. Fetal Liver–Derived Alveolar-like Macrophages: A Self-Replicating Ex Vivo Model of Alveolar Macrophages for Functional Genetic Studies. *ImmunoHorizons* (2022) 6(2):156-69. doi: 10.4049/immunohorizons.2200011

108. Fejer G, Wegner MD, Györy I, Cohen I, Engelhard P, Voronov E, et al. Nontransformed, GM-CSF-dependent macrophage lines are a unique model to study tissue macrophage functions. *Proceedings of the National Academy of Sciences of the United States of America* (2013) 110(24):E2191-E8. doi: 10.1073/pnas.1302877110

109. Rabolli V, Badissi AA, Devosse R, Uwambayinema F, Yakoub Y, Palmai-Pallag M, et al. The alarmin IL-1α is a master cytokine in acute lung inflammation induced by silica micro- and nanoparticles. *Particle and Fibre Toxicology* (2014) 11(1):69-. doi: 10.1186/s12989-014-0069-x

110. Kuroda E, Ozasa K, Temizoz B, Ohata K, Koo CX, Kanuma T, et al. Inhaled Fine Particles Induce Alveolar Macrophage Death and Interleukin-1α Release to Promote Inducible Bronchus-Associated Lymphoid Tissue Formation. *Immunity* (2016) 45(6):1299-310. doi: 10.1016/j.immuni.2016.11.010

111. Wierenga KA, Wee J, Gilley KN, Rajasinghe LD, Bates MA, Gavrilin MA, et al. Docosahexaenoic Acid Suppresses Silica-Induced Inflammasome Activation and IL-1 Cytokine Release by Interfering With Priming Signal. *Front Immunol* (2019) 10:2130. doi: 10.3389/fimmu.2019.02130

112. Rajasinghe LD, Chauhan PS, Wierenga KA, Evered AO, Harris SN, Bates MA, et al. Omega-3 Docosahexaenoic Acid (DHA) Impedes Silica-Induced Macrophage Corpse Accumulation by Attenuating Cell Death and Potentiating Efferocytosis. *Frontiers in Immunology* (2020) 11. doi: 10.3389/fimmu.2020.02179

113. Wong SW, Kwon M-J, Choi AMK, Kim H-P, Nakahira K, Hwang DH. Fatty Acids Modulate Toll-like Receptor 4 Activation through Regulation of Receptor Dimerization and Recruitment into Lipid Rafts in a Reactive Oxygen Species-dependent Manner. *Journal of Biological Chemistry* (2009) 284(40):27384-92. doi: 10.1074/jbc.m109.044065

114. Oh DY, Talukdar S, Bae EJ, Imamura T, Morinaga H, Fan W, et al. GPR120 Is an Omega-3 Fatty Acid Receptor Mediating Potent Anti-inflammatory and Insulin-Sensitizing Effects. (2010). doi: 10.1016/j.cell.2010.07.041

115. Chang HY, Lee HN, Kim W, Surh YJ. Docosahexaenoic acid induces M2 macrophage polarization through peroxisome proliferator-activated receptor gamma activation. *Life Sciences* (2015) 120:39-47. doi: 10.1016/j.lfs.2014.10.014

116. Calder PC. Omega-3 fatty acids and inflammatory processes: from molecules to man. *Biochemical Society Transactions* (2017) 45(5):1105-15. doi: 10.1042/bst20160474

117. Djuricic I, Calder PC. Beneficial Outcomes of Omega-6 and Omega-3 Polyunsaturated Fatty Acids on Human Health: An Update for 2021. *Nutrients* (2021) 13(7):2421. doi: 10.3390/nu13072421

118. Liu T, Zhang L, Joo D, Sun S-C. NF-κB signaling in inflammation. *Signal Transduction and Targeted Therapy* (2017) 2(1):17023. doi: 10.1038/sigtrans.2017.23

119. Giuliani C, Bucci I, Napolitano G. The Role of the Transcription Factor Nuclear Factor-kappa B in Thyroid Autoimmunity and Cancer. *Frontiers in Endocrinology* (2018) 9. doi: 10.3389/fendo.2018.00471

120. Jefferies CA. Regulating IRFs in IFN Driven Disease. *Frontiers in Immunology* (2019) 10. doi: 10.3389/fimmu.2019.00325

121. Han S, Zhuang H, Shumyak S, Yang L, Reeves WH. Mechanisms of autoantibody production in systemic lupus erythematosus. *Front Immunol* (2015) 6(MAY):228. doi: 10.3389/fimmu.2015.00228

122. Yung S, Chan TM. Mechanisms of Kidney Injury in Lupus Nephritis - the Role of Anti-dsDNA Antibodies. *Front Immunol* (2015) 6:475. doi: 10.3389/fimmu.2015.00475

123. Moulton VR, Suarez-Fueyo A, Meidan E, Li H, Mizui M, Tsokos GC. Pathogenesis of Human Systemic Lupus Erythematosus: A Cellular Perspective. *Trends Mol Med* (2017) 23(7):615-35. doi: 10.1016/j.molmed.2017.05.006

124. Wang YF, Zhang Y, Lin Z, Zhang H, Wang TY, Cao Y, et al. Identification of 38 novel loci for systemic lupus erythematosus and genetic heterogeneity between ancestral groups. *Nat Commun* (2021) 12(1):772. doi: 10.1038/s41467-021-21049-y

125. Parks CG, de Souza Espindola Santos A, Barbhaiya M, Costenbader KH. Understanding the role of environmental factors in the development of systemic lupus erythematosus. *Best Pract Res Clin Rheumatol* (2017) 31(3):306-20. doi: 10.1016/j.berh.2017.09.005

126. Fernandez D, Kirou KA. What Causes Lupus Flares? *Curr Rheumatol Rep* (2016) 18(3):14. doi: 10.1007/s11926-016-0562-3

127. Parks CG, Conrad K, Cooper GS. Occupational exposure to crystalline silica and autoimmune disease. *Environ Health Perspect* (1999) 107 Suppl 5(Suppl 5):793-802. doi: 10.1289/ehp.99107s5793

128. Brown JM, Pfau JC, Pershouse MA, Holian A. Silica, apoptosis, and autoimmunity. *J Immunotoxicol* (2005) 1(3):177-87. doi: 714111397 [pii]

10.1080/15476910490911922

129. Hoy RF, Chambers DC. Silica-related diseases in the modern world. *Allergy* (2020) 75(11):2805-17. doi: 10.1111/all.14202

130. Wierenga KA, Harkema JR, Pestka JJ. Lupus, Silica, and Dietary Omega-3 Fatty Acid Interventions. *Toxicol Pathol* (2019) 47(8):1004-11. doi: 10.1177/0192623319878398

131. Bates MA, Brandenberger C, Langohr I, Kumagai K, Harkema JR, Holian A, et al. Silica triggers inflammation and ectopic lymphoid neogenesis in the lungs in parallel with accelerated onset of systemic autoimmunity and glomerulonephritis in the lupus-prone NZBWF1 mouse. *PLoS One* (2015) 10(5):e0125481. doi: 10.1371/journal.pone.0125481

132. Pestka JJ, Akbari P, Wierenga KA, Bates MA, Gilley KN, Wagner JG, et al. Omega-3 Polyunsaturated Fatty Acid Intervention Against Established Autoimmunity in a Murine Model of Toxicant-Triggered Lupus. *Front Immunol* (2021) 12:653464. doi: 10.3389/fimmu.2021.653464

133. Benninghoff AD, Bates MA, Chauhan PS, Wierenga KA, Gilley KN, Holian A, et al. Docosahexaenoic Acid Consumption Impedes Early Interferon- and Chemokine-Related Gene Expression While Suppressing Silica-Triggered Flaring of Murine Lupus. *Front Immunol* (2019) 10:2851. doi: 10.3389/fimmu.2019.02851

134. Rajasinghe LD, Li QZ, Zhu C, Yan M, Chauhan PS, Wierenga KA, et al. Omega-3 fatty acid intake suppresses induction of diverse autoantibody repertoire by crystalline silica in lupus-prone mice. *Autoimmunity* (2020) 53(7):415-33. doi: 10.1080/08916934.2020.1801651

135. Gilley KN, Wierenga KA, Chauhuan PS, Wagner JG, Lewandowski RP, Ross EA, et al. Influence of total western diet on docosahexaenoic acid suppression of silica-triggered lupus flaring in NZBWF1 mice. *PLoS One* (2020) 15(5):e0233183. doi: 10.1371/journal.pone.0233183

136. Tani C, Elefante E, Signorini V, Zucchi D, Lorenzoni V, Carli L, et al. Glucocorticoid withdrawal in systemic lupus erythematosus: are remission and low disease activity reliable starting points for stopping treatment? A real-life experience. *RMD Open* (2019) 5(2):e000916. doi: 10.1136/rmdopen-2019-000916

137. Porta S, Danza A, Arias Saavedra M, Carlomagno A, Goizueta MC, Vivero F, et al. Glucocorticoids in Systemic Lupus Erythematosus. Ten Questions and Some Issues. *J Clin Med* (2020) 9(9). doi: 10.3390/jcm9092709

138. Flammer JR, Rogatsky I. Minireview: Glucocorticoids in autoimmunity: unexpected targets and mechanisms. *Mol Endocrinol* (2011) 25(7):1075-86. doi: 10.1210/me.2011-0068

139. Lamore R, 3rd, Parmar S, Patel K, Hilas O. Belimumab (benlysta): a breakthrough therapy for systemic lupus erythematosus. *P T* (2012) 37(4):212-26. doi:

140. Buttgereit F, da Silva JA, Boers M, Burmester GR, Cutolo M, Jacobs J, et al. Standardised nomenclature for glucocorticoid dosages and glucocorticoid treatment regimens: current questions and tentative answers in rheumatology. *Ann Rheum Dis* (2002) 61(8):718-22. doi: 10.1136/ard.61.8.718

141. Al Sawah S, Zhang X, Zhu B, Magder LS, Foster SA, Iikuni N, et al. Effect of corticosteroid use by dose on the risk of developing organ damage over time in systemic lupus erythematosus-the Hopkins Lupus Cohort. *Lupus Sci Med* (2015) 2(1):e000066. doi: 10.1136/lupus-2014-000066

142. Thamer M, Hernan MA, Zhang Y, Cotter D, Petri M. Prednisone, lupus activity, and permanent organ damage. *J Rheumatol* (2009) 36(3):560-4. doi: 10.3899/jrheum.080828

143. Fryar CD, Carroll MD, Gu Q, Afful J, Ogden CL. Anthropometric Reference Data for Children and Adults: United States, 2015-2018. *Vital Health Stat 3* (2021) 3(46)(36):1-44. doi:

144. Dillberger JE, Cronin NS, Carr GJ. Prednisone is not a mouse carcinogen. *Toxicol Pathol* (1992) 20(1):18-26. doi: 10.1177/019262339202000103

145. Brandenberger C, Rowley NL, Jackson-Humbles DN, Zhang Q, Bramble LA, Lewandowski RP, et al. Engineered silica nanoparticles act as adjuvants to enhance allergic airway disease in mice. *Part Fibre Toxicol* (2013) 10(1):26. doi: 10.1186/1743-8977-10-26

146. Kobayashi-Hattori K, Amuzie CJ, Flannery BM, Pestka JJ. Body composition and hormonal effects following exposure to mycotoxin deoxynivalenol in the high-fat diet-induced obese mouse. *Mol Nutr Food Res* (2011) 55(7):1070-8. doi: 10.1002/mnfr.201000640

147. Tschanz SA, Burri PH, Weibel ER. A simple tool for stereological assessment of digital images: the STEPanizer. *J Microsc* (2011) 243(1):47-59. doi: 10.1111/j.1365-2818.2010.03481.x

148. Weening JJ, D'Agati VD, Schwartz MM, Seshan SV, Alpers CE, Appel GB, et al. The classification of glomerulonephritis in systemic lupus erythematosus revisited. *J Am Soc Nephrol* (2004) 15(2):241-50. doi: 10.1097/01.asn.0000108969.21691.5d

149. Metsalu T, Vilo J. ClustVis: a web tool for visualizing clustering of multivariate data using Principal Component Analysis and heatmap. *Nucleic Acids Res* (2015) 43(W1):W566-70. doi: 10.1093/nar/gkv468

150. Bates MA, Benninghoff AD, Gilley KN, Holian A, Harkema JR, Pestka JJ. Mapping of Dynamic Transcriptome Changes Associated With Silica-Triggered Autoimmune Pathogenesis

in the Lupus-Prone NZBWF1 Mouse. *Front Immunol* (2019) 10(MAR):632. doi: 10.3389/fimmu.2019.00632

151. Benninghoff AD, Hintze KJ, Monsanto SP, Rodriguez DM, Hunter AH, Phatak S, et al. Consumption of the Total Western Diet Promotes Colitis and Inflammation-Associated Colorectal Cancer in Mice. *Nutrients* (2020) 12(2):544. doi: 10.3390/nu12020544

152. Hulsen T, de Vlieg J, Alkema W. BioVenn - a web application for the comparison and visualization of biological lists using area-proportional Venn diagrams. *BMC Genomics* (2008) 9(1):488. doi: 10.1186/1471-2164-9-488

153. Danaher P, Warren S, Dennis L, D'Amico L, White A, Disis ML, et al. Gene expression markers of Tumor Infiltrating Leukocytes. *J Immunother Cancer* (2017) 5(1):18. doi: 10.1186/s40425-017-0215-8

154. Schepper JD, Collins F, Rios-Arce ND, Kang HJ, Schaefer L, Gardinier JD, et al. Involvement of the Gut Microbiota and Barrier Function in Glucocorticoid-Induced Osteoporosis. *J Bone Miner Res* (2020) 35(4):801-20. doi: 10.1002/jbmr.3947

155. Yan SX, Deng XM, Wang QT, Sun XJ, Wei W. Prednisone treatment inhibits the differentiation of B lymphocytes into plasma cells in MRL/MpSlac-lpr mice. *Acta Pharmacol Sin* (2015) 36(11):1367-76. doi: 10.1038/aps.2015.76

156. Teramoto K, Negoro N, Kitamoto K, Iwai T, Iwao H, Okamura M, et al. Microarray analysis of glomerular gene expression in murine lupus nephritis. *J Pharmacol Sci* (2008) 106(1):56-67. doi: 10.1254/jphs.fp0071337

157. Laskewitz AJ, van Dijk TH, Grefhorst A, van Lierop MJ, Schreurs M, Bloks VW, et al. Chronic prednisolone treatment aggravates hyperglycemia in mice fed a high-fat diet but does not worsen dietary fat-induced insulin resistance. *Endocrinology* (2012) 153(8):3713-23. doi: 10.1210/en.2011-1891

158. Sali A, Guerron AD, Gordish-Dressman H, Spurney CF, Iantorno M, Hoffman EP, et al. Glucocorticoid-treated mice are an inappropriate positive control for long-term preclinical studies in the mdx mouse. *PLoS One* (2012) 7(4):e34204. doi: 10.1371/journal.pone.0034204

159. Sagcal-Gironella AC, Sherwin CM, Tirona RG, Rieder MJ, Brunner HI, Vinks AA. Pharmacokinetics of prednisolone at steady state in young patients with systemic lupus erythematosus on prednisone therapy: an open-label, single-dose study. *Clin Ther* (2011) 33(10):1524-36. doi: 10.1016/j.clinthera.2011.09.015

160. Mangin O, Zheng Y, Bouazza N, Foissac F, Benaboud S, Lui G, et al. Free prednisolone pharmacokinetics predicted from total concentrations in patients with inflammatory -

immunonologic conditions. *Fundam Clin Pharmacol* (2020) 34(2):270-8. doi: 10.1111/fcp.12515

161. Cozzani E, Drosera M, Gasparini G, Parodi A. Serology of Lupus Erythematosus: Correlation between Immunopathological Features and Clinical Aspects. *Autoimmune Dis* (2014) 2014:321359. doi: 10.1155/2014/321359

162. Alba P, Bento L, Cuadrado MJ, Karim Y, Tungekar MF, Abbs I, et al. Anti-dsDNA, anti-Sm antibodies, and the lupus anticoagulant: significant factors associated with lupus nephritis. *Ann Rheum Dis* (2003) 62(6):556-60. doi: 10.1136/ard.62.6.556

163. Taves MD, Ashwell JD. Glucocorticoids in T cell development, differentiation and function. *Nat Rev Immunol* (2021) 21(4):233-43. doi: 10.1038/s41577-020-00464-0

164. Foster MH, Ord JR, Zhao EJ, Birukova A, Fee L, Korte FM, et al. Silica Exposure Differentially Modulates Autoimmunity in Lupus Strains and Autoantibody Transgenic Mice. *Front Immunol* (2019) 10:2336. doi: 10.3389/fimmu.2019.02336

165. Lehman AJ. Approximate relation of parts per million in the diet to mg/kg bw/day. *Association of Food and Drug Officials Quarterly Bulletin* (1954) 18. doi:

166. FDA. Estimating the safe starting dose in clinical trials for therapeutics in adult healthy volunteers.: U.S. Department of Health and Human Services 2005 [Available from: https://www.fda.gov/regulatory-information/search-fda-guidance-documents/estimating-maximum-safe-starting-dose-initial-clinical-trials-therapeutics-adult-healthy-volunteers.

167. Richard ML, Gilkeson G. Mouse models of lupus: what they tell us and what they don't. *Lupus Science & Medicine* (2018) 5(1):e000199. doi: 10.1136/lupus-2016-000199

168. Akbar U, Yang M, Kurian D, Mohan C. Omega-3 Fatty Acids in Rheumatic Diseases: A Critical Review. *Journal of Clinical Rheumatology* (2017) 23(6):330-9. doi: 10.1097/RHU.0000000000000563

169. Pestka JJ. n-3 Polyunsaturated fatty acids and autoimmune-mediated glomerulonephritis. *Prostaglandins, Leukotrienes and Essential Fatty Acids (PLEFA)* (2010) 82(4-6):251-8. doi: 10.1016/j.plefa.2010.02.013

170. Dutta S, Sengupta P. Men and mice: Relating their ages. *Life Sci* (2016) 152:244-8. doi: 10.1016/j.lfs.2015.10.025

171. Reeves WH, Lee PY, Weinstein JS, Satoh M, Lu L. Induction of autoimmunity by pristane and other naturally occurring hydrocarbons. *Trends in Immunology* (2009) 30(9):455-64. doi: 10.1016/j.it.2009.06.003

172. Wierenga KA, Strakovsky RS, Benninghoff AD, Rajasinghe LD, Lock AL, Harkema JR, et al. Requisite Omega-3 HUFA Biomarker Thresholds for Preventing Murine Lupus Flaring. *Frontiers in Immunology* (2020) 11:1796-. doi: 10.3389/fimmu.2020.01796

173. Weening JJ. The Classification of Glomerulonephritis in Systemic Lupus Erythematosus Revisited. *Journal of the American Society of Nephrology* (2004) 15(2):241-50. doi: 10.1097/01.asn.0000108969.21691.5d

174. Benninghoff AD, Hintze KJ, Monsanto SP, Rodriguez DM, Hunter AH, Phatak S, et al. Consumption of the Total Western Diet Promotes Colitis and Inflammation-Associated Colorectal Cancer in Mice. *Nutrients* (2020) 12(2):544. doi: 10.3390/nu12020544

175. Metsalu T, Vilo J. ClustVis: a web tool for visualizing clustering of multivariate data using Principal Component Analysis and heatmap. *Nucleic Acids Research* (2015) 43(W1):W566-W70. doi: 10.1093/nar/gkv468

176. Porta S, Danza A, Arias Saavedra M, Carlomagno A, Goizueta MC, Vivero F, et al. Glucocorticoids in Systemic Lupus Erythematosus. Ten Questions and Some Issues. *Journal of Clinical Medicine* (2020) 9(9):2709-. doi: 10.3390/jcm9092709

177. Tsokos GC, Lo MS, Reis PC, Sullivan KE. New insights into the immunopathogenesis of systemic lupus erythematosus. *Nature Reviews Rheumatology* (2016) 12(12):716-30. doi: 10.1038/nrrheum.2016.186

178. Qiu W, Yu T, Deng G-M. The role of organ-deposited IgG in the pathogenesis of multi-organ and tissue damage

in systemic lupus erythematosus. *Front Immunol* (2022) 13:924766. doi: 10.3389/fimmu.2022.924766

179. Cavallo T, Goldman M, Graves K, Lambert PH. Altered glomerular permeability in the early phase of immune complex nephritis. *Kidney Int* (1983) 24(5):632-7. doi: 10.1038/ki.1983.204

180. Cavallo T, Goldman M, Lambert PH. Animal model of human disease. Proliferative glomerulonephritis associated with polyclonal B-cell activation. *Am J Pathol* (1984) 114(2):346-8. doi:

181. Ramos-Niembro F, Fournie G, Lambert PH. INDUCTION OF CIRCULATING IMMUNE-COMPLEXES AND THEIR RENAL LOCALIZATION AFTER ACUTE OR CHRONIC POLYCLONAL B-CELL ACTIVATION IN MICE. *Kidney International* (1982) 21:S29-S38. doi:

182. Cavallo T, Granholm NA. Repeated exposure to bacterial lipopolysaccharide interferes with disposal of pathogenic immune complexes in mice. *Clin Exp Immunol* (1990) 79(2):253-9. doi: 10.1111/j.1365-2249.1990.tb05187.x

183. Cavallo T, Granholm NA. Bacterial Lipopolysaccharide Transforms Mesangial into Proliferative Lupus Nephritis Without Interfering with Processing of Pathogenic Immune Complexes in NZB/W Mice. 1990.

184. Cavallo T, Granholm NA. Lipopolysaccharide from gram-negative bacteria enhances polyclonal B cell activation and exacerbates nephritis in MRL/lpr mice. *Clin Exp Immunol* (1990) 82(3):515-21. doi: 10.1111/j.1365-2249.1990.tb05482.x

185. Granholm NA, Cavallo T. Bacterial lipopolysaccharide enhances deposition of immune complexes and exacerbates nephritis in BXSB lupus-prone mice. *Clin Exp Immunol* (1991) 85(2):270-7. doi: 10.1111/j.1365-2249.1991.tb05717.x

186. Granholm NA, Cavallo T. Bacterial lipopolysaccharide causes variable deposits of diverse immunoglobulin isotypes in kidneys of lupus-prone mice. *Lupus* (1992) 1(4):255-61. doi: 10.1177/096120339200100409

187. Cavallo T, Granholm NA. Accelerated (proliferative) lupus nephritis. *Am J Pathol* (1990) 137(6):1549-51. doi:

188. Fournie GJ, Minh MG, Mignon-Conte MA, Hass S, Lambert PH, Conte JJ. Acceleration of glomerulonephritis in NZB x NZW mice by early immunization with DNA and injection of bacterial lipopolysaccharide. Experimental approach to the treatment of lupus nephritis by use of the accelerated model of NZB x NZW mouse disease. *J Clin Lab Immunol* (1980) 4(2):103-6. doi:

189. Liebers V, Brüning T, Raulf M. Occupational endotoxin exposure and health effects. *Archives of Toxicology* (2020) 94(11):3629-44. doi: 10.1007/s00204-020-02905-0

190. Ebbensgaard A, Mordhorst H, Aarestrup F, Hansen EB. The Role of Outer Membrane Proteins and Lipopolysaccharides for the Sensitivity of *Escherichia coli* to Antimicrobial Peptides. *Front Microbiol* (2018) 9:2153. doi: 10.3389/fmicb.2018.02153

191. Sigsgaard T, Bonefeld-Jørgensen EC, Hoffmann HJ, Bønløkke J, Krü Ger T. Microbial cell wall agents as an occupational hazard. *Toxicol Appl Pharmacol* (2005) 1(207):310-9. doi: 10.1016/j.taap.2004.12.031

192. Wunschel J, Poole JA. Occupational agriculture organic dust exposure and its relationship to asthma and airway inflammation in adults. *Journal of Asthma* (2016) 53(5):471-7. doi: 10.3109/02770903.2015.1116089

193. Illescas-Montes R, Corona-Castro CC, Melguizo-Rodríguez L, Ruiz C, Costela-Ruiz VJ. Infectious processes and systemic lupus erythematosus. *Immunology* (2019) 158(3):153-60. doi: 10.1111/imm.13103

194. Ka SM, Lin JC, Lin TJ, Liu FC, Chao LK, Ho CL, et al. Citral alleviates an accelerated and severe lupus nephritis model by inhibiting the activation signal of NLRP3 inflammasome and enhancing Nrf2 activation. *Arthritis Research and Therapy* (2015) 17(1):331-. doi: 10.1186/s13075-015-0844-6

195. Liu X, Yin S, Chen Y, Wu Y, Zheng W, Dong H, et al. LPS-induced proinflammatory cytokine expression in human airway epithelial cells and macrophages via NF-κB, STAT3 or AP-1 activation. *Molecular Medicine Reports* (2018) 17(4):5484-91. doi: 10.3892/mmr.2018.8542

196. Wu C-Y, Hua K-F, Chu C-L, Yang S-R, Arbiser JL, Yang S-S, et al. Tris DBA Ameliorates Accelerated and Severe Lupus Nephritis in Mice by Activating Regulatory T Cells and Autophagy and Inhibiting the NLRP3 Inflammasome. *The Journal of Immunology* (2020) 204(6):1448-61. doi: 10.4049/jimmunol.1801610

197. Lin T-J, Wu C-Y, Tsai P-Y, Hsu W-H, Hua K-F, Chu C-L, et al. Accelerated and Severe Lupus Nephritis Benefits From M1, an Active Metabolite of Ginsenoside, by Regulating NLRP3 Inflammasome and T Cell Functions in Mice. *Frontiers in Immunology* (2019) 10(AUG):1951-. doi: 10.3389/fimmu.2019.01951

198. Brandenberger C, Rowley NL, Jackson-Humbles DN, Zhang Q, Bramble LA, Lewandowski RP, et al. Engineered silica nanoparticles act as adjuvants to enhance allergic airway disease in mice. *Particle and Fibre Toxicology* (2013) 10(1):26. doi: 10.1186/1743-8977-10-26

199. Stavnezer J, Guikema JEJ, Schrader CE. Mechanism and Regulation of Class Switch Recombination. *Annual Review of Immunology* (2008) 26(1):261-92. doi: 10.1146/annurev.immunol.26.021607.090248

200. Krieg AM, Yi A-K, Matson S, Waldschmidt TJ, Bishop GA, Teasdale R, et al. CpG motifs in bacterial DNA trigger direct B-cell activation. *Nature* (1995) 374(6522):546-9. doi: 10.1038/374546a0

201. Murray PJ. Macrophage Polarization. *Annual Review of Physiology* (2017) 79(1):541-66. doi: 10.1146/annurev-physiol-022516-034339

202. Bissonnette EY, Lauzon-Joset JF, Debley JS, Ziegler SF. Cross-Talk Between Alveolar Macrophages and Lung Epithelial Cells is Essential to Maintain Lung Homeostasis. *Front Immunol* (2020) 11:583042. doi: 10.3389/fimmu.2020.583042

203. Martin TR. Innate Immunity in the Lungs. *Proceedings of the American Thoracic Society* (2005) 2(5):403-11. doi: 10.1513/pats.200508-090js

204. Divangahi M, King IL, Pernet E. Alveolar macrophages and type I IFN in airway homeostasis and immunity. *Trends in Immunology* (2015) 36(5):307-14. doi: 10.1016/j.it.2015.03.005

205. Adler B, Adler H. Type I interferon signaling and macrophages: a double-edged sword? *Cellular & Molecular Immunology* (2021) 19(9):967-8. doi: 10.1038/s41423-020-00609-0

206. Hussell T, Bell TJ. Alveolar macrophages: plasticity in a tissue-specific context. *Nature Reviews Immunology* (2014) 14(2):81-93. doi: 10.1038/nri3600

207. Li Y, Lee PY, Reeves WH. Monocyte and Macrophage Abnormalities in Systemic Lupus Erythematosus. *Archivum Immunologiae et Therapiae Experimentalis* (2010) 58(5):355-64. doi: 10.1007/s00005-010-0093-y

208. Herrada AA, Escobedo N, Iruretagoyena M, Valenzuela RA, Burgos PI, Cuitino L, et al. Innate Immune Cells' Contribution to Systemic Lupus Erythematosus. *Front Immunol* (2019) 10:772. doi: 10.3389/fimmu.2019.00772

209. Udalova IA, Mantovani A, Feldmann M. Macrophage heterogeneity in the context of rheumatoid arthritis. *Nature Reviews Rheumatology* (2016) 12(8):472-85. doi: 10.1038/nrrheum.2016.91

210. Wierenga KA, Harkema JR, Pestka JJ. Lupus, Silica, and Dietary Omega-3 Fatty Acid Interventions. *Toxicologic Pathology* (2019) 47(8):1004-11. doi: 10.1177/0192623319878398

211. Wierenga KA, Riemers FM, Westendrop B, Harkema JR, Pestka JJ. Single cell analysis of docosahexaenoic acid suppression of sequential LPS-induced proinflammatory and interferon-regulated gene expression in the macrophage *Front Immunol* (2022) 13:993614. doi: 10.3389/fimmu.2022.993614

212. Bolger AM, Lohse M, Usadel B. Trimmomatic: a flexible trimmer for Illumina sequence data. *Bioinformatics* (2014) 30(15):2114-20. doi: 10.1093/bioinformatics/btu170

213. Dobin A, Davis CA, Schlesinger F, Drenkow J, Zaleski C, Jha S, et al. STAR: ultrafast universal RNA-seq aligner. *Bioinformatics* (2013) 29(1):15-21. doi: 10.1093/bioinformatics/bts635

214. Love MI, Huber W, Anders S. Moderated estimation of fold change and dispersion for RNA-seq data with DESeq2. *Genome Biology* (2014) 15(12). doi: 10.1186/s13059-014-0550-8

215. Badia-i-Mompel P, Vélez Santiago J, Braunger J, Geiss C, Dimitrov D, Müller-Dott S, et al. decoupleR: ensemble of computational methods to infer biological activities from omics data. *Bioinformatics Advances* (2022) 2(1). doi: 10.1093/bioadv/vbac016

216. Garcia-Alonso L, Holland CH, Ibrahim MM, Turei D, Saez-Rodriguez J. Benchmark and integration of resources for the estimation of human transcription factor activities. *Genome Res* (2019) 29(8):1363-75. doi: 10.1101/gr.240663.118

217. Rönnblom L, Leonard D. Interferon pathway in SLE: one key to unlocking the mystery of the disease. *Lupus Science & Medicine* (2019) 6:270-. doi: 10.1136/lupus-2018-000270

218. Chawla A. Control of Macrophage Activation and Function by PPARs. *Circulation Research* (2010) 106(10):1559-69. doi: 10.1161/circresaha.110.216523

219. Pello OM, De Pizzol M, Mirolo M, Soucek L, Zammataro L, Amabile A, et al. Role of c-MYC in alternative activation of human macrophages and tumor-associated macrophage biology. *Blood* (2012) 119(2):411-21. doi: 10.1182/blood-2011-02-339911

220. Shah A, Lindquist JA, Rosendahl L, Schmitz I, Mertens PR. Novel Insights into YB-1 Signaling and Cell Death Decisions. *Cancers* (2021) 13(13):3306. doi: 10.3390/cancers13133306

221. Sharif MN, ŠOšIć DE, Rothlin CV, Kelly E, Lemke G, Olson EN, et al. Twist mediates suppression of inflammation by type I IFNs and Axl. *Journal of Experimental Medicine* (2006) 203(8):1891-901. doi: 10.1084/jem.20051725

222. Shivshankar P, Fekry B, Eckel-Mahan K, Wetsel RA. Circadian Clock and Complement Immune System-Complementary Control of Physiology and Pathology? *Front Cell Infect Microbiol* (2020) 10:418. doi: 10.3389/fcimb.2020.00418

APPENDIX A: CHAPTER 2 SUPPLEMENTAL MATERIAL

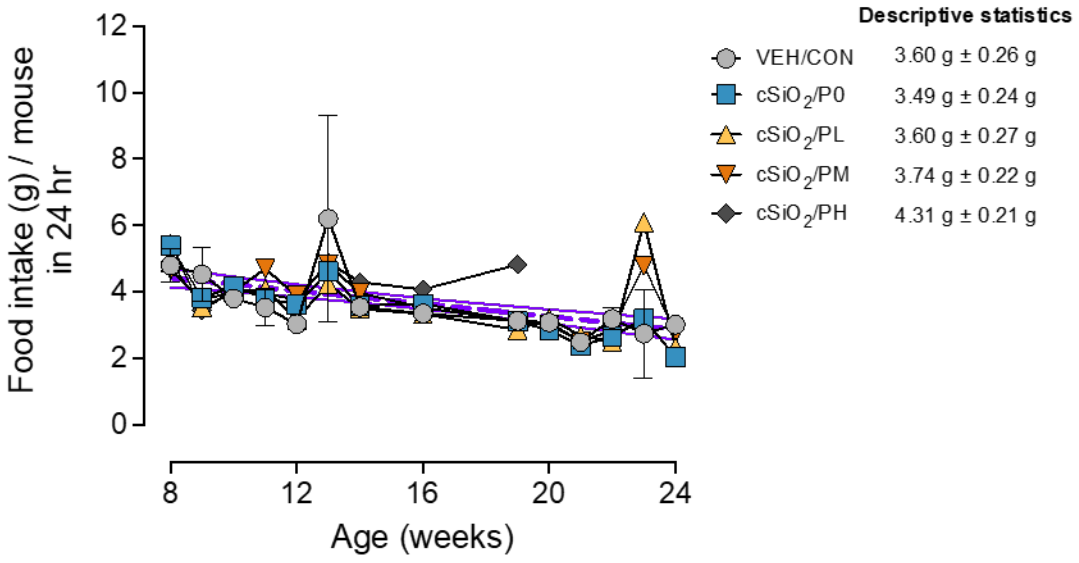

Figure A2.1: Prednisone administration did not result in food refusal throughout the duration of the study. The amount of diet consumed between Monday morning and Tuesday morning (24 hr) was measured 14 out of 16 weeks prior to the Cohort A sacrifice date. Dietary intake per mouse for Cohort A was estimated by 1) calculating the difference between total food administered per cage Monday and total food remaining 24 hr later, then 2) dividing the difference by the number of mice per cage (n=4). Data points represent the estimated diet eaten per mouse for two separate cages (n=2) at each time point. Descriptive statistics represent the 14-week average dietary intake per mouse (g)/24 hr ± SEM for the VEH/P0, $cSiO_2$/P0, $cSiO_2$/PL, and $cSiO_2$/PM groups, and the 9-week average ± SEM for the $cSiO_2$/PH group. Significant differences were not detected between individual slopes for each treatment group based on nonlinear regression analysis. The combined slope of -0.09113 is shown with shaded bands around the regression line illustrating 95% confidence intervals.

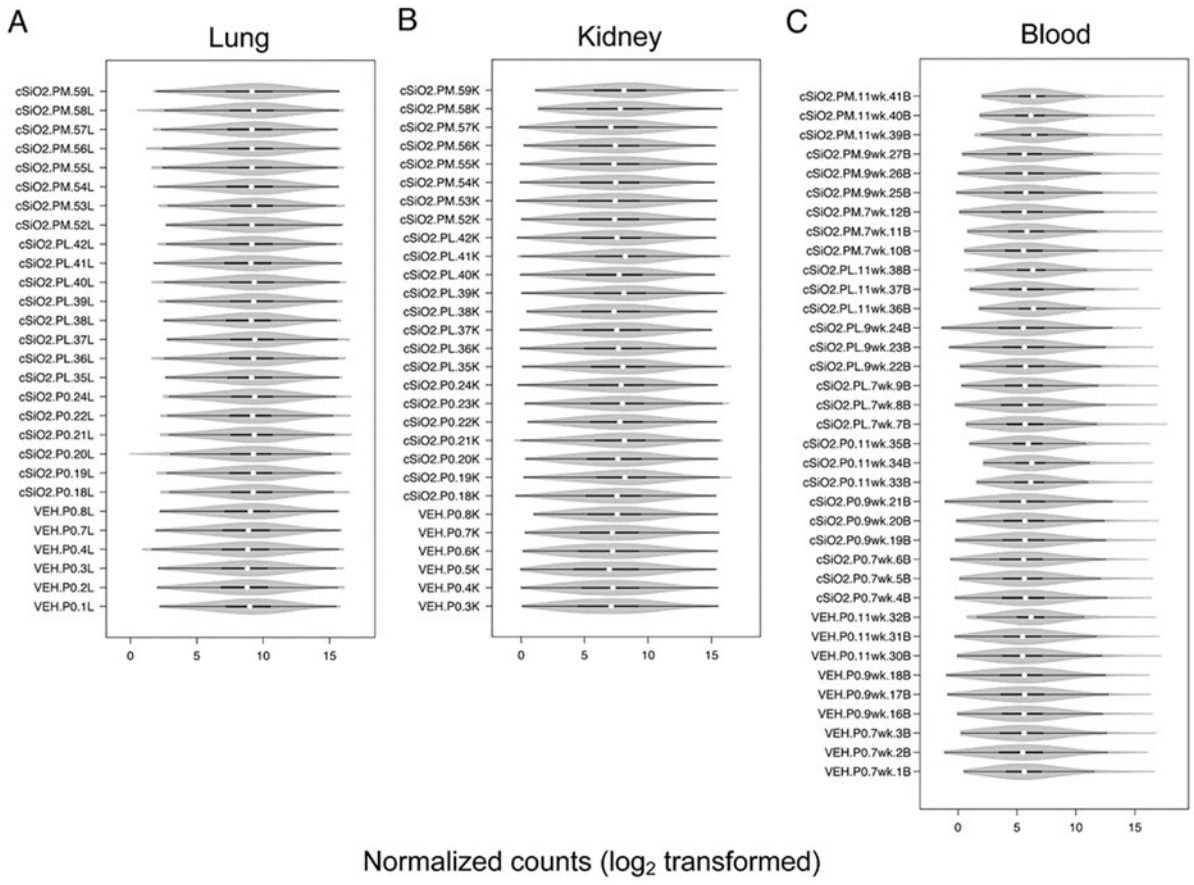

Figure A2.2: Violin plots depicting distribution of normalized counts obtained using NanoString Autoimmune Profiling gene panel for lung (A) and kidney (B) tissues obtained 14 weeks post $cSiO_2$ instillation and (C) for whole blood obtained 7-, 9-, or 11-weeks post $cSiO_2$ instillation. Within the violin distribution polygon, bars represent the 25th to 27th percentile and the white circle indicates the median. Values are shown as the $\log_2$ transformation of normalized counts. Values <20 counts ($\log_2$=4.32) were excluded from analyses.

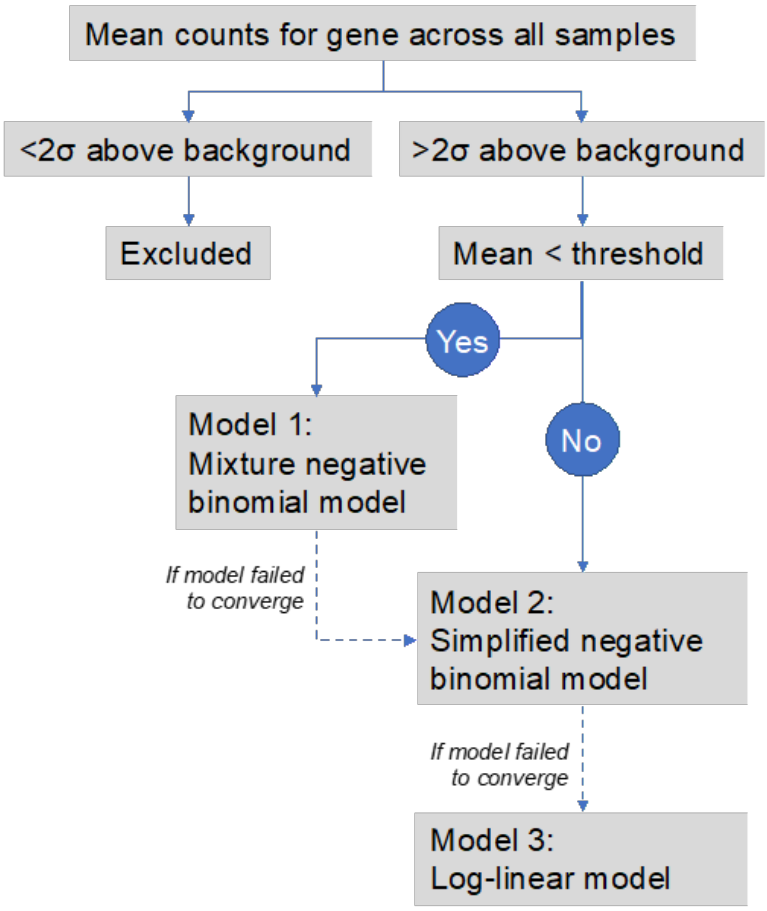

Figure A2.3: Process flow for differential gene expression analysis using nSolver. As outlined by the supplied user manual, the mean of the gene across all samples was compared against the threshold, which is set as 10 times the background signal. If the gene mean was below the threshold, the mixture negative binomial (MLE function in R, Wald test to calculate a p value) was applied; if model 1 did not converge, the simplified model in 2 (glm.nb function in R/Mass) was applied instead. If the gene mean was above the threshold, the mixture model in 1 was simplified to model 2. If model 2 did not converge, the log-linear model 3 was used (lm function in R). [1]

[1] NanoString Technologies, Inc. (2018) nCounter Advanced Analysis 2.0 Plugin for nSolver Software User Manual, vers. Jan 2018 (MAN-10030-03). Accessed at www.nanostring.com.

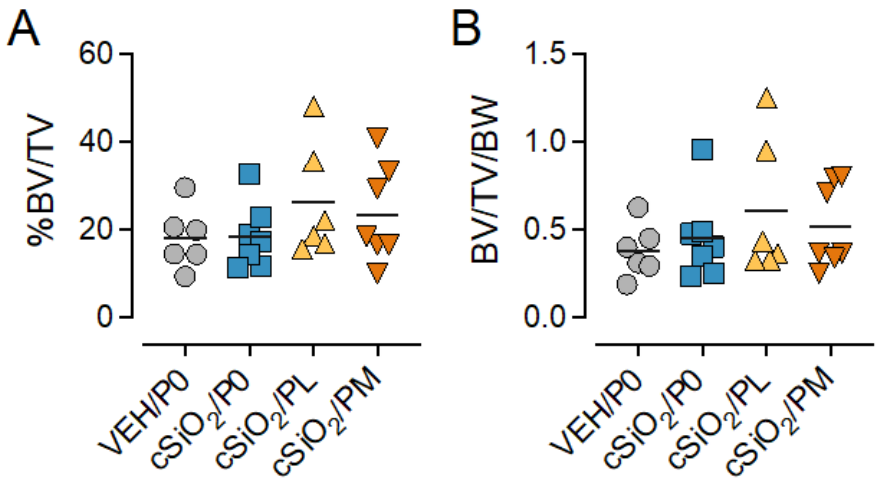

Figure A2.4: Prednisone does not significantly reduce bone density in cSiO2-exposed NZBWF1 mice. Dietary administration of prednisone did not induce trabecular bone loss. Femurs collected from mice at time of necropsy (25 wks of age) were analyzed using µCT. Box-plot whiskers represent the minimum and maximum levels of bone density. No significant differences were detected between VEH/P0 and $cSiO_2$/P0 groups, or between $cSiO_2$/P0 and prednisone-fed groups. BV/TV = bone volume/total volume; BV/TV/BW = bone volume/total volume/body weight.

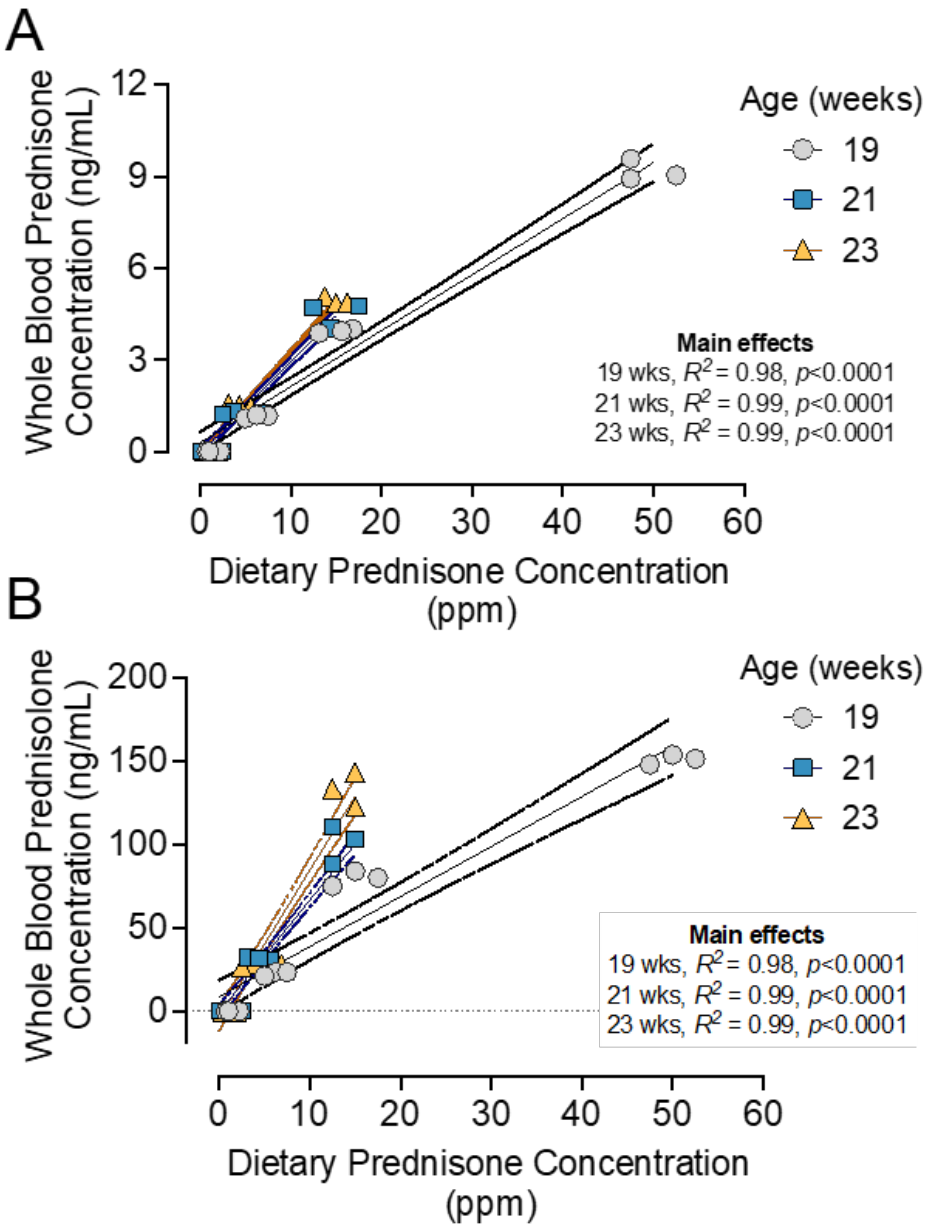

Figure A2.5: Prednisone concentration detected in whole blood is predictable based on dietary prednisone concentrations at multiple timepoints. (A) Levels of prednisone and its active metabolite, prednisolone **(B)**, were detected in whole blood samples taken from mice 19, 21, 23 wk of age determined via LC-MS/MS. Samples were pooled within each cage (n=3/cage), with 3 cages per treatment group resulting in an n=3/group for analysis. For regression analyses, R^2 and p-values are reported for each timepoint. Shaded bands around regression lines represent 95% confidence intervals.

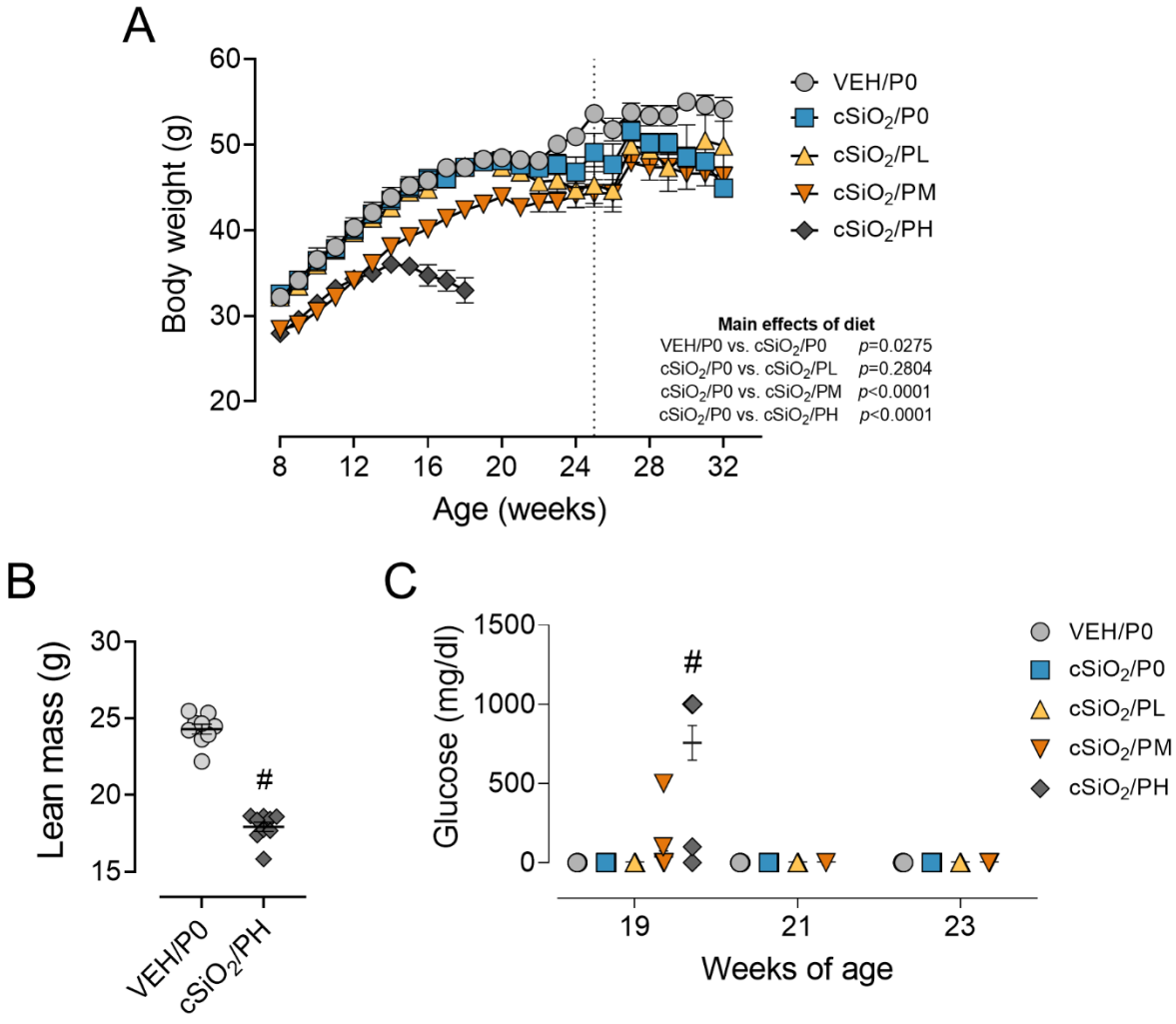

Figure A2.6: High dose prednisone treatment (PH) caused secondary toxicity in $cSiO_2$-instilled mice. (A) Mice from Cohort A and Cohort B were weighed weekly starting at 8 wk of age. Values are shown as mean ± SEM. Unlike PL and PM groups, mice in the PH group experienced weight loss starting at approximately 15-16 wk of age. Body weights were significantly lower in mice provided the PM and PH diets up to 25 wk of age (at time of first necropsy, dashed line) or 18 wk, respectively, as compared to the $cSiO_2$/P0 group. **(B)** At 17 wk of age (5 wk PI) high dose prednisone treatment resulted in significant lean muscle loss compared to VEH/P0 mice. #Indicates $p<0.05$ as determined using a two-tailed Student's t-test. **(C)** At 19 wk of age (7 wk PI) mice were evaluated for urine glucose using clinical dipsticks. High dose prednisone treatment resulted in elevated urine glucose levels compared to all other groups. #Indicates $p<0.05$ compared to $cSiO_2$/P0 as determined by Kruskal-Wallis nonparametric test.

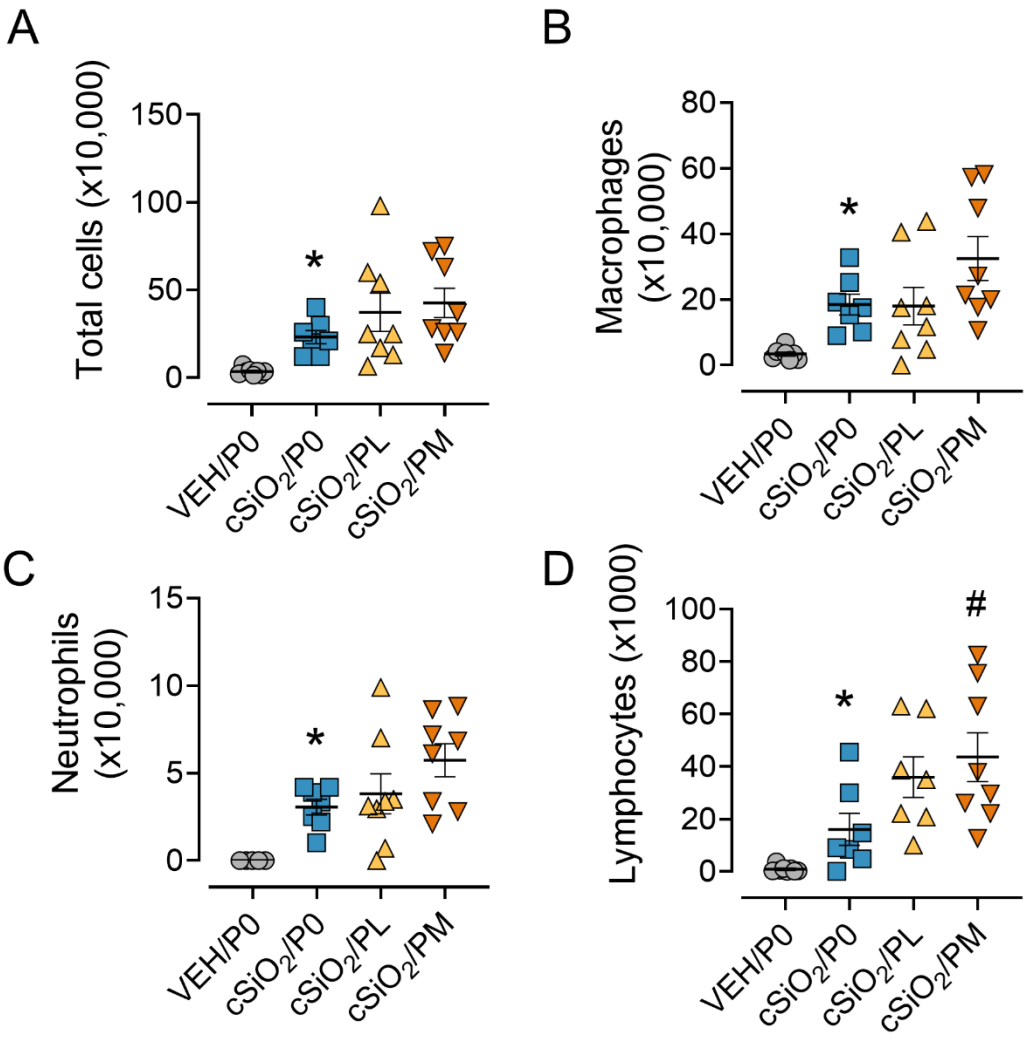

Figure A2.7: Low and medium dose Prednisone did not reduce $cSiO_2$-triggered BALF inflammatory cell counts. SiO_2 instillation caused significant increases in **(A)** total cells, **(B)** macrophages, **(C)** neutrophils, and **(D)** lymphocytes cellular inflammation in the BALF, but these responses were unaffected by PL or PM diets. *Indicates $p<0.05$ for VEH/P0 vs $cSiO_2$/P0; #indicates $p<0.05$ for $cSiO_2$/P0 vs $cSiO_2$/PL or $cSiO_2$/PM group.

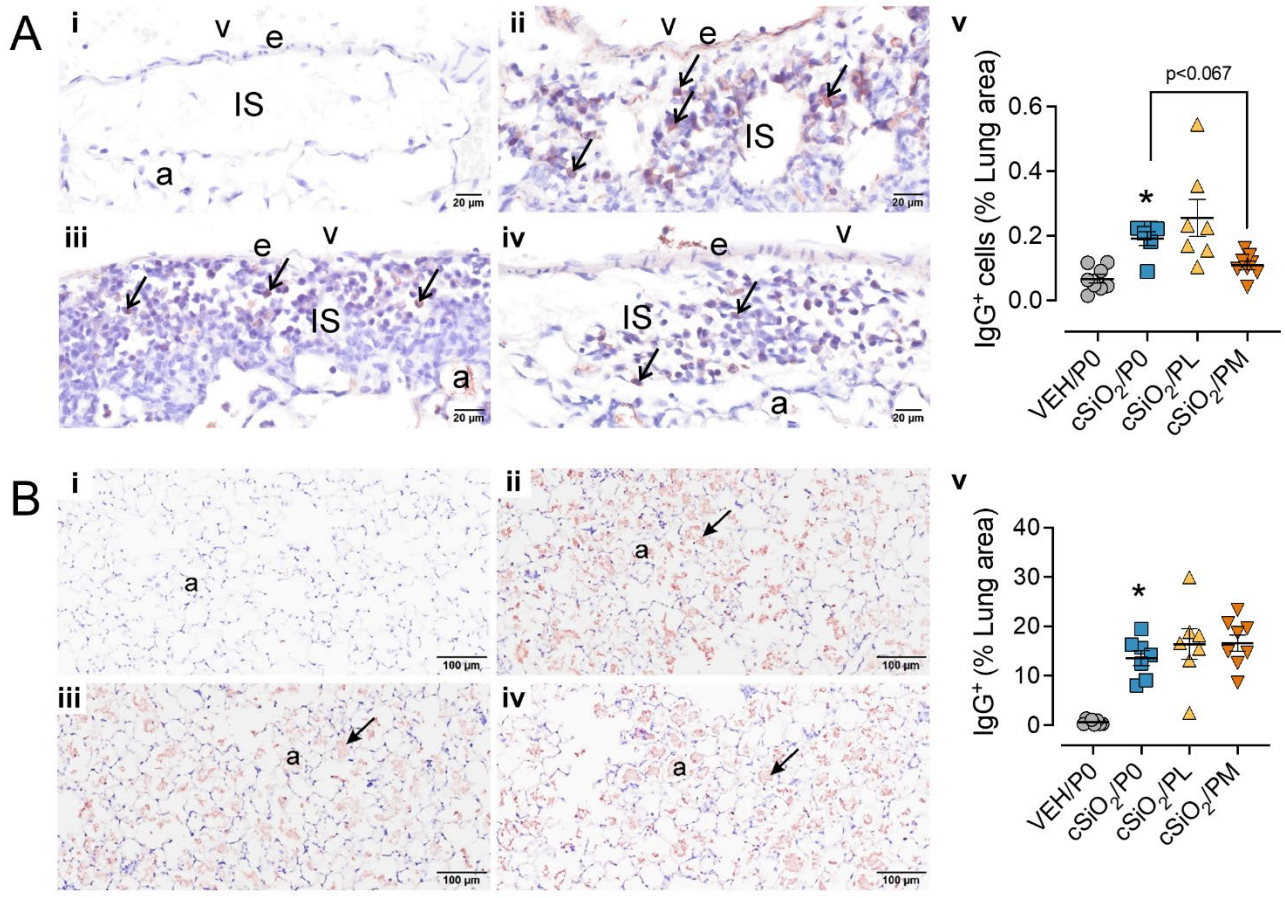

Figure A2.8: Prednisone reduces pulmonary IgG+ plasma cells but not overall IgG deposition. Light photomicrographs of perivenous ectopic lymphoid structures (ELS) immunohistochemically stained for **(A)** IgG+ B plasma cells (arrows) and **(B)** alveolar parenchyma immunohistochemically stained for extracellular IgG+ proteinaceous material (arrows) in alveolar airspace (a) in (i) VEH/P0, (ii) cSiO2/P0, (iii) cSiO2/PL, and (iv) cSiO2/PM mice. e, endothelium; v, venous lumen; IS, perivascular interstitial space; a, alveolus. Graphical representation of morphometrically determined lung density of IgG+ plasma cells (A.v) and total IgG (B.v). PM treatment modestly reduces pulmonary IgG+ plasma cell density (A.v) but has no effect on extracellular IgG (B.v). Tissues counterstained with hematoxylin. *Indicates $p<0.05$ for VEH/P0 vs cSiO2/P0; #indicates $p<0.05$ for cSiO2/P0 vs cSiO2/PL or cSiO2/PM group.

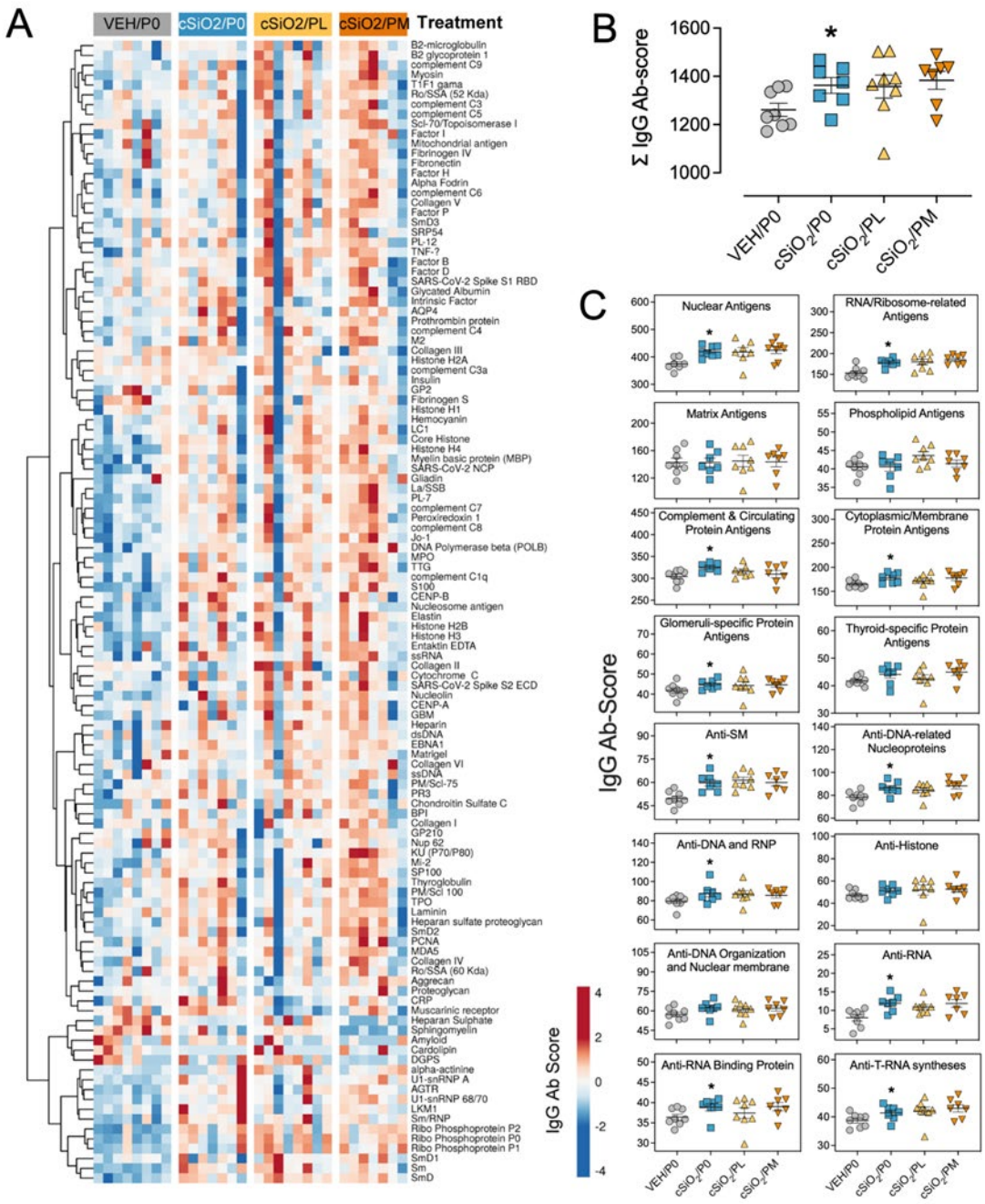

Figure A2.9: Prednisone treatment is not effective in reducing $cSiO_2$-induced AAbs in the plasma. AAbs production was measured in plasma using Cohort A samples collected at time of necropsy (14 wk pi). **(A)** Heat map illustrates unsupervised clustering (Euclidian distance method) of 122 AAbs depict Ab-score values for IgG expression in plasma. Scale bar values reflect the range of variance-stabilized Ab scores, which were centered across rows. **(B)** Prednisone did not reduce overall IgG levels in the plasma compared to $cSiO_2$ controls. **(C)** Prednisone did not alter reduce certain classes of AAbs in the plasma compared to the $cSiO_2$/P0 positive control group. * $p<0.05$ for $cSiO_2$/P0 compared to VEH/P0; $^{\#}$ $p<0.05$ for $cSiO_2$/PL or $cSiO_2$/PM compared to $cSiO_2$/P0 as described in Materials and Methods.

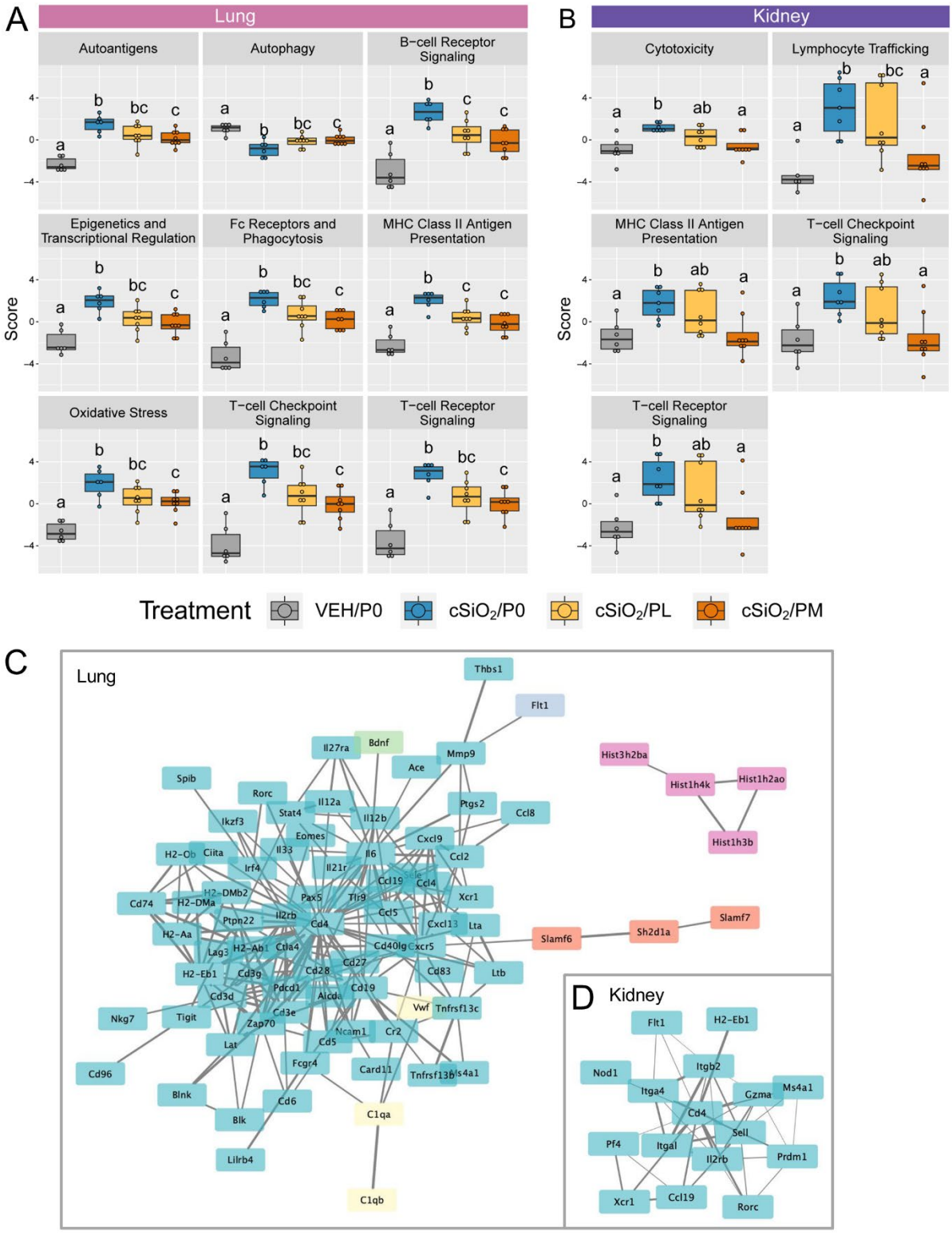

Figure A2.10: Effect of prednisone treatment on select autoimmune pathways in lung and kidney tissues of mice 14 weeks post instillation with $cSiO_2$. (A-B) Pathway Z scores are presented as Tukey box-plots for select pathways of interest for lung **(A)** or kidney **(B)**

Figure A2.10 (cont'd):
tissues. Within a tissue type, different letters indicate that the treatment groups are significantly different ($p<0.05$) as described in Materials and Methods. **(C-D)** Network visualizations of genes significantly affected by prednisone treatment in lung **(C)** or kidney **(D)** tissues. Network interactions for genes differentially regulated by medium-dose prednisone treatment were modeled using the STRING database (string-db.org) with a minimum required interaction score >0.7, and clusters were identified using the Markov Cluster (MCL) algorithm with inflation parameter of 1.5. Networks were visualized in Cytoscape, and edge widths reflect the combined interaction score (thicker edge indicates higher score). Abbreviations: $cSiO_2$, crystalline silica; P0, zero prednisone; PL, low-dose prednisone; PM, medium-dose prednisone; VEH, vehicle control.

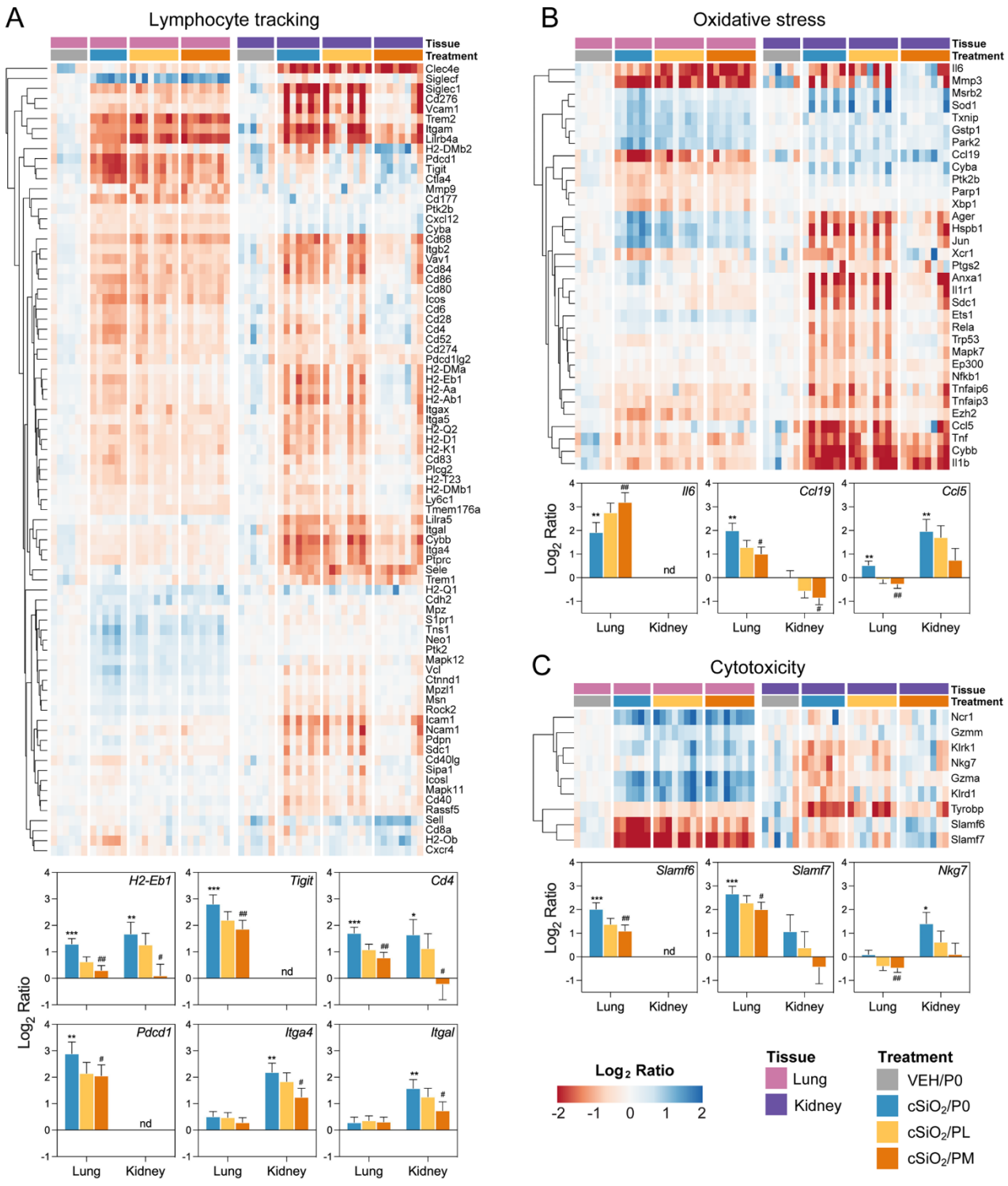

Figure A2.11: Comparison of prednisone-responsive genes associated with (A) lymphocyte tracking, (B) oxidative stress, and (C) cytotoxicity pathways in lung or kidney tissues 14 weeks post instillation with $cSiO_2$. Gene expression data were obtained using the

Figure A2.11 (cont'd):
NanoString Autoimmune Profiling gene panel and are shown as log_2 ratios for $cSiO_2$/P0, $cSiO_2$/PL, and $cSiO_2$/PM treatment groups with respect to the tissue-matched VEH/P0 control group (log_2 ratio = 0). For each pathway, heatmaps with unsupervised hierarchical clustering (Euclidian distance method) by gene show log_2 expression values for all genes identified as differentially expressed in response to either $cSiO_2$ exposure or medium-dose prednisone (FDR $q<0.05$, 1.5-fold change) in either of the selected tissues. The mean log_2 ratio values + SEM for selected genes of interest are also shown for each pathway. For $cSiO_2$/P0 as compared to VEH/P0, *, FDR-corrected $q<0.05$; **, $q<0.01$; and ***, $q<0.001$. For $cSiO_2$/PL or $cSiO_2$/PM vs $cSiO_2$/P0, #, FDR-corrected $q<0.05$; ##, $q<0.01$; and ###, $q<0.001$. See Supplementary File 1 for test specifications and FDR-corrected q-values for all genes in the panel for all comparisons. Abbreviations: $cSiO_2$, crystalline silica; P0, zero prednisone; PL, low-dose prednisone; PM, medium-dose prednisone; VEH, vehicle control.

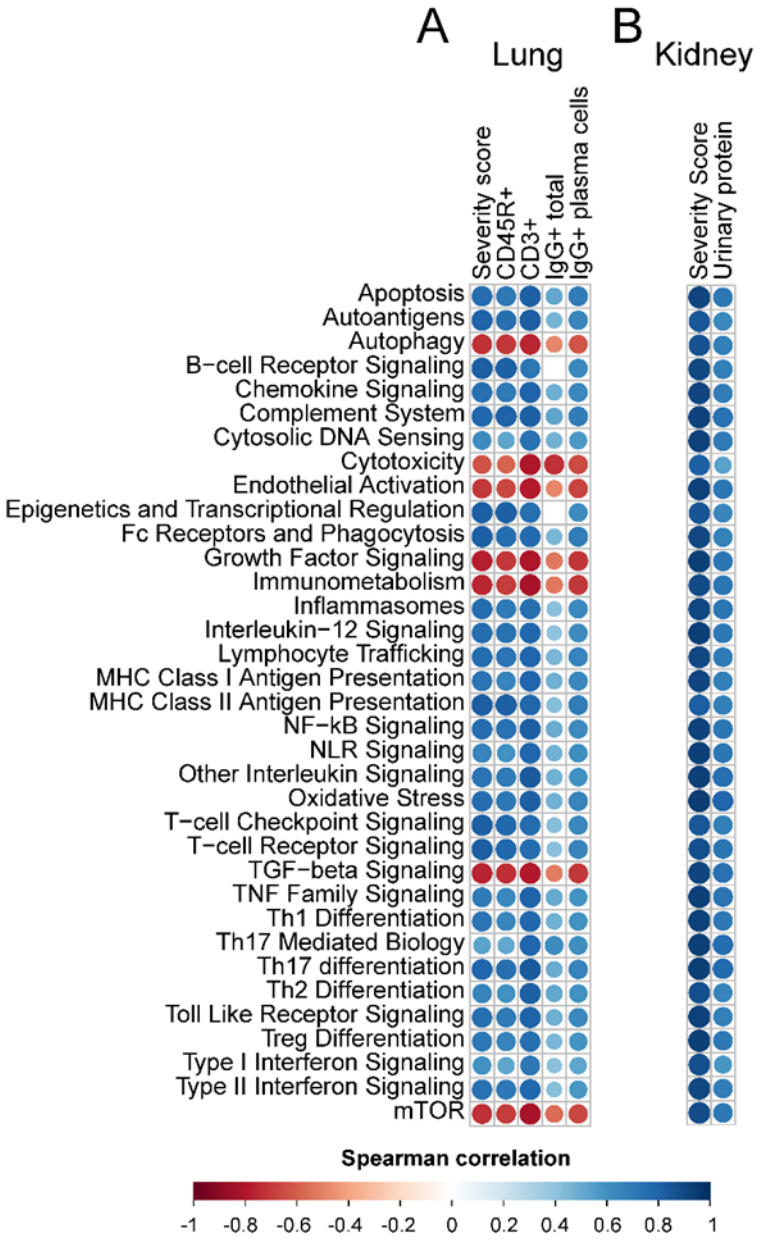

Figure A2.12: Correlation analyses of all pathways represented in the NanoString autoimmune profiling panel. For all treatment groups, spearman ρ values were calculated by correlating pathway Z scores with **(A)** lung severity score or the percent positive staining for CD45R+, CD3+, or IgG+ in lung tissue or IgG+ in lung tissue plasma cells; or **(B)** kidney severity score, kidney blood urea nitrogen (BUN), or kidney urinary protein. Significant correlation values ($p<0.05$) are represented as circles colored by the correlation value (blue, positive; red, negative); non-significant correlations are indicated by blank cells.

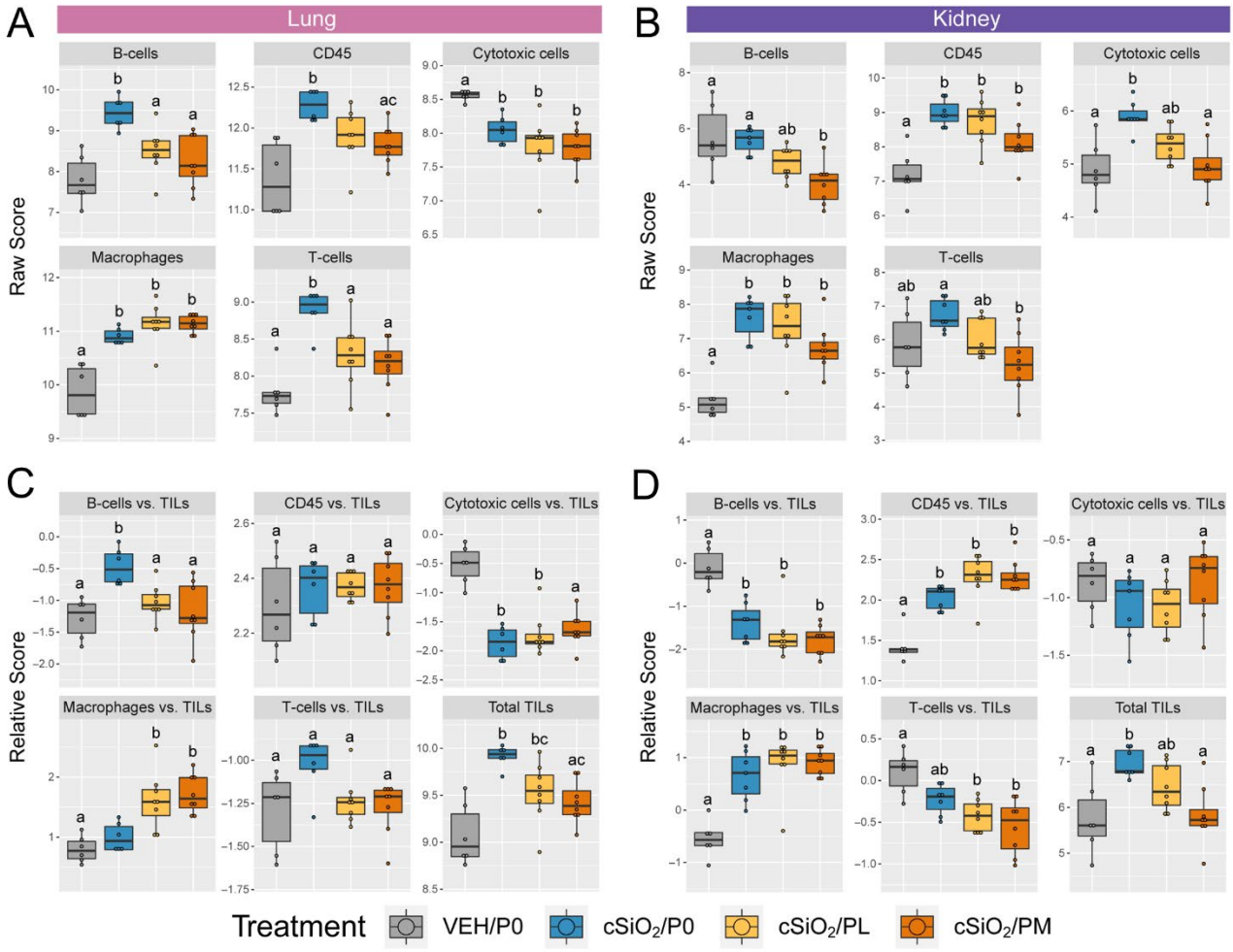

Figure A2.13: Profiling of immune cell types in lung or kidney tissues from mice 14 weeks post instillation with cSiO2. Data shown are the log2 raw scores **(A-B)** or relative scores with respect to total infiltrating leukocytes (TILs) **(C-D)** for the indicated cell types for lung (A,C) and kidney (B,D). Only those cell types passing quality control testing for correlation of marker gene expression for either tissue ($p<0.05$) are shown. Within a tissue type, different letters indicate that the treatment groups are significantly different ($p<0.05$) as described in Materials and Methods. Scores may be compared by treatment within a cell type, but comparisons across cell types are not appropriate for this method of quantitation.

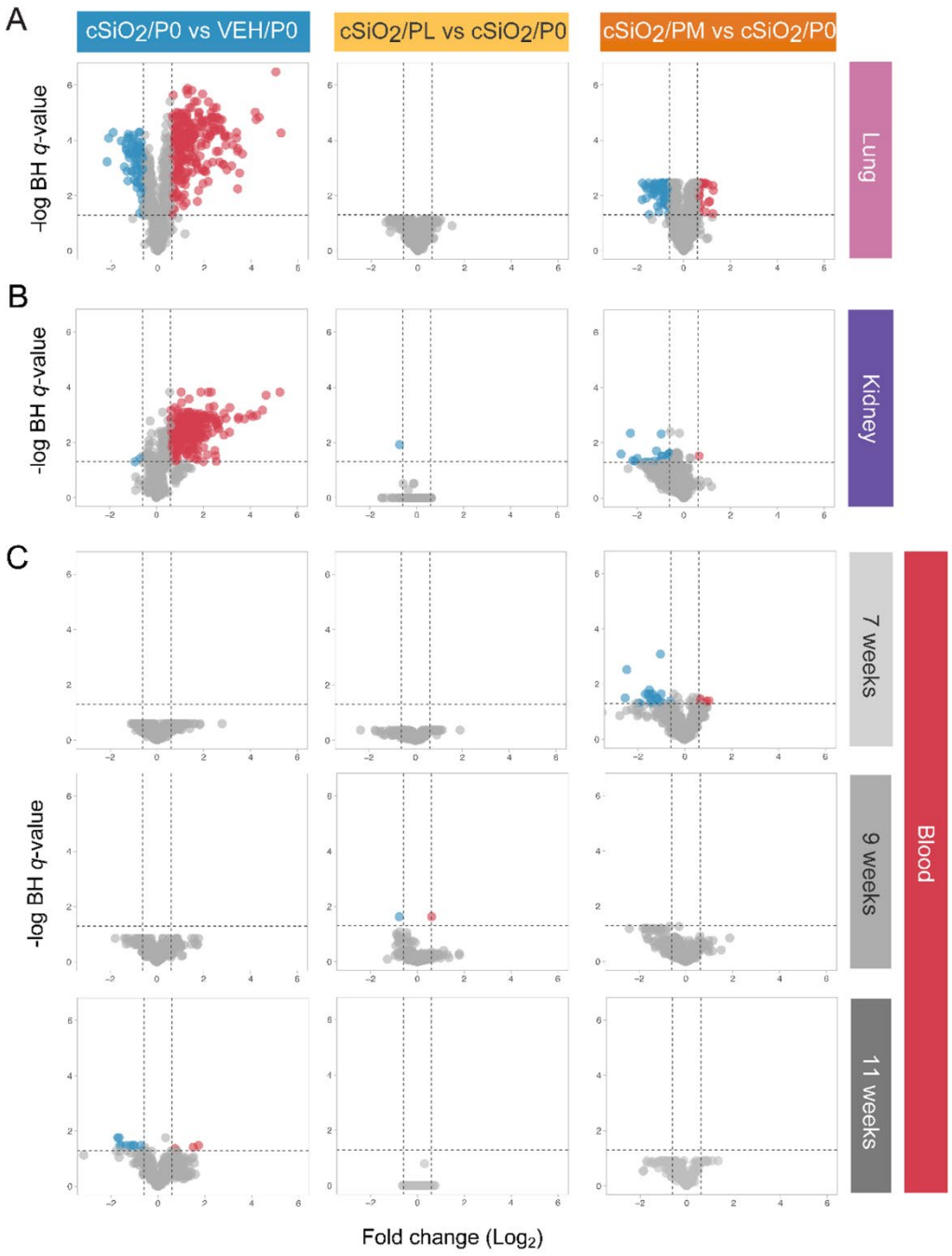

Figure A2.14: Volcano plots depicting gene expression determined using the NanoString Autoimmune Profiling gene panel for (A) lung and (B) kidney tissues obtained 13 weeks post instillation with $cSiO_2$ or whole blood samples obtained 7-, 9-, or 11-weeks post instillation. Values shown are the fold change (log_2 ratio) for $cSiO_2$/P0 treatment vs tissue-matched VEH/P0 control group, or for low-dose ($cSiO_2$/PL) or medium-dose ($cSiO_2$/P0) prednisone versus tissue matched zero prednisone control ($cSiO_2$/P0) plotted against the $-log_{10}$ Benjamini-Hochberg FDR-corrected *q*-value. A significant difference in gene expression was inferred with 1.5-fold change (log_2 <-0.585 or >0.585) with q<0.05.

A

Timepoint & comparison	DEGs Up	Down
Week 7		
$cSiO_2$/P0 vs. VEH/P0	0	0
$cSiO_2$/PL vs $cSiO_2$/P0	0	0
$cSiO_2$/PM vs $cSiO_2$/P0	5	20
$cSiO_2$/PM vs $cSiO_2$/PL	0	0
Week 9		
$cSiO_2$/P0 vs. VEH/P0	0	0
$cSiO_2$/PL vs $cSiO_2$/P0	1	1
$cSiO_2$/PM vs $cSiO_2$/P0	0	0
$cSiO_2$/PM vs $cSiO_2$/PL	0	0
Week 11		
$cSiO_2$/P0 vs. VEH/P0	3	10
$cSiO_2$/PL vs $cSiO_2$/P0	0	0
$cSiO_2$/PM vs $cSiO_2$/P0	0	0
$cSiO_2$/PM vs $cSiO_2$/PL	0	0

B

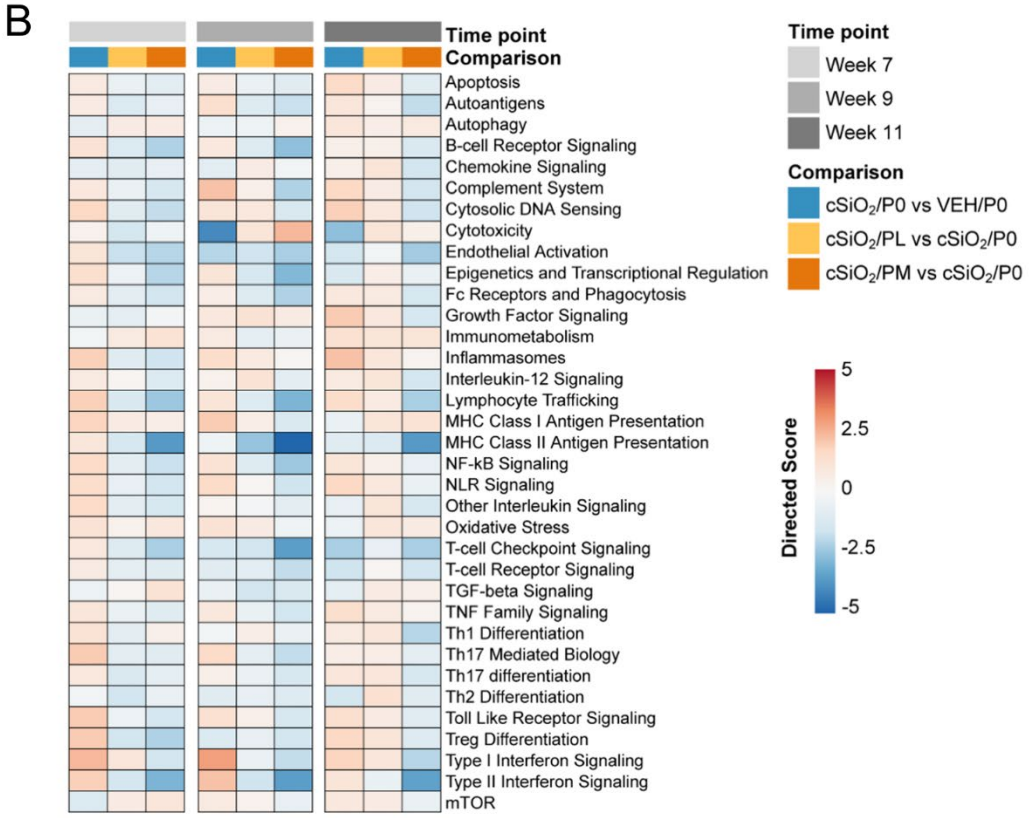

Figure A2.15: Effect of prednisone treatment on $cSiO_2$-induced transcriptional changes in whole blood 7-, 9-, and 11-weeks post instillation. (A) Table indicating the number of differentially expressed genes (FDR q<0.05, 1.5-fold change) at each time point for each treatment comparison of interest. Venn diagrams and principal components analyses of whole blood sample data were not performed due to the low number of differentially expressed genes identified in blood samples. **(B)** Directed significance scores for select autoimmune pathways were determined using nSolver (see Materials and Methods) by comparing $cSiO_2$/P0 to timepoint-matched VEH/P0 control group or by comparing $cSiO_2$/PL or $cSiO_2$/PM treatments to timepoint-matched $cSiO_2$/P0 treatment group.

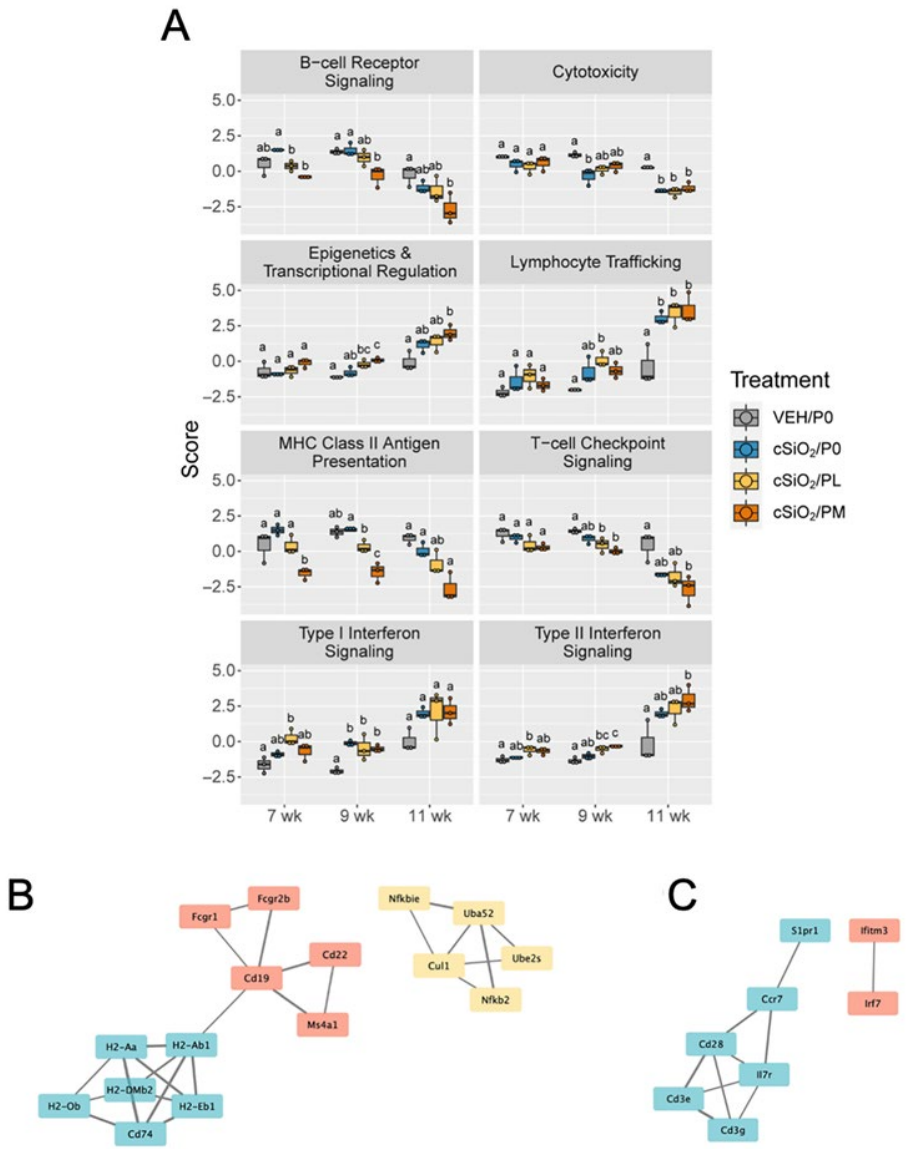

Figure A2.16: Effect of prednisone treatment on select autoimmune pathways in whole blood obtained 7-, 9-, and 11-weeks post instillation with $cSiO_2$. (A) Pathway Z scores ae presented as Tukey box-plots (n=3) for select pathways of interest. Within each time point, different letters indicate that the treatment groups are significantly different ($p<0.05$) as determined by one-way ANOVA with Tukey HSD post-hoc test for multiple comparisons. **(B)** Network visualization of genes significantly affected by medium-dose prednisone compared to control (cSiO2/PM vs cSiO2/P0) in blood at 7-weeks post instillation. **(C)** Network visualization of genes significantly affected by $cSiO_2$ exposure ($cSiO_2$/P0 vs VEH/P0) at 11-weeks post-instillation. Networks were not considered for other comparisons or time points due to few or no identified differentially expressed genes. Network interactions were modeled using the STRING database (string-db.org) with a minimum required interaction score >0.7, and clusters were identified using the Markov Cluster (MCL) algorithm with inflation parameter of 1.5. Networks were visualized in Cytoscape, and edge widths reflect the combined interaction score (thicker edge indicates higher score).

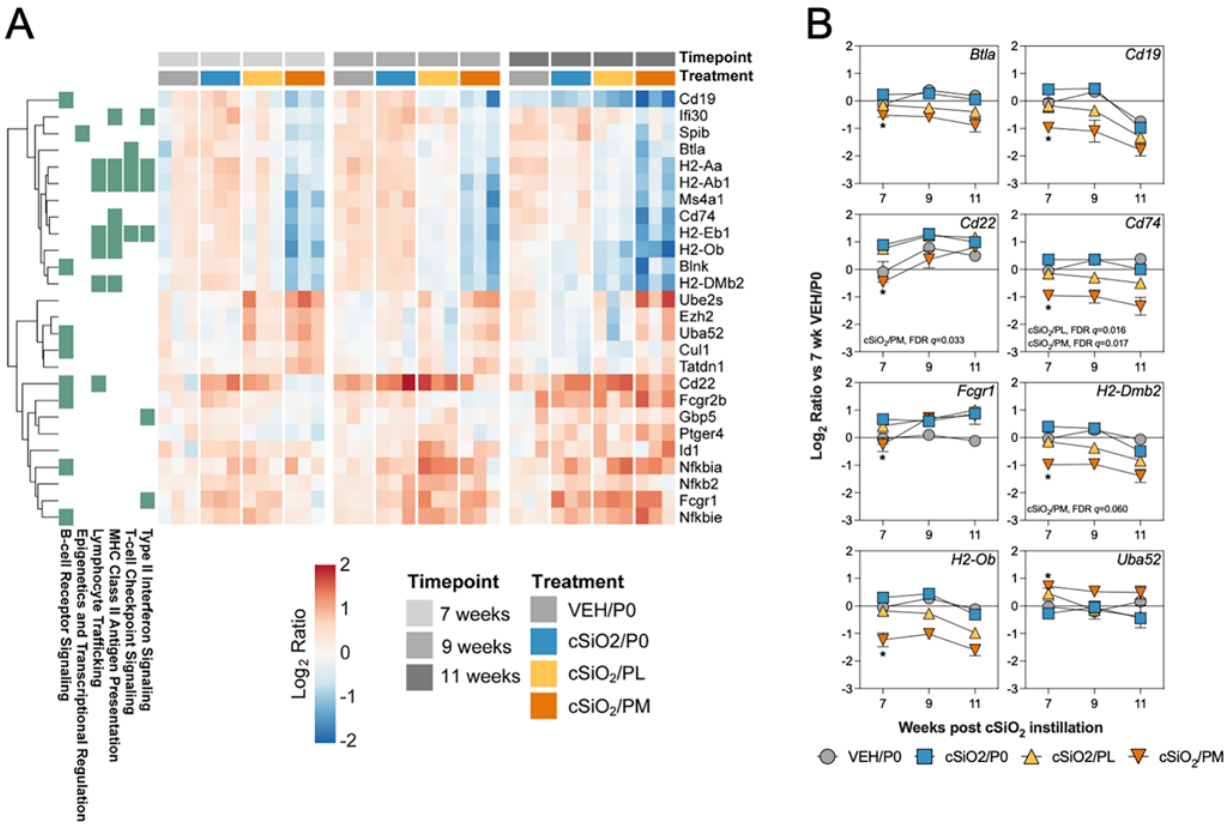

Figure A2.17: Comparison of prednisone-responsive genes associated with selected pathways of interest in whole blood obtained 7-, 9-, and 11-weeks post instillation with $cSiO_2$. Gene expression data were obtained using the NanoString Autoimmune Profiling gene panel and are shown as log_2 ratios for $cSiO_2$/P0, $cSiO_2$/PL, and $cSiO_2$/PM treatment groups with respect to the 7-week, VEH/P0 control group (log_2 ratio = 0). **(A)** Heatmap with unsupervised hierarchical clustering (Euclidian distance method) by gene shows log_2 expression values for all genes identified as differentially expressed in response medium-dose prednisone (FDR q<0.05, 1.5-fold change) at any time point. Membership in autoimmune pathways is indicated to the left (green bar). **(B)** The mean log_2 ratio values + SEM for selected genes of interest are also shown. * Indicates FDR-corrected q<0.05 for $cSiO_2$/PM vs $cSiO_2$/P0. (No significant differences were observed for $cSiO_2$/P0 vs. VEH/P0 or $cSiO_2$/PL vs. cSiO2/P0 comparisons for these genes.) Main effects of the $cSiO_2$/PL or $cSiO_2$/PM treatments vs. $cSiO_2$/P0 are also indicated, when significant (or trending). See Supplementary File 1 for test specifications and FDR-corrected q-values for all genes in the panel for all comparisons.

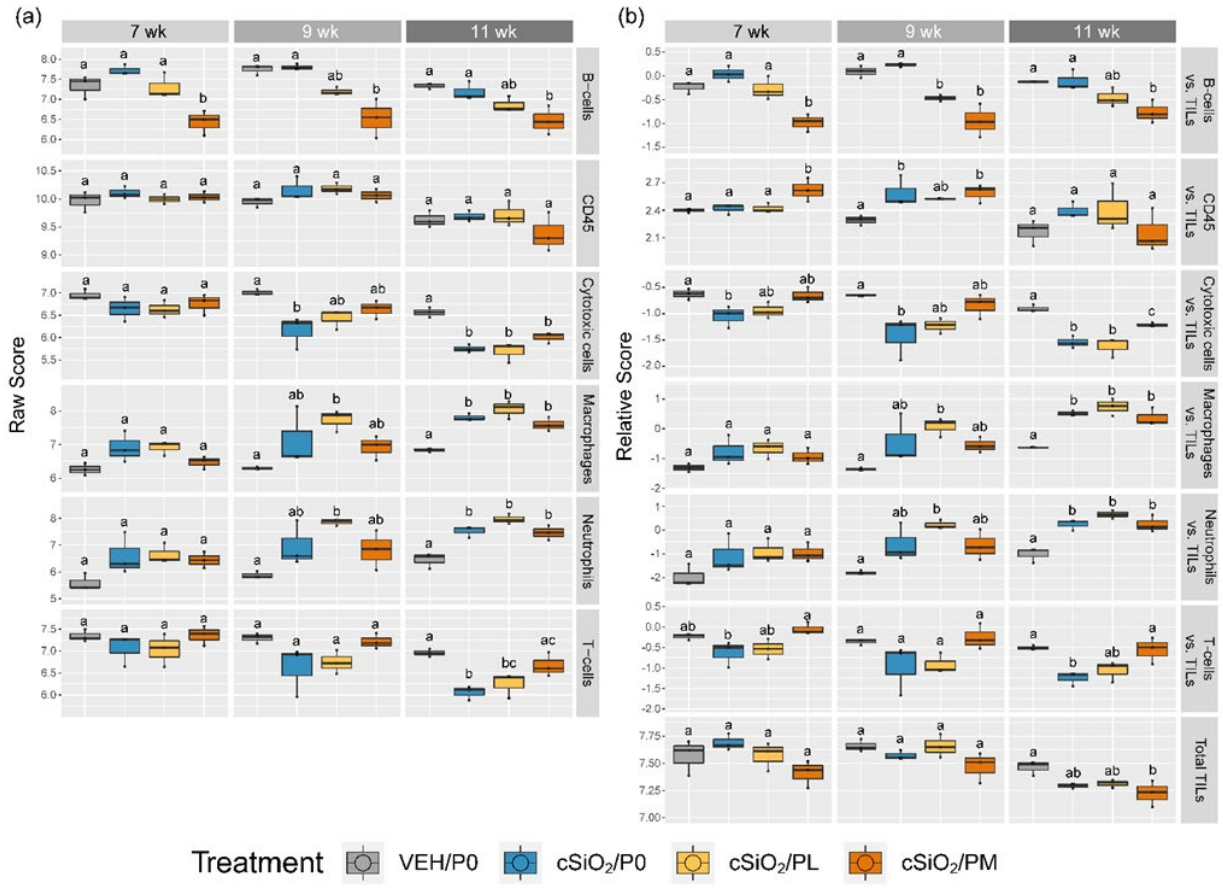

Figure A2.18: Profiling of immune cell types in whole blood from mice 7-, 9-, or 11-weeks post instillation with $cSiO_2$. Data shown are the $\log_2$ raw scores **(A)** or relative scores with respect to total infiltrating leukocytes (TILs) **(B)** for the indicated cell types. Only those cell types passing quality control testing for correlation of marker gene expression for either tissue ($p<0.05$) are shown. Within a tissue type, different letters indicate that the treatment groups are significantly different ($p<0.05$) as described in Materials and Methods. Scores may be compared by treatment within a cell type, but comparisons across cell types are not appropriate for this method of quantitation.

Table A2.1: Experimental diet formulation.

	Experimental Diet			
	CON (P0)	low PR (PL)	medium PR (PM)	high PR (PH)
Ingredient	(g/kg total diet)			
Corn Starch	398	398	398	398
Maltodextrin (dyetrose)	132	132	132	132
Sucrose	100	100	100	100
Cellulose	50	50	50	50
Casein	100	100	100	100
L-Cysteine	3	3	3	3
Corn Oil	10	10	10	10
High-Oleic Safflower Oil	60	60	60	60
AIN93G Mineral Mix	35	35	35	35
AIN93G Mineral Mix	10	10	10	10
Choline Bitartrate	3	3	3	3
TBHQ Antioxidant	0.01	0.01	0.01	0.01
	(mg/kg total diet)			
Prednsione	0	5	15	50

Table A2.2: Criteria for defining moribund condition of silica-treated NZBWF1 mice[a].

Criteria	Method	Response	Score Assigned
Proteinuria[1,2]	Weekly monitoring	<2000 mg/dl = negative (NEG)	0
		>2000 mg/dl = positive (POS)	1
	Note: proteinuria scoring is cumulative over time		
	e.g., POS for proteinuria at 22 wks of age and POS at 23 wks of age = cumulative score of 2		
Weight Loss[2,3,4,5]	Weekly body weight	<10% loss = NEG	0
		10-14% loss = POS	2
		>15% loss = POS	4
	Note #1: loss of body weight will be calculated relative to body weight at onset of nephritis		
	Note #2: onset of nephritis defined as = 300 mg/dl proteinuria (determined in above measurements)		
Dyspenia[1,3,4,5,*]	Daily health check	Qualitative - NO	0
		Qualitative - YES	1
Ambulation[3,4,5,*]	Daily health check	Qualitative - NO	0
		Qualitative - YES	4
Rough Coat[3,4,5,*]	Daily health check	Qualitative - NO	0
		Qualitative - YES	1

[a] Table was reviewed by CAR Veterinarian Dr. Danielle Ferguson at Michigan State University. Mice receiving a score of 4 or more were euthanized. References for criteria previously published indicated by superscripts and noted below.

[1]Gardet et al. (2016) PLOS ONE. 11(10): e 0164423
[2]Frese-Schaper et al. (2010) J Immunology 184 (4) 2175-2182
[3]Toth, L. (2000). Journal of the Institute for Laboratory Animal Research (2000) 41 (2): 72-29
[4]Toth, L. (1997). Contemp. Top Lab Anim Sci 36, 44-48
[5]Tomasovic et al. (1988). Lab Animal 17:31-34,1998.
*The IACUC Handbook (2014) CRC Press. 3rd Edition

Table A2.3: List of Kits, Reagents, and Chemicals.

Reagent/Assay	Vendor	Catalog Number	Lot Number
Prednisone	Spectrum Chemical	PR103	4HF0028
Prednisolone	Toronto Research Chemicals		
Urine InstaTest Reagent Strips	Cortez Diagnostics	URS-2P	82721
AIN-93G Purified Rodent Diet without Vitamin Mix	Dyets Inc.	110700	
AIN-93VX Vitamin Mix	Dyets Inc.	310025	
LouAna Safflower Oil	LouAna Oils		
Mazola Corn Oil	Mazola		
Polyclonal Rabbit Anti-CD3 Antibody	Abcam	ab5690	
Monoclonal Rat Anti-Mouse CD45R Antibody	BD Pharmingen	550268	
Polyclonal Goat Anti-IgG Antibody	Bethyl Labs - FORTIS Life Sciences	A-90-100A	
Diff-Quick	Fisher Scientific		
XT_Mm_AIProfiling_CSO	NanoString	115000269	XT-CSO-MAIP1-12
nCounter Master Kit	NanoString	100054	NAA-AKIT-048

APPENDIX B: CHAPTER 3 SUPPLEMENTAL MATERIAL

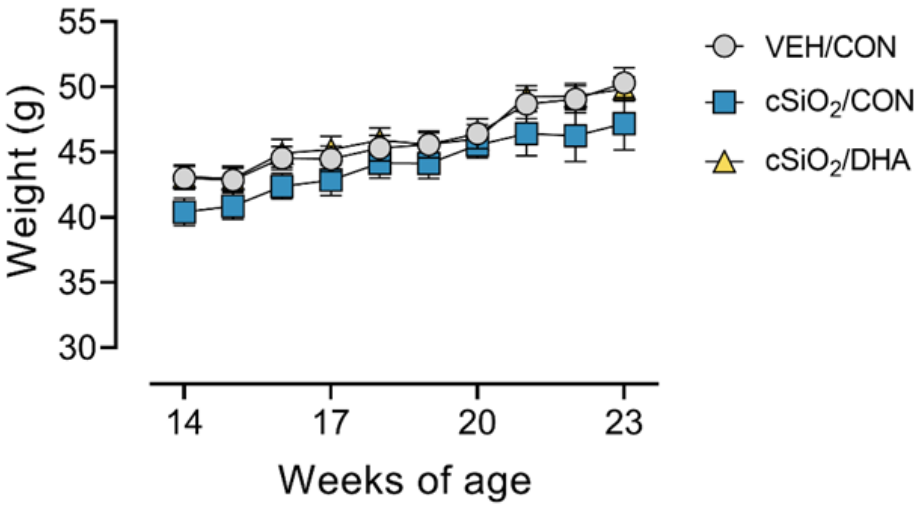

Figure A3.1: Body weights were not altered by exposure or diet. $cSiO_2$/CON mice did not have significant alterations in body weight compared to VEH/CON mice throughout the study. Similarly, $cSiO_2$/DHA mice did not have significant changes in weight compared to VEH/CON or $cSiO_2$/CON mice.

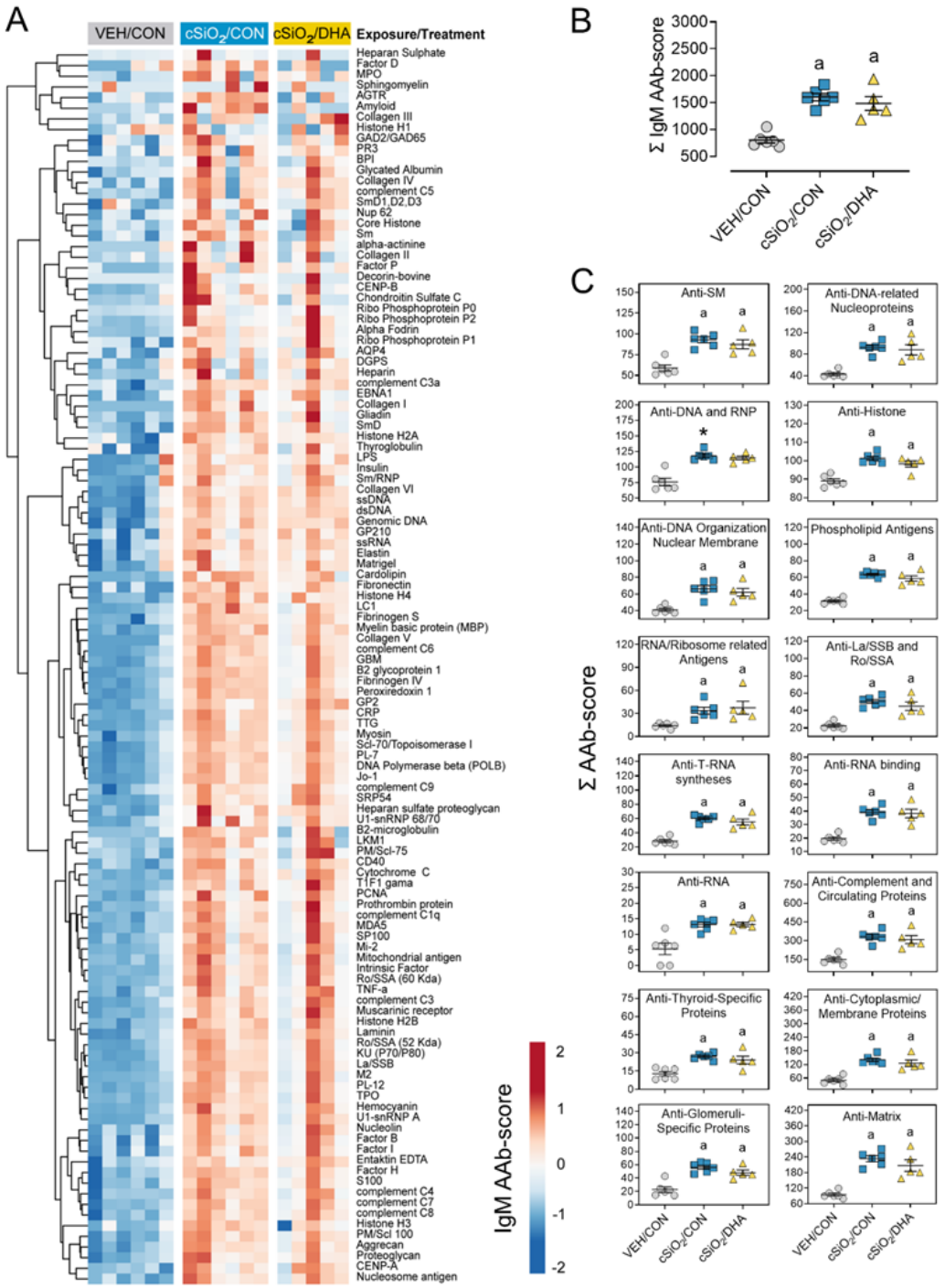

Figure A3.2: $cSiO_2$ exposure induces significant IgM AAb response detected in the BALF of adult mice necropsied at 5-wks PI. (A) Ab-score values for the expression of 120 IgM AAbs are illustrated in a heatmap using unsupervised clustering (Euclidian distance method). Scale bar values reflect the range of variance-stabilized Ab scores, which are centered across rows. **(B)** DHA does not significantly reduce the $cSiO_2$-triggered increase of total IgM in the BALF. **(C)** $cSiO_2$ exposure significantly increases various classes of autoimmunity-related AAbs remain elevated in DHA-fed mice. $p<0.05$; a, Significant compared to VEH/CON.

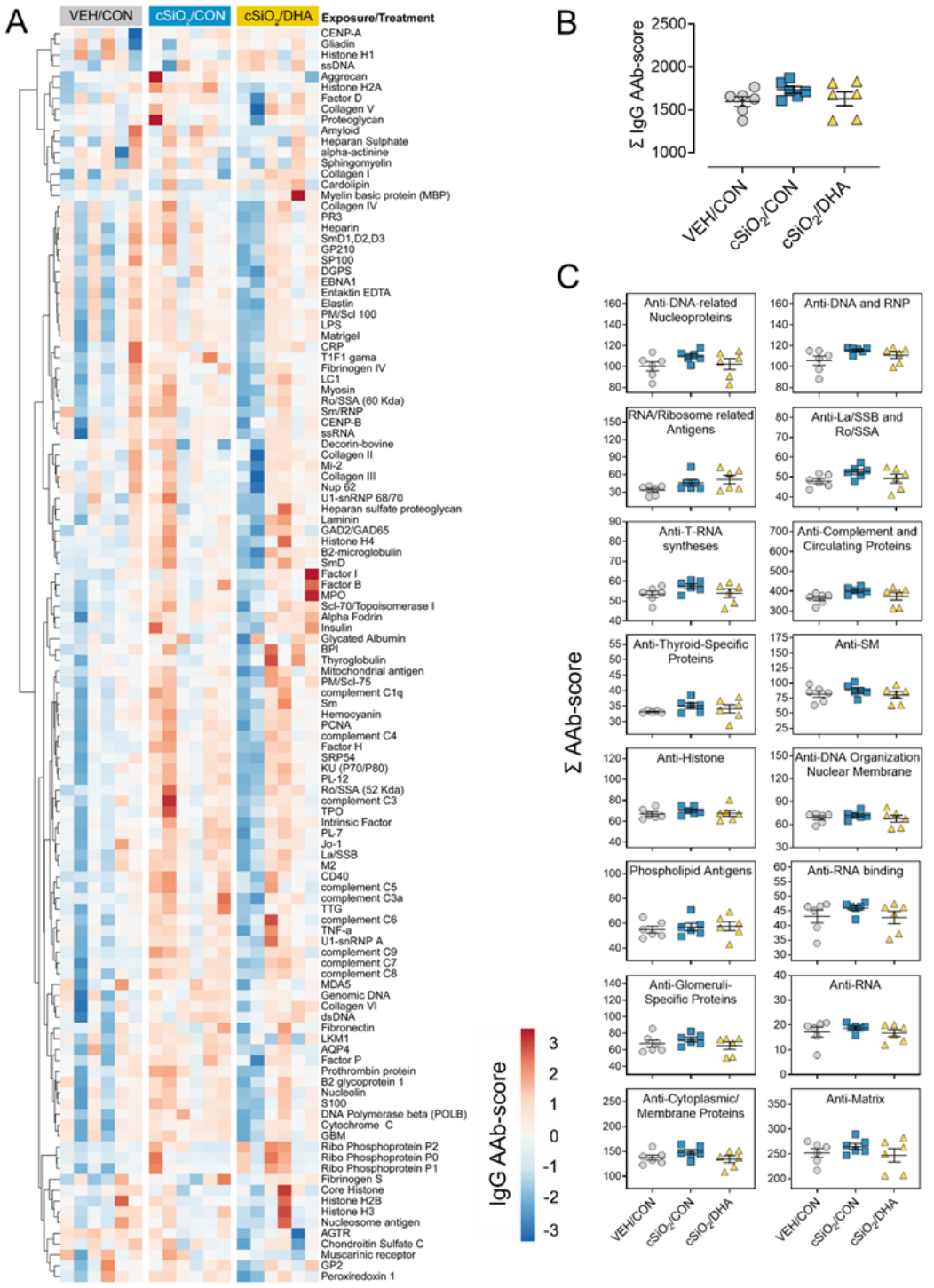

Figure A3.3: $cSiO_2$ exposure did not lead to increased IgG AAb levels detected in the plasma of adult mice necropsied at 5-wks PI. (A) Ab-score values for the expression of 120 IgM AAbs are illustrated in a heatmap using unsupervised clustering (Euclidian distance method). Scale bar values reflect the range of variance-stabilized Ab scores, which are centered across rows. **(B)** Exposure to $cSiO_2$ and diet did not impact IgG AAb summation scores in the plasma, nor various classes of autoimmunity-related AAbs in the plasma **(C)**.

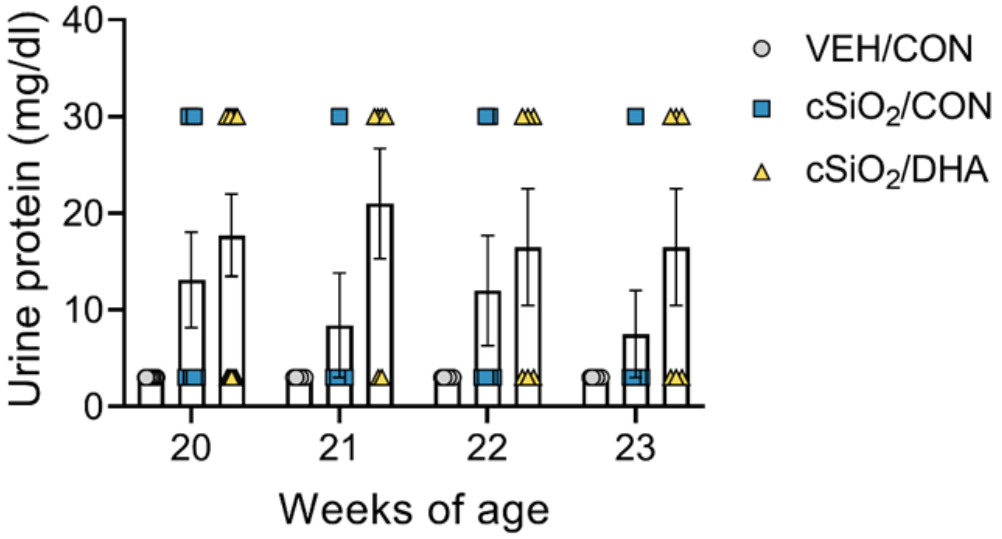

Figure A3.4: $cSiO_2$ exposure did not lead to elevated proteinuria indicative of glomerulonephritis. All experimental groups had trace amounts of protein detected in the urine using diagnostic dipsticks.

Table A3.1: List of Kits, Reagents, and Chemicals.

Reagent/Assay	Vendor	Catalog Number	Lot Number
DHASCO microalgal oil containing 40% Docosahexaenoic Acid	Martek Biosciences Corporation		
Urine InstaTest Reagent Strips	Cortez Diagnostics	URS-2P	82721
AIN-93G Purified Rodent Diet without Vitamin Mix	Dyets Inc.	110700	
AIN-93VX Vitamin Mix	Dyets Inc.	310025	
LouAna Safflower Oil	LouAna Oils		
Mazola Corn Oil	Mazola		
Polyclonal Rabbit Anti-CD3 Antibody	Abcam	ab5690	
Monoclonal Rat Anti-Mouse CD45R Antibody	BD Pharmingen	550268	
Polyclonal Goat Anti-IgG Antibody	Bethyl Labs - FORTIS Life Sciences	A-90-100A	
Human Autoimmunity, Allergy, and Infection Autoantigen Panel	GeneCopoeia	PA010	
NanoString Autoimmune Profiling Panel - Master Kit	NanoString	100052	

APPENDIX C: CHAPTER 4 SUPPLEMENTAL MATERIAL

Table A4.1: List of Kits, Reagents, and Chemicals.

Reagent/Assay	Vendor	Catalog Number	Lot Number
Lipopolysacchrides from Escherichia coli O55:B5	Sigma-Aldrich	L2880	12190801
Urine InstaTest Reagent Strips	Cortez Diagnostics	URS-2P	82721
AIN-93G Purified Rodent Diet without Vitamin Mix	Dyets Inc.	110700	0260-1
AIN-93VX Vitamin Mix	Dyets Inc.	310025	0210-A
LouAna Safflower Oil			
Mazola Corn Oil			